University of Oxford

Department of Chemistry



Group III permethylindenyl-phenoxy complexes for biorenewable polymer synthesis

Justin A. Hayden

Wadham College

July 2024

This Thesis is submitted in partial fulfilment of the requirement for the degree of Doctor of Philosophy at the University of Oxford

For my friends and family

Preface

The work described in this Thesis was carried out in the Chemistry Research Laboratory at the University of Oxford between October 2020 and July 2024 under the supervision of Professor Dermot O'Hare. All work was performed by the author unless otherwise stated, and no part has been previously submitted for another degree at this or any other university.

Part of the work contained in this Thesis **(Chapter 2)** has been published in the following journal paper:

C. G. Collins Rice, **J. A. Hayden**, A. D. Hawkins, L. J. Morris, Z. R. Turner, J. C. Buffet and D. O'Hare, Organometallics. **2024**, *43, 4,* 540-556

DOI: 10.1021/acs.organomet.3c00503

And presented at the following conferences (**Chapter 2** and **4**):

Canadian Chemistry Conference and Exhibition 2023

Dalton 2023

Abstract

Group III permethylindenyl-phenoxy complexes for biorenewable polymer synthesis

Justin A. Hayden **D.Phil Thesis**

Wadham College **Trinity Term 2024**

Chapter One introduces the mechanism of ring opening polymerisation of cyclic esters and the importance of biodegradable and renewable polymers have in modern society. The history of organometallic synthesis is examined in the context of the evolution of asymmetric catalysts for the polymerisation.

Chapter Two contains the synthesis and characterisation of PHENI* (M = Sc, Y, La, and Al) complexes with a focus on scandium. Ligand substitutions are used to synthesis initiators for ring opening polymerisation and particular consideration is given to the stereochemistry of the complexes both in solution and the solid state.

Chapter Three investigates the dynamic equilibrium that are present in solution of PHENI* complexes. This chapter is designed as a guide to understanding the fluxionality of the system and the operations and mechanisms that relate the various isomeric forms.

Chapter Four examines the use of PHENI* and CGC amino scandium complexes for the ROP of ϵ-caprolactone and *L*-Lactide homo- and co-polymerisation and mechanisms for polymerisation are explored. Coordination complexes of 4-coodinate PHENI* scandium monomer adducts of *L*-lactide, ϵ-caprolactone, and ω-pentadecalactone are discussed.

Chapter Five details experimental procedure for all experiments in this thesis in addition to supplementary information

Chapter Six provides overall conclusions for the work in this thesis and an outlook.

Acknowledgments

I would like to thank Professor Dermot O'Hare for the invaluable supervision throughout my project. I am also deeply thankful to Dr. Zoë Turner and Dr. Louis Morris for their continuous patience guidance and discussion. JC, Peace, Jess L, and the various postdocs to inhabit S2, thank you for all your help during the early stages of this work. To (Dr and Dr) Clem and Rebecca, I extend my heartfelt appreciation for your continuous inspiration and general know-how at all point during the lab-work and write up. Your keen eye(s) for detail and encouragement have been a real drive over the past four years. Thanks are due to the entire O'Hare group, including Sam, Alex, Gabi, and Matt(s), as well as the part IIs over the years (Joanna, Izzy, Matt(s) Ollie), for their collaboration, camaraderie, and shared passion for scientific exploration. Thanks to those in the Williams and Aldridge group who put up with my conversation in the corridor(s) around the floor and gave oft needed advice. To my housemates over the years: thank you for your patience and friendship. Good Luck! The triathlon club, Wadham ball committee, and OSFSS (and all those involved) also deserve recognition for facilitating my impulsive interests and desire to be a part of something greater. Niv, Steve, and Tom, your unwavering support and encouragement throughout this journey has been the foundation to all I have, and will, achieve. Your support, encouragement, and friendship have made this journey both rewarding and fulfilling. Lastly to Katie, thanks for making this last year so special, long may it last.

Nomenclature

[L], L_n	Ligand
[η]	Intrinsic viscosity
{^{1}H}	Proton decoupled
$^{3\text{-Ph}}$Ind$^{\#}$	3-phenyl-pentamethylindenyl
Å	Ångström, 10^{-10} m
A	Polymerisation activity
Allyl	CH_2=CH_2CH_3
Ar	Aryl, C_6H_n
atm	Standard atmosphere, 1 atm = 101.325 kPa
b	Broad
BHT	3,5-di-*tert*-butyl-4-hydroxytoluene
Bn	Benzyl, CH_2Ph
cent	Centroid
CGC	Constrained geometry complex
CGCI*	Permethylindenyl constrained geometry complex
COSY	Correlation spectroscopy
Cp	Cyclopentadienyl
Cp*	Permethylcyclopentadienyl
Cumyl	CMe_2Ph
d	Doublet
d	*Deuterated*
$Đ_M$	Molecular mass dispersity , M_w/M_n
Da	Dalton, g mol^{-1}
DEPT	Distortionless enhancement by polarisation transfer

DFT	Density functional theory
Dipp	2,6-di*iso*propylphenyl
DMAP	4-Dimethylaminopyridine
EB	Ethylene bridge, $–C_2H_4–$
EBI	Ethylene-1,2-bis(1-indenyl)
Et	Ethyl, CH_2CH_3
eq.	Equivalents
ϵ-CL	ϵ-Caprolactone
Cp	Cyclopentadiene
ΔH	Enthalpy of activation
ΔS	Entropy of activation
GPC	Gel Permeation Chromatography
h	Hours
HMBC	Heteronuclear multiple bond correlation
HSQC	Heteronuclear single-quantum coherence
HPLC	High-performance liquid chromatography
Ind, I	Indenyl
$Ind^{\#}$, $I^{\#}$	Hexamethylindenyl, $C_{15}H_{20}$
Ind*, I*	Permethylindenyl, $C_{16}H_{22}$
IR	Infrared
k_{app}	Apparent rate constant
k_i	Initiation rate constant
k_{obs}	Observed rate constant
k_p	Propagation rate constant
k_{tr}	Transfer rate constant
KTFA	Potassium trifluoroacetate, $KO_2C_2F_3$

KHMDS	Potassium hexamethyldisilazide, $K(NSiMe_3)_2$
LA	Lactide
M	mol dm^{-3}
Me	Methyl, CH_3
^{Me2}SB	Dimethylsilane bridged, $–SiMe_2–$
M_n	Number-average molecular weight
mol%	Percent by mole fraction
M_w	Weight-average molecular weight
m/z	Mass to charge ratio
^{n}Bu	*n*-Butyl, $CH_2CH_2CH_2CH_3$
Neosilyl	CH_2SiMe_3
NHC	*N*-Heterocyclic carbene
NMR	Nuclear magnetic resonance
NOESY	Nuclear Overhauser Effect Spectroscopy
^{n}Pr	*n*-Propyl $CH_2CH_2CH_3$
Ph	Phenyl, C_6H_5
PHENI*	*ansa*-Permethylindenyl-phenoxy
PHENICS	Phenoxy-Induced Complex of Sumitomo
PLA	Polylactide
PCL	Polycaprolactone
PDL	ω-Pentadecalactone
ppm	Parts per million
PTFE	Polytetrafluoroethylene, Teflon®
q	Quartet
r, *rac*	Racemic
R_{tot}	Total reflectance

ROP	Ring-opening polymerisation
ROCOP	Ring-opening co-polymerisation
RT	Room temperature
s	Singlet
SB	Silyl bridged
t	Triplet
TA’	Characteristic torsion angle
^{t}Bu	*tert*-Butyl
THF	Tetrahydrofuran
TMEDA	Tetramethyl ethylenediamine
TMS	Trimethylsilyl
TOF	Turnover frequency
T_p	Temperature of polymerisation
VT	Variable temperature
Z’	Number of symmetry-independent molecules
δ	Chemical shift
Δ_{M-C}	Ring-slip parameter
η^x	Hapticity
μ	Mean; bridging ligand
ρ	Density

Table of Contents

Preface ..... **iii**

Abstract ..... **iv**

Acknowledgments ..... **v**

Nomenclature ..... **vi**

Chapter 1 – Introduction **1**

1.1. Overview **1**

1.1.1. The future of polymers 1

1.1.2. Polymers derived from renewable feedstocks 2

1.1.3. Thermodynamics of ROP 5

1.1.4. Kinetics of living polymerisation 6

1.1.5. Cyclic polymers 10

1.1.6. Role of the neutral donor in ROP 12

1.1.7. Metal radii and Lewis acidity effects on polymerisation activity 13

1.2. Polymerisation Characterisation **13**

1.2.1. Molecular Weight 13

1.2.2. Size Exclusion Chromatography (SEC) 14

1.2.3. Matrix Assisted Laser Desorption/Ionisation Time-of-Flight mass spectrometry (MALDI-TOF MS) 16

1.3. Initiators for the ROP of ϵ-CL and LA **16**

1.3.1. Common catalysts 16

1.3.2. Rare earth initiators 18

1.4. Metal-complexes with cyclopentadienyl-derived ligands **23**

1.4.1. Cyclopentadienyl ligands 23

1.4.2. The indenyl effect 24

1.4.3. Constrained Geometry Catalysts 26

1.4.4. Stereochemistry in metallocene complexes 27

1.4.5. Asymmetric initiators for ROP of cyclic esters 30

1.4.1. Permethylindenyl catalysts for ROP of cyclic esters 32

1.5. Scope of thesis **33**

1.6. References **34**

Chapter 2 – Group three permethylindenyl-phenoxy (PHENI*) complexes 40

2.1. Introduction 40

2.1.1. Phenoxy-Induced Complexes of Sumitomo (PHENICS) and constrained geometry complexes (CGCs) 40

2.1.2. Permethylindenyl phenoxy PHENICS-type (PHENI*) complexes 40

2.1.3. Chapter synopsis 42

2.2. Synthesis of Ligands 42

2.2.1. Synthesis of proligands ^{Me_2}SB($^{R,R'}$ArOAllyl,I*)H (R = R′ = ^{t}Bu, CMe$_2$Ph; R = ^{t}Bu, R′ = Me; Cumyl = CMe$_2$Ph) 42

2.2.2. Synthesis of other proligands 44

2.3. Synthesis of ^{Me_2}SB($^{R,R'}$ArO,I*)Sc(Cl)THF {R = R′ = ^{t}Bu (1) and Cumyl (2); R = ^{t}Bu, R′ = Me (3)} 46

2.3.1. Characterisation of complexes 1 and 2 48

2.3.2. NMR spectroscopic characterisation of ^{Me_2}SB(^{Cumyl_2}ArO,I*)Sc(Cl)THF (2) 52

2.3.3. Solid-state structures of ^{Me_2}SB($^{R,R'}$ArO,I*)Sc(Cl)THF (R = R′ = ^{t}Bu (1) and Cumyl (2)) 53

2.4. Synthesis and characterisation of ^{Me_2}SB($^{R,R'}$ArO,I*)Sc(ODipp)THF R = R′ = ^{t}Bu (5) and Cumyl (6) 55

2.4.1. NMR spectroscopic characterisation of ^{Me_2}SB($^{R,R'}$ArO,I*)Sc(ODipp)THF (5) ... 55

2.4.2. NMR spectroscopic characterisation of ^{Me_2}SB(^{Cumyl_2}ArO,I*)Sc(ODipp)THF (6) 57

2.4.3. Solid-state structure of ^{Me_2}SB(^{tBu_2}ArO,I*)Sc(ODipp)THF (5) 57

2.4.4. Synthesis and solid-state characterisation of ^{Me_2}SB(^{tBu}N,I*)Sc(X)THF X = Cl (4) and ODipp (7) 58

2.5. Comparison of solid-state structure of 1, 2, 4, 5, and 7 59

2.5.1. Ligand Shielding 65

2.5.2. Structure and catalytic activity 68

2.6. Ligand substitution reactions with 1, 5, and 7 69

2.6.1. NMR spectroscopic characterisation of ^{Me_2}SB([η^1],I*)Sc(X)DMAP ([η^1] = ^{tBu_2}ArO and X = Cl (8), X = ODipp (9); [η^1] = ^{tBu_2}N and X = ODipp (10)) 71

2.6.2. NMR spectroscopic characterisation of ^{Me_2}SB([η^1],I*)Sc(X)OPPh$_3$ ([η^1] = ^{tBu_2}ArO and X = Cl (11), X = ODipp (12), [η^1] = ^{tBu}N and X = ODipp (13)) 73

2.7. DFT calculations on isomers of PHENI* and CGCI* complexes 76

2.8. ^{45}Sc NMR spectroscopy 78

2.9. Attempted synthesis of M(III) PHENI* complexes 80

2.9.1. General synthesis of ^{Me_2}SB(^{tBu_2}ArO,I*)M(Cl)THF$_x$ (M = Y, La, and Al) 81

2.9.2. Attempted preparation of alkyl complexes. 83

2.10. Conclusions **85**
2.11. References **86**
Chapter 3 – Solution Dynamics of PHENI* complexes **88**
3.1. Introduction **88**
3.1.1. Stereogenic units 88
3.1.2. Chapter synopsis 88
3.2. Isomerism in PHENICS **89**
3.2.1. Conformational isomerism 89
3.2.2. Stereogenicity at tetrahedral metal centre 91
3.2.3. Asymmetric Ligand 93
3.2.4. Operations and mechanisms for isomerism 94
3.2.5. Metallocyclic ring puckering 96
3.2.6. Ligand/solvent exchange 98
3.2.7. Disassociation, rotation, and reassociation of the indenyl moiety (I* face flip) 106
3.3. Conclusion **110**
3.4. References **111**
Chapter 4 – Using scandium complexes for the polymerisation of cyclic esters ... **101**
4.1. Introduction **101**
4.1.1. Chapter synopsis / Overview 101
4.1.2. Organometallic Scandium Catalysts for polymerisation 102
4.1.3. Reaction kinetics 105
4.1.4. Polymerisation conditions 106
4.1.5. Considerations regarding Mark Houwink correction factor 107
4.2. ϵ-CL polymerisation studies using PHENI* scandium chlorides (1–3) **107**
4.2.1. The effect of BnOH 107
4.3. Polymerisation studies using PHENI*/CGCI* scandium aryloxide complexes **111**
4.3.1. Polymerisation of ϵ-CL varying the hetero atom (5 and 7) 112
4.3.2. Initiator concentration dependency for 5 and 7 113
4.3.3. The effects of a competing neutral donor on polymerisation 115
4.3.4. Temperature variation 118
4.3.5. Polymerisation of ϵ-CL using scandium tris-aryloxide complexes (29 and 30) 122
4.3.6. Polymer characterisation 123
4.3.7. Discussion on proposed reaction mechanism for 5, 7, 29 and 30 128
4.4. *L*-LA polymerisation using 5 and 7 ..... **130**
4.5. Synthesis and solid-state characterisation of scandium-cyclic ester adducts ... **132**
4.6. *L*-Lactide and ϵ-CL copolymerisation using 5 and 7 ..... **140**

4.6.1. Literature reports and mechanism 140
4.6.2. Preliminary Results 141
4.7. Conclusion 144
4.8. References 146
Chapter 5 – Experimental Detail 149
5.1. Compound Key 149
5.2. General procedures 152
5.2.1. Literature preparations and commercially supplied reagents 152
5.2.2. Solvent Preparation 154
5.2.3. Solution NMR spectroscopy 154
5.2.4. X-ray crystallography 155
5.2.5. Elemental analysis 155
5.2.6. Infrared spectroscopy 156
5.2.7. Gel permeation chromatography 156
5.2.8. Proligand synthesis 156
5.3. Experimental Detail for Chapter 2 158
5.3.1. Synthesis of ^{Me_2}SB($^{t Bu_2}$ArOAllyl,I*)H 158
5.3.2. Synthesis ^{Me_2}SB(^{Cumyl_2}ArOAllyl,I*)H of 159
5.3.3. Synthesis of ^{Me_2}SB($^{t Bu_2}$ArOAllyl,I*)$Li_2.(NEt_3)_x$ 160
5.3.4. Synthesis of ^{Me_2}SB(Furan,I*)H 161
5.3.5. Synthesis of ^{Me_2}SB(Furan,I*)Li 162
5.3.6. Synthesis of $I^{\#}SiMe_3$ 163
5.3.7. Synthesis of ^{Me_2}SB($^{R,R'}$ArO,I*)Sc(Cl)THF R = R′ = ^{t}Bu (1) and Cumyl (2); R = ^{t}Bu, R′ = Me (3) 164
5.3.8. Synthesis of ^{Me_2}SB(^{Cumyl_2}ArO,I*)Sc(Cl)THF (2) 165
5.3.9. Synthesis of ^{Me_2}SB($^{t Bu,\ Me}$ArO,I*)Sc(Cl)THF (3) 166
5.3.10. Synthesis of ^{Me_2}SB($^{t Bu_2}$ArO,I*)Sc(ODipp)THF (5) 167
5.3.11. Synthesis of ^{Me_2}SB(^{Cumyl_2}ArO,I*)Sc(ODipp)THF (6) 168
5.3.12. General synthesis of DMAP (8–10) and $OPPh_3$ (11–13) adducts 169
5.3.13. Synthesis of ^{Me_2}SB($^{t Bu_2}$ArO,I*)Sc(Cl)DMAP (8) 170
5.3.14. Synthesis of ^{Me_2}SB($^{t Bu_2}$ArO,I*)Sc(ODipp)DMAP (9) 170
5.3.15. Synthesis of ^{Me_2}SB($^{t Bu}$N,I*)Sc(ODipp)DMAP (10) 171
5.3.16. Synthesis of ^{Me_2}SB($^{t Bu_2}$ArO,I*)Sc(Cl)$OPPh_3$ (11) 172
5.3.17. Synthesis of ^{Me_2}SB($^{t Bu_2}$ArO,I*)Sc(ODipp)$OPPh_3$ (12) 173
5.3.18. Synthesis of ^{Me_2}SB($^{t Bu}$N,I*)Sc(ODipp)$OPPh_3$ (13) 174

5.3.19. Synthesis of [^{Me_2}SB(^{tBu_2}ArO,I*)Y(Cl)THF]$_2$ (14) 174
5.3.20. ^{Me_2}SB(^{tBu_2}ArO,I*)LaCl (15) 176
5.3.21. Synthesis of ^{Me_2}SB(^{tBu_2}ArO,I*)Al(Cl)THF (16) 177
5.4. Experimental for unsuccessful chemistries in Chapter 2 178
5.4.1. Synthesis of ^{Me_2}SB($^{R,R'}$ArO,I*)Sc(CH$_2$(SiMe$_3$))$_2$-μ^2Li.THF R = R′ = ^{t}Bu (17) and Cumyl (18) 178
5.4.2. Synthesis of ^{Me_2}SB(^{tBu_2}ArO,I*)Sc(N(SiMe$_3$)$_2$)$_2$.E.THF (E = Li (19) and K (20)) 180
5.4.3. Synthesis of ^{Me_2}SB($^{R,R'}$ArO,I*)Sc(BH$_4$)THF R = R′ = ^{t}Bu (21) and Cumyl (22) 181
5.5. Experimental detail for Chapter 4 183
5.5.1. Synthesis of ^{Me_2}SB(^{tBu_2}ArO,I*)Sc(X)L, X = Cl; L = ϵ-CL (23), L-La, (24) and PDL (25); X = ODipp, L = ϵ-CL (26), L-La (27) and PDL (28) 183
5.5.2. Synthesis of Sc(OAr)$_3$.2THF 187
5.6. References 187
Chapter 6 – Conclusions and outlook 189

Chapter 1 – **Introduction**

1.1. Overview

1.1.1. The future of polymers

A polymer is a molecule of high relative molecular mass, and its structure consists of the multiple repetition of units (monomers) derived from molecules of low relative molecular mass. Plastics, synthetic or semi-synthetic materials that use polymers as a main ingredient, are ubiquitous to our daily life and needs in the 21st century and are found in nearly all markets. Recent estimates have predicted the yearly consumption of plastics will double in the next 20 years.[1, 2] The estimated production of plastics in 2024 was over 450mn tonnes. The need to form a robust circular economy, defined through eliminating waste, rebuilding natural capital and creating value from sustainable use of resources, is key to improving the currently unsustainable relationship between plastics and modern society.[3-5] Emerging technologies such as chemically recyclable, biodegradable,, depolymerisable polymers, and use of waste chemicals and resources as feedstocks are critical areas of research at present.[6-11]

Waste feedstocks occur as substances that were previously considered as unwanted process waste, but can reform the beginning of a new supply chain. They often take the form of small molecules like carbon dioxide (CO_2) or biowaste (e.g. citrus peel). Immense potential can be provided through the use of such building blocks for the synthesis of value-added chemicals or polymers.[12-14] However, their use is often limited by high kinetic and thermodynamic stability and limited supply chains. Transformations may remain difficult under ambient conditions, although great interest persists due to the apparent abundance and low cost of such substances.[13, 15]

1.1.2. Polymers derived from renewable feedstocks

The production of renewable, biodegradable, and biocompatible polymers is becoming increasingly sought after. The high standards required and competition against conventional petrochemical-based polymers set a high bar for commercial entry. In addition, the cost and time to modify existing optimised industrial processes acts as a barrier for their adoption for existing petrochemical companies. These new materials can stand in for a range of applications; products such as single use packaging and biomedical devices are currently being manufactured from these materials (**Table 1.1**).[16-19]

Table 1.1 Polymer feedstock and application for selected commercial polymers applications.[5, 20, 21]

Polymer	Feedstocks	Applications
Polyethylene (PE)	**Ethylene** (from naphtha or ethane)	Packaging, construction, consumer goods
Polypropylene (PP)	**Propylene** (from naphtha or natural gas)	Automotive, consumer products, packaging
Polyvinyl Chloride (PVC)	**Vinyl chloride monomer** (from ethylene and chlorine)	Construction (pipes, flooring), healthcare
Polystyrene (PS)	**Styrene** (from ethylbenzene, benzene, and ethylene)	Packaging, insulation, disposable products
Polyethylene Terephthalate (PET)	**Terephthalic acid** (PTA) and ethylene glycol (from petroleum)	Beverage bottles, food packaging, textiles (fibres)
Acrylonitrile Butadiene Styrene (ABS)	**Acrylonitrile**, **butadiene**, **styrene** (from crude oil derivatives)	Automotive parts, household appliances, electronics
Polylactic Acid (PLA)	**Corn starch**, **sugarcane**	Packaging, food service ware, biomedical devices
Polyhydroxyalkanoates (PHA)	**Organic waste**, **plant oils**	Packaging, agriculture, biomedical devices
Bio-based Polyethylene (Bio-PE)	**Bio-ethanol** (from sugarcane, corn)	Packaging, consumer goods, industrial applications

As of the early 2020s, the market size for renewables is still dwarfed by that of conventional petrochemicals. For example with the volume of polylactic acid (PLA), one of the main types of renewable, biodegradable polyesters, is produced in the region of 0.2 – 0.3 Mn tonnes compared to over 110 Mn tonnes of various types of polyethylene (PE).[22]

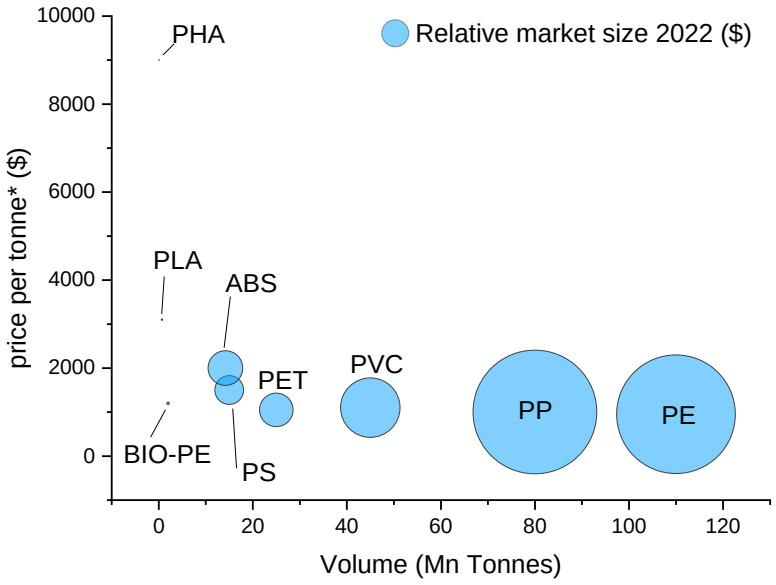


Figure 1.1 Estimated volume traded against average price per tonne (2022) (prices not fixed).[23]

Table 1.2 Polymer with market data including market size, estimated volume traded, and average price per tonne.[23]

Polymer	**Market Size (2022 Bn$)**	**Volume (Mn Tonnes)**	Price Per Tonne (2022, $)
Polyethylene (PE)	120	110	950
Polypropylene (PP)	125	80	1000
Polyvinyl Chloride (PVC)	60	45	1100
Polystyrene (PS)	30	15	1500
Polyethylene Terephthalate (PET)	35	25	1050
Acrylonitrile Butadiene Styrene (ABS)	35	15	2000
Polylactic Acid (PLA)	< 2	< 1	3100
Polyhydroxyalkanoates (PHA)	< 1	0.1	> 9000
Bio-based Polyethylene (Bio-PE)	3	2	1200

Poly(lactide) (PLA) and poly(ϵ-caprolactone) (PCL) are among the most used and studied polyesters. Polyesters are enticing materials as they are generally biodegradable through hydrolyses of the ester bonds, in addition to being biocompatible. The feedstocks to produce cyclic esters are often bio-sourced. For example, lactide, is sourced from plant-based matter such as corn or sugar beets. ϵ-caprolactone (ϵ-CL) can be synthesised *via*

Bayer Williger oxidation of cyclohexanone or a multistep synthesis from starch (**Figure 1.1**).[24-27]

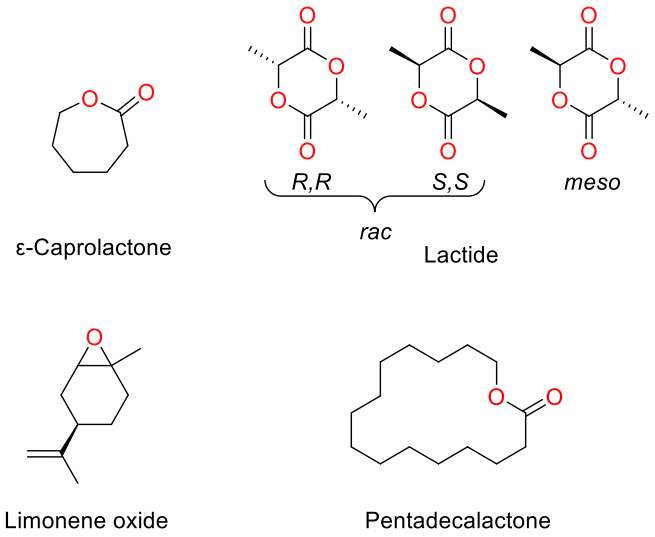


Figure 1.2 A selection of monomers capable of ROP to form biodegradable and/or biocompatible polymers.[28] ϵ-CL (starch), lactide (corn and beets), and limonene oxide (citrus peel) can all be bio-sourced.

In order for polyesters to be viable replacements to plastics made from petrochemicals, a requirement to tune properties, such as tensile strength, processability, and degradability (possible through altering crystallinity) is necessary.[29, 30] In addition, use of copolymers through polymerisation of two monomers into the same polymer chain and can lead to materials with differing properties such as hydrophobicity.[28, 31, 32] The choice of composition and monomers used is crucial to the final material properties.[33-39] For example, poly(3-hydroxyburtyrate) (H3PB) is a polyester part of the wider polyhydroxyalkonates (PHA) family. It is a brittle and readily decomposable polymer that can be extracted from bacteria. A synthetic variation can be produced through the polymerisation of β-butyrolactone (BBL) and modified through copolymerisation with lactide or ϵ-CL. The copolymers exhibit improved ductility and elasticity, in addition to improving the biodegradability.[34, 40-43]

The development of sustainable feedstocks and scalable polyester production has the potential to disrupt the plastics market; however, in order to achieve this, effective catalysts are required to make polymers with desired performance and functionality. Ring-opening polymerisation (ROP), a type of chain-growth polymerisation where the growing polymer chain has a reactive end that opens another cyclic monomer, has proven successful for the synthesis of many of these polymers.[44]

1.1.3. Thermodynamics of ROP

Cyclic molecules, or monomers, can polymerise when both thermodynamic and kinetic towards the polymer, and there is an allowed mechanism to form repeating polymer units. Ring strain is an important factor to consider when discussing the thermodynamic driving forces for the reactivity of ring like molecules. Understanding the entropic *vs* enthalpic pay-off is key to knowing where the monomer–macromolecule equilibrium will lie, and to understand under what conditions a monomer may be reactive.[45, 46] Where the Gibbs free energy is less than 0 for the ring opening of a cyclic ester, there is a thermodynamic drive for polymerisation to occur (**Figure 1.3**).

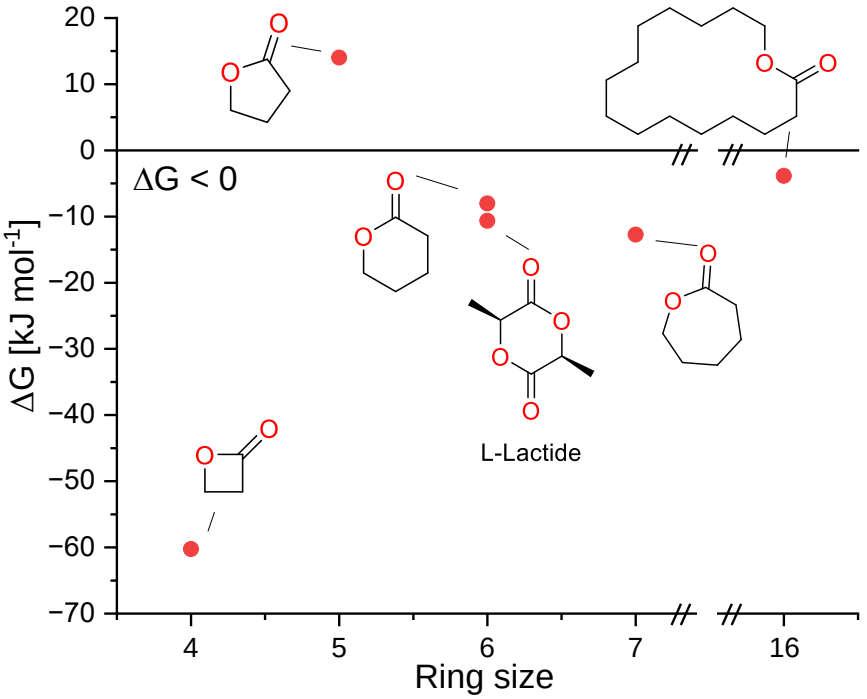


Figure 1.3 ΔG *vs* ring size for selected cyclic esters, calculated at 298 K.[47] Where ΔG < 0, under the line, polymerisation is thermodynamically favourable at room temperature.

The main mechanisms for ring opening polymerisation involve coordination, covalent, ionic (anionic or cationic) metathetic, radical and enzymatic polymerisation; the type of which is dependent on the catalyst/initiator and the monomer used.[47] However, for larger cyclic esters (ring size >7) it has been suggested that the strain of the ring is not a main driving force for the formation of polymer from monomer.[48] In these cases, lower activation energy mechanisms are required to polymerise these monomers.[49]

1.1.4. Kinetics of living polymerisation

Extensive studies have been undertaken to understand the kinetics of the ring opening polymerisations of cyclic esters.[50-56] The coordination-insertion mechanism of ROP of cyclic esters using metal alkoxide complexes involves a number of steps (**Figure 1.4**). Initiation: coordination proceeds via coordination to the carbonyl oxygen of the cyclic ester, then the ring opening of the first cyclic ester.[57] Faster coordination is general linked

to increased electrophilicity, and unsaturated steric and coordination environment around the active metal centre (**Figure 1.3** (a)).[58] Propagation: chain lengthening by coordination and ring opening of subsequent monomers. (**Figure 1.3** (b)). Termination: reaction with a deactivating agent.

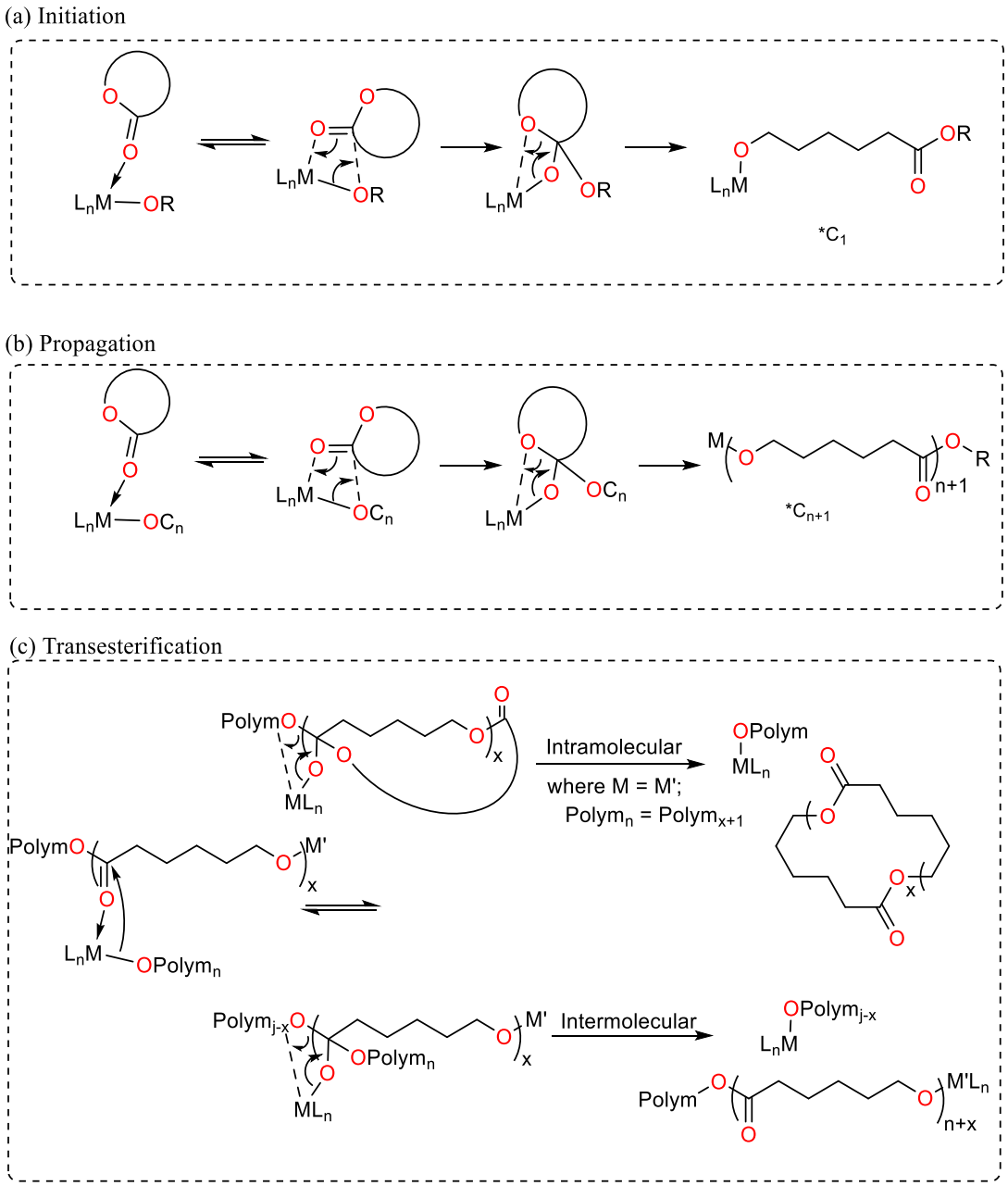


Figure 1.4 Kinetic scheme involving (a) initiation, (b) propagation, and (c) transesterification for the coordination, insertion polymerisation of cyclic esters using metal alkoxides initiator.[54, 56]

Living polymerisation as defined by IUPAC is "a chain polymerisation from which chain transfer and chain termination are absent. In many cases, the rate of chain initiation is fast compared with the rate of chain propagation, so that the number of kinetic chain carriers is essentially constant and defined by throughout the polymerisation."[59] Living, reversible ROP dates back to as early as the 1940s with the anionic propagation of ethylene oxide, which occurs without side reactions such as irreversible transfer and termination.[60] Cationic polymerisation was developed later in the 1970s, with the same living nature attached to it.[61] Immortal ROP; a living polymerisation in which the growing chains do not die, makes use of chain transfer agents, often alcohols such as 2-propanol or benzyl alkoxide, to provide great control over the active propagating polymer chains. The rapid chain transfer allows the formation of polymers with very narrow molecular weight distributions and controlled molecular weights. However, chain transfer agents have also have the potential to poison ROP initiators through protonation of ligand framework.[62] Polymerisation control is often important as transesterification can compromise the molecular weights and lead to unwanted oligomerisation reactions (**Figure 1.5**(c)).

Where transesterification is involved, there are two types of chain transfer: Int**ra**- and int**er**-molecular: Intramolecular leads to cyclic polymer formation, and intermolecular leads to formation of other chain length linear oligomers.

Kinetic schemes are useful models that assist with understanding the possible reactions and active species present. For polymerisation reaction schemes are used to discuss the order of selectivity that reactions and equilibria occur (**Figure 1.5**).[52-54]

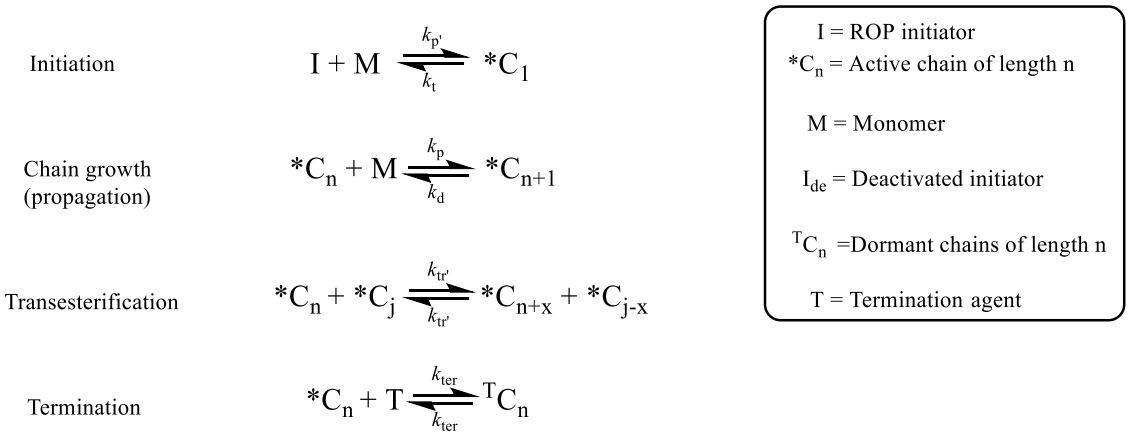


Figure 1.5 Kinetic scheme for the simplified variation of ROP of cyclic esters such as lactones. Initiation, followed by propagation and termination either through addition of a quenching agent (i.e. wet pentane/solvent) or impurity in reaction.*C_n is involved in multiple equilibria during polymerisation.

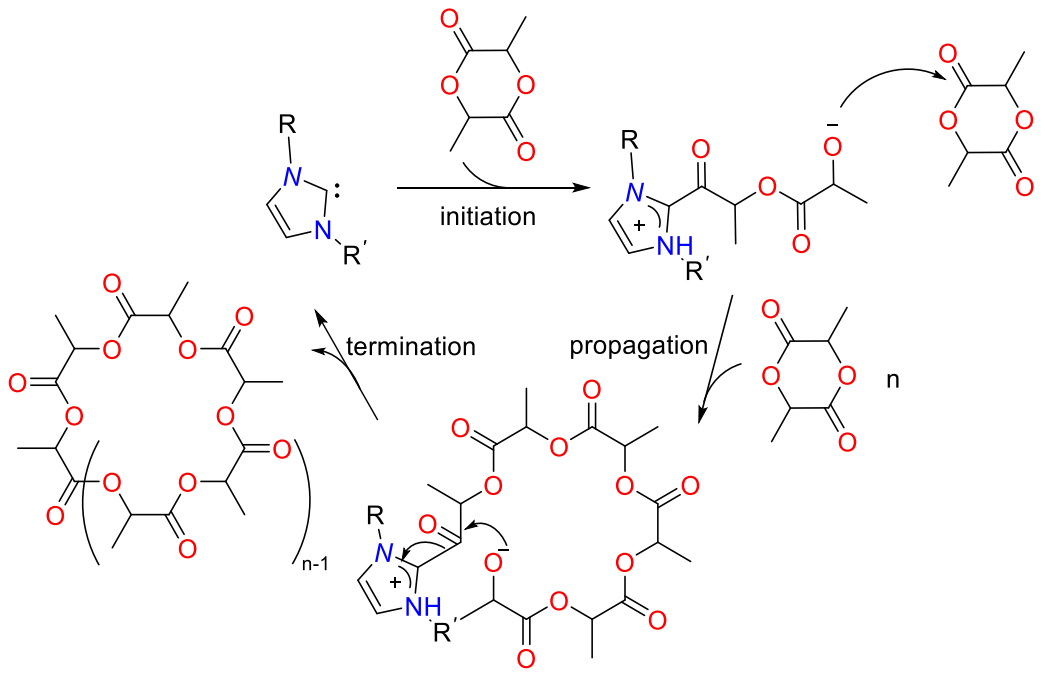
The selectivity of polymerisation, defined in this case as the likelihood of the active centre favouring activating monomer over polymer, hence propagation over chain transfer reactions, is dependent on the reactivity (k_p) and size of the species.[63] Although chain transfer reactions do not change the number of active chain ends, they act to compete against propagation. This can change the rate at which monomer is consumed, hence the observed rate constant k_{obs} is defined in ROP as the rate at which monomer concentration changes over time. Thus, in cases where activity k_p is large, and selectivity is poor (where k_{tr} is also great), the final distribution of molecular weights' are highly dependent on the concentrations of monomer (M) and chains (both active and dormant or dead) in the reaction.

When $[M] \gg [C_n]$, propagation is favoured over transesterification; the molecular weight distribution ($Đ_M$) will be closer to 1.0 and display 'living' like polymerisation, where there is no termination and side reactions such as chain transfer. When $[M] \ll [C_n]$, transesterification is favoured over propagation; $Đ_M$ will be higher, with extensive side reactions even if no termination is present.

Techniques such as MALDI-TOF mass spectroscopy, or by analysis of the topology through chromatography, the polymer can be examined at different stages of polymerisation for evidence of transesterification. characterising the polymer resulting from the reaction, it is possible to determine which reactions are preferred during the polymerisation process.

1.1.5. Cyclic polymers

The lack of chain ends on cyclic polymers leads to different properties with respect to linear systems. The topology affects reptation (molecules ability to slide over one another) and leads to a reduction in hydrodynamic radii.[64, 65] Selective cyclic polymer synthesis is possible through chain end-coupling, use of anionic species to promote cyclisation and ring expansion polymerisation.[66-70] Conditions such as temperature and monomer concentration can have a large impact to the degree of cyclisation.[71] One of the most facile routes is through zwitterionic catalysts such as N-heterocyclic carbene (NHC) organo-catalysts reported by Waymouth *et al.* for the synthesis cyclic PLA (M_n > 26 kDa) (**Scheme 1.1**).[72]



Scheme 1.1 NHC-mediated zwitterionic polymerisation of lactide. Adapted with permission from Wiley. (*Angew. Chem.* Int. Ed. 2007, 119, 2681–2684.)[72]

Arnold, Williams and co-workers reported both ultra-rapid activity and high molecular weights with a cerium-NHC catalyst to form large cyclic polymers (M_n = 250 kDa, $Đ_m$ = 1.53) (**Figure 1.6 (a)**). In this case, intrinsic viscosity and GPC comparison to linear counterpart was used due as NMR and MALDI-ToF analysis only being possible for polymers in the lower M_w regime. The catalyst forms a zwitterionic intermediate which reduces entropy limitations and enhances backbiting. Okuda and co-workers reported a ring expansion mechanism that involved in the amide ligand that was tethered through a Cp moiety to the active carbon. This led to properties as above forming with only linear polymer forming as part of the quenching process (**Figure 1.6 (b)**).[66]

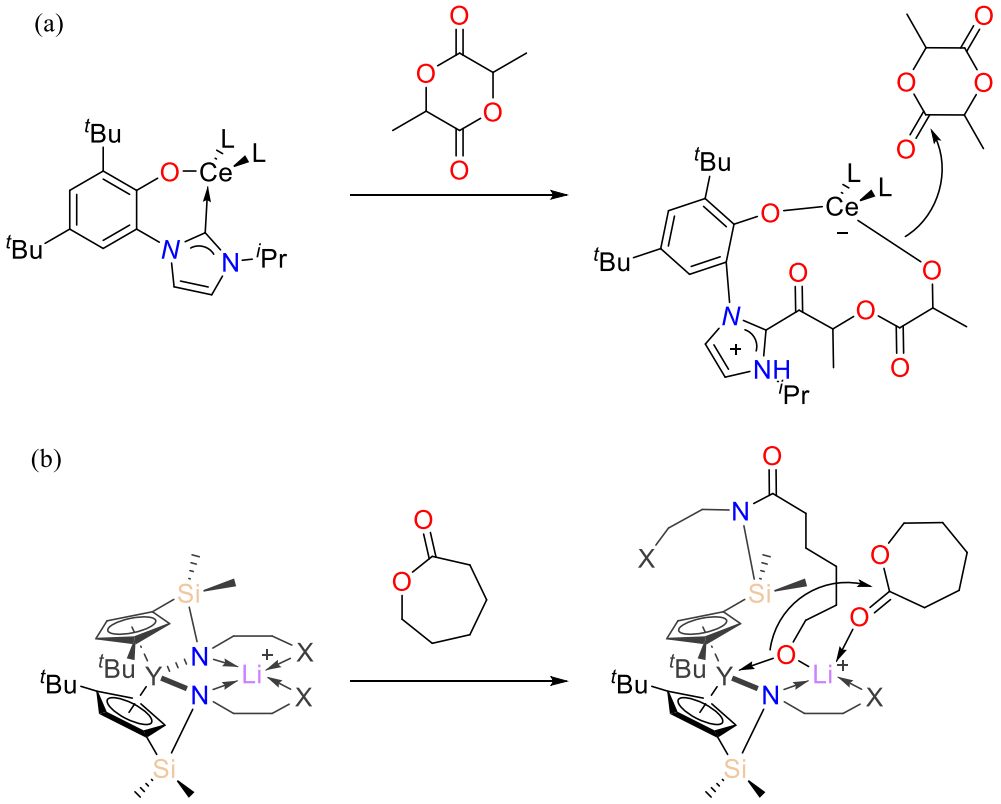


Figure 1.6 Ring expansion polymerisation of (a) lactide with NHC-Ce initiator by Williams and co-workers.[73](b) ϵ-CL with chiral lanthanocene by Okuda and co-workers.[74]

1.1.6. Role of the neutral donor in ROP

Introduction of neutral donors ligands have emerged as attractive opportunity to tune catalysts performance.[75] Use of neutral donor ligands during ROP of cyclic esters can lead to improved propagation and stereo control, regulation of catalyst aggregation,[76] promotion of Lewis pair polymerisation, and suppressing degradation pathways such as chain transfer or termination.[77, 78] The reader is directed towards a review on recent developments.[75] In most cases, the initiator contains a neutral donor in the form of a coordinating solvent, such as THF.[79] However, the use of large neutral donors such as $OPPh_3$, has been shown to increase axial steric pressure such that donor steric profile has been proposed to impart control over polymerisation. Further, strong neutral donors can

also outcompete the reversible coordination of ester linkages and suppress undesirable chain-terminating side-reactions (**Figure 1.7**).[80, 81]

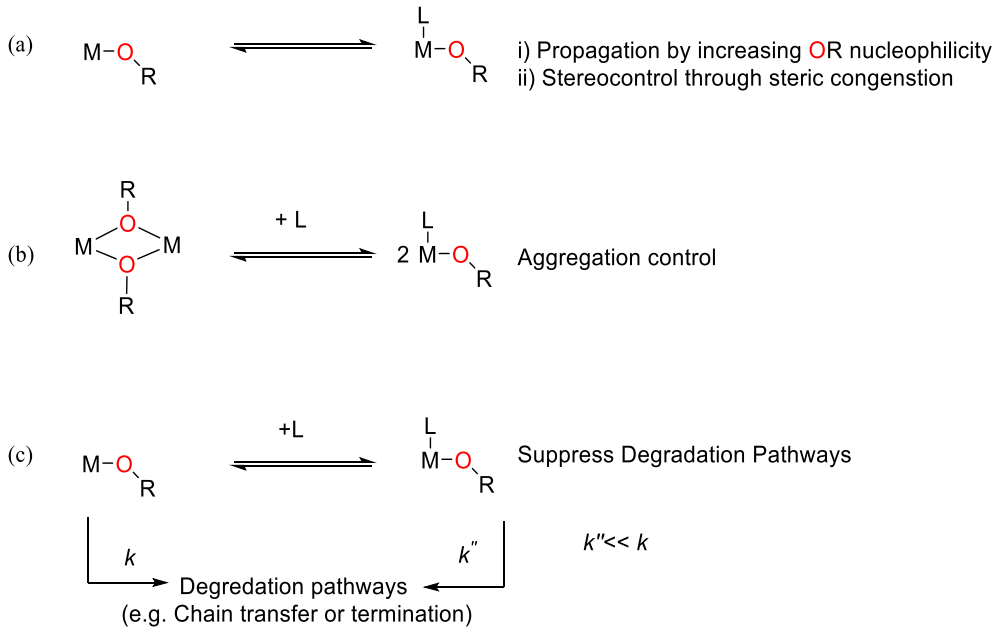


Figure 1.7 Ways in which a neutral donor ligand can influence catalyst performance in ROP of cyclic esters.

1.1.7. Metal radii and Lewis acidity effects on polymerisation activity

The effect of ionic size of activity has been studied, with smaller metal radii linked to controlled and slower ROP of cyclic esters, and larger ionic radii displaying higher reaction rate but poor iso-selectivity (for lactide polymerisation).[58, 69, 82, 83] Further, greater Lewis acidity on the active metal centre accelerates the reaction *via* stabilisation of the transition state and increases bonding between the ester carbonyl and the metal ion, activating the ester carbonyl carbon for facile nucleophilic attack.[84]

1.2. Polymerisation Characterisation

1.2.1. Molecular Weight

Molar mass distributions of polymers are reported as statistical averages as number average molecular weight (M_n) (**Equation 1.1**) , weight average molecular weight (M_w)

(**Equation 1.2**) and the molar mass dispersity ($Đ_m$), which measures the broadness of the distribution where $Đ_m = M_w/M_n$.

Equation 1.1 $M_n = \frac{\Sigma N_i M_i}{\Sigma N_i}$ **Equation 1.2** $M_W = \frac{\Sigma W_i M_i}{\Sigma W_i} = \frac{\Sigma N_i M_i^2}{\Sigma N_i M_i}$

N_i = number of molecules of weight 'i'; M_i = molecular weight of molecules 'i'; $W_i = N_i M_i$ total weight of molecules of weight 'i'.

In general, having a narrow molecular weight distribution will give a $Đ_m$ of close to 1 (< 1.2) and is preferable and is indicative of good reaction control. For those in the region of 1.2–2.0, slow initiation and side reactions maybe be the cause for deviation from ideal; in cases where $Đ_m > 2$, polymerisation is considered uncontrolled, likely with significant proportion of side reactions or poor initiation.[47]

1.2.2. Size Exclusion Chromatography (SEC)

Gel Permeation Chromatography (GPC), or Size Exclusion Chromatography (SEC) is a well-known size-based separation technique that makes use of a solid and mobile phase. Based on known or estimated interaction between the sample and the phases, information about the molecular weight can be collected. The mobile phase, containing the sample dissolved in a chosen solvent (often chloroform or THF) is pumped at elevated pressures through a column packed with beads of polystyrene containing different pore sizes. Large molecules cannot enter the pores, hence have smaller retention times and are eluted first.[85] However, interactions between the sample and the stationary phase of the column occurs, and calibration is used to offset this. These interactions lead to distortions in the molecular weight distribution, especially if the sample interacts differently with the column compared to the calibration standards. In most cases, polymers do not behave ideally in GPC. Additional factors, such as coil conformation, branching, and abnormal interactions

with the column phases can impact the elution behaviour, leading to alteration in M_w recorded.[86]

The intrinsic viscosity of a polymer in a certain solvent can correlated with molar mass *via* the Mark-Houwink equation (**Equation 1.3**).

Equation 1.3 $[\eta] = KM^{\alpha}$ **Equation 1.4** $g' = \frac{[\eta]_c}{[\eta]_l}$

[η] = intrinsic viscosity; K and a = Mark-Houwink constants; M = molar mass. $[\eta]_c$ intrinsic viscosity of cyclic counterpart. $[\eta]_l$ cyclic viscosity of linear counterpart.

Intrinsic viscosity is dependent on temperature, solvent, type of polymer, concentration of polymer, and molar mass. When a polymer is dissolved in a solvent, the flow of the mixture is highly depended on the molecular structure of the polymer as well as the interactions between the molecules.

The ratio of intrinsic viscosity of cyclic and linear polymers of identical molecular weights (g′) can be used to compare the hydrodynamic properties of linear and cyclic polymers (**Equation 1.4**). Consistent comparisons are difficult due to the obtaining high purity samples of cyclic polymer. Typically, the g′ for PS, PLA and PCL has been reported in the range of g′ = 0.4 – 0.8, dependent on temperature, solvent and molecular weight. Cyclic polymers will in general have a lower hydrodynamic ratio than their linear counterparts.[87, 88]

1.2.3. Matrix Assisted Laser Desorption/Ionisation Time-of-Flight mass spectrometry (MALDI-TOF MS)

MALDI-ToF mass spectrometry can be used to provide structural characterisation on a polymer sample. The sample is mixed with a matrix and cationising agent. The matrix acts as an absorbent for the ionising lasers pulses which convert large molecules into ion fragments in the form $[M+ion]^+$. The fragments desorb and are accelerated through a fixed voltage flight chamber towards a detector. As the field is known in the flight chamber, the 'time-of-flight' can be used with the mass to charge ratio (m\z) to produce a spectrum of the mass sequences recorded. Issues arise from this technique when assessing mixtures of polymers and high molecular weights (>3000 M_n) due to poor mass discrimination against high-mass oligomers and calibration issues.[89] In addition, structural differences, such as end groups, can affect the ionisation efficiency; hence, MALDI TOF MS cannot be used to quantify distinct species in a sample.[90-92] As side products are present in ROP, improved techniques such as MALDI spiral-TOF MS can be used to discriminate between species of known mixed materials.[93] Use of a longer flight path (17m up for 2m) allows for a greater mass-resolution across the spectrum.

1.3. Initiators for the ROP of ϵ-CL and LA

1.3.1. Common catalysts

Commercial catalysts such as tin(II) octanoate ($Sn(Oct)_2$, aluminium(III) isopropoxide, and zinc(II) lactate now compete with organocatalysts such as NHCs and thiourea-amine catalysts for polymerisation of cyclic esters such as LA (**Figure 1.8**).[94, 95]

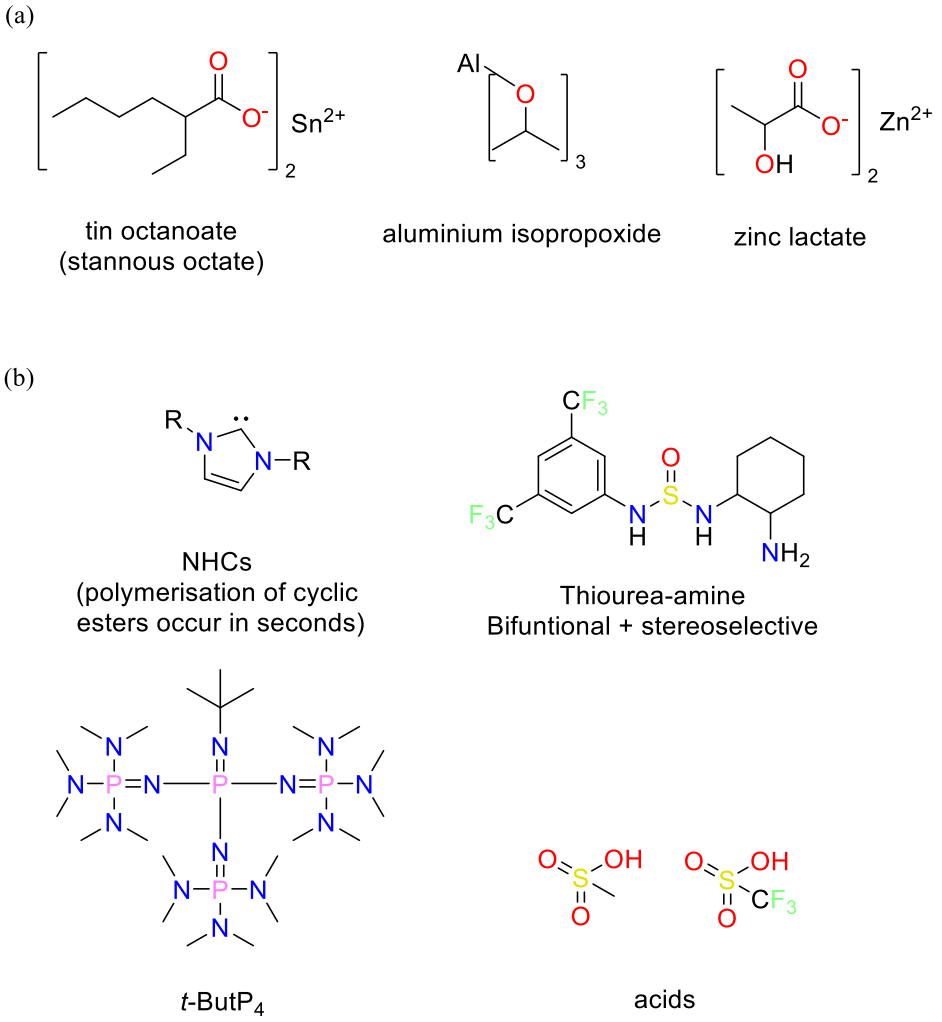


Figure 1.8 (a) Tin(II) octanoate ($Sn(Oct)_2$), aluminium(III) isopropoxide, and zinc(II) lactate. (b) organocatalysts basic NHCs and phosphazene,[72] thiourea-amine, capable of stereocontrol and methanesulfonic and triflic acid. Exhibit high activities for ROP of cyclic esters.[96, 97]

$Sc(Oct)_2$ is currently used as the catalyst of choice for the bulk production of PLA. At temperatures of >140 °C and in the presence of a co-initiator, high molecular weights (100–1000 kg mol^{-1}) are produced. The potential toxicity of tin and other metals has not prevented polymers produced through this method from use as biomedical applications.[98] Finding effective catalysts that can produce polyesters with required properties such as hydrophobicity or hydrophilicity, improved cell binding and overall mechanical strength expands the use of these catalysts.[99] Organocatalysts (**Figure 1.8 (b)**) such as thiourea-

amine complexes, NHCs, phosphazenes and various acids have gained popularity as catalysts for polymerisation of cyclic esters. The have shown to provide good control and high activities showing polymerisation of lactide with some reported reactions occurring in a matter of seconds at high loadings (200 equiv. in < 2 s).[100]

1.3.2. Rare earth initiators

The need for well controlled initiators that have low toxicity provides avenues for new catalyst design. The rare earth metals have been shown to be highly active and exhibit relatively low toxicity in animals, although have been shown to interreact negatively with proteins by competing with calcium in protein binding pockets.[101 102] Radii of the +3 ions of Sc, Y, La plays an important part in their reactivity with yttrium and lanthanum showing vastly superior activities to scandium in general.[58] This is due to the increase if ionic radius of lanthanum (1.032 Å) and yttrium over scandium (0.745 Å).[151, 154]

Studies reported in late 90s and early 00s used simple metal alkoxides and aryloxides.[103] A number of reviews exist that cover the recent developments of using rare earth metals for ROP and the reader is directed to them here.[24, 58] A number of multidentate ligand structures have also been implemented, to control the coordination to the active metal centre. These include phenoxy-imine, metallocene and other derivatives to explore the possible activity and stereo control possible with these metals (**Figure 1.9**).

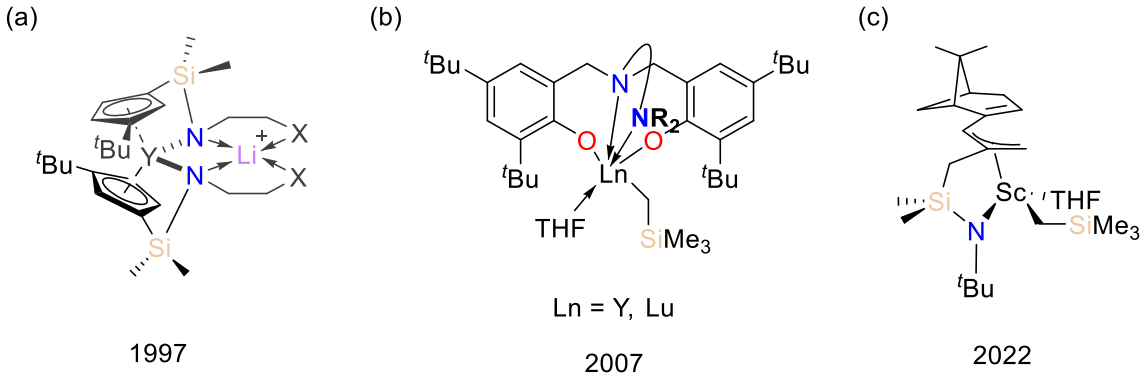


Figure 1.9 (a) Yttrium complexes that produces cyclic esters.[74] (a) Lanthanide alkyl complex that produces heterotactic PLA[79] (c) Enantiomeric scandium[104]

In general, post metallocene catalysts for ROP include both half-sandwich and other coordination complexes. These include catalysts with Cp-amido (CGC), phosphine-imide, imino-amino and phenoxy-imine architectures.[105-107]

Okuda and co-workers explore the ROP of ϵ-CL using titanium-alkoxy piano-stool complexes as initiators.[108, 109] By altering the η^5- moiety, it the polymerisation activity followed the order of Cp < ^{SiMe_3}Cp < $^{(SiMe_3)_2}$Cp< Indenyl.

Similarly, cationic scandium imitators have found use polymerisation systems are used for the (co)polymerisation of ϵ-caprolactone and vinyl containing olefins such as ethylene and styrene.[110] Materials with superior properties can be synthesised through this such as poly(styrene)-block-poly(caprolactone) (sPS-b-PCL) copolymers that show greater material properties, such as increased flexibility, tensile strength and stiffness over the homo or polymer blends.[111]

In 1879, scandium was discovered from the minerals euxenite and gadolinite in Scandinavia, produced in the form of scandium oxide (Sc_2O_3). It was not until 1937 that it was isolated in the form of $ScCl_3$, through electrolysis at 700 °C.[112] Even though it is

fairly abundant, scandium is costly. It is well distributed in the earth's crust in the form of thortveitite ($Sc_2Si_2O_7$) but mainly produced as a by-product of uranium extraction.[113] The interest in scandium, the smallest transition metal, arises due to its chemistry resembling both group three and lanthanide elements. Scandium has an electronic configuration of [Ar] $4s^2$ $3d^1$ occurring in the trivalent state in nature (example of +1[114] and +2[115] have also been reported in the literature).[116, 117]

Although generally unused commercially, organo-scandium complexes have been employed for a range of uses including enantio- and regio- selective catalytic synthesis including hydrosilation of alkenes,[118] C-H alkylation[119] and for carbon dioxide[120-122] and other small molecule activation.[123-126] Scandium organometallic complexes, of the form **Figure 1.10** (b), are used for the polymerisation of styrene,[111, 127] ethylene,[128] isoprene,[129, 130] and ROP of cyclic esters.[131-135]

The extreme Lewis acidity of scandium provides a very high reactivity towards Lewis bases.[136] Scandium triflates ($Sc(OTf)_3$) were shown to polymerise ϵ-CL through cationic living polymerisation involving a activated monomer mechanism (**Figure 1.10** (a)).[137] In addition $Sc(OTf)_3$ has also been highly effective where strong Lewis acids are needed for catalysis, showing good water resistance unlike ACl_3, BF_3 and $SnCl_4$.[138]

Cationic scandium half metallocenes, have also been incredible effective for the copolymerisation of polar and non-polar polymerisation which has been the main focus for scandium metallocene chemistry since 2010.[111, 139, 140]

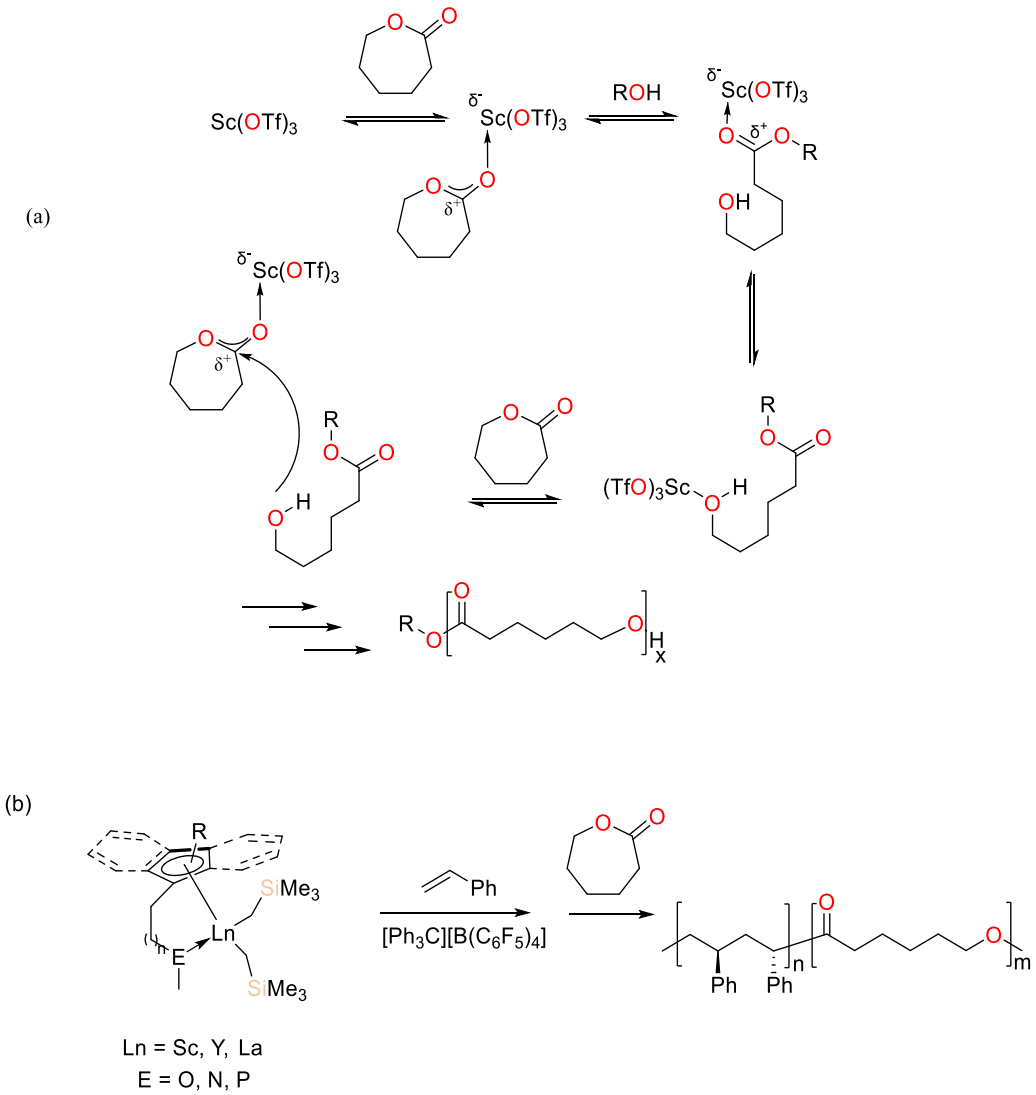


Figure 1.10 (a) activated monomer mechanism with $Sc(OTf)_3$.[137] (b) Ln post metallocene complexes can be used for α-olefin (such as styrene), ϵ-calprolactone copolymerisation.[111] δ

Metallocene catalysts for ring opening polymerisation asymmetric half metallocene scandium complexes for polymerisation of olefins and cyclic esters have developed over the past 20 years. This includes use of indenyl and Cp ligands with scandium in the cationic state when activated for polymerisation (**Figure 1.11**).

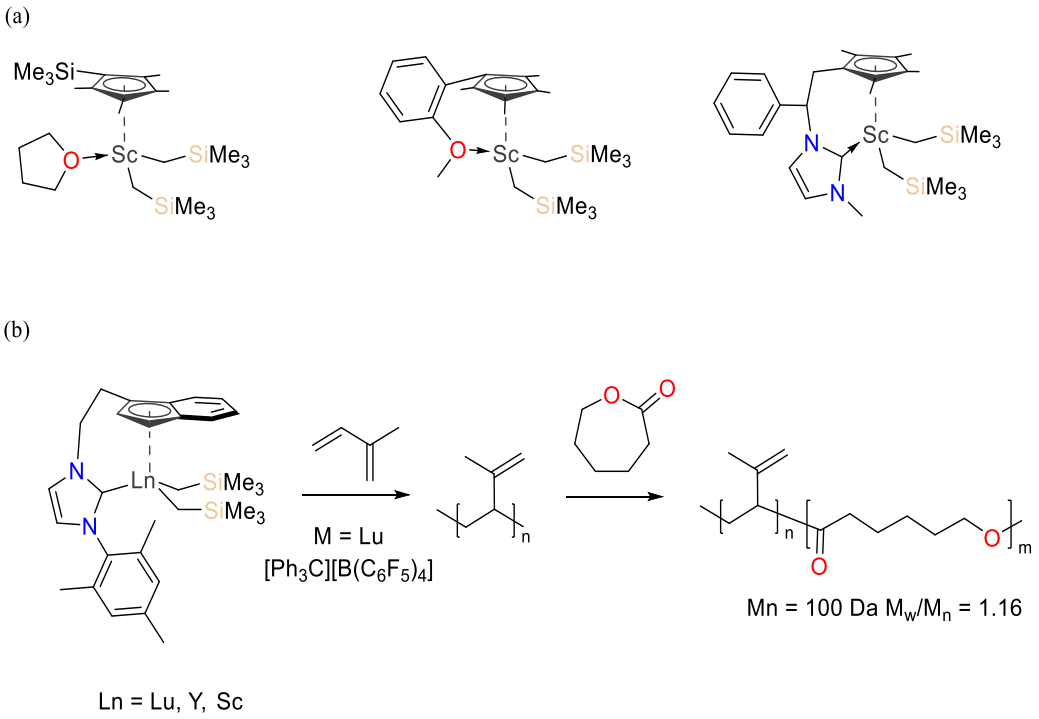


Figure 1.11 (a) Selection of bis(alkyl) rare earth (III) complexes[141, 142] THF free scandium complexes, which (b) when activated with $[Ph_3C][B(C_6F_5)_4]$ and show highly active polymerisation of esters and olefins.

The highly 3,4-selective living polymerization of isoprene, followed by copolymerisation with ε-Cl by an amidino N-heterocyclic carbene ligated lutecium bis(alkyl) is an example of the stepwise copolymerisation using post-metallocene scandium complexes.

Homo-polymerisation of cyclic esters using metallocene complexes has also been reported. The M(III) rare earth metallocene, the samarium Cp aryloxide complex (**Figure 1.12** (**a**)) showed rapid polymerisation (>99%) of 500 eq. of ϵ-CL in 2 minutes (M_n = 120 kDa, $Đ_m$ = 1.40).[143] Further, bis-indenyl Yb and Eu complexes displayed polymerisation of ϵ-CL, only when $SiMe_3$ functionality was present on the ligands (**Figure 1.12** (b)).[143, 144]

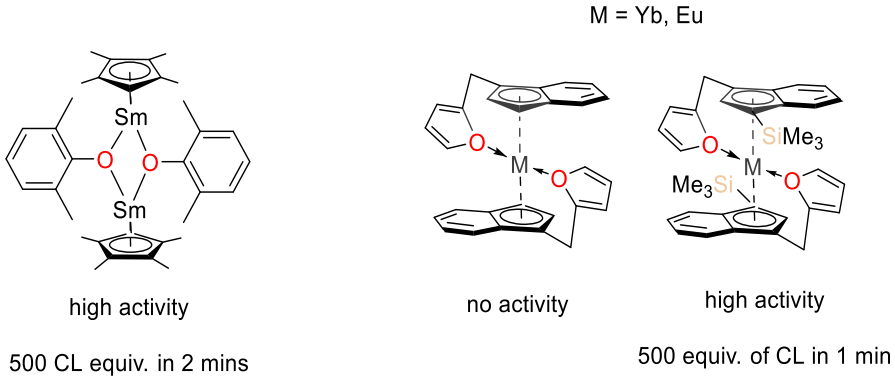


Figure 1.12 (a) samarium aryloxide[144], (b) Bis-tetrahydrofurfuryl-indenyl complexes of Yb and Eu.[145]

1.4. Metal-complexes with cyclopentadienyl-derived ligands

1.4.1. Cyclopentadienyl ligands

'The use of η^5-cyclopentadienyl ($C_5H_5^-$, Cp) ligands, originally in 1951 for the synthesis of ferrocene, started the rich field of sandwich and half-sandwich compounds.[146] The extensive coordination chemistry of Cp is found for a large range of elements. This is linked to the good σ- and π- donor ability of Cp, which in part is due to η^5 coordination and the thermodynamic stability gained in achieving aromaticity.[144, 147-153] Tuning is also possible, substitution of the hydrogens for methyl groups results in the permethylcyclopentadienyl ($C_5Me_5^-$, Cp*) ligand, that shows variable steric and electronic properties that effect the selectivity and stability of the complexes.

In the D_{5h} point group, Cp has an electronic configuration of $\sigma^2\pi^4\delta^0$, able to act as a σ donor through the filled a_2'' orbital, a π donor through the filled doubly degenerate e_1'' pair of orbitals and as a δ acceptor through the vacant e_2'' pair.[154] As well as good orbital overlap between the molecular orbitals of Cp and those of the metal, the Coulombic attraction between the formally anionic ligand and a formally positive metal centre leads to strong bonding interactions and stable complexes. Bonding in sandwich compounds, like ferrocene, occurs principally through π- and δ-type interactions. The metal d_{z^2} has a

nodal cone in its spatial distribution function hence σ bonding is weak due to the poor orbital overlap.[155]

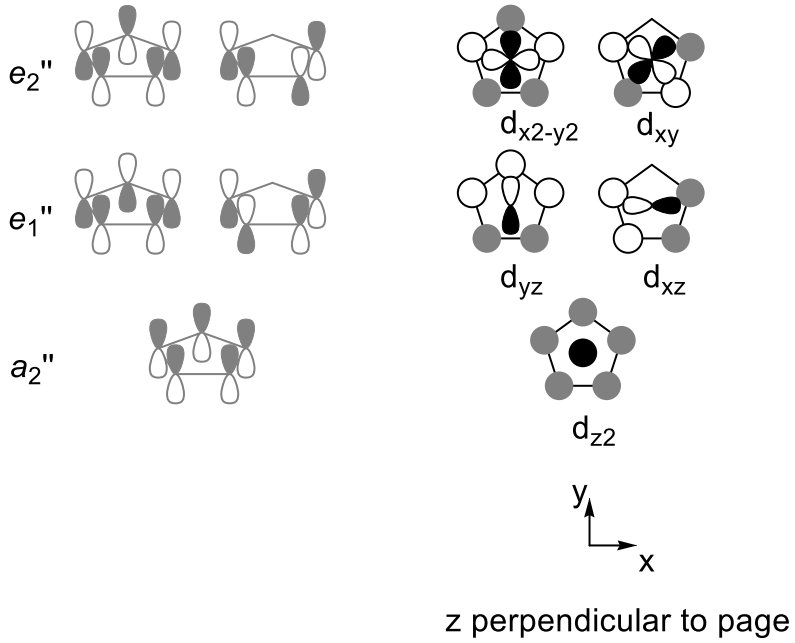


Figure 1.13 Molecular orbital diagram of the cyclopentadienyl ligand, showing interactions with transition metallic d orbitals. Figure adapted from *Inorganic Chemistry*, 7th ed. (OUP).[154]

As a ligand, the properties of Cp can be tuned both sterically and electronically through substitution with electron donating or withdrawing groups, or bulky substituents.[156, 157] In particular, the increased steric bulk caused by per-methylation increases the kinetic stability of these complexes.[158]

1.4.2. The indenyl effect

Indenyl ligands ($C_9H_7^-$, Ind, I) are also common η^5 cyclic polyenes. Bonding through the C_5 ring as η^5- ligand is the most common, although η^6-, η^3-, η^2- and η^1-indenyl complexes have also been reported. such as the η^3- and a η^5- bis indenyl tungsten complex reported by Nesmeyanov *et al.* (**Figure 1.14 (a)**).[159-161] Kullnig *et al.* reported an iron indenyl complex capable of alkyl-CO migration insertion. Tautomerisation of the indenyl through

η^5-η^3-η^5 ring slip of the indenyl was key to understanding the mechanism (**Figure 1.14 (b)**).[162] This η^5-η^3 ring slip is formally a two-electron oxidation of the metal which becomes electrophilic and coordinatively unsaturated, hence allowing associative substitution processes not common for 18 electron complexes.[163] This has been shown to lead to an increase in the rate of ligand substitution on the order of ~10^3.[164, 165] In general η^5- bonding is better described as 3 + 2 coordination and compared to η^5- Cp, there is a decreased kinetic barrier and increased thermodynamic driving force for η^5-Ind to undergo a η^3,η^5-haptotropic ring slip. Under the right stimuli, re-aromatisation of the aryl group combined with low folding energy, favour bonding through η^3- allyl mode (**Figure 1.14 (c)**). [166-168]

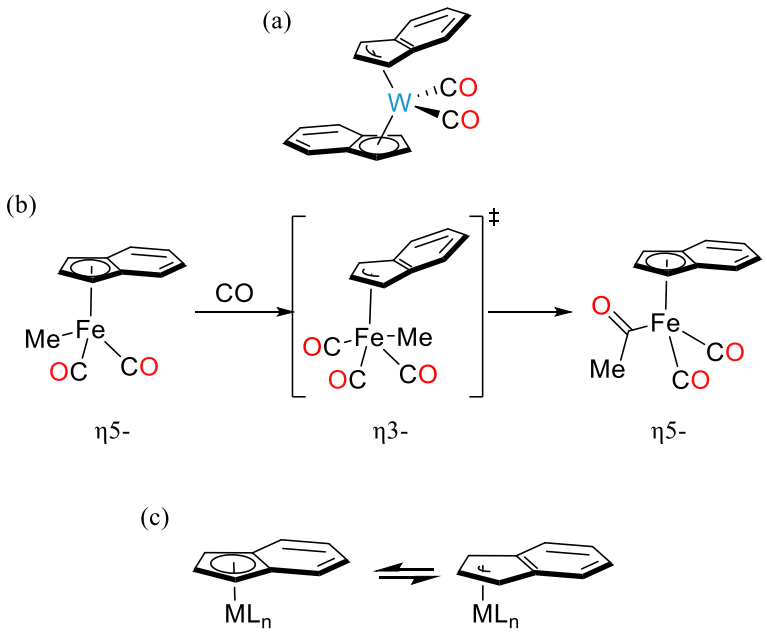


Figure 1.14 (a) Structure of (η^5-C_9H_7)(η^3-C_9H_7)$W(CO)_2$ reported by Nesmeyanov *et al.*.[161] (b) Structure of (η^5-C_9H_7)$Fe(CO)_3$ reported by Kullnig *et al.*.[162] (c) η^5-η^3 ring slip in metallo-indenyl complexes, driven by re-aromatisation of the C_6 ring

Similarly, permethylation confers kinetic stability to permethylindenyl ($C_9Me_7^-$, Ind*, I*) complexes as the increased steric bulk reduced the probability of reactive collision. In addition, the methyl groups induce a positive inductive effect through $\sigma_{CH} \rightarrow \pi^*_{CC}$

hyperconjugation which increases the thermodynamic stability.[169] I* metallocenes have been reported for a wide range of f- and d- block elements (Figure 1.11).[170-176] The electronic properties of the I* ligand in FeI^*_2 were studied by O'Hare *et al.* and showed quantitatively the electron donating nature of the I* ligand by a reduction in the first ionisation energies and redox potentials compared to $FeCp^*_2$.[170]

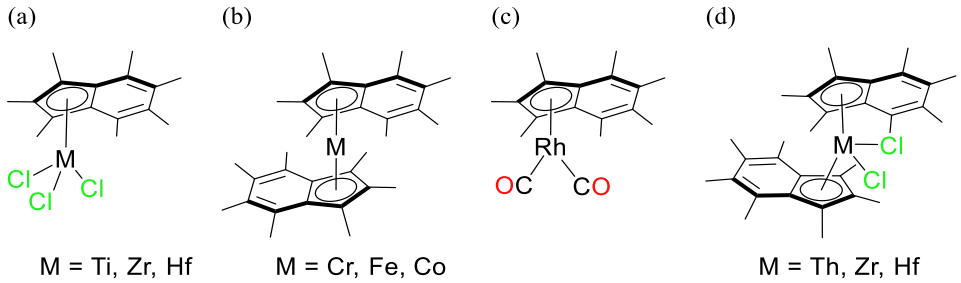


Figure 1.15 Permethylindenyl complexes of d- and f-block elements. (a) I^*MCl_3 (M = Ti, Zr, Hf),[173] (b) I^*_2M (M = Cr, Fe, Co),[170, 171] (c) $I^*Rh(CO)_2$,[172] (d) $I^*_2MCl_2$ (M = Th, Zr, Hf).[174, 176]

1.4.3. Constrained Geometry Catalysts

The term "Constrained Geometry Catalyst" was coined to describe a specific ligand architecture that constrains the coordination geometry around the metal centre. The original design focused on a ligand that involved both η^5- pi moiety η^1- heteroatom bonded to the same metal centre. Through a short *ansa*- bridge, the more open coordination sphere and small η^5-(π bonded) -M-η^1(σ bonded) angle reduce the readiness of chain-transfer.[177, 178]

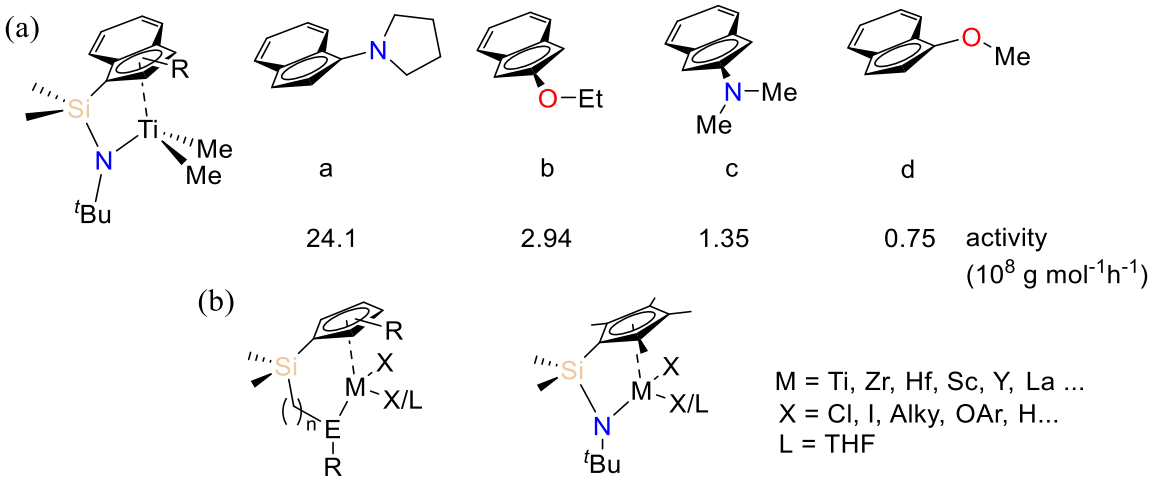


Figure 1.16 (a) Changes in activity for ethylene polymerisation through altering the R group on indenyl. (b) General structure for constrained geometry complexes that have been reported. Ti[179] Sc Yb and Sm[180]

For olefin polymerisation, the structure-activity relationship is put down to a correlation between increasing electron density at the metal centre with increasing ethylene polymerisation activity. Substitution of both the cyclopentadienyl moiety and the η^1 chelating ligand with more donating groups have been used to test this across the literature.[178]

1.4.4. Stereochemistry in metallocene complexes

As ligand scaffolds grew more intricate, the stereochemistry of metallocene, [181] half-metallocene, and *ansa*- bridged[74, 182] species became a significant topic of discussion in the late 1980s and early 2000s. [162, 163] The presence of the bridge can enhance the activity and stereoselectivity of olefin polymerisation by expanding the reaction space at the metal centre. This more defined structure imposes steric effects, resulting in improved stereo control.[107, 133, 183-185] The stereo configuration control of polyolefins has been shown to be essential for the material properties of the produced polymers. This created an explosion of research in the field and development of many enantiomeric complexes,

such as ethylenebis(indenyl) (EBI) and oscillating zirconocene metallocene catalysts developed by Kaminsky and Waymouth (**Figure 1.17**).[186, 187-190]

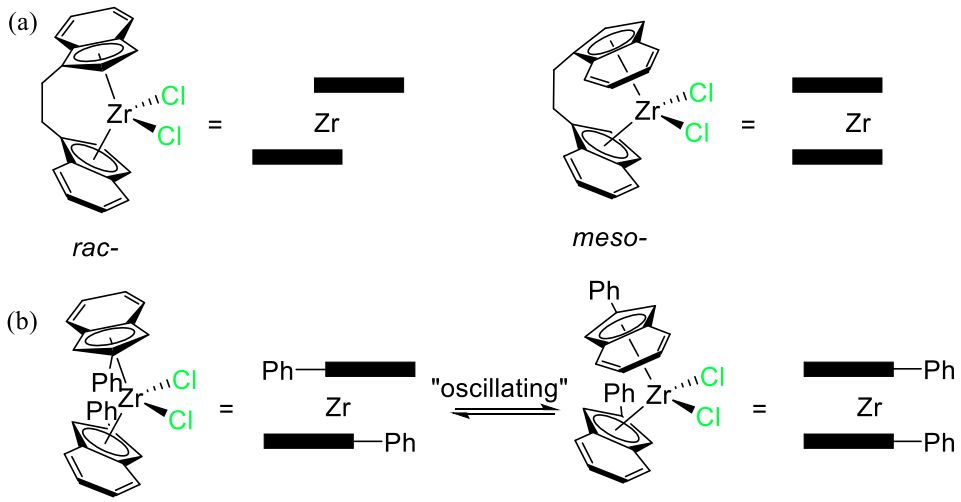
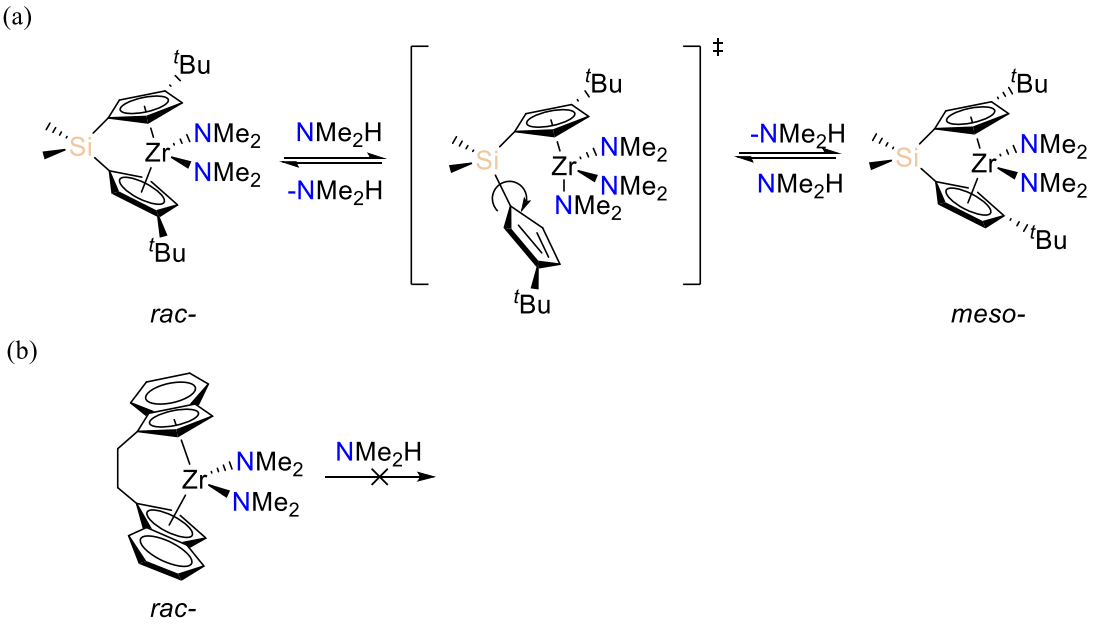


Figure 1.17 (a) *rac*- and *meso* $(EBI)ZrCl_2$.[186](b) "oscillating" $(2\text{-}PhInd)_2ZrCl_2$ produces elastomeric stereo block polypropylene[189]

However, in the synthesis of enantiomeric compounds, thermodynamics dictate that an equilibrium mixture will always include both enantiomers in a 1:1 ratio. Nonetheless, the thermodynamic stability of diastereomers can vary, causing deviations from this 1:1 ratio. Achiral ligands, such as half-metallocene complexes, can influence the equilibrium and shift the ratio to favour one diastereomer.[191] It is crucial, however, to determine whether the formation of these diastereomers is irreversible (under kinetic control) or if the products are in equilibrium (under thermodynamic control). For complexes that are chiral at the metal centre, this distinction is vital for understanding the species present, particularly regarding the possible stereo control during catalysis.[192, 193] Considerations must also be made if the addition of other reactants can catalyse the interconversion of isomers. For example, the addition of dimethylamine catalyses the interconversion of

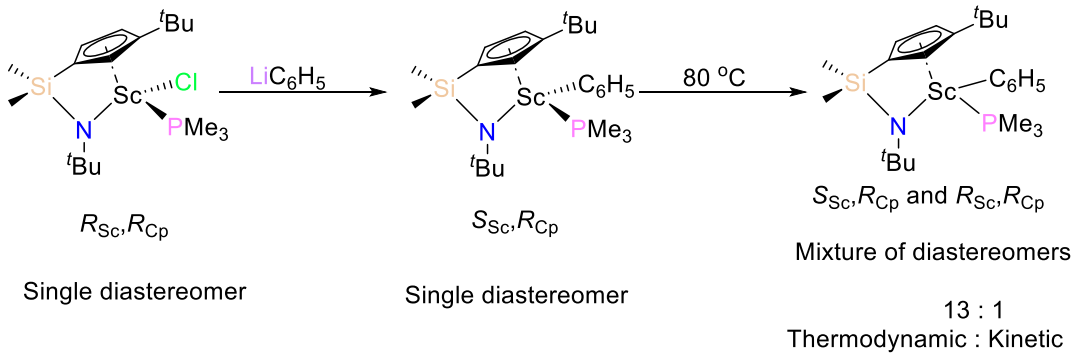
rac- and *meso*-^{Me_2}SB((Cp-3-^{t}Bu)$_2$)Zr(NMe$_2$)$_2$ but not for *rac*-(EBI)Zr(NMe$_2$)$_2$ (**Scheme 1.2**).[186, 194]



Scheme 1.2 (a) NMe$_2$H catalysed epimerisation process through dissociation, rotation, and re-coordination with the opposite face of the cyclopentadienyl ring of ^{Me_2}SB((Cp-3-^{t}Bu)$_2$)Zr(NMe$_2$)$_2$.[186, 194] (b) no reaction with thermodynamically stable *rac-*(EBI)Zr(NMe$_2$)$_2$ and NMe$_2$H

Known isomerisation routes including hetero-atom assisted enantioface exchange,[195] photochemical[196] or thermal homolysis,[197] and silatropic rearrangement for Cp and Indenyl sandwich complexes.[198] For half metallocene complexes, various mechanisms have been proposed where isomerisation has been observed. Once such mechanism involves a zwitterionic ring-slipped intermediate with a cationic metal centre and anionic Cp/I$^-$, stabilised by a polar Lewis-basic species such as THF and free Li$^+$. The Li$^+$ originates from a salt metathesis synthetic route that forms LiCl salt.[182, 195, 199, 200] Donors, anions and cations in solution act to stabilise the racemisation transition state as the η_x (x = 3, 5) "Cp" bond dissociates and reforms, with addition of salt accelerating isomerisation.[198, 201]

In 1990, Bercaw and co-workers synthesised scandium CGC complexes of the formula ^{Me_2}SB($^{t Bu}$N,Cp-3-^{t}Bu)Sc(X)L *via* salt metathesis. Initially, these complexes served as single-component catalysts for α-olefin polymerisation, valued for their well-defined structure and ease of ligand modification.[202, 203] However, it was observed that the chiral scandium centre undergoes isomerisation at elevated temperatures. (**Scheme 1.3**)



Scheme 1.3 Isomerisation of ^{Me_2}SB($^{t Bu}$N,Cp-3-^{t}Bu)Sc(C_6H_5)PMe_3 at 80 °C produces an equilibrium of a thermodynamic and kinetic product. Stereo labels presented for enantiomer(s) shown.[202]

In addition, the ligands -C_6H_5 and -PMe_3 are described as non-labile and no mechanism for isomerisation was proposed, though the species are in equilibrium.

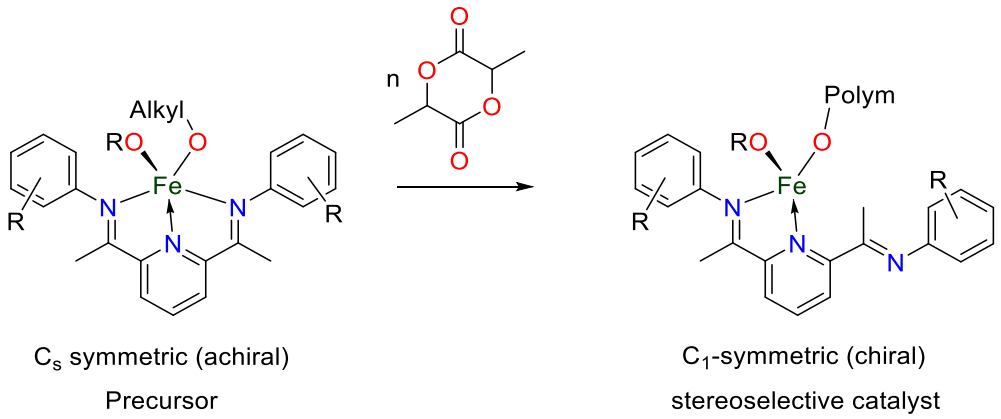
1.4.5. Asymmetric initiators for ROP of cyclic esters

Synthesis of stereoregular polymers from racemic monomers is of great importance in ROP. When using lactide, which contains two stereogenic centres, the opportunity for a diverse range of PLA microstructures is possible which will result in different material characteristics.[204] Stereo control can occur through chain end control or enantiomorphic site control. Chain end control is dependent on a chiral propagating chain end bound to a hindered achiral catalyst.

Enantiomorphic site control occurs when a chiral catalysts is used; stereo control in this case is not dependent on chiral chain end or monomer used.[205] The parameters P_r and P_m

are used which refer to the probability of forming racemic (syndiotactic) or meso (isotactic) chain links respectively.[205] Values of P_r or $P_m \geq 0.7$ are considered noteworthy of consideration rather than a simple control bias. For coordination insertion mechanisms, the coordination of the lactide monomer to the metal centre, through a carbonyl oxygen, is significant for the stereo control of the system. Attack from the alkoxide chain end to the activated carbonyl carbon and further ring-opening leads to the formation of the new chain-extended metal alkoxide species, where the close proximity of the carbonyl group is proposed to stabilise the propagating species.

A wide range of studies have employed asymmetric catalysts with sterically demanding ligands to explore the kinetics, mechanisms, and methods to control the structure of polymer produced.[79, 205-207] The structure of active species is often overlooked, however is of extreme important to understand reaction mechanisms. For example, Byers and co-workers reported the enantiomorphic site controlled stereoselective polymerisation of lactides using an achiral iron catalysts (**Equation 1.5**).[208]



Equation 1.5 Stereogenic iron centres in equilibrium.[208]

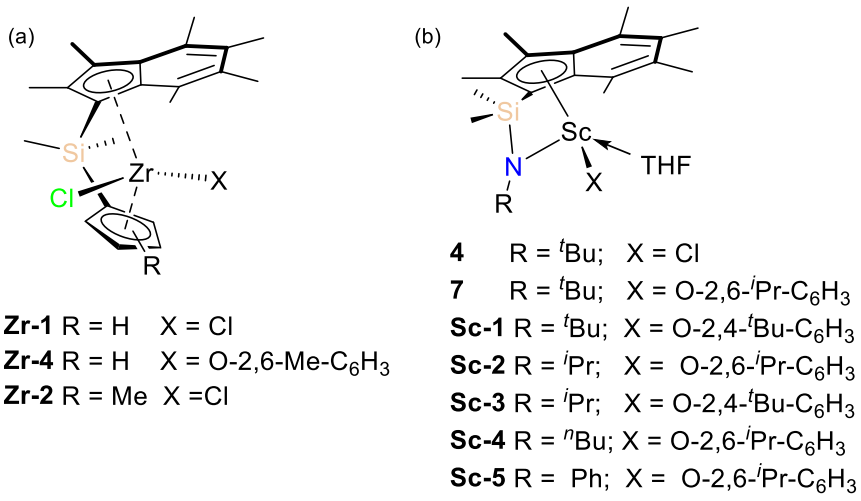
As reported, the initiator is achiral and contains Cs symmetry. However, it was shown, during polymerisation, the achiral precursor forms a chiral stereoselective catalyst, which produced heterotactic enriched PLA.

1.4.1. Permethylindenyl catalysts for ROP of cyclic esters

Work done by O'Hare *et al*, has previously been focused around ROP of *L*- and *rac*-lactide to study the activity and stereo control of a number of metallocene and half metallocene Group III and IV systems.

Variation of the R, R' groups on the on the PHENI* scaffold was used to scope the effect of steric and electronic effects of the phenoxy- substituent with respect to accessibility and Lewis acidity of the metal centre. Similar scoping was done in the O'Hare group by Collins-Rice for titanium and group IV using the same ligand system for slurry phase olefin polymerisation

Two systems of note are the constrained geometry permethylindenyl complexes (CGC-I*) of scandium and Zirconium *ansa*-bridged I*-Cp (**Figure 1.18**).[133, 134, 209, 210] CGC-I* scandium of the formula ^{Me_2}SB(^{R}N,I*)Sc(X)THF polymerised *L*- and *rac*- LA to form poly(*L*-lactide) (PLLA) both in and without the presence of BnOH. The activity with BnOH was greater for all complexes tested. For example, with **4** the activity at 70 °C in benzene was k_{obs} = 3.85 (BnOH) and 0.40 h^{-1}.



Zr-1 R = H X = Cl
Zr-4 R = H X = O-2,6-Me-C_6H_3
Zr-2 R = Me X =Cl

4 R = ^{t}Bu; X = Cl
7 R = ^{t}Bu; X = O-2,6-^{i}Pr-C_6H_3
Sc-1 R = ^{t}Bu; X = O-2,4-^{t}Bu-C_6H_3
Sc-2 R = ^{i}Pr; X = O-2,6-^{i}Pr-C_6H_3
Sc-3 R = ^{i}Pr; X = O-2,4-^{t}Bu-C_6H_3
Sc-4 R = ^{n}Bu; X = O-2,6-^{i}Pr-C_6H_3
Sc-5 R = Ph; X = O-2,6-^{i}Pr-C_6H_3

Figure 1.18 Summary of I* complexes for ROP of lactide.(a) ansa-bridged I*-CP zirconium complexes (b) CGC-I* ^{Me_2}SB(^{R}N,I*)Sc(Cl)THF

1.5. Scope of thesis

The scope of this thesis is two parts: (a) the synthesis and characterisation of group three permethylindenyl phenoxy compounds, (b) the testing of these as initiators for the ring opening polymerisation of select cyclic esters.

Through exploration of synthesis, characterisation and reactivity of these complexes, understanding regarding the mechanism of polymerisation, solution dynamics, and feasibility as these catalysts for the polymerisation and copolymerisation of cyclic esters. This work builds on half-metallocene complexes, and permethylindenyl complexes developed by O'Hare and co-workers.

Chapter 2 discusses the synthesis and characterisation of new PHENI* Sc complexes with a range of substituents. **Chapter 3** forms a dialogue on the isomerisation and fluxionality exhibited in these complexes. **Chapter 4** shows the capability of the scandium systems for the ROP of ϵ-CL and comparisons to LA, then details the material polymer produced from the ROP and conclude with mechanistic explanation. **Chapter 5**

contains experimental information and characterising data. **Chapter 6** discusses conclusions and outlook.

1.6. References

1. L. Lebreton and A. Andrady, *Palgr Commun*, 2019, **5**, 6.
2. R. Wei, T. Tiso, J. Bertling, K. O'Connor, L. M. Blank and U. T. Bornscheuer, *Nat Catal*, 2020, **3**, 867-871.
3. M. Linder, *Green Chem Lett Rev*, 2017, **10**, 428-435.
4. F. Vidal, E. R. van der Marel, R. W. F. Kerr, C. McElroy, N. Schroeder, C. Mitchell, . . . C. K. Williams, *Nature*, 2024, **626**, 45-57.
5. Y. Zhu, C. Romain and C. K. Williams, *Nature*, 2016, **540**, 354-362.
6. G. W. Coates and Y. D. Y. L. Getzler, *Nat Rev Mater*, 2020, **5**, 501-516.
7. M. Hong and E. Y. X. Chen, *Green Chem*, 2017, **19**, 3692-3706.
8. T. Keijer, V. Bakker and J. C. Slootweg, *Nat Chem*, 2019, **11**, 190-195.
9. S. Tian, Q. Yue, C. Liu, M. Li, M. Yin, Y. Gao, . . . L. Luo, *J Am Chem Soc*, 2021, **143**, 10054-10058.
10. X. Y. Tang and E. Y. X. Chen, *Chem-Us*, 2019, **5**, 284-312.
11. G. Q. Xu and Q. G. Wang, *Green Chem*, 2022, **24**, 2321-2346.
12. K. Tomishige, M. Tamura and Y. Nakagawa, *Chem Rec*, 2019, **19**, 1354-1379.
13. W. Li, H. Wang, X. Jiang, J. Zhu, Z. Liu, X. Guo and C. Song, *RSC Adv*, 2018, **8**, 7651-7669.
14. B. Grignard, S. Gennen, C. Jerome, A. W. Kleij and C. Detrembleur, *Chem Soc Rev*, 2019, **48**, 4466-4514.
15. C. Hepburn, E. Adlen, J. Beddington, E. A. Carter, S. Fuss, N. Mac Dowell, . . . C. K. Williams, *Nature*, 2019, **575**, 87-97.
16. J. C. Middleton and A. J. Tipton, *Biomaterials*, 2000, **21**, 2335-2346.
17. P. Chandika, S. Y. Heo, T. H. Kim, G. W. Oh, G. H. Kim, M. S. Kim and W. K. Jung, *Int J Biol Macromol*, 2020, **164**, 2329-2357.
18. A. C. Albertsson and I. K. Varma, *Biomacromolecules*, 2003, **4**, 1466-1486.
19. R. E. Drumright, P. R. Gruber and D. E. Henton, *Adv Mater*, 2000, **12**, 1841-1846.
20. M. Kumar, S. Bolan, L. P. Padhye, M. Konarova, S. Y. Foong, S. S. Lam, . . . N. Bolan, *Appl Energy*, 2023, **345**, 121307.
21. J.-G. Rosenboom, R. Langer and G. Traverso, *Nat Rev Mater*, 2022, **7**, 117-137.
22. T. M. McGuire, A. Buchard and C. Williams, *J Am Chem Soc*, 2023, **145**, 19840-19848.
23. Statista, chemicals & Resources, https://www.statista.com/markets/410/chemicals-resources/).
24. A. Arbaoui and C. Redshaw, *Polym Chem-Uk*, 2010, **1**, 801-826.
25. R. Auras, B. Harte and S. Selke, *Macromol Biosci*, 2004, **4**, 835-864.
26. I. Palard, M. Schappacher, B. Belloncle, A. Soum and S. M. Guillaume, *Chemistry*, 2007, **13**, 1511-1521.
27. M. A. Woodruff and D. W. Hutmacher, *Prog Polym Sci*, 2010, **35**, 1217-1256.
28. V. R. Sinha, K. Bansal, R. Kaushik, R. Kumria and A. Trehan, *Int J Pharm*, 2004, **278**, 1-23.
29. M. Bartnikowski, T. R. Dargaville, S. Ivanovski and D. W. Hutmacher, *Prog Polym Sci*, 2019, **96**, 1-20.
30. R. M. Cywar, N. A. Rorrer, C. B. Hoyt, G. T. Beckham and E. Y. X. Chen, *Nat Rev Mater*, 2022, **7**, 83-103.
31. P. Lecomte and C. Jérôme, in *Synthetic Biodegradable Polymers*, eds. B. Rieger, A. Kunkel, G. W. Coates, R. Reichardt, E. Dinjus and T. A. Zevaco, 2012, vol. 245, pp. 173-217.
32. M. A. Woodruff and D. W. Hutmacher, *Prog Polym Sci*, 2010, **35**, 1217-1256.
33. W. Gruszka and J. A. Garden, *Nat Commun*, 2021, **12**, 3252.
34. X. Y. Tang, C. X. Shi, Z. Zhang and E. Y. X. Chen, *Macromolecules*, 2021, **54**, 9401-9409.
35. X. Li, R. L. Duan, C. Y. Hu, X. Pang and M. X. Deng, *Polym Chem-Uk*, 2021, **12**, 1700-1706.
36. T. Rheinberger, J. Wolfs, A. Paneth, H. Gojzewski, P. Paneth and F. R. Wurm, *J Am Chem Soc*, 2021, **143**, 16673-16681.
37. S. Inkinen, M. Hakkarainen, A. C. Albertsson and A. Sodergard, *Biomacromolecules*, 2011, **12**, 523-532.
38. T. J. Neal, E. D. Neal, J. Cumby and J. A. Garden, *Polym Chem-Uk*, 2024, **15**, 1704-1713.

39. R. L. Webster, N. Noroozi, S. G. Hatzikiriakos, J. A. Thomson and L. L. Schafer, *Chem Commun (Camb)*, 2013, **49**, 57-59.
40. X. Tang and E. Y. Chen, *Nat Commun*, 2018, **9**, 2345.
41. A. B. Samui and T. Kanai, *Int J Biol Macromol*, 2019, **140**, 522-537.
42. S. Shahid, S. Razzaq, R. Farooq and Z. I. Nazli, *Int J Biol Macromol*, 2021, **166**, 297-321.
43. Z. B. Li, J. Yang and X. J. Loh, *Npg Asia Mater*, 2016, **8**, e265-e265.
44. G. Cama, D. E. Mogosanu, A. Houben and P. Dubruel, in *Science and Principles of Biodegradable and Bioresorbable Medical Polymers*, ed. X. Zhang, Woodhead Publishing, 2017, DOI: 10.1016/b978-0-08-100372-5.00003-9, pp. 79-105.
45. A. Duda, A. Kowalski, S. Penczek, H. Uyama and S. Kobayashi, *Macromolecules*, 2002, **35**, 4266-4270.
46. M. Save, M. Schappacher and A. Soum, *Macromol Chem Phys*, 2002, **203**, 889-899.
47. A. Duda and A. Kowalski, in *Handbook of Ring-Opening Polymerization*, 2009, DOI: 10.1002/9783527628407.ch1, pp. 1-51.
48. P. Olsen, K. Odelius and A. C. Albertsson, *Biomacromolecules*, 2016, **17**, 699-709.
49. D. Myers, T. Witt, A. Cyriac, M. Bown, S. Mecking and C. K. Williams, *Polym Chem-Uk*, 2017, **8**, 5780-5785.
50. L. F. Wang, M. Bochmann, R. D. Cannon, J. F. Carpentier, T. Roisnel and Y. Sarazin, *Eur J Inorg Chem*, 2013, **2013**, 5896-5905.
51. D. J. Gilmour, R. L. Webster, M. R. Perry and L. L. Schafer, *Dalton Trans*, 2015, **44**, 12411-12419.
52. D. Meimaroglou, P. Pladis and C. Kiparissides, *Macromol React Eng*, 2016, **11**, 1600039.
53. G. P. Paul and N. Virivinti, *Iran Polym J*, 2022, **31**, 59-81.
54. Y. C. Yu, G. Storti and M. Morbidelli, *Ind Eng Chem Res*, 2011, **50**, 7927-7940.
55. F. Y. Weng, X. H. Li, Y. J. Wang, W. J. Wang and S. J. Severtson, *Macromol React Eng*, 2015, **9**, 535-544.
56. Y. Zhang, M. Schmitt, L. Falivene, L. Caporaso, L. Cavallo and E. Y. Chen, *J Am Chem Soc*, 2013, **135**, 17925-17942.
57. W. Rao, C. Cai, J. Tang, Y. Wei, C. Gao, L. Yu and J. Ding, *Chin J Chem*, 2021, **39**, 1965-1974.
58. D. M. Lyubov, A. O. Tolpygin and A. A. Trifonov, *Coordin Chem Rev*, 2019, **392**, 83-145.
59. in *The IUPAC Compendium of Chemical Terminology*, International Union of Pure and Applied Chemistry (IUPAC), 3.0.1 edn., 2014, DOI: 10.1351/goldbook.L03597, ch. L03597.
60. P. J. Flory, *J Am Chem Soc*, 1940, **62**, 1561-1565.
61. S. Penczek, *J Polym Sci Pol Chem*, 2000, **38**, 1919-1933.
62. B. N. Mankaev and S. S. Karlov, *Materials (Basel)*, 2023, **16**, 6682.
63. S. Penczek, R. Szymanski, A. Duda and J. Baran, *Macromol Symp*, 2003, **201**, 261-269.
64. F. M. Haque and S. M. Grayson, *Nat Chem*, 2020, **12**, 433-444.
65. H. R. Kricheldorf, *J Polym Sci Pol Chem*, 2010, **48**, 251-284.
66. K. C. Hultzsch, T. P. Spaniol and J. Okuda, *Organometallics*, 1998, **17**, 485-488.
67. E. Rabinovich, S. Aharonovich, M. Botoshansky and M. S. Eisen, *Dalton Trans*, 2010, **39**, 6667-6676.
68. M. Visseaux, C. H. Brachais, C. Boisson and K. Tortosa, *Cr Acad Sci Ii C*, 2000, **3**, 631-638.
69. V. Nieboer, N. Fanjul-Mosteirín, P. Olsen and K. Odelius, *Macromolecules*, 2024, **57**, 3397-3406.
70. H. Ma and J. Okuda, *Macromolecules*, 2005, **38**, 2665.
71. H. R. Kricheldorf and S. M. Weidner, *Eur Polym J*, 2023, **185**, 111822.
72. D. A. Culkin, W. Jeong, S. Csihony, E. D. Gomez, N. P. Balsara, J. L. Hedrick and R. M. Waymouth, *Angew Chem Int Ed Engl*, 2007, **46**, 2627-2630.
73. R. W. F. Kerr, P. M. D. A. Ewing, S. K. Raman, A. D. Smith, C. K. Williams and P. L. Arnold, *Acs Catal*, 2021, **11**, 1563-1569.
74. K. C. Hultzsch, T. P. Spaniol and J. Okuda, *Organometallics*, 1997, **16**, 4845-4856.
75. X. Dong and J. R. Robinson, *New J Chem*, 2022, **46**, 444-453.
76. K. Y. Ding, M. O. Miranda, B. Moscato-Goodpaster, N. Ajellal, L. E. Breyfogle, E. D. Hermes, . . . W. B. Tolman, *Macromolecules*, 2012, **45**, 5387-5396.
77. E. Piedra-Arroni, C. Ladaviere, A. Amgoune and D. Bourissou, *J Am Chem Soc*, 2013, **135**, 13306-13309.
78. P. Degée, P. Dubois, S. Jacobsen, H. G. Fritz and R. Jérôme, *J Polym Sci Pol Chem*, 2000, **37**, 2413-2420.
79. X. L. Liu, X. M. Shang, T. Tang, N. H. Hu, F. K. Pei, D. M. Cui, . . . X. B. Jing, *Organometallics*, 2007, **26**, 2747-2757.
80. X. Dong, A. M. Brown, A. J. Woodside and J. R. Robinson, *Chem Commun (Camb)*, 2022, **58**, 2854-2857.

81. X. Dong and J. R. Robinson, *Chem Sci*, 2020, **11**, 8184-8195.
82. F. Fiorentini, W. T. Diment, A. C. Deacy, R. W. F. Kerr, S. Faulkner and C. K. Williams, *Nat Commun*, 2023, **14**, 4783.
83. C. Bakewell, A. J. P. White, N. J. Long and C. K. Williams, *Angew Chem Int Ed*, 2014, **53**, 9226-9230.
84. M. O. Miranda, Y. DePorre, H. Vazquez-Lima, M. A. Johnson, D. J. Marell, C. J. Cramer and W. B. Tolman, *Inorg Chem*, 2013, **52**, 13692-13701.
85. C.-S. Wu, *Handbook Of Size Exclusion Chromatography And Related Techniques*, CRC Press, Boca Raton, 2 edn., 2003.
86. S. Mori and H. G. Barth, *Size Exclusion Chromatography*, Springer, 1999.
87. Y. Jeong, Y. Jin, T. Chang, F. Uhlik and J. Roovers, *Macromolecules*, 2017, **50**, 7770-7776.
88. L. Xiang, W. Ryu, H. Kim and M. Ree, *Polymers (Basel)*, 2018, **10**.
89. H. Rashidzadeh and B. Guo, *Anal Chem*, 1998, **70**, 131-135.
90. C. Puglisi, F. Samperi, R. Alicata and G. Montaudo, *Macromolecules*, 2002, **35**, 3000-3007.
91. M. Florczak, A. Michalski, A. Kacprzak, M. Brzezinski, T. Biedron, A. Pajak, . . . T. Biela, *React Funct Polym*, 2016, **104**, 71-77.
92. F. M. Haque, C. M. Schexnayder, J. M. Matxain, F. Barroso-Bujans and S. M. Grayson, *Macromolecules*, 2019, **52**, 6369-6381.
93. H. Sato, S. Nakamura, K. Teramoto and T. Sato, *J Am Soc Mass Spectrom*, 2014, **25**, 1346-1355.
94. J. Ahmed and S. K. Varshney, *Int J Food Prop*, 2011, **14**, 37-58.
95. O. Dechy-Cabaret, B. Martin-Vaca and D. Bourissou, *Chem Rev*, 2004, **104**, 6147-6176.
96. A. P. Dove, *ACS Macro Letters*, 2012, **1**, 1409-1412.
97. N. E. Kamber, W. Jeong, R. M. Waymouth, R. C. Pratt, B. G. G. Lohmeijer and J. L. Hedrick, *Chem Rev*, 2007, **107**, 5813-5840.
98. I. Cota, *Phys Sci Rev*, 2017, **2**.
99. I. Manavitehrani, A. Fathi, H. Badr, S. Daly, A. Negahi Shirazi and F. Dehghani, *Polymers*, 2016, **8**, 20.
100. X. Zhang, G. O. Jones, J. L. Hedrick and R. M. Waymouth, *Nat Chem*, 2016, **8**, 1047-1053.
101. C. Sanchez-Gonzalez, C. Lopez-Chaves, L. Rivas-Garcia, P. Galindo, J. Gomez-Aracena, P. Aranda and J. Llopis, *ScientificWorldJournal*, 2013, **2013**, 782745.
102. Z. Y. Hu, H. Richter, G. Sparovek and E. Schnug, *J Plant Nutr*, 2004, **27**, 183-220.
103. N. Nomura, A. Taira, T. Tomioka and M. Okada, *Macromolecules*, 2000, **33**, 1497-1499.
104. K. Munster, J. Raeder and M. D. Walter, *Dalton Trans*, 2022, **51**, 986-997.
105. M. C. Baier, M. A. Zuideveld and S. Mecking, *Angew Chem Int Ed Engl*, 2014, **53**, 9722-9744.
106. M. Bochmann, *Organometallics*, 2010, **29**, 4711-4740.
107. Z. M. Hou and Y. Wakatsuki, *Coordin Chem Rev*, 2002, **231**, 1-22.
108. J. Okuda, *J Organomet Chem*, 2023, **1000**, 122833.
109. J. Okuda, P. König, I. L. Rushkin, H.-C. Kang and W. Massa, *J Organomet Chem*, 1995, **501**, 37-39.
110. J. Hitzbleck and J. Okuda, *Z Anorg Allg Chem*, 2006, **632**, 1947-1949.
111. L. Pan, K. Y. Zhang, M. Nishiura and Z. M. Hou, *Macromolecules*, 2010, **43**, 9591-9593.
112. M. V. Orna and M. Fontani, in *150 Years of the Periodic Table*, Springer International Publishing, 2021, DOI: 10.1007/978-3-030-67910-1_10, ch. Chapter 10, pp. 227-257.
113. K. Hans Wedepohl, *Geochimica et Cosmochimica Acta*, 1995, **59**, 1217-1232.
114. P. L. Arnold, F. G. N. Cloke, P. B. Hitchcock and J. F. Nixon, *J Am Chem Soc*, 1996, **118**, 7630-7631.
115. J. C. McGuire and C. P. Kempter, *J Chem Phys*, 1960, **33**, 1584-1585.
116. I. M. Samson and M. Chassé, in *Encyclopedia of Geochemistry*, ed. W. M. White, Springer International Publishing, Cham, 2016, DOI: 10.1007/978-3-319-39193-9_281-1, ch. Chapter 281-1, pp. 1-5.
117. P. L. Arnold, F. G. N. Cloke, P. B. Hitchcock and J. F. Nixon, *J Am Chem Soc*, 1996, **118**, 7630-7631.
118. G. Zhan, H. L. Teng, Y. Luo, S. J. Lou, M. Nishiura and Z. Hou, *Angew Chem Int Ed Engl*, 2018, **57**, 12342-12346.
119. J. Oyamada and Z. Hou, *Angew Chem Int Ed Engl*, 2012, **51**, 12828-12832.
120. D. H. Woen, G. P. Chen, J. W. Ziller, T. J. Boyle, F. Furche and W. J. Evans, *Angew Chem Int Ed Engl*, 2017, **56**, 2050-2053.
121. D. W. Beh, W. E. Piers, I. Del Rosal, L. Maron, B. S. Gelfand, C. Gendy and J. B. Lin, *Dalton Trans*, 2018, **47**, 13680-13688.
122. J. Liu, X. Kong, L. Zheng, X. Guo, X. Liu and J. Shui, *ACS Nano*, 2020, **14**, 1093-1101.

123. P. L. Arnold, I. A. Marr, S. Zlatogorsky, R. Bellabarba and R. P. Tooze, *Dalton Trans*, 2014, **43**, 34-37.
124. M. E. Thompson, S. M. Baxter, A. R. Bulls, B. J. Burger, M. C. Nolan, B. D. Santarsiero, . . . J. E. Bercaw, *J Am Chem Soc*, 2002, **109**, 203-219.
125. T. Chu, W. E. Piers, J. L. Dutton and M. Parvez, *Organometallics*, 2013, **32**, 1159-1165.
126. B. Wang, M. Nishiura, J. Cheng and Z. Hou, *Dalton Trans*, 2014, **43**, 14215-14218.
127. Y. Wang, C. L. Zhou and J. H. Cheng, *Macromolecules*, 2020, **53**, 3332-3338.
128. F. Guo, M. Nishiura, H. Koshino and Z. M. Hou, *Macromolecules*, 2011, **44**, 6335-6344.
129. F. Guo, M. Nishiura, Y. Li and Z. Hou, *Chem Asian J*, 2013, **8**, 2471-2482.
130. M. Deng, S. H. Chi and Y. J. Luo, *New J Chem*, 2015, **39**, 7575-7581.
131. Y. Chapurina, J. Klitzke, L. Casagrande Ode, Jr., M. Awada, V. Dorcet, E. Kirillov and J. F. Carpentier, *Dalton Trans*, 2014, **43**, 14322-14333.
132. C. Bakewell, A. J. White, N. J. Long and C. K. Williams, *Inorg Chem*, 2015, **54**, 2204-2212.
133. N. Diteepeng, J. C. Buffet, Z. R. Turner and D. O'Hare, *Dalton Trans*, 2019, **48**, 16099-16107.
134. N. Diteepeng, I. A. P. Wilson, J.-C. Buffet, Z. R. Turner and D. O'Hare, *Polym Chem-Uk*, 2020, **11**, 6308-6318.
135. A. Takasu, M. Oshimura and T. Hirabayashi, *J Polym Sci Pol Chem*, 2008, **46**, 2300-2304.
136. W. E. Piers, P. J. Shapiro, E. E. Bunel and J. E. Bercaw, *Synlett*, 1990, **1990**, 74-84.
137. N. Nomura, A. Taira, T. Tomioka and M. Okada, *Macromolecules*, 2000, **33**, 1497-1499.
138. S. Kumar, A. Arora, S. Sapra, R. Chaudhary, B. K. Singh and S. K. Singh, *Asian Journal of Organic Chemistry*, 2024, **n/a**, e202400295.
139. X. F. Li, X. Y. Wang, X. Tong, H. X. Zhang, Y. Y. Chen, Y. Liu, . . . Z. M. Hou, *Organometallics*, 2013, **32**, 1445-1458.
140. G. L. Zhou, X. H. Kang, X. B. Wang, Z. M. Hou and Y. Luo, *Organometallics*, 2018, **37**, 551-558.
141. B. Wang, D. Wang, D. Cui, W. Gao, T. Tang, X. Chen and X. Jing, *Organometallics*, 2007, **26**, 3167-3172.
142. X. Xu, Y. Chen, J. Feng, G. Zou and J. Sun, *Organometallics*, 2010, **29**, 549-553.
143. M. Nishiura, Z. M. Hou, T. Koizumi, T. Imamoto and Y. Wakatsuki, *Macromolecules*, 1999, **32**, 8245-8251.
144. S. Arndt and J. Okuda, *Chem Rev*, 2002, **102**, 1953-1976.
145. Y. Wu, S. Wang, C. Qian, E. Sheng, M. Xie, G. Yang, . . . X. Tang, *J Organomet Chem*, 2005, **690**, 4139-4149.
146. T. J. Kealy and P. L. Pauson, *Nature*, 1951, **168**, 1039-1040.
147. J. Mas-Rosello, A. G. Herraiz, B. Audic, A. Laverny and N. Cramer, *Angew Chem Int Ed Engl*, 2021, **60**, 13198-13224.
148. S. Harder, *Coordin Chem Rev*, 1998, **176**, 17-66.
149. M. A. Beswick, J. S. Palmer and D. S. Wright, *Chem Soc Rev*, 1998, **27**, 225-225.
150. T. P. Hanusa, *Organometallics*, 2002, **21**, 2559-2571.
151. R. Poli, *Chem Rev*, 1991, **91**, 509-551.
152. B. E. Bursten and R. J. Strittmatter, *Angew Chem Int Edit*, 1991, **30**, 1069-1085.
153. J. M. O'Connor and C. P. Casey, *Chem Rev*, 2002, **87**, 307-318.
154. M. Weller, T. Overton, F. Armstrong and J. Rourke, *Inorganic Chemistry*, Oxford University Press, 2018.
155. P. L. Pauson, *Q Rev Chem Soc*, 1955, **9**, 391-414.
156. T. Piou, F. Romanov-Michailidis, M. Romanova-Michaelides, K. E. Jackson, N. Semakul, T. D. Taggart, . . . T. Rovis, *J Am Chem Soc*, 2017, **139**, 1296-1310.
157. T. Senda, H. Hanaoka, T. Hino, Y. Oda, H. Tsurugi and K. Mashima, *Macromolecules*, 2009, **42**, 8006-8009.
158. D. C. Calabro, J. L. Hubbard, C. H. Blevins, A. C. Campbell and D. L. Lichtenberger, *J Am Chem Soc*, 1981, **103**, 6839-6846.
159. I. A. Lobanova and V. I. Zdanovich, *Russian Chemical Reviews*, 1988, **57**, 967-980.
160. M. Stradiotto*, *Coordin Chem Rev*, 2001, **219-221**, 311-378.
161. A. N. Nesmeyanov, N. A. Ustynyuk, L. G. Makarova, V. G. Andrianov, Y. T. Struchkov, S. Andrae, . . . S. G. Malyugina, *J Organomet Chem*, 1978, **159**, 189-199.
162. T. C. Forschner, A. R. Cutler and R. K. Kullnig, *Organometallics*, 1987, **6**, 889-891.
163. A. J. Hart-Davis and R. J. Mawby, *J Chem Soc A*, 1969, **0**, 2403-2407.
164. A. J. Hart-Davis, C. White and R. J. Mawby, *Inorganica Chimica Acta*, 1970, **4**, 441-446.
165. L. F. Veiros, *Organometallics*, 2000, **19**, 3127-3136.

166. M. J. Calhorda and L. F. Veiros, *Coordin Chem Rev*, 1999, **185-6**, 37-51.
167. M. E. Rerek, L.-N. Ji and F. Basolo, *J Chem Soc, Chem Commun*, 1983, DOI: 10.1039/c39830001208, 1208-1209.
168. M. J. Calhorda, C. C. Romao and L. F. Veiros, *Chemistry*, 2002, **8**, 868-875.
169. T. K. Miyamoto, M. Tsutsui and L.-B. Chen, *Chemistry Letters*, 1981, **10**, 729-730.
170. D. Ohare, J. C. Green, T. Marder, S. Collins, G. Stringer, A. K. Kakkar, . . . S. Pugh, *Organometallics*, 1992, **11**, 48-55.
171. D. Ohare, V. J. Murphy and N. Kaltsoyannis, *J Chem Soc Dalton*, 1993, **3**, 383-392.
172. T. M. Frankcom, J. C. Green, A. Nagy, A. K. Kakkar and T. B. Marder, *Organometallics*, 2002, **12**, 3688-3697.
173. D. Ohare, V. Murphy, G. M. Diamond, P. Arnold and P. Mountford, *Organometallics*, 1994, **13**, 4689-4694.
174. T. M. Trnka, J. B. Bonanno, B. M. Bridgewater and G. Parkin, *Organometallics*, 2001, **20**, 3255-3264.
175. M. Tsutsui, L. B. Chen, D. E. Bergbreiter and T. K. Miyamoto, *J Am Chem Soc*, 1982, **104**, 855-856.
176. D. O'Hare, V. Murphy, G. M. Diamond, P. Arnold and P. Mountford, *Organometallics*, 2002, **13**, 4689-4694.
177. R. A. Collins, A. F. Russell and P. Mountford, *Appl Petrochem Res*, 2015, **5**, 153-171.
178. H. Braunschweig and F. M. Breitling, *Coordin Chem Rev*, 2006, **250**, 2691-2720.
179. J. Okuda, *Chemische Berichte*, 2006, **123**, 1649-1651.
180. Z. M. Hou, T. Koizumi, M. Nishiura and Y. Wakatsuki, *Organometallics*, 2001, **20**, 3323-3328.
181. P. S. Steinlandt, L. Zhang and E. Meggers, *Chem Rev*, 2023, **123**, 4764-4794.
182. M. Amako, J. Schinkel, M. A. Brook, M. J. McGlinchey and J. F. Britten, *Organometallics*, 2005, **24**, 1533-1543.
183. B. Q. Wang, *Coordin Chem Rev*, 2006, **250**, 242-258.
184. E. Laur, E. Louyriac, V. Dorcet, A. Welle, A. Vantomme, O. Miserque, . . . E. Kirillov, *Macromolecules*, 2017, **50**, 6539-6551.
185. E. Louyriac, E. Laur, A. Welle, A. Vantomme, O. Miserque, J. M. Brusson, . . . E. Kirillov, *Macromolecules*, 2017, **50**, 9577-9588.
186. G. M. Diamond, R. F. Jordan and J. L. Petersen, *Organometallics*, 1996, **15**, 4030-4037.
187. S. Collins, B. A. Kuntz and Y. Hong, *J Org Chem*, 1989, **54**, 4154-4158.
188. G. W. Coates and R. M. Waymouth, *Science*, 1995, **267**, 217-219.
189. K. B. Wagener, *Science*, 1995, **267**, 191.
190. W. Kaminsky, O. Rabe, A. M. Schauwienold, G. U. Schupfner, J. Hanss and J. Kopf, *J Organomet Chem*, 1995, **497**, 181-193.
191. S. Akine and H. Miyake, *Coordin Chem Rev*, 2022, **468**.
192. H. Brunner, *Angew Chem Int Ed Engl*, 1999, **38**, 1194-1208.
193. J. Morvan, F. Vermersch, Z. Zhang, T. Vives, T. Roisnel, C. Crévisy, . . . M. Mauduit, *Organometallics*, 2023, **42**, 495-504.
194. G. M. Diamond, R. F. Jordan and J. L. Petersen, *Organometallics*, 1996, **15**, 4045-4053.
195. S. Bellemin-Laponnaz, M. M. C. Lo, T. H. Peterson, J. M. Allen and G. C. Fu, *Organometallics*, 2001, **20**, 3453-3458.
196. F. R. W. P. Wild, L. Zsolnai, G. Huttner and H. H. Brintzinger, *J Organomet Chem*, 1982, **232**, 233-247.
197. M. Ringwald, R. Stürmer and H. H. Brintzinger, *J Am Chem Soc*, 1999, **121**, 1524-1527.
198. O. J. Curnow and G. M. Fern, *Organometallics*, 2002, **21**, 2827-2829.
199. O. J. Curnow, G. M. Fern, M. L. Hamilton and E. M. Jenkins, *J Organomet Chem*, 2004, **689**, 1897-1910.
200. R. M. Buck, N. Vinayavekhin and R. F. Jordan, *J Am Chem Soc*, 2007, **129**, 3468-3469.
201. C. M. Haar, C. L. Stern and T. J. Marks, *Organometallics*, 1996, **15**, 1765-1784.
202. P. J. Shapiro, PhD, California Institute of Technology, 1991.
203. P. J. Shapiro, E. Bunel, W. P. Schaefer and J. E. Bercaw, *Organometallics*, 2002, **9**, 867-869.
204. O. Dechy-Cabaret, B. Martin-Vaca and D. Bourissou, *Chem. Rev.*, 2004, **104**, 6147-6176.
205. M. J. Stanford and A. P. Dove, *Chem Soc Rev*, 2010, **39**, 486-494.
206. S. Gesslbauer, G. Hutchinson, A. J. P. White, J. Burés and C. Romain, *Acs Catal*, 2021, **11**, 4084-4093.
207. A. Amgoune, C. M. Thomas, T. Roisnel and J. F. Carpentier, *Chemistry*, 2005, **12**, 169-179.

208. C. M. Manna, A. Kaur, L. M. Yablon, F. Haeffner, B. Li and J. A. Byers, *J Am Chem Soc*, 2015, **137**, 14232-14235.
209. Z. R. Turner, J. V. Lamb, T. P. Robinson, D. Mandal, J. C. Buffet and O. H. D, *Dalton Trans*, 2021, **50**, 4805-4818.
210. J. V. Lamb, J. C. Buffet, J. E. Matley, C. M. R. Wright, Z. R. Turner and D. O'Hare, *Dalton Trans*, 2019, **48**, 2510-2520.

Chapter 2 – Group three permethylindenyl-phenoxy (PHENI*) complexes

2.1. Introduction.

2.1.1. Phenoxy-Induced Complexes of Sumitomo (PHENICS) and constrained geometry complexes (CGCs)

Constrained geometry complexes (CGCs), a family of *ansa*-cyclopentadienyl-amido complexes, laid the building blocks for the development of **Ph**enoxy-**I**nduced **C**omplexes of **S**umitomo (PHENICS) (**Figure 2.1**).[1-6]

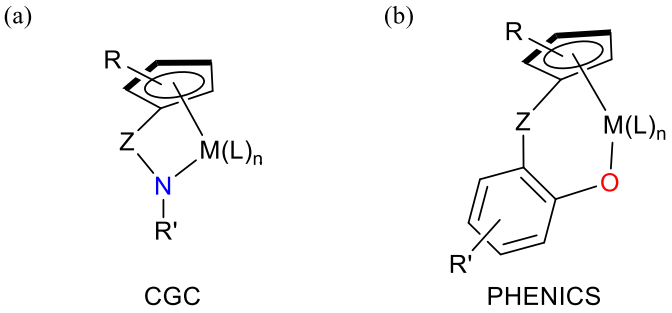


Figure 2.1 General structures of ansa-bridged (a) CGC and (b) PHENICS compounds with link 'Z'. R = Me, R′ = alkyl, (e.g. ^{t}Bu, ^{n}Bu), Ph;[2, 3] L = Cl, Me, Et, I, OAr).[7]

These complexes are composed of an η^5-coordinating π donor, such as cyclopentadienyl (Cp = η^5-C_5H_4), indenyl (I = η^5-C_9H_6), with an η^1- heteroatom terminated pendant arm attached through a silicon or carbon containing bridging group. PHENICS complexes provide greater conformational flexibility over CGC through extending the pendant arm *via* a phenoxy group.

2.1.2. Permethylindenyl phenoxy PHENICS-type (PHENI*) complexes

Single-site catalysts provide a foundation to study polymerisation in terms of performance and controllability *via* pre*proximal*e design of architecture and conditions.[8]

The initial ligand framework used in this investigation is the silyl bridged permethylindenyl (I* = I where H = Me) phenoxy PHENICS-type ligand (PHENI*), which combines the features of PHENICS and established I* metallocenes (**Figure 2.2**).[1, 9, 10]

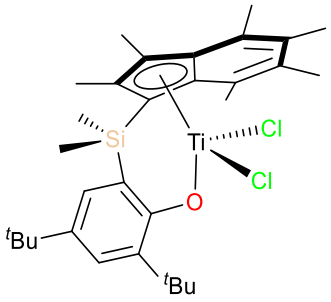


Figure 2.2 Silyl bridged permethylindenyl phenoxy titanium complexes (PHENI*) {(η^5-C_9Me_6)^{Me_2}Si(2-R-4-R′-C_6H_2O)}$TiCl_2$: ^{Me_2}SB(^{tBu_2}ArO,I*)$TiCl_2$.[10]

The facile ability to alter the *R, R′* groups in addition to the silyl bridge allow a route to designing new ligands that offer different steric/electronic/conformational features thereby impacting the reactivity of the organometallic complex (**Figure 2.3**).

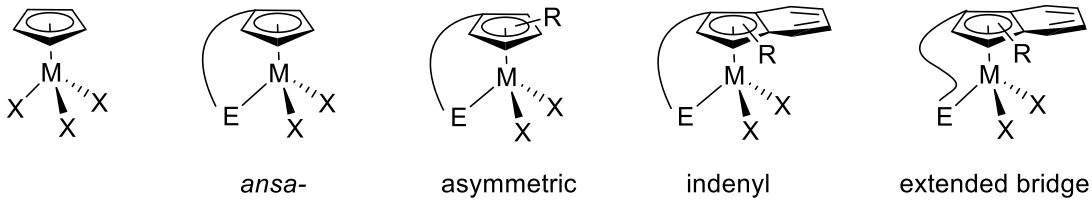


Figure 2.3 Evolution from half sandwhich complexes to PHENI* complexes

The different ligands, developed by O'Hare *et al.*, presented in **Figure 2.4** have unique solution dynamics which will be discussed in detail in **Chapter 3**.

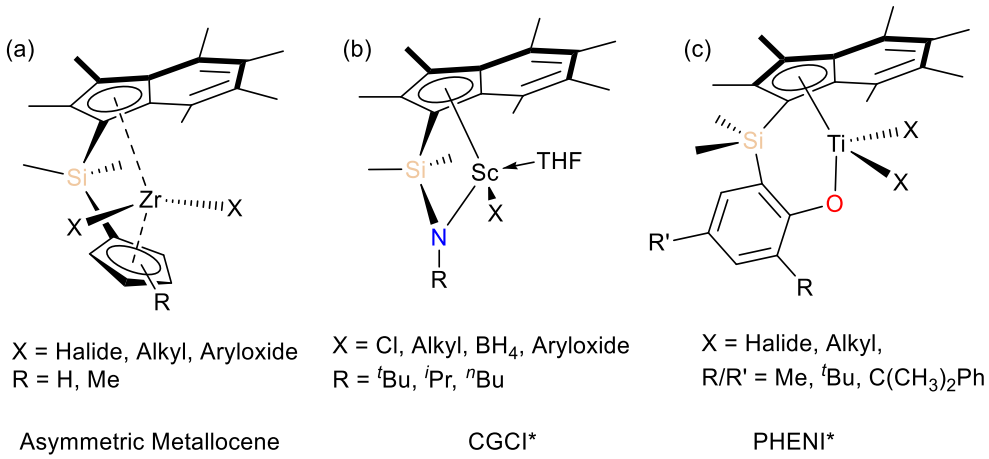


Figure 2.4 Selected permethylindenyl *ansa*-bridged systems studied by O'Hare *et al*. as polymerisation catalysts (a) Zr complexes[11-14] (b) Ti and Sc CGC-permethylindenyl (CGCI*)[15-17] (c) Ti PHENI* complexes.[7, 10, 18, 19]

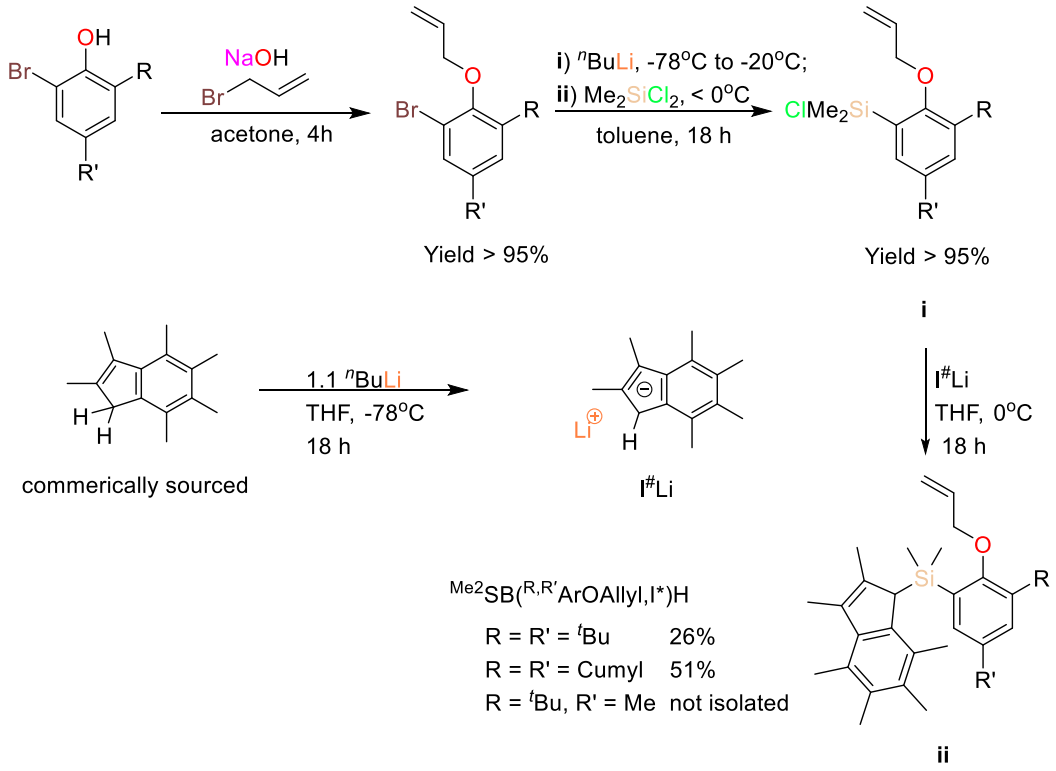
2.1.3. Chapter synopsis

Chapter 2 describes the synthesis and characterisation of a family of trivalent complexes using CGCI* and PHENI* ligands. A variety of substitution patterns on the aryloxide ring are reported along with a range of substitutions for the neutral donor ligand on the M(III) centre.

2.2. Synthesis of Ligands

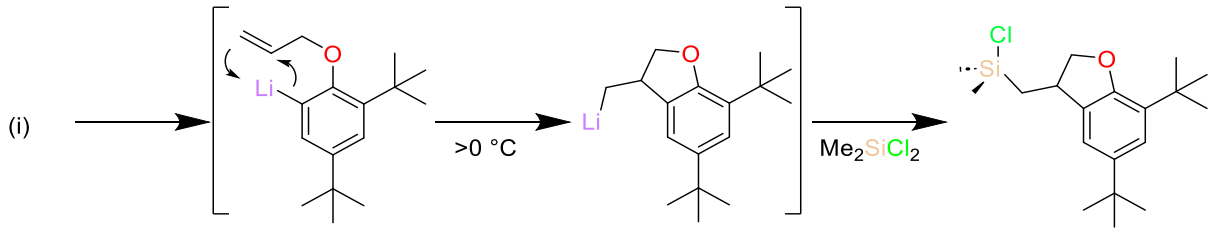
2.2.1. Synthesis of proligands ^{Me2}SB($^{R,R'}$ArOAllyl,I*)H (R = R′ = ^{t}Bu, CMe$_2$Ph; R = ^{t}Bu, R′ = Me; Cumyl = CMe$_2$Ph)

The PHENI* ligands ^{Me2}SB($^{R,R'}$ArOAllyl,I*)H were prepared following the route reported by O'Hare *et al.*, (Scheme 2.1)[10] where the crude products (Me$_2$Cl)Si($^{R,R'}$ArOAllyl)H (i) and ^{Me2}SB($^{R,R'}$ArOAllyl,I*)H (ii) (R = R′ = ^{t}Bu or CMe$_2$Ph, cumyl; R = ^{t}Bu, R′ = Me), were originally reported as orange oils.



Scheme 2.1 General synthesis route for proligands ^{Me_2}SB($^{R,\,R'}$ArOAllyl,I*)H (Where R,R′ = ^{t}Bu, ^{t}Bu; CMe_2Ph, CMe_2Ph; ^{t}Bu, Me; Cumyl = CMe_2Ph).

During the formation of ^{Me_2}SB($^{R,R'}$ArOAllyl,I*)H the temperature must be kept below −20 °C during the lithiation step to avoid the formation of a dihydrobenzofuran by intramolecular rearrangement (Scheme 2.2).[6]



Scheme 2.2 Rearrangement of *ortho*-aryl lithium intermediate due to thermal instability above 0 ℃ .

Crystallisation from cold hexanes (−20 °C) was found to yield colourless crystals of **ii** (R = R′ = ^{t}Bu; Cumyl) suitable for an X-ray crystallographic study. Collection of supernatant

solution followed by concentration and cooling was used to produce a series of crops. Characterisation of these proligands is described in published work from O'Hare *et al*.[7]

2.2.1.1. Solid state structures of ^{Me2}SB($^{R,R'}$ArOAllyl,I)H {R = R' = ^{t}Bu; Cumyl}*

^{Me2}SB(^{tBu2}ArOAllyl,I*)H was found to crystallise in the monoclinic *I2/a* space group with 8 molecules in the unit cell. ^{Me2}SB(^{Cumyl2}ArOAllyl,I*)H was found to crystallise in the triclinic $P\bar{1}$ space group with 2 molecules in the unit cell. All bond lengths were consistent with similar structures (**Figure 2.5**).[7]

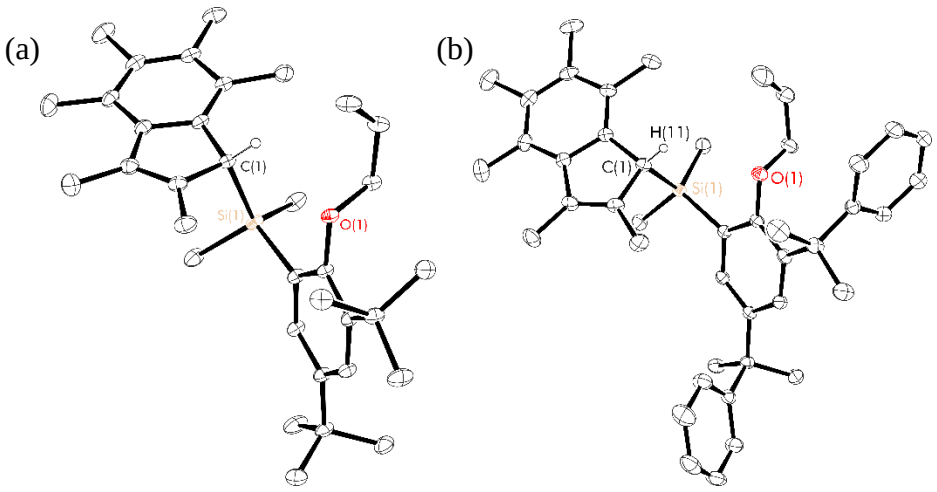
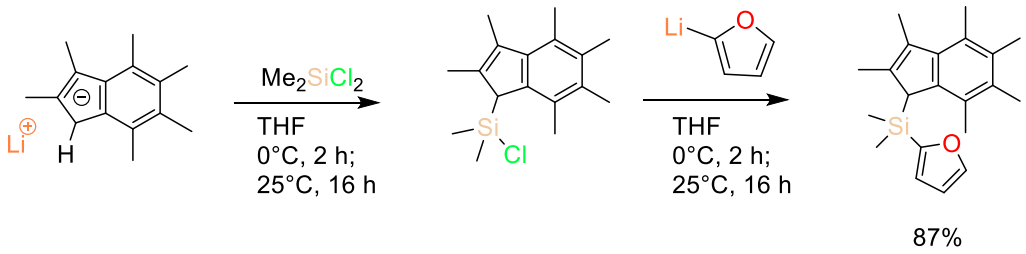


Figure 2.5 Solid state structure of (a) ^{Me2}SB(^{tBu2}ArOAllyl,I*)H and (b) ^{Me2}SB(^{Cumyl2}ArOAllyl,I*)H Ellipsoids are drawn at 30% probability and all hydrogen atoms other than those at C(1) stereocentres are omitted for clarity.

2.2.2. Synthesis of other proligands

The I*-Furan proligand (C_9Me_6)H^{Me2}Si(C_4H_3O) (^{Me2}SB(Furan,I*)H) was prepared following an adapted route as employed for analogous Cp-derivatives.[12, 20] Furan-2-yl lithium was synthesised following literature procedure.[21] ^{Me2}SB(Furan,I*)H was isolated as an orange waxy solid in in 87% yield following a two-step procedure (**Scheme 2.3**).



Scheme 2.3 Synthesis of proligand ^{Me_2}SB(Furan,I*)H.

The ^{1}H NMR spectrum of ^{Me_2}SB(Furan,I*)H shows six resonances for I*Me protons between δ 1.86 and 2.50 ppm. In addition, two singlets at δ 0.06 and 0.08 correspond to the SiMe_2 proton resonances, which couple to the I*-C_1 protons in the ^{1}H-^{13}C HMBC 2D NMR spectrum. A singlet at δ 3.62 ppm corresponds to the I*H proton. Two doublets at δ 6.39 and 7.43 ppm couple to the doublet of doublets at δ 6.17 ppm, which are all resonances for the protons on the furan substituent. (**Figure 2.6**)

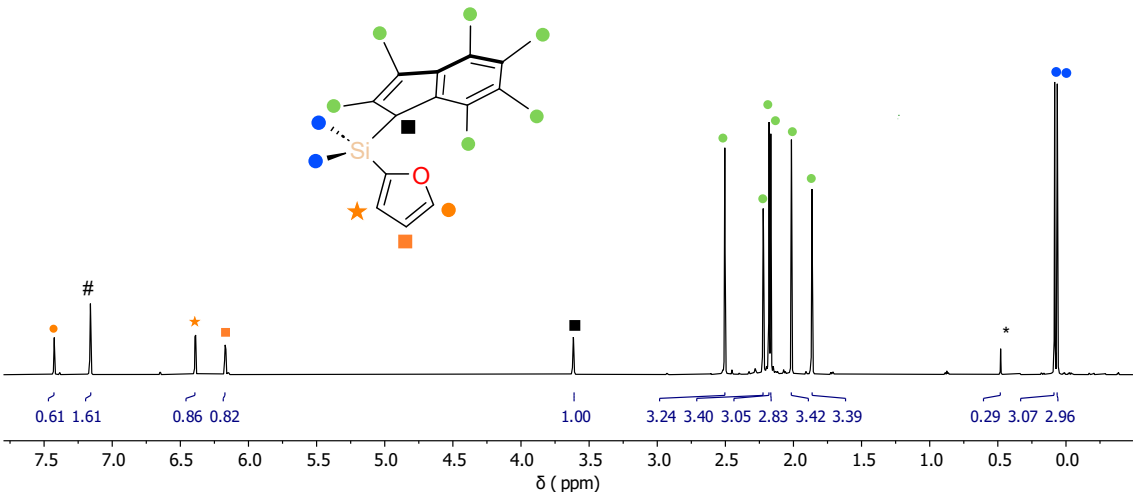
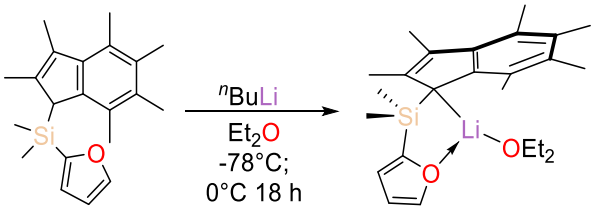


Figure 2.6 ^{1}H NMR spectrum (600 MHz, benzene-d_6, 298 K) of ^{Me_2}SB(Furan,I*)H. # denotes residual protio solvent and * denotes residual protio species.

Reaction of 1.1 eq ^{n}BuLi in Et_2O with ^{Me_2}SB(Furan,I*)H produced the crude ether-lithium salt adduct ^{Me_2}SB(Furan,I*)Li·Et_2O as a pale-yellow precipitate in 12% yield that was unstable at room temperature (**Equation 2.1**).

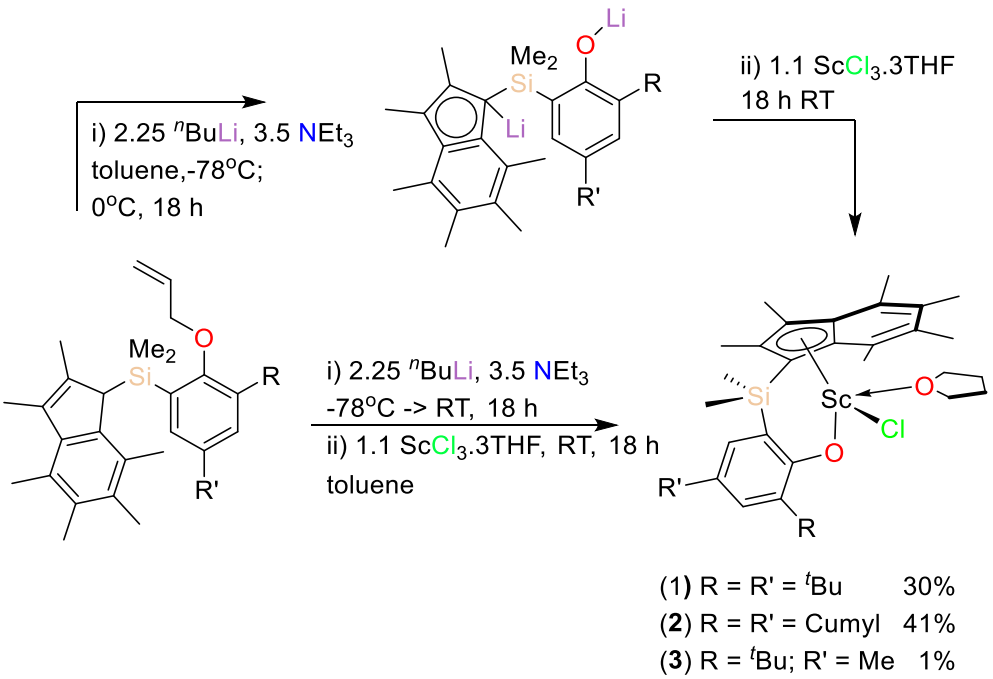


Equation 2.1 Synthesis of ^{Me2}SB(Furan,I*)Li·OEt$_2$.

Further salt metathesis reaction with ^{Me2}SB(Furan,I*)Li·OEt$_2$ produced only mixtures of products, of which none were isolated. Bulky amide bases such as M(N(SiMe$_3$)$_2$) (M = Li, K) showed no reactivity with ^{Me2}SB(Furan,I*)H. In addition, homoleptic scandium bases Sc(CH$_2$SiMe$_3$)$_3$(THF)$_2$ and Sc(N(SiMe$_3$)$_2$)$_3$ also produced no reaction. ^{Me2}SB(Furan,I*)Li·OEt$_2$ was not used from this point onwards.

2.3. Synthesis of ^{Me2}SB($^{R,R'}$ArO,I*)Sc(Cl)THF {R = R′ = ^{t}Bu (1) and Cumyl (2); R = ^{t}Bu, R′ = Me (3)}

Reaction of ScCl$_3$·3THF and the lithium salt ^{Me2}SB($^{R,R'}$ArO,I*)Li$_2$, which was prepared and utilised *in situ*, afforded ^{Me2}SB($^{R,R'}$ArO,I*)Sc(Cl)THF (R = R′ = ^{t}Bu (**1**); Cumyl (**2**); R = ^{t}Bu, R′ = Me (**3**)) complexes as off-white powders in 30%, 41% and 1% yield respectively (**Scheme 2.4**).



Scheme 2.4 Synthesis of ^{Me_2}SB($^{R,R'}$ArO,I*)Sc(Cl)THF (R = R′ = ^{t}Bu (**1**); Cumyl (**2**); R = ^{t}Bu, R′ = Me (**3**)). Synthesis of crude lithiate proligand followed by addition of $ScCl_3$.3THF.

While the lithiated ligand salts can be isolated and characterised *ex situ* by NMR spectroscopy (**Figure 2.7**), the highest yields of scandium complexes (>30% vs <10%)) are achieved through one pot synthesis.[7] The crude ^{1}H NMR spectrum of ^{Me_2}SB($^{t Bu_2}$ArOAllyl,I*)Li_2.$(NEt_3)_{0.3}$ shows the presence of NEt_3 as a quartet at δ 2.43 ppm and a triplet at δ 0.98 ppm both with $^3J_{H-H}$ = 6.5 Hz. The presence of NEt_3 in the NMR after washing with hexanes, suggests the formation of an adduct, in a ratio of approximately 1:0.3, between the lithiate clusters.[7] Six singlets between δ 2.95 and 2.31 ppm correspond to the I**Me* protons and integrate to 3H each. The bridging silyl-*Me* protons are in distinct environments assigned to broad singlets at δ 1.03 (Si*Me*), which integrates to 6H. The 2,4-^{t}*Bu*-C_6H_2 environments can be assigned to two resonances at δ 1.86 and 1.56 ppm respectively which integrate to 9H each.

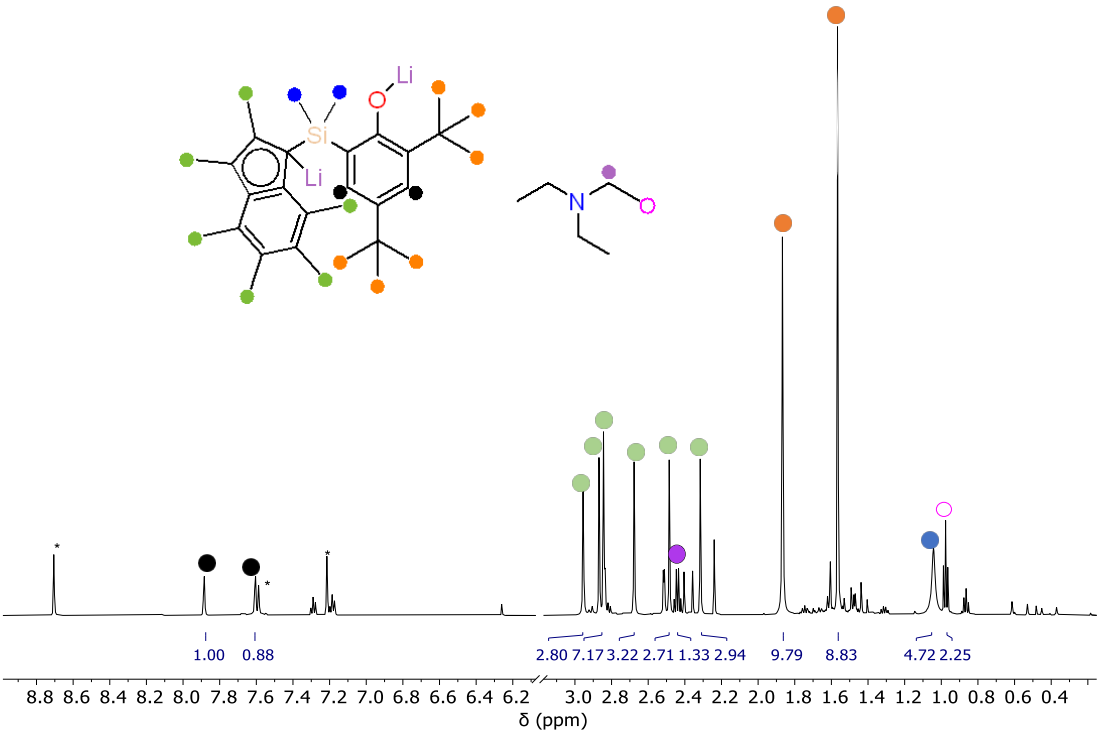


Figure 2.7 ^{1}H NMR spectrum (pyridine-d_5, 600 MHz, 298 K) of ^{Me_2}SB(^{tBu_2}ArOAllyl,I*)Li$_2$.(NEt$_3$)$_{0.3}$

2.3.1. Characterisation of complexes 1 and 2

2.3.1.1. Conformational labels of PHENI complexes*

Labels A-"*proximal*" and B-"*distal*" are defined by the torsion angle (TA(M)) between the I*-Me$^{\alpha}$ and metal-bonded heteroatom on the pendant arm in the solid state. **T**he term "proximal" from the Latin word *proximus*, meaning close or near, indicates proximity. In contrast, "distal", derived from the Latin prefix *dis*-, meaning "apart". In this case, *proximal* and *distal* describes the relative distance of phenoxy- substituent relative to the 6-membered ring of the Indenyl (blue in **Figure 2.8**). A-*proximal* TA(M) > 72°, and B-*distal* TA(M) < 72° (a complete definition is found in the **Appendix A.1.1**). The angular range derives from measurements of the solid-state structures, but can be generally applied to the ligand arrangements in solution. (**Figure 2.8)**.[22]

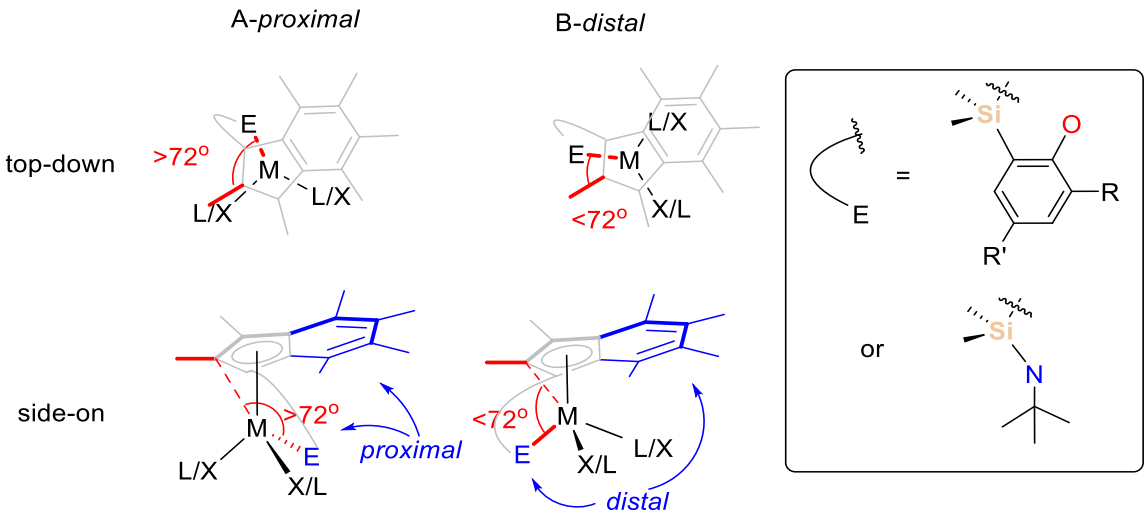


Figure 2.8 Conformers, A-*proximal* and B-*distal*, with TA(M) highlighted red. L is Lewis base/neutral donor, X is anionic donor (X^-).

Where the ligands are sufficiently small, the B-*distal* conformation is preferred, with one of the η^1- ligands (X or L) positioned underneath the I*-C_6Me_4 ring. Where the substituents X and L are larger, the A-*proximal* conformation has lower energy, with ligands positioned facing outwards, away from the I* moiety.

2.3.1.2. NMR spectroscopic characterisation of ^{Me_2}SB(^{tBu_2}ArO,I)Sc(Cl)THF (1)*

The ^{1}H NMR spectrum of **1** in benzene-d_6 at 298 K is consistent with a mixture of 2 isomers with the formula ^{Me_2}SB(^{tBu_2}ArO,I*)Sc(Cl)THF (**1**) in a ratio of 7:1. (**Figure 2.9**).

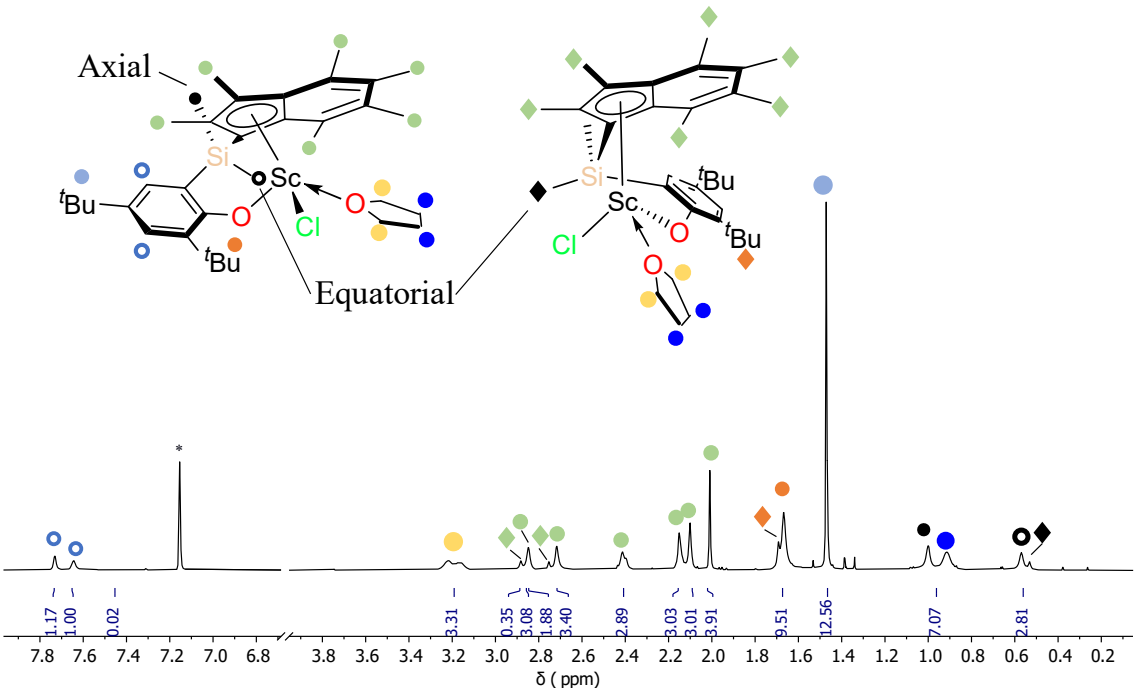


Figure 2.9 ^{1}H NMR spectrum (500 MHz, benzene-d_6, 298 K) of ^{Me_2}SB(^{tBu_2}ArO,I*)Sc(Cl)THF (**1**) The S_I enantiomer from each pair (B-*distal*,R_{Sc},S_I)-**1** (major, left) and (A-*proximal*,R_{Sc},S_I)-**1** (minor, right) is drawn. Diamonds denote the minor resonances.

The major isomer is the (B-*distal*,R_{Sc},S_I)/(B-*distal*,S_{Sc},R_I)-**1** enantiomer pair. Six singlets between δ 2.85 and 2.02 ppm correspond to the I**Me* protons and integrate to 3H each. The bridging silyl-*Me* protons are in distinct environments assigned to broad singlets at δ 1.05 (Si*Me*$_{axial}$) and 0.58 ppm (Si*Me*$_{equatorial}$), which both integrate to 3H each. Using ^{1}H-^{1}H NOESY spectroscopy, the 2-^{t}*Bu*-C_6H_2 and 4-^{t}*Bu*-C_6H_2 environments can be assigned to two resonances at δ 1.67 and 1.47 ppm respectively which integrate to 9H each. A secondary set of resonances, consistent with the (A-*proximal*,R_{Sc},S_I)/(A-

proximal,S_{Sc},R_I)-**1** enantiomer pair, is observed in the ^{1}H NMR spectrum. For example, resonances at δ 2.87 and 2.73 ppm corresponding to two of the I*Me* environments. The low temperature ^{1}H NMR spectrum in toluene-d_8, at 210 K, shows the sharpening of all resonances (**Figure 2.10**).

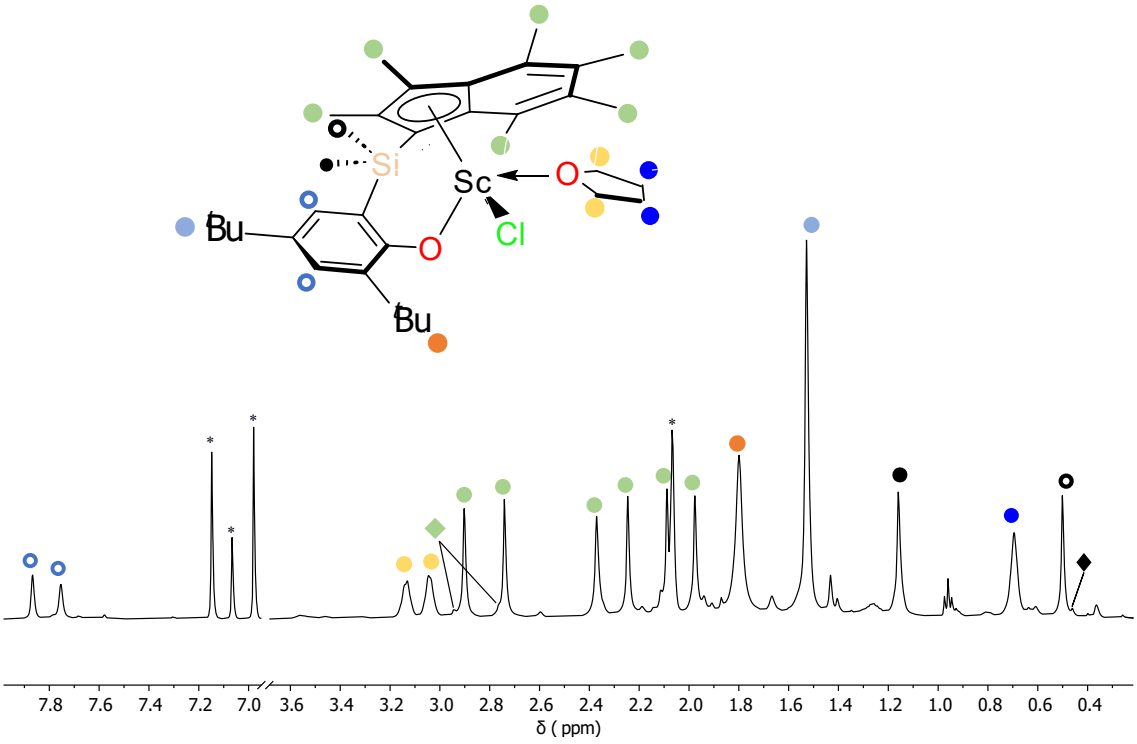


Figure 2.10 ^{1}H NMR spectrum (500 MHz, toluene-d_8, 210 K) of ^{Me_2}SB(^{tBu_2}ArO,I*)Sc(Cl)THF (**1**) (B-*distal*,R_{Sc},S_I)-**1** drawn in figure. ◆ denotes a minor resonance. * denotes residual protio solvent.

Coalescence does not occur at elevated temperatures (374 K) which suggests the energetic barrier between the species is $\gg k_BT$. Both positive (red) and negative (blue) cross peaks are present in the ^{1}H-^{1}H NOESY spectrum of **1**, arising from through-space interactions and chemical exchange respectively.[23, 24] The signals for the interactions between Sc-O-1,4-C$_4$*H*$_8$ and Si*Me*$_{equatorial}$ (black circle), four I**Me*, and the -2-^{t}*Bu* protons (orange dot, δ 1.67 ppm) indicates the THF adduct is held near Si*Me*$_{equatorial}$, hence suggestive of the *distal* conformation for the major species. The ^{7}Li NMR spectrum of **1**

contained a single resonance at δ –0.05 ppm in toluene-d_8. Bercaw *et al.* published a similar CGCI* scandium chloride complex with the formula ^{Me_2}SB(Cp*$^{t_{bu}}$N)ScCl $(LiCl)_n$ THF_x where LiCl was observed through NMR. ^{n}BuLi was used in Bercaw and co-workers' reported synthesis. As there are no other species present in the ^{1}H NMR spectrum for **1**, the lithium environment must be LiCl in solution.

2.3.2. NMR spectroscopic characterisation of ^{Me_2}SB(^{Cumyl_2}ArO,I*)Sc(Cl)THF (2)

The ^{1}H NMR spectrum of ^{Me_2}SB(^{Cumyl_2}ArO,I*)Sc(Cl)THF (**2**), similar to **1**, displays two species (B-*distal*,R_{Sc},S_I)/(B-*distal*,S_{Sc},R_I)-**2** enantiomer pair and (A-*proximal*,R_{Sc},S_I)/(A-*proximal*,S_{Sc},R_I)-**2** enantiomer pair in a ratio of approximately 15:1 in benzene-d_6 at 298 K. For (B-*distal*,R_{Sc},S_I)/(B-*distal*,S_{Sc},R_I)-**2**, the 2,4-CMe_2Ph proton resonances appear as 4 singlets at δ 2.03, 1.51 and 1.85 ppm with integrals corresponding to 3, 3, and 6 protons respectively. Additional aromatic resonances, corresponding to the CMe_2*Ph* protons, which integrate to 10 H in total occur in the spectrum between δ 7.48 and 6.73 ppm as a series of broadened triplets and doublets. The Si*Me* and I**Me* proton resonances are all present as expected. Interestingly, the ligated THF protons, 1,4-OC_4H_8, are present as two broad signals at δ 2.56 and 2.72 ppm, at a lower frequency than the same environment for **1**, suggesting close proximity to the I*-C_6 ring in solution and restricted rotation around the Sc–O bond (**Figure 2.11**).

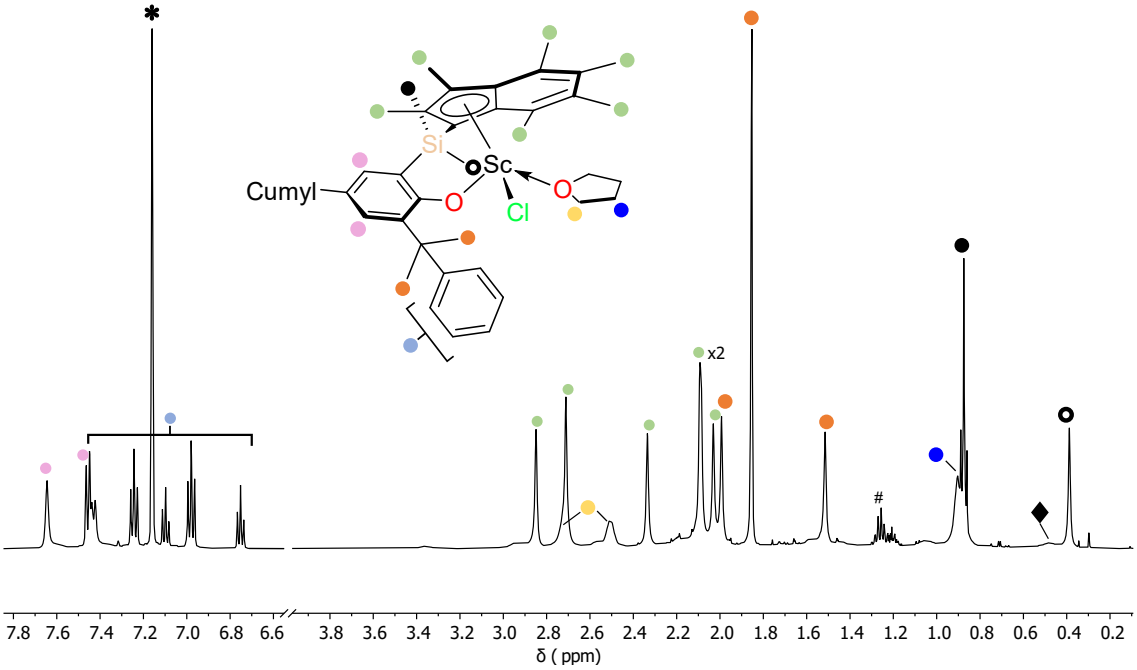


Figure 2.11 ^{1}H NMR spectrum (400 MHz, benzene-d_6, 298 K) of ^{Me_2}SB(^{Cumyl_2}ArO,I*)Sc(Cl)THF (**2**). Drawn in figure (B-*distal*,R_{Sc},S_I)-**2**. * denotes residual protio solvent, # denotes residual solvent and ◆ denotes the minor Si*Me* resonance.

2.3.3. Solid-state structures of ^{Me_2}SB($^{R,R'}$ArO,I*)Sc(Cl)THF (R = R′ = ^{t}Bu (1) and Cumyl (2))

Crystals suitable for X-ray diffraction studies of **1** and **2** were grown from slow evaporation of a hexane solution at –30 °C (**Figure 2.12**). The solid-state structure of **1** was found to crystallise in the monoclinic space group, $P2_1/n$ and **2** in the triclinic space group, $P\bar{1}$; as non-Sohncke space groups. Both **1** and **2** were found in the B-*distal* conformations in the solid-state, with TA(M) of 31.44(17)° and 31.4(3)° respectively. In addition, the unit cells contained enantiomer pairs (B-*distal*,R_{Sc},S_I)/(B-*distal*,S_{Sc},R_I) for **1** and **2**, in agreement with the major isomer identified in solution**.** .

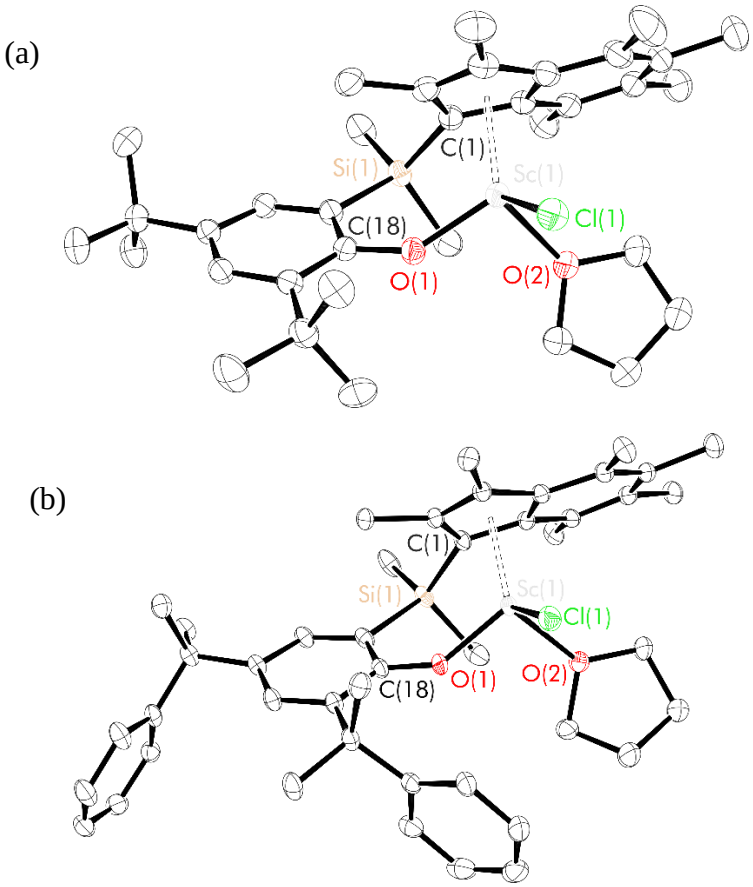


Figure 2.12 Solid state structures of (a) (B-*distal*,R_{Sc},S_I)-**1** and (b) (B-*distal*,R_{Sc},S_I)-**2**. Enantiomer (B-*distal*,S_{Sc},R_I) for **1** and **2** are present in the unit cell but not shown. Ellipsoids are drawn at 30% probability and all hydrogen atoms are omitted for clarity.

Selected distances and angles are presented in **Table 2.1**. The geometry about the 4-coordinate scandium centre is observed as distorted tetrahedral for **1** and **2**. The nature of the 4-coordinate centre can be quantified though the τ_4' parameter:

$$\tau 4' = \frac{\beta - \alpha}{360° - \theta} + \frac{180° - \beta}{180° - \theta}$$

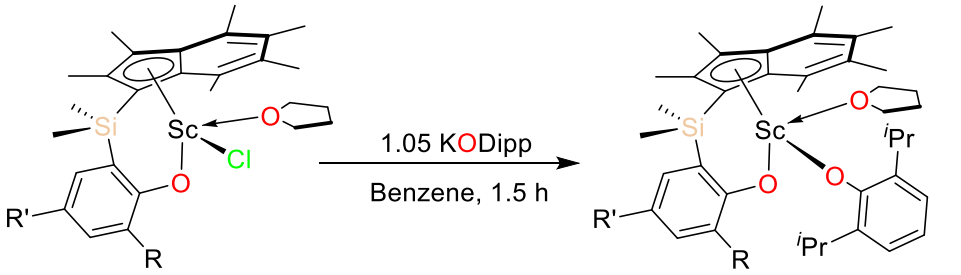
Equation 2.1 τ_4' = 0 for square planar. τ_4' = 1 for tetrahedral; $\theta = \cos^{-1}(-1/3) = 109.471°$; β > α, two greatest valency angles (for example for **1**, α, I*cent–Sc–X = 118.17(3) and β, I*cent–Sc–O^{THF} = 120.94(5)).[25]

where β > α are defined as the two greatest valency angles. For **1** and **2**, τ'_4 = 0.8633(10) and 0.8605(16)) respectively. This a slight increase in distortion with respect to analogous

Ti PHENI* complex ^{Me2}SB(^{tBu2}ArO,I*)TiCl$_2$ which are reported to have a shorter M-I* bond at 2.0242(9) compared to 2.1522(3) Å for **1**, and less distorted tetrahedral metal centre $\tau'_4 = 0.90$.[7] The Sc–(OAr) bond lengths increase as the R, R′ groups increase in steric bulk (^{t}Bu to Cumyl) from **1** (1.8191(14) Å) to **2** (1.920(2) Å). They are both shorter than reported values in literature for Sc–^{R,R}OAr (R = alkyl) complexes with typical bond lengths between 1.9–2.0 Å.[26, 27] Sc-O^{THF} and Sc-Cl bond lengths fall into the ranges for related bond types; 2.1–2.3 Å, [28-30] and 2.37–2.44 Å,[31-34] respectively.

2.4. Synthesis and characterisation of ^{Me2}SB($^{R,R'}$ArO,I*)Sc(ODipp)THF R = R′ = ^{t}Bu (5) and Cumyl (6)

To a benzene solution of scandium chloride complexes **1** or **2**, potassium(2,6-diisopropyl)phenoxide (KODipp) was added (1.05 equiv.) to give the respective PHENI* scandium phenoxide ^{Me2}SB($^{R,R'}$ArO,I*)Sc(ODipp)THF (R = R′ = ^{t}Bu (**5**) and Cumyl (**6**)) complexes as off white powders in 56% and 26% yield respectively (**Scheme 2.5**).



R = R' = ^{t}Bu (**1**)
CMe$_2$Ph (**2**)

R = R' = ^{t}Bu (**5**) 56%
CMe$_2$Ph (**6**) 26%

Scheme 2.5 Synthesis of scandium aryloxide complexes ^{Me2}SB($^{R,R'}$ArO,I*)Sc(ODipp)THF (R = R′ = ^{t}Bu (**5**) and Cumyl (**6**)).

2.4.1. NMR spectroscopic characterisation of ^{Me2}SB($^{R,R'}$ArO,I*)Sc(ODipp)THF (5)

A first inspection, the ^{1}H NMR spectrum of ^{Me2}SB(^{tBu2}ArO,I*)Sc(ODipp)THF (**5**) shows the synthesis of a single isomeric product of the form (A-*proximal*,S_{Sc},S_I)/(A-

proximal,R_{Sc},R_I)-**5** from **1** (**Figure 2.13**). However, secondary resonances are present, similar to **1**–**3,** in a very small ratio (approx. 40:1) that correspond to proton environments for the (B-*distal*,S_{Sc},S-$_I$)/(B-distal,R_{Sc},R_I)-**5** enantiomer pair related. Correlations in the ^{1}H-^{1}H NOESY spectrum was used to confirm the species are in chemical exchange and are isomers with the same molecular formula (Expansion in **Figure 2.13**).[23] For the major enantiomer pair (A-*proximal*,S_{Sc},S_I)/(A-*proximal*,R_{Sc},R_I)-**5,** distinct isopropyl environments are present as seen by two doublets at δ 1.29 and 1.16 ppm which integrate to 6H each. The ^{t}*Bu* proton signals integrate to 9H each with resonances at δ 1.48 and 1.42 ppm. The Si*Me* proton resonances at δ 0.94 and 0.85 ppm integrate to 3H each.

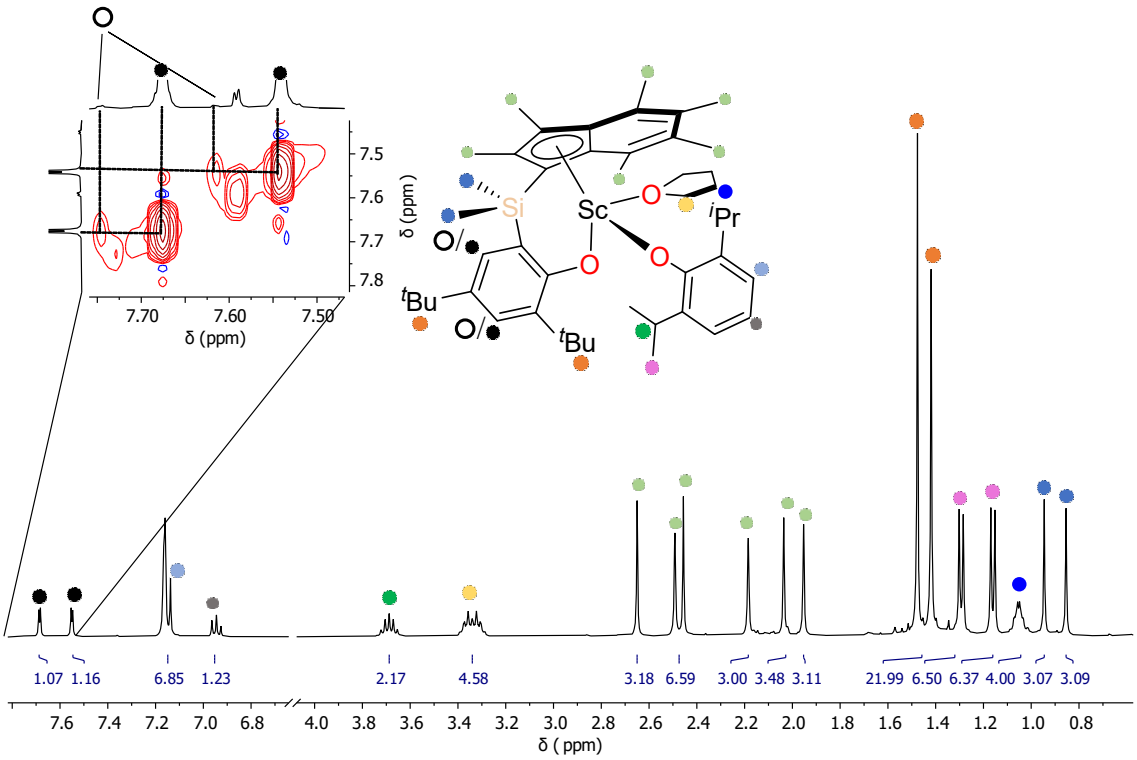


Figure 2.13 ^{1}H NMR spectrum (400 MHz, benzene-d_6, 298 K) of **5.** (A-*proximal*,S_{Sc},S_I)-**5** drawn in figure. *denotes residual protio solvent. Expansion: ^{1}H-^{1}H NOESY spectrum (benzene-d_6, 500 MHz, 298 K) for 3,5-C_6H_2 protons between δ 7.80–7.50 ppm.

2.4.2. NMR spectroscopic characterisation of ^{Me_2}SB(^{Cumyl_2}ArO,I*)Sc(ODipp)THF (6)

The ^{1}H NMR spectrum of ^{Me_2}SB(^{Cumyl_2}ArO,I*)Sc(ODipp)THF (**6**) displays similar spectrum to **5**, and shows the formation of two set of enantiomer pairs (A-*proximal*,S_{Sc},S_I)/(A-*proximal*,R_{Sc},R_I)-**6** and (B-*distal*,S_{Sc},S_I)/(B-distal,R_{Sc},R_I)-**6** in a ratio of 40:1. For (A-*proximal*,S_{Sc},S_I)/(A-*proximal*,R_{Sc},R_I)-**6**, the major species, distinct isopropyl environments are present as seen by two doublets at δ 1.26 and 1.19 ppm. All resonances in the ^{1}H NMR spectrum of **6** appear significantly sharper than the ^{1}H NMR spectrum of **2**. The dynamics of this are discussed in **Chapter 3**.

2.4.3. Solid-state structure of ^{Me_2}SB(^{tBu_2}ArO,I*)Sc(ODipp)THF (5)

Crystals suitable for X-ray diffraction studies were grown for **5** by slow evaporation from a hexane solution at –30 °C. The solid-state structure of **5** present as the enantiomer pair (A-*proximal*,S_{Sc},S_I)/(A-*proximal*,R_{Sc},R_I)-**5** in the unit cell as was solved in the triclinic $P\bar{1}$ space group. The 4 coordinate scandium centre has τ'_4 = 0.8751(14) indicating distorted tetrahedral conformation around the scandium, although closer to tetrahedral than either **1** or **2**. The Sc–ODipp bond distance is shorter at 1.928(2) Å compared to the Sc–Cl bond distance of 2.4311(6) Å for **1** but lies within the range of previously reported Sc–ODipp bond distances of 1.90–1.95 Å.[16, 17, 35] The order of the bond lengths (Sc–O < Sc–Cl) is in line with the expected sum of covalent radii for Sc (1.44 Å) and O (0.66(2)Å) where ∑ = 2.1 Å and for Sc and Cl (1.02(4) Å) where ∑ = 2.46Å.[2, 36] Additionally, the Sc–O^{THF} bond distance, at 2.160(2) Å for **5**, is longer than the respective bond Sc–O^{THF} in **1** of 2.1296(15) Å. This would suggest a weaker coordination of THF in **5** than **1** in the solid-state possibly due to steric crowding of the scandium centre, forcing the THF molecule further from the metal centre. In the solid-state, **5** is in the A-*proximal* conformation, where TA(M) = 106.5°.

2.4.4. Synthesis and solid-state characterisation of ^{Me2}SB(^{tBu}N,I*)Sc(X)THF X = Cl (4) and ODipp (7)

The CGCI* complex ^{Me2}SB(^{tBu}N,I*)Sc(Cl)THF (**4**) reported by O'Hare *et al*. was prepared following the literature preparation. [16] However, for the first time, yellow crystals suitable for an X-ray crystallographic study were obtained from cold (4 °C) hexanes. The solid-state structure of **4** was present as the enantiomer pair (R_{Sc},S_I)/(S_{Sc},R_I) and was found to have an orthorhombic space group, *Pbca*. (**Figure 2.14**). The 4-coordinate scandium centre has a $\tau'_4 = 0.8811(11)$, indicating some distortion from tetrahedral geometry, but less than the PHENI* direct comparison **1** ($\tau'_4 = 0.8633(10)$).

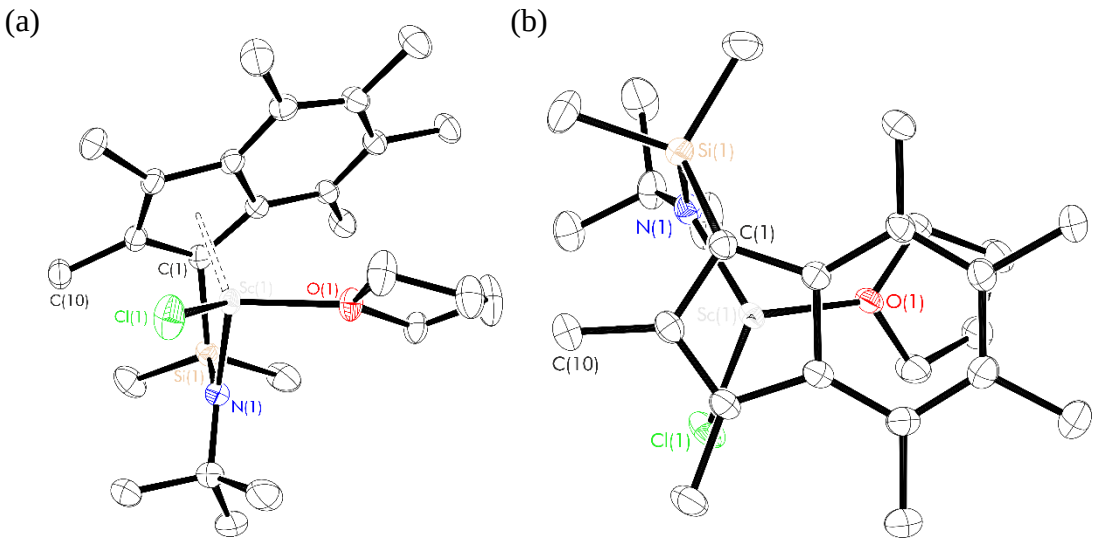


Figure 2.14 Side (a) and top down (b) view of solid-state structure of (R_{Sc},S_I)-**4.** (S_{Sc},R_I)-**4** not shown, but present in the unit cell. Ellipsoids are drawn at 30% probability and all hydrogen atoms are omitted for clarity.

The Sc–N bond length of 2.033(2) Å is shorter than the covalent radius sum for Sc and N (1.44 Å and 0.70(1) Å) of 2.14 Å.[2, 36] This is expected and has been reported by Bercaw *et al*. for the CGCI*-Sc complex [(Cp*SiNR)(PMe_3)Sc]$_2$(μ-H)$_2$, where the Sc–N bond distance is reported as 2.058(3) Å. Sc–N bond distances specifically reported for CGCI* scandium complexes have been reported between 2.026–2.086 Å (mean 2.049 Å).[17, 37, 38]

Bercaw *et al*. suggested that the electronegativity difference between Sc and N causes the bond distance to be shorter than expected.[2] The Sc–I*$_{cent}$ bond length of **4** (2.1426(12) Å) is shorter than reported Sc–I*$_{cent}$ distances for phenoxy substituted **7** and ^{Me_2}SB(^{t}Bu,N,I*)Sc(O-2,4-^{t}Bu$_2$C$_6$H$_3$)THF (2.1718(1) and 2.1786(1)).[16]

In general, the Sc–I*$_{cent}$ bond distances for **1**, **2**, **4**, **5**, and **7** are shorter when compared to Sc–Cp*$_{cent}$ bond lengths for scandium metallocene and half metallocene complexes, which are reported between 2.163–2.206 Å[37-39] or Sc–I$_{cent,}$ bond lengths which range between 2.228–2.253 Å.[40, 41] In this case, the order follows bond strength in general which has been shown to follow I* ≥ Cp* > I.[42] In general, the η^5-Cp-M bond is stronger than the η^5-I-M bond and the η^3-Cp-M bond is weaker than the η^3-I-M bond.[42] *Ansa*--bridge complexes have inherent distortion that leads to distortion of the Cp/Ind bonding mode. This leads to worse orbital overlap and lower bond strength. More η^3 character leads to a shorter, stronger bond, which more readily accessible for I/I* ligands.

2.5. Comparison of solid-state structure of 1, 2, 4, 5, and 7

The top-down view of the **1** (**Figure 2.15**) and **5** (**Figure 2.16**) present examples of the conformation A-*proximal*, **5**; and B-*distal*, **1**. Bulkier X ligands (ODipp) favour the A-*proximal* conformation over the B-*distal.* A list of selected parameters is presented in **Table 2.1** for **1**, **2**, **4**, **5**, and **7**.[16]

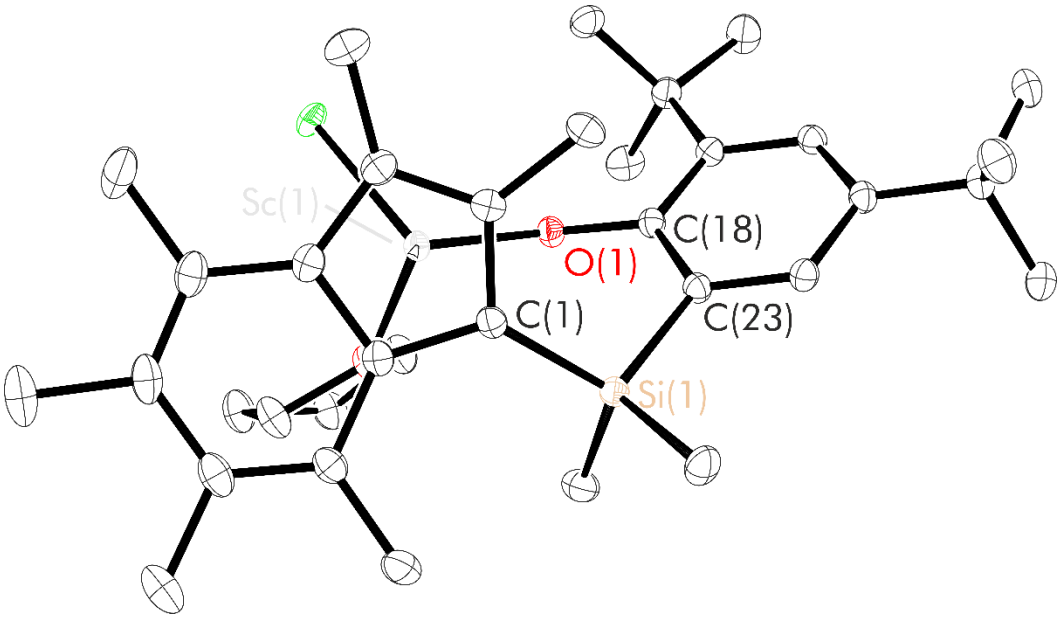


Figure 2.15 (Top down view) Solid state structure of (B-*distal*,R_{Sc},S_I)-**1**. (B-*distal*,S_{Sc},R_I)-**1** not shown, but present in the unit cell. Ellipsoids are drawn at 30% probability and all hydrogen atoms are omitted for clarity.

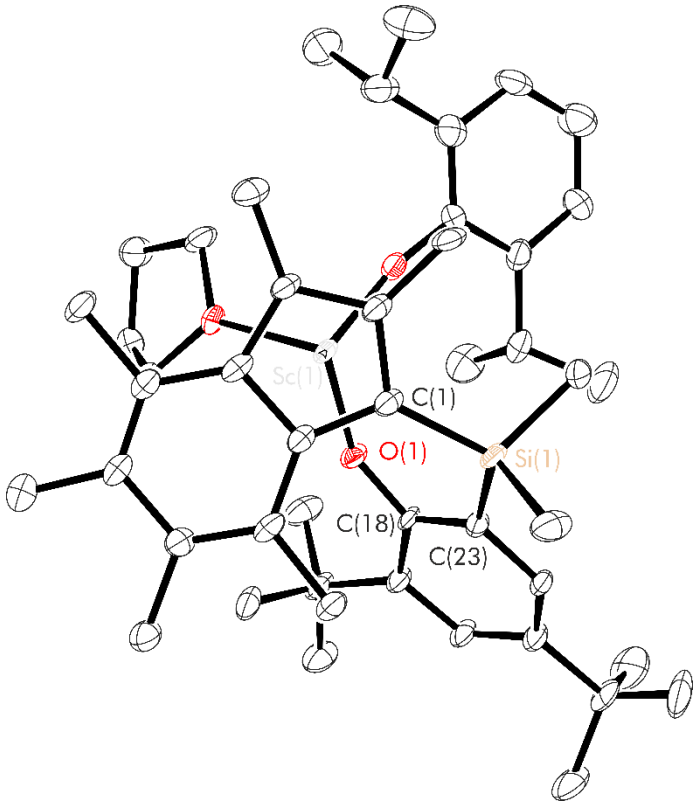


Figure 2.16 (Top town view) Solid state structure of (A-*proximal*,S_{Sc},S_I)-**5.** (A-*proximal*,$R_{Sc,}R_I$)-**5** not shown, but present in the unit cell. Ellipsoids are drawn at 30% probability and all hydrogen atoms are omitted for clarity

Table 2.1 Experimental metrical parameters (bond lengths (Å) and angles (°)) for **1**, **2**, **4**, **5**, and **7.** Estimated standard deviations shown in brackets

Parameter	**1**	**2**	**4**	**5**	**7**[16]
X[a]	Cl	Cl	Cl	ODipp	ODipp
^{Me_2}SB([**η^1**],I*)[b]	^{tBu_2}Ar**O**	^{Cumyl_2}Ar**O**	^{tBu}**N**	^{tBu_2}Ar**O**	^{tBu}**N**
Conformation	B-*distal*	B-*distal*	-	A-*proximal*	-
Sc–I*$_{cent}$	2.1522(3)	2.1443(15)	2.1426(12)	2.1574(15)	2.1718(1)
Sc–X	2.4311(6)	2.3917(10)	2.3890(9)	1.928(2)	1.9450(1)
Sc–O^{THF}	2.1296(15)	2.127(2)	2.1471(18)	2.160(2)	2.1686(1)
Sc–E[c]	1.8191(14)	1.920(2)	2.033(2)	1.9201(18)	2.0593(1)
I*$_{cent}$–Sc–X	*118.17(3)	118.39(5)	119.05(4)	120.06(7)	119.70(1)
I*$_{cent}$–Sc–O^{THF}	*120.94(5)	121.09(8)	117.37(7)	117.36(7)	112.56(1)
I*$_{cent}$–Sc– E	*114.48(5)	114.34(8)	104.92(7)	111.60(7)	103.99(1)
X–Sc–O^{THF}	94.02(5)	95.34(7)	96.91(5)	96.27(8)	102.13(1)
X–Sc– E	108.01(4)	106.74(7)	113.02(7)	107.72(8)	116.88(1)
O^{THF}–Sc– E	97.84(6)	97.54(9)	105.01(8)	101.44(8)	100.03(1)
TA(M) ϕ	31.44(17)	31.4(3)	58.4(2)	106.5(2)	60.61(1)
τ'_4	0.8633(10)	0.8605(16)	0.8811(11)	0.8751(14)	0.8813(1)
Δ_{M-C}	0.106	0.054	0.150	0.103	0.140
Fold angle[d]	5.94	5.94	3.17	5.41	4.16

For ^{Me_2}SB([**η^1**],I*)Sc(X).THF, [a] X is anionic ligand [b] [η^1] represents ^{tBu_2}Ar**O,** ^{Cumyl_2}Ar**O,** or ^{tBu}**N** where specified and [c] **E** is hetero atom on *ansa*-[η^1] moiety. [d] The angle between the plane containing C1, C2, and C3 and the plane containing C1, C3, C4, and C9.

With respect to the Sc-E (where E is the hetero atom on the [η^1] moiety which represents ^{tBu_2}Ar**O,** ^{Cumyl_2}Ar**O,** or ^{tBu}**N),** the Sc–N bonds on both **4** and **7** are shorter on average than the Sc–O bonds on **1**, **2**, and **5**. There is an inverse correlation between the length of the Sc–E bonds and the length of the Sc–O (THF) bond (**Figure 2.17**).

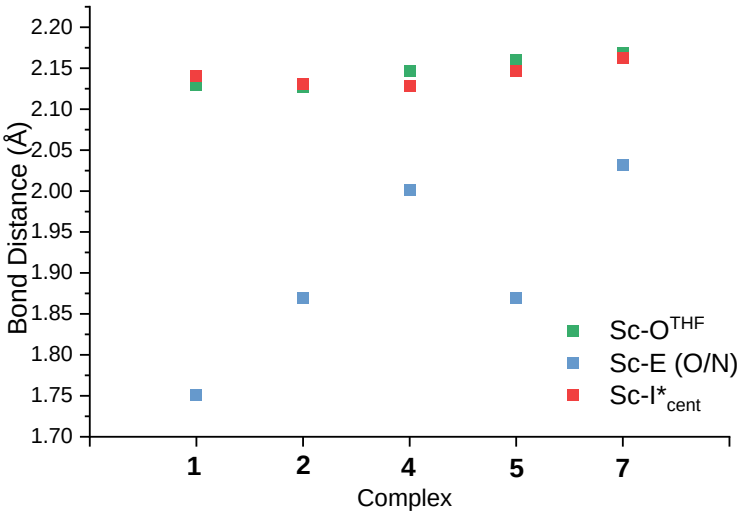


Figure 2.17 Selected bond-lengths for **1**, **2**, **4**, **5**, and **7** (Sc-O^{THF}; Sc-E, where E is hetero atom on *ansa*-[η^1] moiety; Sc-I*$_{cent}$).

This suggests that the stronger the bond between the scandium and the pendant heteroatom, the weaker the bond between the scandium and the ligated THF. The scandium is accepting more charge from the heteroatom and less from the ligated THF. Further, the substitution of Cl to ODipp from **1** to **5**, leads to an increase in Sc-O bond length of the phenoxy-scandium bond from 1.8191(14) to 1.9201(18) Å. Conformational rearrangement, from *proximal* to *distal* and bond to lengthening are both features of the substitution.

Additionally, the Sc–I*$_{cent}$ bond distance also decreases slightly across the series: 2.1296(15) ≥ 2.127(2) > 2.033(2) Å for **1** ≥ **2** > **4**. It is likely that Sc–I*$_{cent}$ bond distance changes are a combination of alleviation of intramolecular steric strain and electronic effects from the neutral donor (ligated THF in this case).

For equivalent PHENI* titanium(IV) complexes, where X = L = I, as for ^{Me2}SB(^{tBu2}ArO,I*)TiI$_2$, both of the A-*proximal* and B-*distal* conformations of the complex are present in the solid-state.[7] However, where the non-methylated indenyl is

used, only the B-*distal* conformation is reported in the literature as for ^{Me_2}SB(^{tBu,Me}ArO,I)TiCl$_2$.[6]

For CGCI* complexes, the *ansa*-bridge contains only a silicon and nitrogen atom, whereas the PHENI* has a more flexible, longer I*-SiCCO arm with more degrees of freedom.[43] Distortion in CGCI* complexes is minimal. TA(M) is close to 60° for both **4** and **7** (TA(M) 6 = 58.4°; **7** = 60.61°).

It has previously been reported that η^5-I is better described as $\eta^2 + \eta^3$ coordination.[42] Indicators of the amount of η^2 bonding involved include: the ring slip parameter ($\Delta_{M\text{-}C}$) which indicates the degree of η^5- or η^3- coordination (where completely η^5- coordination (or equal $\eta^2 + \eta^3$) $\Delta_{M\text{-}C} = 0$) and fold angle where lower angles around ~4° related to η^5-coordination compared to η^3- coordination around ~21°.[44, 45] A complete definition of $\Delta_{M\text{-}C}$ is found in the appendix (**A.1.1**).

$\Delta_{M\text{-}C}$ is greater for **4** and **7** at $\Delta_{M\text{-}C}$ = 0.150 and 0.140 than for the PHENI* complexes **1**, **2**, and **5** which range from $\Delta_{M\text{-}C}$ = 0.054–1.06. This would suggest greater distortion towards η^3- coordination for the CGCI* complexes, however the fold angle for **1**, **2**, **4**, **5** and **7** was found to be in the region of 3.17–5.94°, close the that of η^5- coordination complex showing that all occur with η^5- coordination to the scandium centre (**Figure 2.18**).

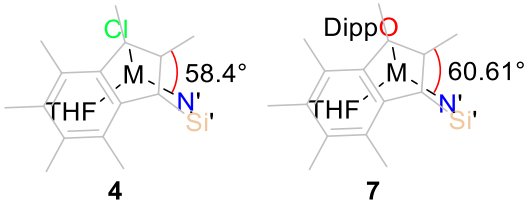


Figure 2.18 Top down conformational comparision of **4** and **7**. Solid-state TA(M) angle shown in red.

The additional degrees of freedom by from -amido to -phenoxy allows more conformations to be possible and stable in solution. Local energy minima for the A-*proximal* and B-*distal* conformations of the PHENI* Sc systems was calculated using r^{2}SCAN-3c: an efficient composite electronic structure method that uses semi-local density-functional theory (DFT).[46] By combing conformational isomerisation, A-*proximal* and B-*distal* and R_{Sc}/S_{Sc} isomerisation a set of 4 diastereomers are created: (A-*proximal*,R_{Sc}), (A-*proximal*,S_{Sc}), (B-*distal*,R_{Sc}), and (B-*distal*,S_{Sc}); and were used as inputs for the calculations (indenyl chirality is constant, i.e. always (S_I)). The lowest energy isomer is the structure observed experimentally in the solid state for **1** and **5** as shown in **Figure 2.19**. For **(**B-*distal*,R_{Sc},S_I)-**5**, the calculated dihedral angle for the optimised structure is smaller at 99.11° than the recorded solid-state dihedral angle (SSA) of 106.5°. By comparison, the r^{2}SCAN-3c optimised structure of (A-*proximal*,R_{Sc},S_I)-**1** is much closer at 31.51° to the solid-state angle of 31.44°. ΔG between the optimised conformations of **(**A-*proximal*,S_{Sc},S_I)**/(**B-*distal*,S_{Sc},S_I))-**5** is larger, at 3.96 kcal mol^{-1}, than for the optimised conformations of (A-*proximal*,R_{Sc},S_I)/(B-*distal*,R_{Sc},S_I)-**1**, of 2.20 kcal mol^{-1}.

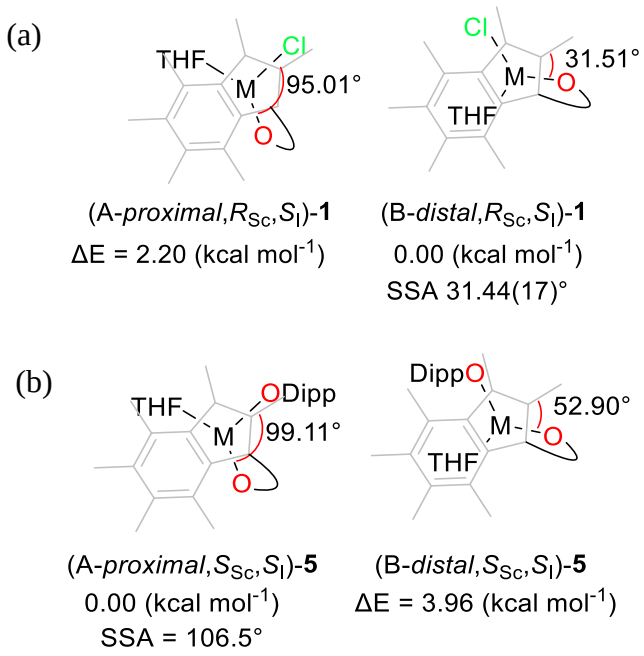


Figure 2.19 Computed Gibbs energy profile of (a) (A-*proximal*,R_{Sc},S_I)-**1**, (B-*distal*,R_{Sc},S_I)-**1** and (b) (A-*proximal*,S_{Sc},S_I)-**5**, **(**B-*distal*, S_{Sc},S_I)-**5**. The relative energies are computed using r^{2}SCAN-3c and presented as ΔG (kcal mol^{-1}) relative to the solid-state structure. Calculated dihedral angle ϕ TA(M) shown in red. Measured solid state dihedral angle (SSA) shown below strucutre where appropriate.

2.5.1. Ligand Shielding

Analysis of ligand coverage or 'shielding' of the metal centre can help to rationalise the influence of the ligand scaffold on reactivity, with increased shielding of the metal centre often correlated with decreased catalytic activity in polymerisation.[47] By blocking the active site, the metal centre in the case of polymerisation, polymerisation activity of the complexes can be rationalised. Algorithms have been developed to quantify metal-ligand coordination interactions, such as the percentage of the metal sphere shielded. Using the *SuperG* program developed by Guzei and Wendt,[48] the parameter $G_{2.28}$(Ligand) is calculated for each ligand as the percentage coverage of the ligands if the metal centre were a light source projecting on a sphere (**Figure 2.20**).

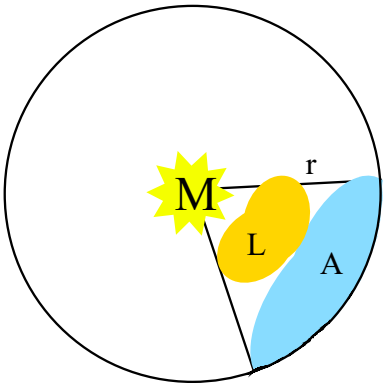


Figure 2.20 Ligand casting a shadow (A) related to the solid angle Ω. Where $\Omega = A/r^2$.

The sum of the coverage minus the overlap gives the proportion of the sphere shielded by the ligands: *G(%)*:∑*G*(Ligand)-overlap. Overlap can be calculated by considering each ligand individually, or pairs of ligands to analyse specific overlap. More complex 'shadows' can be analysed; an improvement over Tolman cones angles.[49] This allows improved ligand comparison. M-Ligand distance is normalised to 2.28 Å in most cases to provide a quantitative comparison between values.

2.5.1.1. Ligand shielding comparisons of 1, 2, 4, 5, and 7

Using the solid-state structures, the results for PHENI* scandium chloride complexes **1** and **2** are detailed in **Table 2.2** and visual representations shown in **Figure 2.21**.

Table 2.2 Summary of ligand solid angles (*Ω*) for **1**, **2** and **4**. *Ω*(Lignad) solid angle of the ligand *G*(Ligand): proportion of the sphere shielded by the ligand. *G(%)*:∑*G*(Ligand)-overlap. *G*(Sc): proportion of the scandium surface shielded by the ligated atoms only. *S*(Sc): proportion of the Sc surface "in contact" with the ligated atoms.

	***Ω*(*P*) (sr)**	***Ω*(X) (sr)**	***Ω*(L) (sr)**	***G*(P) (%)**	***G*(L) (%)**	***G*(R) (%)**	***G*(%)**	$G_{2.28}$**(P) (%)**	$G_{2.28}$**(X) (%)**	$G_{2.28}$**(L) (%)**	***G*(Sc) (%)**	***S*(Sc) (%)**
[a]**1**	7.61	1.62	2.24	60.56	12.89	17.82	90.12	54.18	14.40	16.67	73.42	68.88
[b]**2**	7.94	1.61	2.07	63.17	12.84	16.47	90.57	58.39	14.36	14.72	73.90	69.55
[c]**4**	7.52	1.62	1.99	59.88	12.87	15.86	87.92	54.34	14.39	14.41	71.81	67.59

[a]*P* = ^{Me_2}SB(^{tBu_2}ArO,I*); [b]*P* = ^{Me_2}SB(^{Cumyl_2}ArO,I*); [c]*P* = ^{Me_2}SB(^{tBu}N,I*). X = Cl, L = THF.

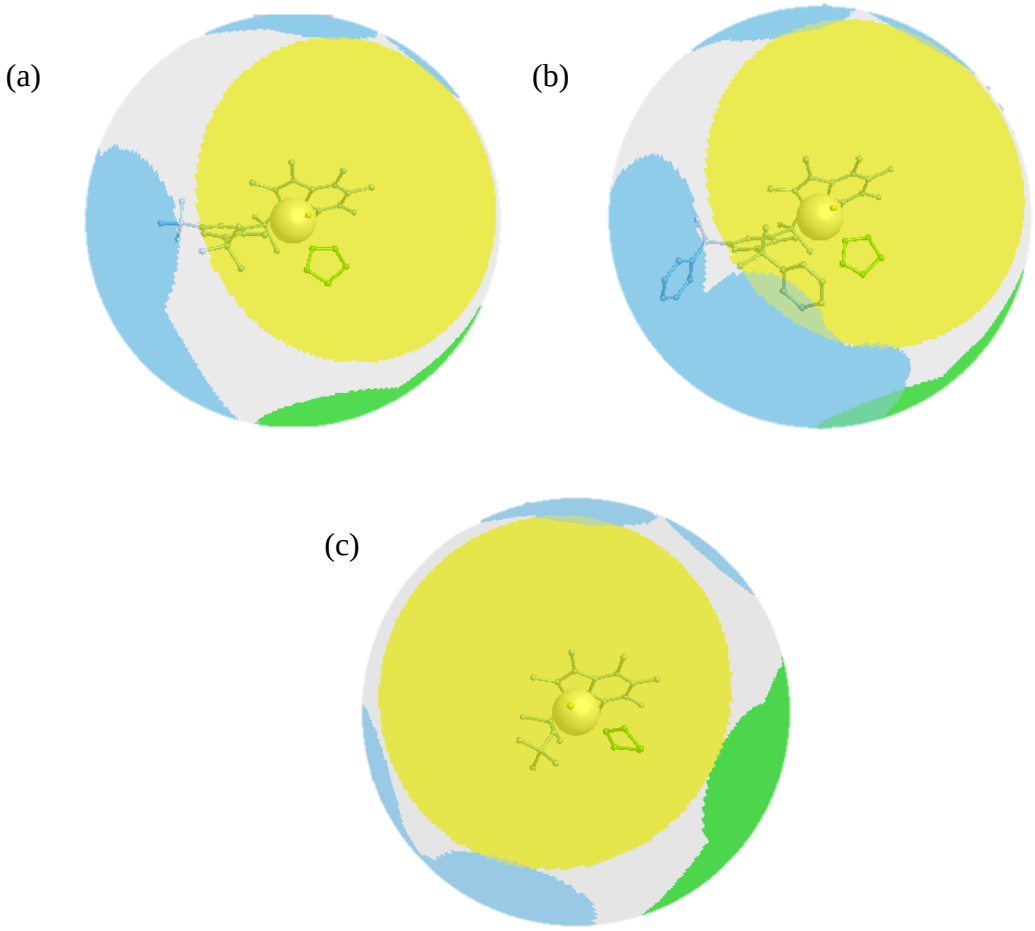


Figure 2.21 Visualisation of G(L) values for **1** (a), **2** (b), and **4** (c) showing the proportion of the complex sphere shielded by each ligand (blue = ^{Me_2}SB([η^1],I*); yellow = Cl; green = THF).

Complexes **1** and **2** exhibit similar steric coverage for the PHENI* ligand, slightly increased in **2** due to the larger cumyl groups and both larger than the equivalent value for the CGCI* scaffold. The calculated ligand coverage (G(Ω)) increase from **2** > **1** > **4**; 63.17% > 60.56% > 59.88% is relatively minor.[50] From this, electronic effects of the substituents are more likely to have an impact on changes to activity. As discussed in **Section 2.6**, the energy between conformations in small as the bridge does not contain rigidity.

The ligand coverage is greater for **5** than for either **1** or **2**, which is expected due to the size difference of the ODipp *vs* Cl ligands. *G*(Sc) = 76.47% of the metal surface is

shielded by the ligands compared to 73.42% for **1**. The ligand coverage is summarised in **Table 2.3** with visual representation of complex sphere in **Figure 2.22**.

Table 2.3 Summary of ligand solid angles (Ω) for **5** and **7**. *Ω*(Ligand) solid angle of the ligand $G_{2.28}$(Ligand):% of the sphere shielded by the ligand,. *G*(Sc):% of the Scandium surface shielded by the ligated atoms only. *S*(Sc):% of the Sc surface "in contact" with the ligated atoms.

	***Ω*(P) (sr)**	***Ω*(X) (sr)**	***Ω*(L) (sr)**	***G*(P) (%)**	***G*(X) (%)**	***G*(L) (%)**	***G***	$G_{2.28}$**(P) (%)**	$G_{2.28}$**(X) (%)**	$G_{2.28}$**(L) (%)**	***G*(Sc) (%)**	***S*(Sc) (%)**
[b]**5**	7.39	2.87	2.02	58.84	22.80	16.06	93.42	51.77	18.77	15.43	76.47	72.50
[a]**7**	7.30	2.84	1.99	58.07	22.56	15.83	93.32	52.90	18.78	15.78	74.41	70.21

[a]P = ^{Me_2}SB($^{t Bu_2}$ArO,I*); [b] P = ^{Me_2}SB($^{t Bu}$N,I*). X = ODipp, L = THF

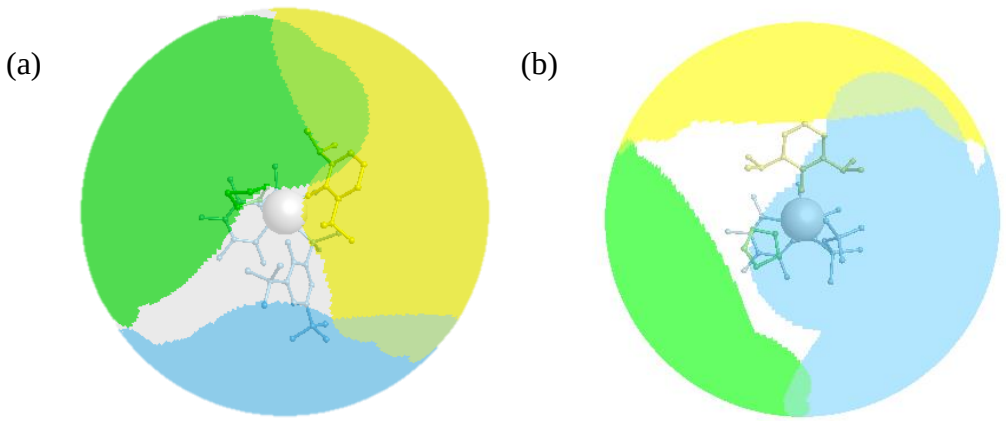


Figure 2.22 Visualsation of G(L) values for **5** (a), **7** (b) showing the percentage of the complex sphere shielded by each ligand (Blue = ^{Me_2}SB([η^1],I*)); Yellow = ODipp; Green = THF).

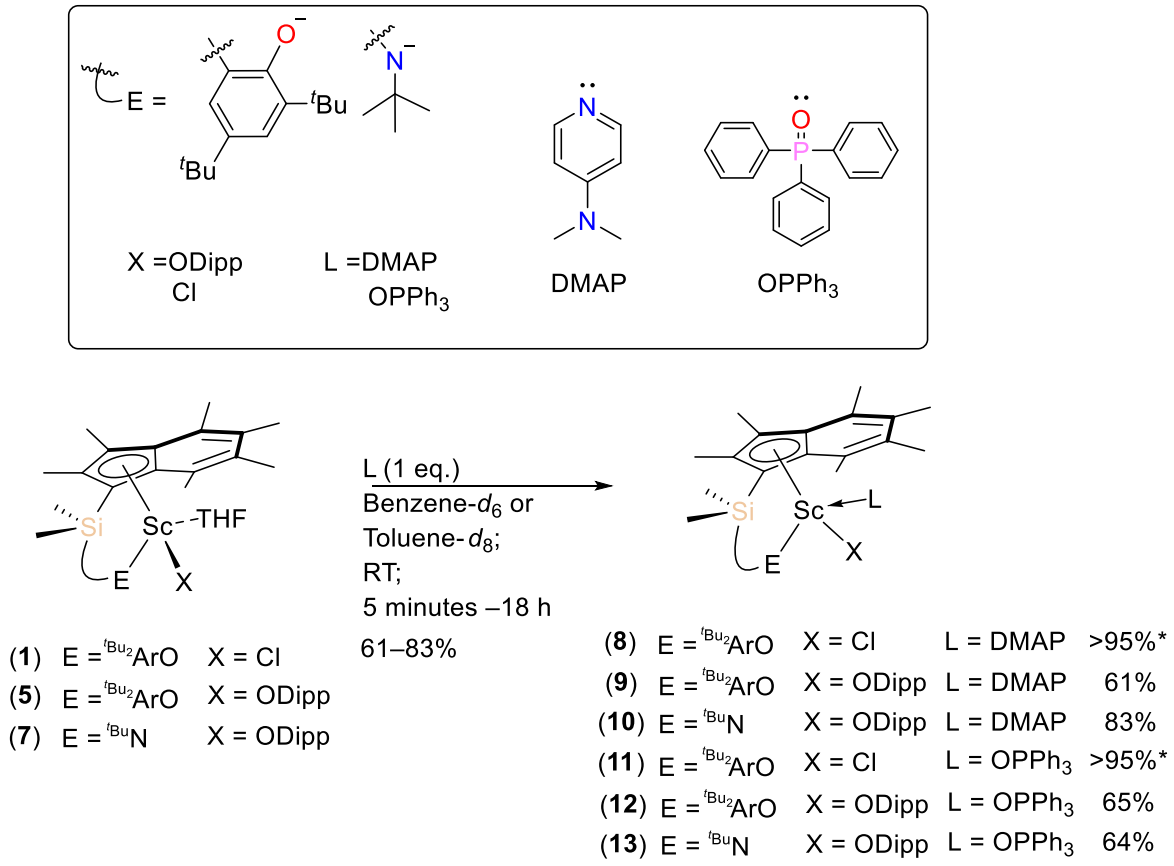
2.5.2. Structure and catalytic activity

Although a comparison can be drawn between the A-*proximal* and B-*distal* conformations using sphere shielding, there is a small difference between different conformations of the same the ligand coverage. For ^{Me_2}SB($^{t Bu_2}$ArO,I*) ligand coverage is

60.56% for A-*proximal* and 58.84% for the B-*distal* conformation. As the difference in coverage is small, the steric effects are likely less impactful than the electronic effects when rationalising reactivity.[50] Monomer approach, stabilisation of the active species,[1] and flexibility of ligand allows uptake of different sized substrates or monomers.[6] In addition, changes to substituents seemingly remote from the active site have been previously shown to have a profound effect on the activity of catalysts.[7, 50-52]

2.6. Ligand substitution reactions with 1, 5, and 7

Substitution of the ligated THF with different neutral donors provides additional information on the conformational, electronic, and steric properties of the PHENI* complexes. 4-Dimethylaminopyridine (DMAP) and triphenylphosphine oxide ($OPPh_3$) were reacted with **1, 5**, or **7** in benzene-d_6 or toluene-d_8, displacing THF to form DMAP (**8**–**10**) and $OPPh_3$ (**11**–**13**) complexes of the form ^{Me_2}SB([η^1],I*)Sc(X)L (where: ^{Me_2}SB($^{t Bu_2}$ArO,I*)Sc(Cl)DMAP (**8**), ^{Me_2}SB($^{t Bu_2}$ArO,I*)Sc(ODipp)DMAP (**9**), ^{Me_2}SB($^{t Bu}$N,I*)Sc(ODipp)DMAP (**10**), ^{Me_2}SB($^{t Bu_2}$ArO,I*)Sc(Cl)$OPPh_3$ (**11**), ^{Me_2}SB($^{t Bu_2}$ArO,I*)Sc(ODipp)$OPPh_3$ (**12**), ^{Me_2}SB($^{t Bu}$N,I*)Sc(ODipp)$OPPh_3$ (**13**). The resulting pale-yellow solutions were freeze dried to afford off-white microcrystalline powders of **9**, **10**, **12** and **13** in 63–85% yields (**Scheme 2.6**).



(**1**) E = ^{tBu_2}ArO X = Cl
(**5**) E = ^{tBu_2}ArO X = ODipp
(**7**) E = ^{tBu}N X = ODipp

(**8**)	E = ^{tBu_2}ArO	X = Cl	L = DMAP	>95%*
(**9**)	E = ^{tBu_2}ArO	X = ODipp	L = DMAP	61%
(**10**)	E = ^{tBu}N	X = ODipp	L = DMAP	83%
(**11**)	E = ^{tBu_2}ArO	X = Cl	L = $OPPh_3$	>95%*
(**12**)	E = ^{tBu_2}ArO	X = ODipp	L = $OPPh_3$	65%
(**13**)	E = ^{tBu}N	X = ODipp	L = $OPPh_3$	64%

Scheme 2.6 Synthesis of ^{Me_2}SB([η^1],I*)Sc(X)L ^{Me_2}SB(^{tBu_2}ArO,I*)Sc(Cl)DMAP (**8**), ^{Me_2}SB(^{tBu_2}ArO,I*)Sc(ODipp)DMAP (**9**), ^{Me_2}SB(^{tBu}N,I*)Sc(ODipp)DMAP (**10**), ^{Me_2}SB(^{tBu_2}ArO,I*)Sc(Cl)$OPPh_3$ (**11**), ^{Me_2}SB(^{tBu_2}ArO,I*)Sc(ODipp)$OPPh_3$ (**12**), ^{Me_2}SB(^{tBu}N,I*)Sc(ODipp)$OPPh_3$ (**13**).* as calculated *via* NMR spectroscopy.

During the ligand exchange, the stronger Lewis base exchanges with THF either by associative or dissociative substitution and this is explored in **Chapter 3**. Enthalpy of complexation with boron trifluoride ($\Delta H^o_{BF_3}$) has been developed by Gal and co-workers to provide a method for comparing donor strength of Lewis bases. As there is no universal method for comparison of Lewis bases, a reference Lewis acid (BF_3 in this case) is required to generate a relative order.[53] A general order from literature for the enthalpy of formation is presented where DMAP > OPR_3 > THF (36.2 ± 0.18 > 28.2 ± 0.22–29.3 ± 0.03 > 21.6 ± 0.07 kcal mol^{-1}) (**Table 2.4**).

Lewis base (L)	$\Delta H^{o}_{BF_3}$ (CH_2Cl_2)[a]
THF	21.6 ± 0.07
γ-Butyrolactone	18.2 ± 0.3
PMe_3	23.6 ± 0.07
$OP(NC_4H_8)_3$	28.2 ± 0.22
$OP(NC_5H_{10})_3$	29.3 ± 0.03
DMAP	36.2 ± 0.18

Table 2.4 [a] Enthalpies of complex formation with boron trifluoride in dichloromethane in kcal mol^{-1}.[54-57]

The reactions were monitored using ^{1}H NMR spectroscopy; release of THF and the formation of new organometallic complexes with C_1 molecular symmetry consistent with proposed formulas are observed. Isomers in chemical exchange are observed for **8**, **9**, and **11** through positive correlation in ^{1}H-^{1}H NOESY spectra and is discussed in **Chapter 3**.

Ligand substitution has been reported by Bercaw *et al.* using scandium half metallocene complexes for the formation of THF free ^{Me2}Si($^{t\text{Bu}}$N,Cp*)Sc(C_6H_5)PMe_3, ^{Me2}Si($^{t\text{Bu}}$N,Cp*)Sc(H)PMe_3 and ^{Me2}SB($^{t\text{Bu}}$N,$^{t\text{Bu}}$Cp)ScCl(PMe_3) from THF-scandium adducts.[2, 58]

2.6.1. NMR spectroscopic characterisation of ^{Me2}SB([η^1],I*)Sc(X)DMAP ([η^1] = $^{t\text{Bu}2}$ArO and X = Cl (8), X = ODipp (9); [η^1] = $^{t\text{Bu}2}$N and X = ODipp (10))

^{1}H NMR spectroscopy of complex **9** presented an equilibrium mixture of two species in an approximate ratio 40:1 (**Figure 2.23**). The aromatic 2,6-NC_6H_4 and 3,5-NC_6H_4 proton resonances appear as doublets of doublets at δ 7.39 and 5.63 ppm and integrate to 2H each. The 2,6-NC_6H_4 protons have coupling constants of $^3J_{H-H}$ = 5.6 and $^4J_{H-H}$ = 1.6 Hz for coupling with the neighbouring *proximal/distal* protons. 3,5-NC_6H_4 protons show

coupling, with $^{3}J_{H–H}$ = 5.6, $^{4}J_{H–H}$ = 1.3 Hz. A singlet at δ 1.88 ppm integrating to 6H, corresponds to the DMAP-N*Me*$_2$ signal. The diagnostic features of the PHENI* backbone are present. The secondary resonances were suggestive of a single additional rotamer in solution, which was confirmed through positive correlation in the ^{1}H-^{1}H NOESY spectrum.

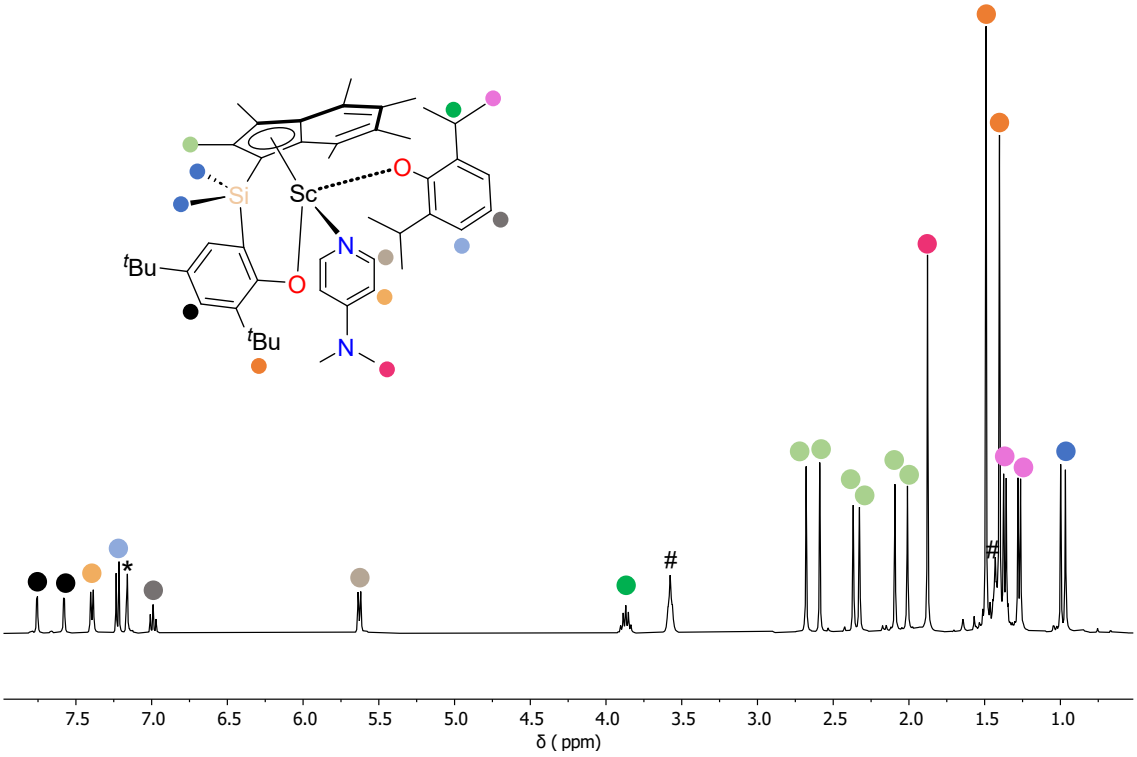


Figure 2.23 ^{1}H NMR spectrum (400 MHz, benzene-d_6, 298 K) of (**9**). * denotes residual protio solvent, # denotes free THF at δ 3.58 and 1.43 ppm.

The PHENI* ScCl DMAP complex **8** exists as a mixture of conformers in dynamic equilibrium in benzene in a ratio of 13:1 as judged by ^{1}H-^{1}H NOESY spectroscopy. The CGCI* complex **10** only displays a single product forming with the displacement 1 equiv. of THF indicting complete conversion.

2.6.2. NMR spectroscopic characterisation of ^{Me_2}SB([η^1],I*)Sc(X)OPPh$_3$ ([η^1] = ^{tBu_2}ArO and X = Cl (11), X = ODipp (12), [η^1] = ^{tBu}N and X = ODipp (13))

The reactions of **1**, **5** and **7** with $OPPh_3$ each formed a mixture of species consistent with a 4-coordinate Sc metal complex, with bound η^5-,η^1-PHENI*, ODipp/Cl, and labile $OPPh_3$ ligands (**11–13**) in C_1 symmetry. **12** and **13** formed a mixture of kinetic (**K**) and thermodynamic (**T**) products where **12-T** and **13-T** products were the major species once dynamic equilibrium has been reached. For **12**, the signals corresponding to **12-T** in the ^{1}H NMR spectrum show characteristic I*Me proton as six resonances that integrate to 3H each in the range δ 2.75–1.97 ppm; the signal pattern is very similar to that of (A-*proximal*,S_{Sc},S_I)/(A-*proximal*,R_{Sc},R_I)-**5**. Two SiMe protons are present as singlet resonances at δ 1.06 and 1.05 ppm and integrate to 3H each. The OPPh protons present as multiplet resonances between δ 7.30–6.82 ppm and integrate to 15H in total. The -CHMe_2 protons resonances appear as very broad signals in the baseline at 25 °C but at elevated temperature (373 K) are observed as two broad singlets at δ 1.18 and 0.83 ppm that integrate to 6H each (**Figure 2.24**).

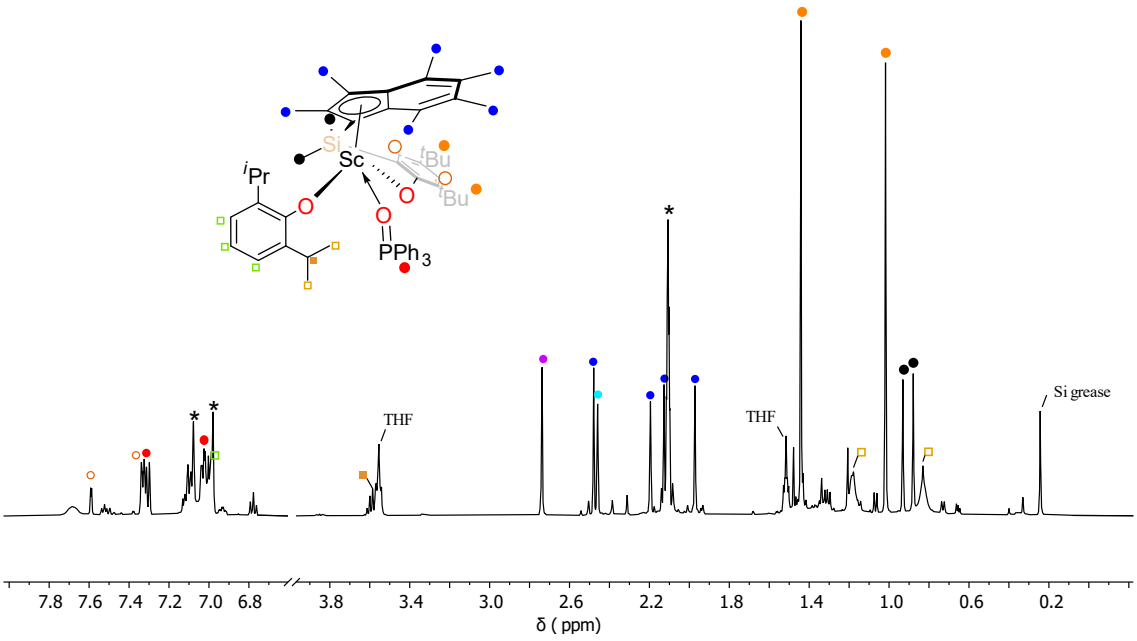


Figure 2.24 ^{1}H NMR spectrum (500 MHz, toluene-d_8, 373 K) of ^{Me_2}SB(^{tBu_2}ArO,I*)Sc(ODipp)OPPh$_3$ (**12**). (A-*proximal*,S_{Sc},S_I)/(A-*proximal*,R_{Sc},R_I)-**12 (12-T)** labelled.

Analysis of the ^{1}H-^{1}H NOESY spectrum of **12**, the thermodynamic product **12-T** is confirmed as the (A-*proximal*,S_{Sc},S_I)/(A-*proximal*,R_{Sc},R_I) enantiomer pair; through space correlation between the ^{i}Pr-ODipp proton signals to the two 2,3-I*Me* proton resonances and one Si*Me* proton resonance. In addition, the Si*Me* proton resonances are very close together, with a splitting of Δ 0.01 ppm, similar to the close splitting in **5** of 0.03 ppm suggesting a A-*proximal* conformation is solution.

A similar study was conducted for the PHENI* Sc Cl complex **1**. The addition of OPPh$_3$ to **1** was monitored *via* ^{1}H NMR spectroscopy. At *t* = 5 minutes, the spectrum shows the formation of a mixture of isomers of the formula ^{Me_2}SB(^{tBu_2}ArO,I*)Sc(Cl)OPPh$_3$ (**11**) (**Figure 2.25**). The species was not isolated. For the major species, six resonances corresponding to the I*Me* are present between δ 2.83 and 1.82 ppm. The 2,4-^{t}*Bu*

resonances can be distinguished, 2-^{t}*Bu* at δ 1.60 ppm and 4-^{t}*Bu* at δ 1.50 ppm, by analysis of the ^{1}H-^{1}H NOESY NMR spectrum. The Si*Me* singlet resonances occur at δ 1.06 and 0.65 ppm with a large separation of δ 0.43 ppm, suggesting the same conformation, B-*distal*, as **1** is present in solution. Resonances of the P-2,6-C_6H_5 protons on the $OPPh_3$ ligand display as a multiplet at δ 7.44–7.36 ppm and correlated through space with the 2-^{t}*Bu* resonance and the Si*Me* proton resonance at δ 0.65 ppm. The 3-C_6H_2 and 5-C_6H_2 protons can also be assigned to resonances that present as two doublets at δ 7.77 and 7.65 ppm, integrating at 1H each and with $^{4}J_{H\text{-}H}$ = 2.5 Hz.

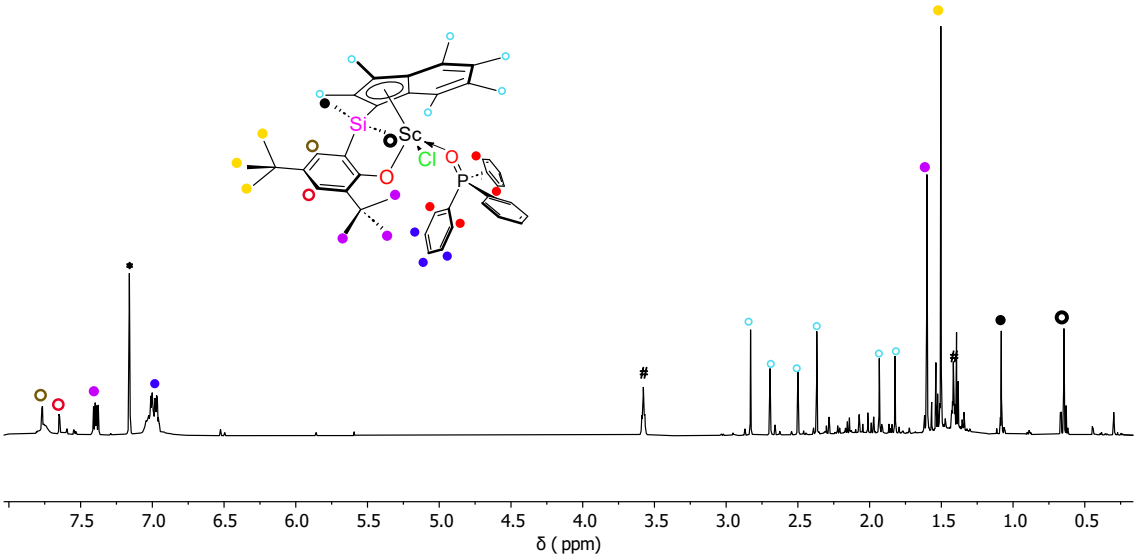


Figure 2.25 ^{1}H NMR spectrum of ^{Me_2}SB($^{t Bu_2}$ArO,I*)Sc(Cl)$OPPh_3$ **11** (600 MHz, benzene-d_6 298 K).* denotes residual protio solvent; # denotes THF.

The reaction of $OPPh_3$ with **7** to form ^{Me_2}SB($^{t Bu}$N,I*)Sc(ODipp)$OPPh_3$ (**13**) shows the same characteristics as the formation of **12**, where two major species form initially in a ratio of 3:1, interconverting to form an equilibrium in the ratio of 1:10, after a 16 h period at 25 ℃.

The $^{31}P\{^{1}H\}$ NMR spectra of **11**, **12**, and **13** show multiple resonances at in the region of δ 41–39 ppm confirming multiple scandium phosphine adducts corresponding to the different isomers present in solution. Resonance of similar scandium OPR_3 coordination complexes also show ^{31}P resonances around δ 40 ppm such as for tethered $^{Me2}SBMe(Cp,O(PPh_2))Sc(SiMe_3)_2$ (δ 46.6 ppm). The ^{31}P signal is reported to occur at δ 27.9 ppm for uncoordinated $C_5HMe_4CH_2SiMe_2(O)PPh_2$ ligand.[59-61]

2.7. DFT calculations on isomers of PHENI* and CGCI* complexes

The relative energies of the structures of **1**, **5**, 7, **11**, **12,** and **13** were considered. The set of *n* isomers with S_I geometry (*n* = 4 for **1**, **5**, **11**, and **12;** *n* = 2 for **7** and **13**) are considered. The stereogenic units altered were the metal stereocentre S_{Sc}/R_{Sc} in addition to the metallocyclic ring puckering for **1**, **5**, **11**, and **12** to form A-*proximal*/B-*distal* isomers. Energies were calculated using r^{2}SCAN-3c though analysis of local minima (**Figure 2.26**).[46] A discussion on the method can be found in section **3.2.6**.

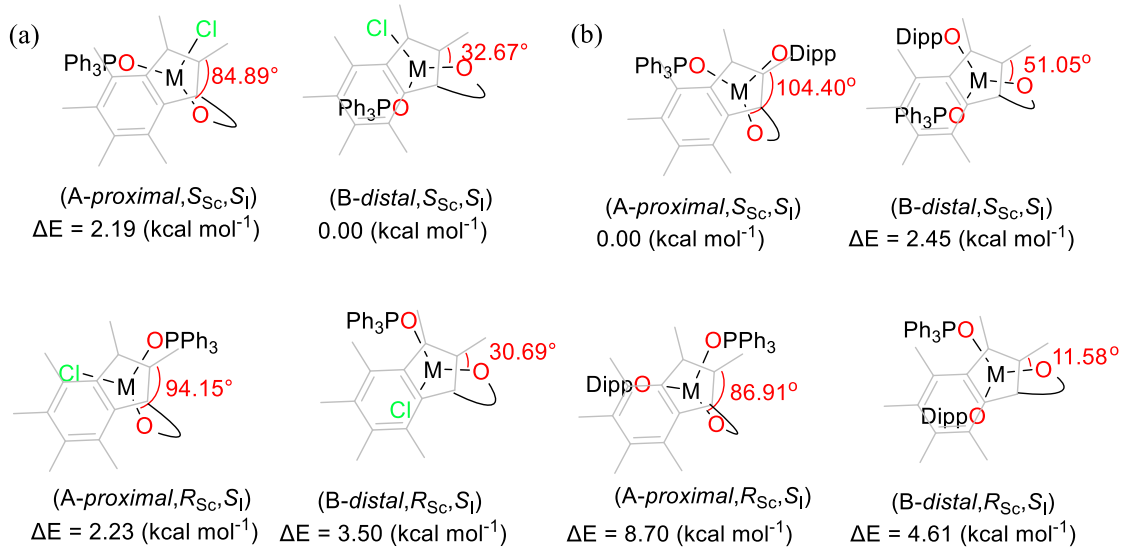


Figure 2.26 Computed Gibbs energy profile for isomers of (a) **11** and (b) **12**. The energies are computed using r^{2}SCAN-3c and presented as Δ*G* (kcal mol^{-1}) relative to the lowest energy conformation. Dihedral angle ϕ TA(M) shown in red.

The relative predicted lowest energy of the isomers of **1**, **5**, 7, **11**, **12,** and **13** was confirmed by experimental data from NMR spectroscopy data in addition to the solid-state data for **1** and **5** (**Table 2.5 and Figure 2.27**). For **1** and **11**, the three species – (A-*proximal*,S_{Sc}), (B-*distal*,S_{Sc}), and (A-*proximal*,R_{Sc}) are proposed to be the isomers observed in the ^{1}H NMR spectra at 298 K. DTF is consistently predicting structures that are relatively close in energy all calculated at < 2.23 kcal mol^{-1}. For **12**, the free energy calculations would predict the lowest energy conformation to be (A-*proximal*,S_{Sc}), and (B-*distal*,S_{Sc}). However, the species present in for **12** solution at RT are (A-*proximal*,S_{Sc}) and (B-*distal*,R_{Sc}).

Table 2.5 Computed Gibbs energy profile for isomers of **1**, **5**, **7**, **11**, **12**, and **13**. The energies are computed using r^{2}SCAN-3c and presented as Δ*G* (kcal mol^{-1}) relative to the lowest energy conformation.

	1	**5**	**7**	**11**	**12**	**13**
A-*proximal*,*S*$_{Sc}$	2.20	0.00	-	2.19	0.00	-
B-*distal*,*S*$_{Sc}$	0.00	3.96	0.00	0.00	2.45	0.00
A-*proximal*,*R*$_{Sc}$	1.52	4.69	-	2.23	8.70	-
B-*distal*,*R*$_{Sc}$	6.10	5.24	3.63	3.50	4.61	4.57

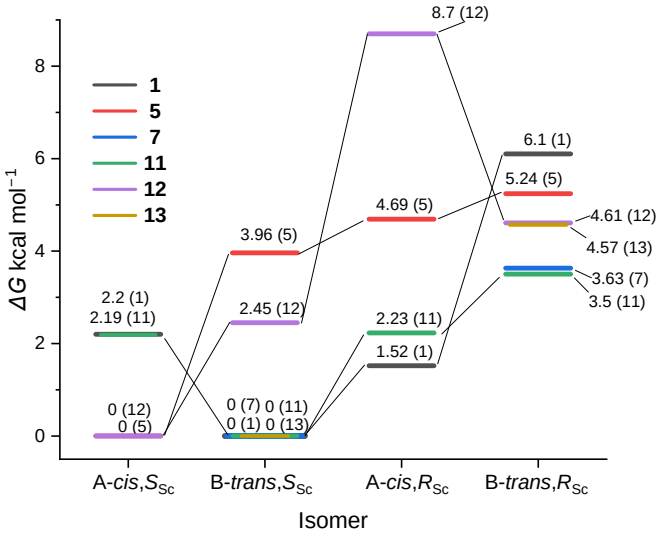


Figure 2.27 ΔG (kcal mol^{-1}) of **1**, **5**, **7**, **11**, **12**, and **13** [energy (complex)]. The relative energies are computed using r^{2}SCAN-3c and presented as ΔG (kcal mol^{-1}) relative to the lowest energy isomer.

2.8. ^{45}Sc NMR spectroscopy

^{45}Sc (100% abundant, $I = 7/2$) NMR spectra are often not reported in literature. Resonances are typically broad due to interaction of the quadrupolar nucleus with the electric field gradients due to a non-spherical distribution of charge. Anisotropy leads to line shape alteration and significant broadening compared to spin ½ nuclei.[62-64] A solid state ^{45}Sc NMR spectroscopy study reported by Conley *et al.* used DFT and experimental observations to examine scandocene halides Cp*$_2$Sc(X)THF (X = F, Cl, Br, and I; n = 0, 1; Cp* = C_5Me_5) complexes.[62] Of the tetrahedral coordinate complexes studied, Cp*$_2$Sc(F)THF had the smallest reported solid state ^{45}Sc NMR shift of δ^{iso} 12 ppm and

$Cp^*_2Sc(I)$ the largest at δ^{iso} 132 ppm.[62] (δ^{iso} is the isotropic chemical shift value used in solid-state NMR. This allows comparison of anisotropic chemical shifts)

As reported, for the $Cp^*_2Sc(X)$ compounds, the Sc-F bond (1.9274(12) Å) is significantly shorter than the Sc-I bond (2.8194(3) Å). This shorter distance increases the contribution from halide orbitals to the filled core scandium orbitals, resulting in greater shielding and an up-field shift. Additionally, the contribution is influenced by the polarisation of halide core electrons by valence orbitals, which depends on bonding distance and polarisability. Hence, as you move down the series, where halides become more polarisable, core contributions increase. However, the magnitude of the polarisability contribution is small when compared to the bonding contribution. The final conclusion is that both bond distance and polarisability should be considered when discussing the shift to high frequency in the ^{45}Sc NMR spectrum.

The CGCI* and PHENI* scandium complexes show three clear trends in the ^{45}Sc NMR resonances as presented in **Table 2.6**. The signal for CGCI* complexes in general is higher frequency with respect to the analogous complex with a PHENI*. For example, the signal for **4** vs **1** which are observed at δ 253 and 141 ppm respectively. Secondly, where Cl is substituted by ODipp, a lower chemical shift of the signal is observed such as that of **1** vs **5** at δ 141 and 52 ppm respectively. In this case, Cl is more polarisable but has a longer M-X bond, hence upon substitution, $OPPh_3$ provides increased shielding leading to the shift. Substitution of THF with DMAP and $OPPh_3$ results in a up field shift for $OPPh_3$ by δ 16–24 ppm and a downfield shift for DMAP of δ 7–9 ppm. This leads to the shielding trend which increases from DMAP < THF < $OPPh_3$.

Table 2.6 ^{45}Sc NMR (121 MHz) resonances for **1**, **4** ,**5** ,**7**–**13**.

	^{Me2}SB([**η^1**],I*)[a]	X	L	Sc-E[b,c]	Sc-X[c]	Sc-O^{THF}[c]	δ[d]	$\Delta\nu_{1/2}$
11	[O]	Cl	$OPPh_3$				125	8950
1	[O]	Cl	THF	1.8191(14)	2.4311(6))	2.1296(15)	141	5493
8	[O]	Cl	DMAP				148	5900
12	[O]	ODipp	$OPPh_3$				35	7788
5	[O]	ODipp	THF	1.9201(18)	1.928(2)	2.160(2)	52	8448
9	[O]	ODipp	DMAP				61	6218
4	[N]	Cl	THF	2.033(2)	2.3890(9)	2.1471(18)	253	1497
13	[N]	ODipp	$OPPh_3$				124	6946
7	[N]	ODipp	THF	2.0593(1)	1.9450(1)	2.1686(1)	148	8765
10	[N]	ODipp	DMAP				156	6714

[a][O] = ^{tBu2}ArO and [N] = ^{tBu}N, [b]E = [O], [N]. [c] in Å . [d]δ in (ppm)

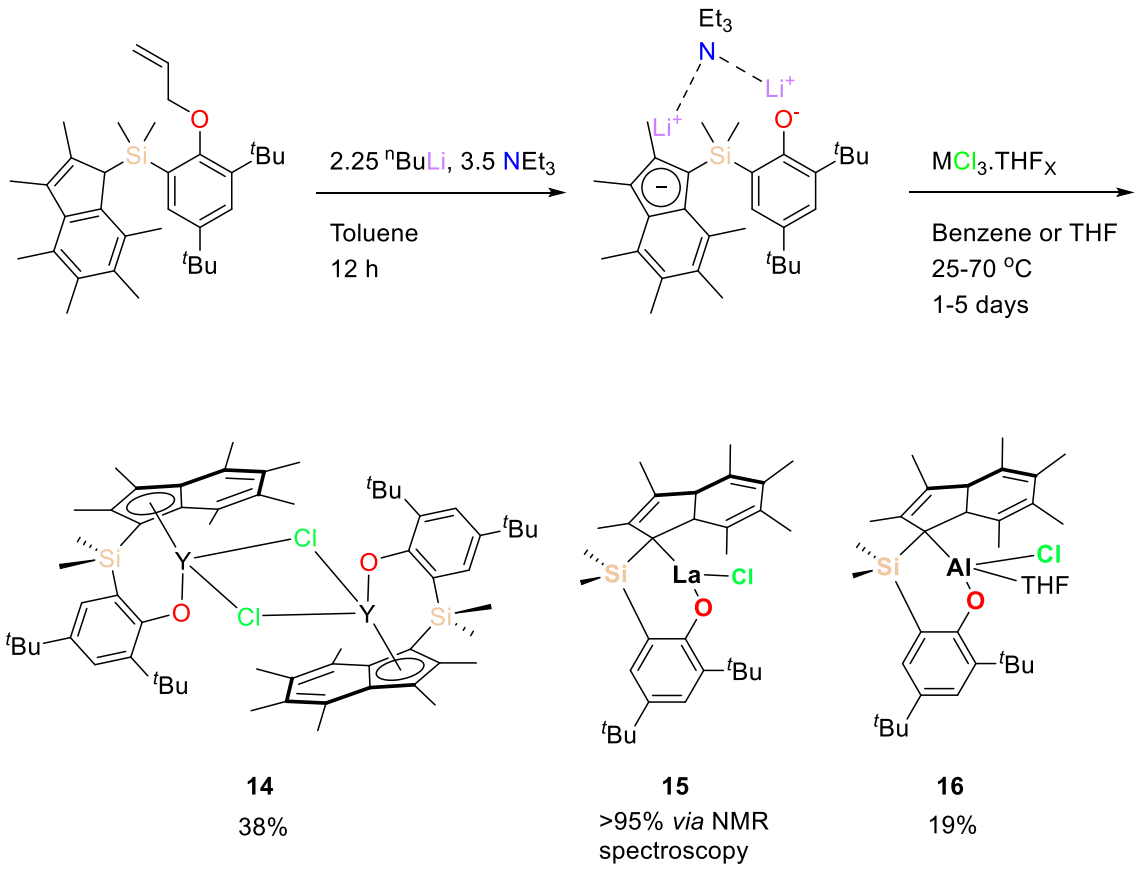
Ligand proximity to the scandium atom being the most significant indicator that relates to shielding, with Sc-O bonds being the shortest of those presented. Chloride provides less core contribution to the scandium valence orbital and hence the scandium resonance is at a higher frequency. Further, the Sc-N^{tBu} bond is longer than the Sc-OAr bond hence contributes less to shield the scandium nucleus. Sc-O^{OPPh3} bonds in literature have been reported from 2.036–2.068Å[65, 66] and Sc-N^{DMAP} bonds reported between 2.327–2.351 Å.[67, 68]

2.9. Attempted synthesis of M(III) PHENI* complexes

In addition to these scandium complexes, PHENI* complexes of groups 4/5 have been reported demonstrating the general applicability of the ligand. Complexes of tantalum, titanium, hafnium, and zirconium have been synthesised in yields of 1–31% and characterised by NMR spectroscopy and X-ray crystallography.[7]

2.9.1. General synthesis of ^{Me2}SB(^{tBu2}ArO,I*)M(Cl)THF$_x$ (M = Y, La, and Al)

From a modified preparation of the ligand, from which the lithiated PHENI* ligand is isolated, several different metal chloride complexes syntheses were attempted forming dimeric (Y) and σ- bonded complexes (La and Al) with the PHENI* ligand (**Scheme 2.7**). The ligand ^{Me2}SB(^{tBu2}ArOAllyl,I*)H was reacted with 1.05 or 1.1 equiv. of $MCl_3 \cdot THF_x$ (Y, x = 0; La, x = 3; Al, x = 1) in benzene, THF or toluene and heated if required. The reactions were tracked *via* ^{1}H NMR spectroscopy and performed at preparatory scale (approx. 1 g) in the case of **14**, **16**. (**14** 38%; **16**, 19%)



Scheme 2.7 Synthesis of the [^{Me2}SB(^{tBu2}ArO,I*)YCl]$_2$ **14**, ^{Me2}SB(^{tBu2}ArO,I*)LaCl **15**, [^{Me2}SB(^{tBu2}ArO,I*)Al(Cl)THF **16** .

2.9.1.1. NMR spectroscopic characterisation of ^{Me2}SB(^{tBu2}ArO,I)LaCl 15*

The synthesis of ^{Me2}SB(^{tBu2}ArO,I*)LaCl (**15**) follows the general procedure outline in **Scheme 2.7.** A large-scale attempt was made however poor yield was recorded due to low solubility of $LaCl_3$ toluene. A reaction in THF-d_8 allowed the reaction to be monitored via ^{1}H NMR spectroscopy (**Figure 2.28)**.

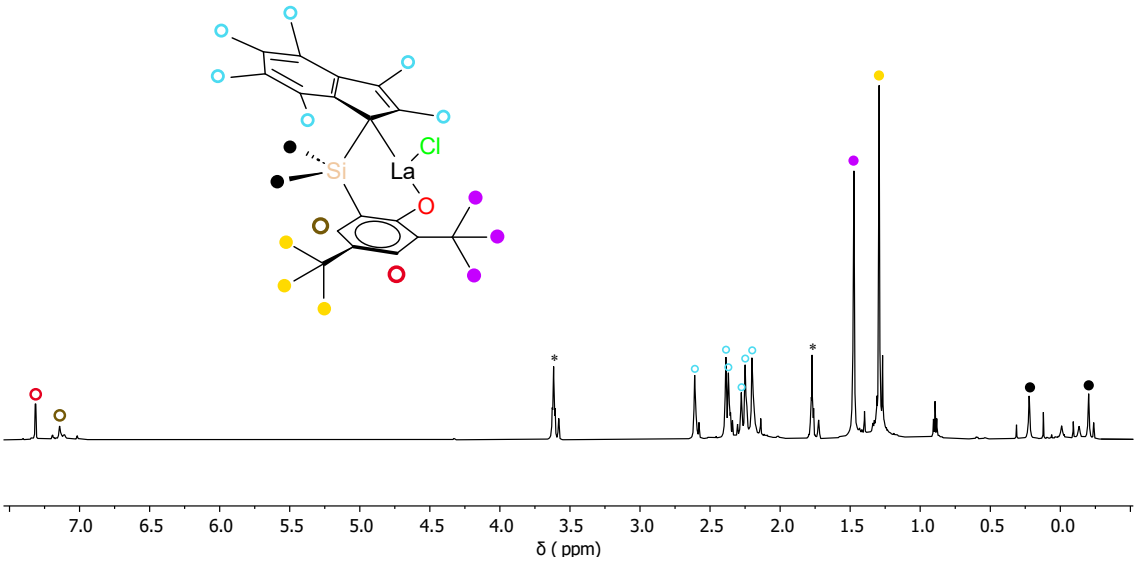


Figure 2.28 The ^{1}H NMR spectrum of ^{Me2}SB(^{tBu2}ArO,I*)LaCl (**15**) (600 MHz, THF-d_8, 298 K). * denotes residual protio solvent

The ^{1}H NMR spectrum shows the presence of a major and minor product in a ratio of 93:7. Six broad I**Me* resonances are found between δ 2.62 and 2.21 ppm and integrate to 3H each. The 2-^{t}*Bu* and 4-^{t}*Bu* proton resonances can be distinguished *via* the ^{1}H-^{1}H NOESY spectrum, integrate to 3H each at δ 1.48 and 1.30 ppm respectively. No further reactivity studies were carried out with this species and it was not isolated.

2.9.1.2. NMR spectroscopic characterisation of ^{Me2}SB(^{tBu2}OAr,I)Al(Cl)THF (16)*

The ^{1}H NMR spectrum of ^{Me2}SB(^{tBu2}OAr,I*)Al(Cl)THF **16** is similar to the CGCI* complex ^{Me2}SB(^{tBu}N,I*)Al(Cl)THF published by O'Hare *et al.*[17] The ^{1}H NMR spectrum shows two distinct products of the molecular formula of **16** that do not interconvert on the NMR timescale at 298 K (**Figure 2.29**). A distinctive feature of the aluminium complexes is the M-I* σ bond rather than through π bonding. ^{13}C{H} NMR spectroscopy can be used to identify the Si-**C(I*)** carbon resonance involved in metal bonding. For **16,** the carbon resonance is present at δ 128.66 ppm. The carbon resonance in **1**, bonded through η^5, occurs at δ 99.88 ppm.

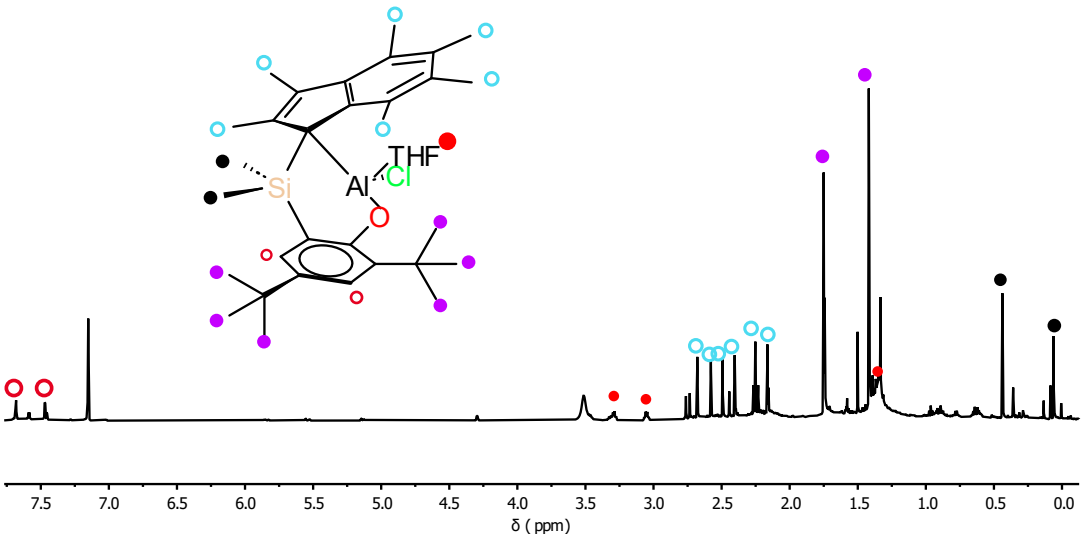
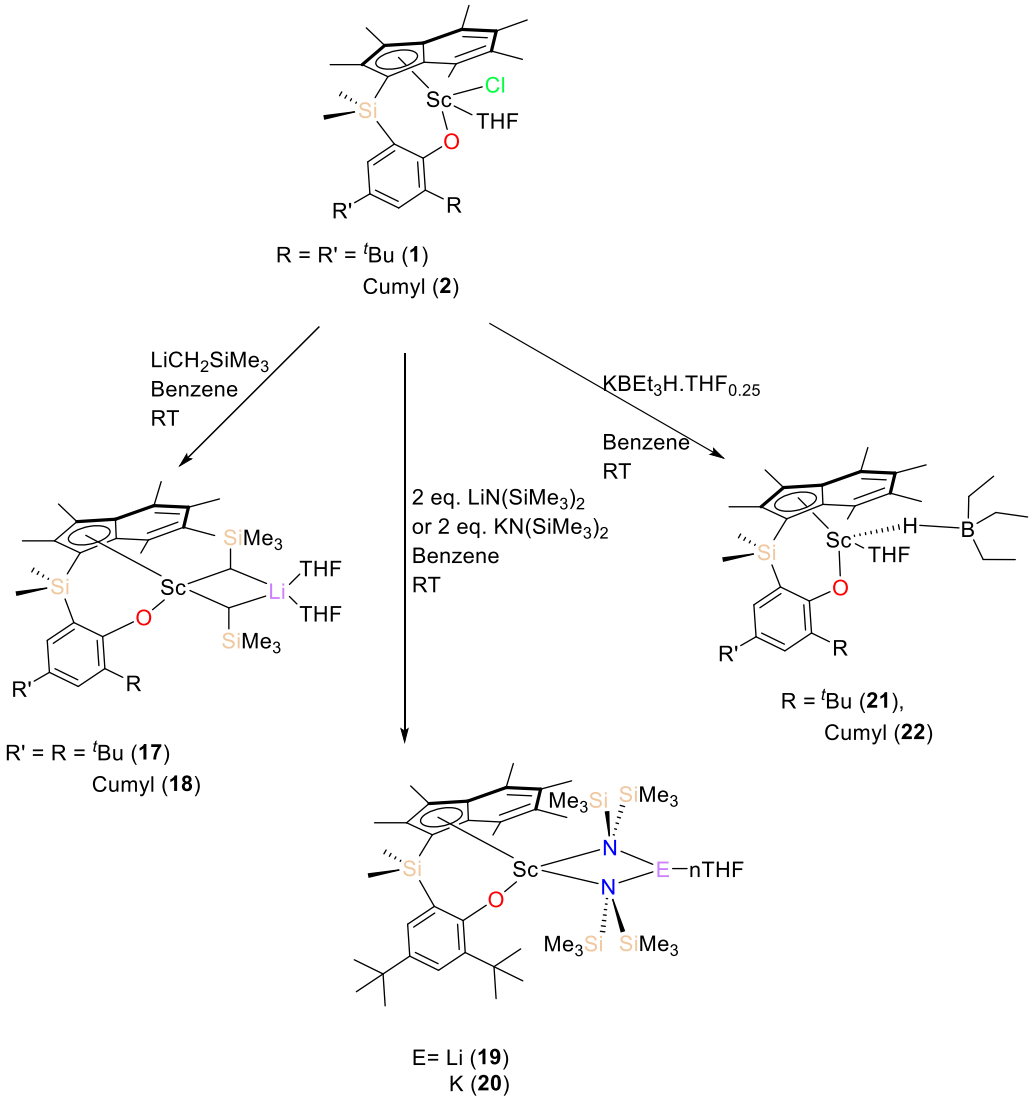


Figure 2.29 ^{1}H NMR spectrum of ^{Me2}SB(^{tBu2}OAr,I*)Al(Cl)THF (**16**) (600 MHz, benzene-d_6, 298 K), showing the presence of a minor product in a ratio of 3:1.

2.9.2. Attempted preparation of alkyl complexes.

The preparation of a number of alkyl scandium complexes was attempted *via* salt metathesis with either **1** and/or **2** and monitored *via* ^{1}H NMR spectroscopy in benzene-d_6. The reactions in all cases were indicative of decomposition in solution and full

characterisation was not undertaken. **Scheme 2.8** provides a summary of reactions. 2 equiv. of $LiCH_2SiMe_3$ with **1** and **2** to form new 'scandiate' species of the formula $^{Me_2}SB(^{t}Bu_2ArO,I^*)Sc(CH_2SiMe_3)_2Li$ (R, R′ = ^{t}Bu (**17**), Cumyl (**18**)).[69] **1** was reacted with lithium and potassium amide $EN(SiMe_3)_2$ to form species of the formula $^{Me_2}SB(^{t}Bu_2ArO,I^*)Sc(NSiMe_3)_2E$ (E = Li (**19**), K (**20**)). **1** and **2** were reacted with $KBEt_3H.THF_{0.25\ to}$ form species of the formula $^{Me_2}SB(^{R,R'}ArO,I^*)Sc(HBEt_3)THF$ (R, R′ = ^{t}Bu (**21**), Cumyl (**22**)). Collected data can be found in **Appendix A.2**



Scheme 2.8 Synthesis of **17**–**22** from **1** and **2.**

2.10. Conclusions

PHENI* complexes **1–3**, **5**, **6**, **8**–**22** and CGCI* complexes **4** and **7**, have been synthesised with a variety of phenoxide substituents, ancillary ligands, and trivalent metals. They have been characterised by multinuclear NMR spectroscopy, elemental analysis, IR spectroscopy, and through single-crystal X-ray diffraction studies. PHENI* complexes **1**, **2**, **5**, **8**, **9**, **11**, **12** present as a mixture of distinct fluxional isomers in solution where I* and phenoxy- substituent can be *proximal* or *distal*. Solid state studies showed the larger ODipp ligand favoured the A-*proximal* conformation and smaller Cl favoured the B-*distal* conformation.

The change in ligand coverage was quantified through solid angle calculations. There was a 2% increase in total ligand coverage for A-*proximal* over B-*distal* conformation. CGCI* complexes (**4** and **7**), previously reported by O'Hare *et al.*, were synthesised and a solid-state X-ray structure has been presented for **4**. Solid-state structures of **1**, **2**, **4**, **5**, and **7** were used to probe the conformation potential energy surface *in silico*. Additional conformations were scoped and used to confirm that other low energy sates are accessible at RT, hence assisting with assigning the NMR spectroscopy data.

The electronic effects of the ligands were probed *via* ^{45}Sc NMR spectroscopy. Bond distance relates significantly to the shielding of the scandium centre and the reported signal with scandium metal in PHENI* complexes being more shielded than in CGCI* complexes. The prediction, when considering catalysis, is that the CGCI* complex is more readily able to accept electron density than the PHENI* complexes leading to increased reactivity. This will be discussed in **Chapter 4**.

2.11. References

1. M. Nabika, H. Katayama, T. Watanabe, H. Kawamura-Kuribayashi, K. Yanagi and A. Imai, *Organometallics*, 2009, **28**, 3785-3792.
2. P. J. Shapiro, E. Bunel, W. P. Schaefer and J. E. Bercaw, *Organometallics*, 2002, **9**, 867-869.
3. J. Okuda, *Chemische Berichte*, 2006, **123**, 1649-1651.
4. M. E. Thompson, S. M. Baxter, A. R. Bulls, B. J. Burger, M. C. Nolan, B. D. Santarsiero, . . . J. E. Bercaw, *J Am Chem Soc*, 2002, **109**, 203-219.
5. I. E. Nifant'ev and P. V. Ivchenko, *Organometallics*, 1997, **16**, 713-715.
6. H. Hanaoka, T. Hino, H. Souda, K. Yanagi, Y. Oda and A. Imai, *J Organomet Chem*, 2007, **692**, 4059-4066.
7. C. G. Collins Rice, J. A. Hayden, A. D. Hawkins, L. J. Morris, Z. R. Turner, J. C. Buffet and D. O'Hare, *Organometallics*, 2024, **43**, 540-556.
8. T. Senda, H. Hanaoka, S. Nakahara, Y. Oda, H. Tsurugi and K. Mashima, *Macromolecules*, 2010, **43**, 2299-2306.
9. J. Klosin, P. P. Fontaine and R. Figueroa, *Acc Chem Res*, 2015, **48**, 2004-2016.
10. C. G. Collins Rice, J. C. Buffet, Z. R. Turner and D. O'Hare, *Chem Commun (Camb)*, 2021, **57**, 8600-8603.
11. J. V. Lamb, D.Phil. D.Phil. Thesis, University of Oxford, 2019.
12. J. V. Lamb, J. C. Buffet, J. E. Matley, C. M. R. Wright, Z. R. Turner and D. O'Hare, *Dalton Trans*, 2019, **48**, 2510-2520.
13. J. V. Lamb, J. C. Buffet, Z. R. Turner and D. O'Hare, *Polym Chem-Uk*, 2019, **10**, 1386-1398.
14. Z. R. Turner, J. V. Lamb, T. P. Robinson, D. Mandal, J. C. Buffet and O. H. D, *Dalton Trans*, 2021, **50**, 4805-4818.
15. T. J. Williams, J. V. Lamb, J. C. Buffet, T. Khamnaen and D. O'Hare, *RSC Adv*, 2021, **11**, 5644-5650.
16. N. Diteepeng, J. C. Buffet, Z. R. Turner and D. O'Hare, *Dalton Trans*, 2019, **48**, 16099-16107.
17. N. Diteepeng, I. A. P. Wilson, J.-C. Buffet, Z. R. Turner and D. O'Hare, *Polym Chem-Uk*, 2020, **11**, 6308-6318.
18. C. G. Collins Rice, J. C. Buffet, Z. R. Turner and D. O'Hare, *Polym Chem-Uk*, 2022, **13**, 5597-5603.
19. C. G. Collins Rice, L. J. Morris, J. C. Buffet, Z. R. Turner and D. O'Hare, *Chem Commun (Camb)*, 2023, **59**, 12128-12131.
20. L. Pan, K. Y. Zhang, M. Nishiura and Z. M. Hou, *Macromolecules*, 2010, **43**, 9591-9593.
21. R. Mykura, R. Sánchez-Bento, E. Matador, V. K. Duong, A. Varela, L. Angelini, . . . D. Leonori, *Nat Chem*, 2024, **16**, 771-779.
22. T. Arnold, D.Phil. Thesis, Oxford University, UK, 2015.
23. G. Binsch, *J Am Chem Soc*, 1969, **91**, 1304-1310.
24. T. D. W. Claridge, in *High-Resolution NMR Techniques in Organic Chemistry*, ed. T. D. W. Claridge, Elsevier, Boston, 3 edn., 2016, DOI: 10.1016/b978-0-08-099986-9.00009-9, ch. 9, pp. 315-380.
25. A. Okuniewski, D. Rosiak, J. Chojnacki and B. Becker, *Polyhedron*, 2015, **90**, 47-57.
26. K. Chang and X. Xu, *Dalton Trans*, 2017, **46**, 4514-4517.
27. K. Chang, X. Wang, Z. Fan and X. Xu, *Inorg Chem*, 2018, **57**, 8568-8580.
28. B. D. Ward, S. R. Dubberley, A. Maisse-François, L. H. Gade and P. Mountford, *J Chem Soc Dalton*, 2002, DOI: 10.1039/b209382k, 4649-4657.
29. M. A. Putzer and G. P. Bartholomew, *Zeitschrift Fur Anorganische Und Allgemeine Chemie*, 1999, **625**, 1777-1778.
30. Y. Luo, J. Baldamus and Z. Hou, *J Am Chem Soc*, 2004, **126**, 13910-13911.
31. T. Jia, S. Y. Xu, L. C. Huang and W. Gao, *Polyhedron*, 2018, **145**, 182-190.
32. S. D. Bennett, S. J. A. Pope, R. L. Jenkins and B. D. Ward, *Eur J Inorg Chem*, 2016, **2016**, 2932-2941.
33. J. L. Atwood and K. D. Smith, *J Chem Soc Dalton*, 1974, **9**, 921-923.
34. S. Giessmann, S. Blaurock, V. Lorenz and F. T. Edelmann, *Inorg Chem*, 2007, **46**, 10956-10958.
35. L. N. Grant, B. Pinter, B. C. Manor, H. Grutzmacher and D. J. Mindiola, *Angew Chem Int Ed Engl*, 2018, **57**, 1049-1052.
36. B. Cordero, V. Gomez, A. E. Platero-Prats, M. Reves, J. Echeverria, E. Cremades, . . . S. Alvarez, *Dalton Trans*, 2008, DOI: 10.1039/b801115j, 2832-2838.
37. Y. J. Luo, S. H. Chi and J. Chen, *New J Chem*, 2013, **37**, 2675-2682.
38. J. Oyamada, M. Nishiura and Z. Hou, *Angew Chem Int Ed Engl*, 2011, **50**, 10720-10723.
39. F. Mazzotta and D. Kunz, *Organometallics*, 2021, **40**, 3003-3011.
40. Y. L. Lei, Y. B. Wang and Y. J. Luo, *J Organomet Chem*, 2013, **738**, 24-28.

41. Z. Chai, J. Chu, Y. Y. Qi, M. J. Tang, J. S. Hou and G. S. Yang, *Rsc Advances*, 2017, **7**, 1759-1765.
42. M. J. Calhorda, C. C. Romao and L. F. Veiros, *Chemistry*, 2002, **8**, 868-875.
43. J. H. Fu, Z. Y. Wang, F. L. Xue and J. P. Huo, *Acta Crystallogr Sect E Struct Rep Online*, 2010, **67**, o73.
44. P. Ransom, A. Ashley, A. Thompson and D. O'Hare, *J Organomet Chem*, 2009, **694**, 1059-1068.
45. M. J. Calhorda and L. F. Veiros, *Coordin Chem Rev*, 1999, **185-6**, 37-51.
46. S. Grimme, A. Hansen, S. Ehlert and J. M. Mewes, *J Chem Phys*, 2021, **154**, 064103.
47. I. Cota, *Phys Sci Rev*, 2017, **2**.
48. I. A. Guzei and M. Wendt, *Dalton Trans*, 2006, DOI: 10.1039/b605102b, 3991-3999.
49. C. A. Tolman, *Chem Rev*, 1977, **77**, 313-348.
50. A. F. Zahrt, S. V. Athavale and S. E. Denmark, *Chem Rev*, 2020, **120**, 1620-1689.
51. H. B. Hansen, H. Wadepohl and M. Enders, *Chemistry*, 2021, **27**, 11084-11093.
52. J. Klosin, W. J. Kruper, P. N. Nickias, G. R. Roof, P. De Waele and K. A. Abboud, *Organometallics*, 2001, **20**, 2663-2665.
53. J.-F. G. Christian Laurence, *Lewis Basicity and Affinity Scales: Data and Measurement*, Wiley, 2010.
54. P. C. Maria and J. F. Gal, *J Phys Chem*, 1985, **89**, 1296-1304.
55. R. H. Morris, *Chem Rev*, 2016, **116**, 8588-8654.
56. J. F. Gal, P. C. Maria, M. Yanez and O. Mo, *Molecules*, 2021, **26**, 1-13.
57. K. Udomsasporn, S. Haesuwannakij, P. Piromjitpong, P. Chumsaeng and K. Phomphrai, *Dalton Trans*, 2020, **49**, 14378-14382.
58. P. J. Shapiro, PhD, California Institute of Technology, 1991.
59. L. D. Henderson, G. D. MacInnis, W. E. Piers and M. Parvez, *Can J Chem*, 2004, **82**, 162-165.
60. F. Guo, M. Nishiura, Y. Li and Z. Hou, *Chem Asian J*, 2013, **8**, 2471-2482.
61. G. E. Maciel and R. V. James, *Inorg Chem*, 2002, **3**, 1650-1651.
62. W. Huynh, D. B. Culver, H. Tafazolian and M. P. Conley, *Dalton Trans*, 2018, **47**, 13063-13071.
63. T. J. Boyle, R. E. Cramer, F. A. Fasulo and N. Padilla, *Polyhedron*, 2021, **208**, 115437.
64. A. Mortis, D. Barisic, K. Eichele, C. Maichle-Mossmer and R. Anwander, *Dalton Trans*, 2020, **49**, 7829-7841.
65. L. Deakin, W. Levason, M. C. Popham, G. Reid and M. Webster, *J Chem Soc Dalton*, 2000, DOI: 10.1039/b001669l, 2439-2447.
66. F. A. H. A.M.Arif, M.B.Hursthouse, *CSD Communication*, 2012, DOI: 10.5517/ccyzhlz.
67. W. F. Rong, J. H. Cheng, Z. H. Mou, H. Y. Xie and D. M. Cui, *Organometallics*, 2013, **32**, 5523-5529.
68. E. Lu, Y. Li and Y. Chen, *Chem Commun (Camb)*, 2010, **46**, 4469-4471.
69. A. Mortis, F. Kracht, T. Berger, J. Lebon, C. Maichle-Mossmer and R. Anwander, *Dalton Trans*, 2022, **52**, 44-51.

Chapter 3 – **Solution Dynamics of PHENI* complexes**

3.1. Introduction

3.1.1. Stereogenic units

The Cahn-Ingold-Prelog (CIP) rules are used to assign the configuration of the entire molecule. In general, they are used when specific isomers are required to be identified. In organometallic chemistry, in general, the descriptions are not used. In order for the descriptions to be used successfully, they must be interpretable to produce a structural diagram from a formula. Creating descriptions and understanding them improves discussion for these systems and can assist the rationalisation of reactivity.

A molecule can contain any number of stereogenic units and in general, a molecule with *n* stereogenic units will have 2^n stereoisomers and 2^{n-1} diastereomers each with an associated pair of enantiomers. Three basic types of stereogenic units are defined as: (a) chiral centres, (b) stable conformations caused by bond rotation about the central bond in a chain of four non-coplanar atoms (atropisomers, conformers), (c) *proximal-distal* isomerism involving a double bond.[1, 2]

3.1.2. Chapter synopsis

Chapter 3 discusses the dynamic equilibrium between isomers of complexes in solution, synthesised in **Chapter 2**. Complexes **1, 5, 7,** and **12** are presented as examples of the three stereogenic units found in PHENI* complexes. The distinct operations and mechanisms that relate the isomers of these chiral scandium(III) complexes are discussed in detail. The conformational stereogenic unit is explored using comparisons between literature examples, **5,** and **7.** The inversion of the metal centre was studied *via* associative

substitution using $OPPh_3$ and explored with DFT. The isomerisation of the asymmetric ligand is explored using **1** and NMR spectroscopic experiments.

3.2. Isomerism in PHENICS

Within the PHENI* scandium systems, there exist a possible set of 2^n isomers that occur due to the presence of *n* stereogenic units, which fall into three classes: conformation, stereogenic metal, and asymmetric ligand. A general set of descriptors is presented to universally describe this particular class of complex. The behaviour of these systems and related isomerism has often been overlooked in previous reported complexes during characterisation which provides an opportunity to deepen understanding.

3.2.1. Conformational isomerism

Distinct conformational isomers can exist due to significant energy barriers. This can impact both reactivity and stereoselectivity in catalysis.[3] However, the population and number of isomers is temperature dependent: at higher temperatures, distinct species converge as molecules possess sufficient energy to overcome conformational energy barriers and are observed to be a single species.[4] Retaining geometries is important with respect to activity or stereo control of polymerisation.[5] Rotation around the I^*_{cent}–Sc and C(1)–Si bonds in bridged metallocenes results in the possibility of different conformers. Indenyl sandwich complexes have been employed to great effect in stereo block polymerisation of α-olefins, through allowed conversion, *via* oscillation around the M-I bond, between isomers during polymerisation.[6-8]

A*nsa*-bridged systems were designed to add stereorigidity to "oscillating" metallocenes. As additional atoms are added to the metallocyclic ring, more conformations are

thermodynamically stable. This is analogous to increasing chair/boat/twist boat conformations and ring puckering in cyclic hydrocarbon rings (**Figure 3.1**).[9-11]

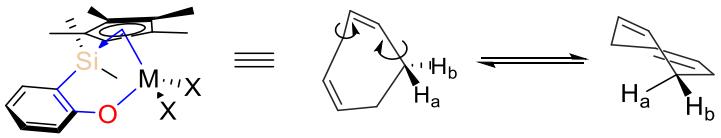


Figure 3.1 PHENICS/PHENI* metallocyclic ring pucking analogous to ring puckering of the 7 membered 1,4-cycloheptadiene.[10]

For CGC-amido complexes of the formula ^{Me2}SB($^{t Bu}$N,I*)Sc(X)THF, the *ansa* bridge contains only a silicon and nitrogen atom. Only one stable conformer exists at room temperature. In contrast, the larger metallocyclic ring in PHENI* can results in multiple stable conformations. If the energy barrier to interconversion is sufficiently large, multiple conformations can be observed simultaneously (**Figure 2.17**).[12]

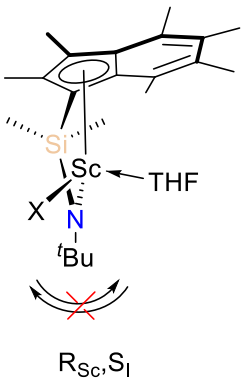


Figure 3.2 At room temperature, ^{Me2}SB($^{t Bu}$N,I*)Sc(X)THF exhibits only one stable conformation. The CGC-I* ligand has less metallocylic flexibility compared to the PHENI* ligand.

In all cases, the stereogenic centre linked to conformation, is highly dependent on both temperature and solvent environment.

3.2.2. Stereogenicity at tetrahedral metal centre

A tetrahedral metal centre creates the same opportunity for chirality as a tetrahedral carbon when coordination involves four different ligands (**Figure 3.3** (a)).[13] The label *R* is assigned if the cyclic sequence of priority numbers, from the viewed perspective looking down the vector from the tetrahedral centre to the lowest priority substituent, occurs in a clockwise direction. *S* where the sequence is anticlockwise.[14]

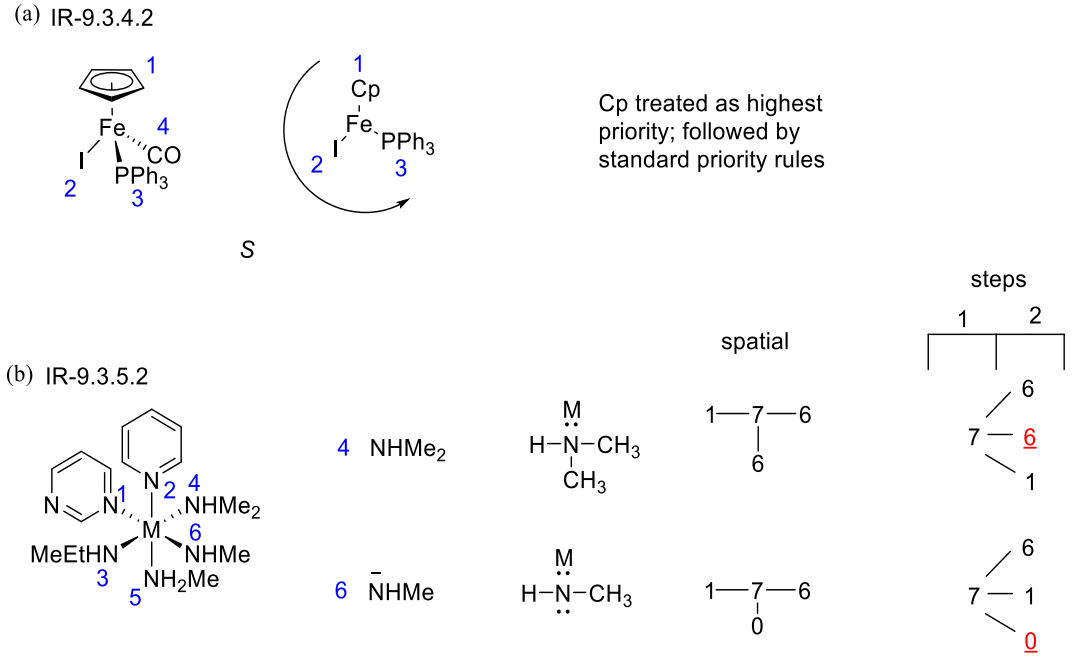


Figure 3.3. (a) IUPAC recommendation example for assigning a) tetrahdedral half-sandwhich complexes and (b) priority sequence for ligands.[14]

When it comes to forming a priority list, Cp is generally giving the highest priority according to the IUPAC recommendations. The Cahn, Ingold, and Prelog (CIP) rules are generally used on each ligand, proceeding along the branches of the molecules until an order is formed.[15, 16]

Scandium complexes **1–13** have a tetrahedral coordination geometry with four unique ligands. Inversion of the metal centre is possible in solution where one of the bonds is labile and associative or dissociative substitution is possible. Where substitution occurs

with an identical molecule to that being displaced, chirality inversion is ensured. Using a simplified version of chloride complex **1**, assigning the chirality of the scandium stereogenic centre can be examined (**Figure 3.4**).

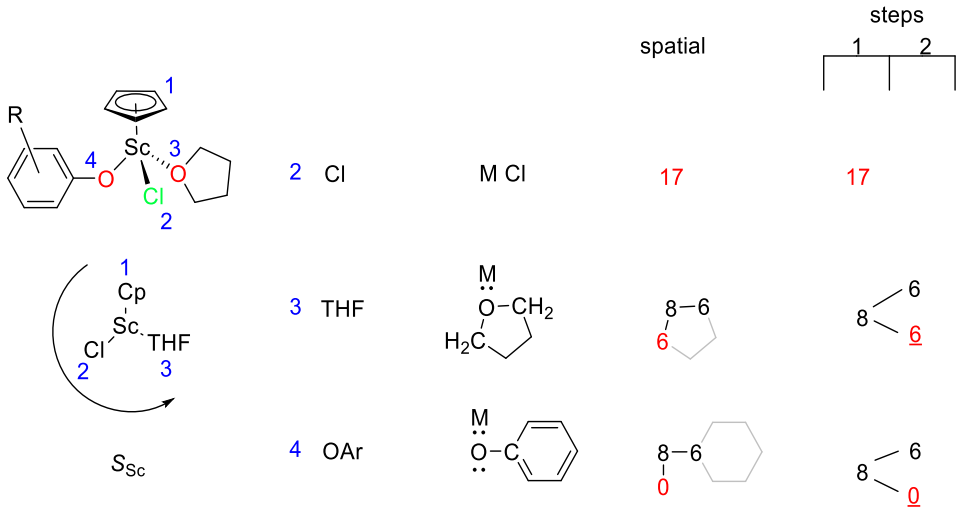


Figure 3.4 Priority for cases presented in this thesis Cp > Cl > THF > OAr leading to S_{Sc} discriptor.

Proceeding along the branches of the ligand constituents allows priorities to be assigned. The numbers in are the atomic numbers of the atoms in the structures, with those in brackets accounting for the presence of multiple bonds. Averaging techniques are used in the case of resonance structures. For the case where ligands are I*, triphenylphosphine oxide ($OPPh_3$), 2,6-diisoprophenyl oxide (ODipp), and aryloxide silicon bridged ($O^{SB}Ar$) ligands, the 1st and 2nd priority are assigned to η^5-I then the $OPPh_3$. To discern the order of the two aryloxide groups, the atoms further from along the branches are considered, where after the 3rd step, the silicon on the *ansa*- bridge places the ODipp ligand in the lowest priority (**Figure 3.5**).

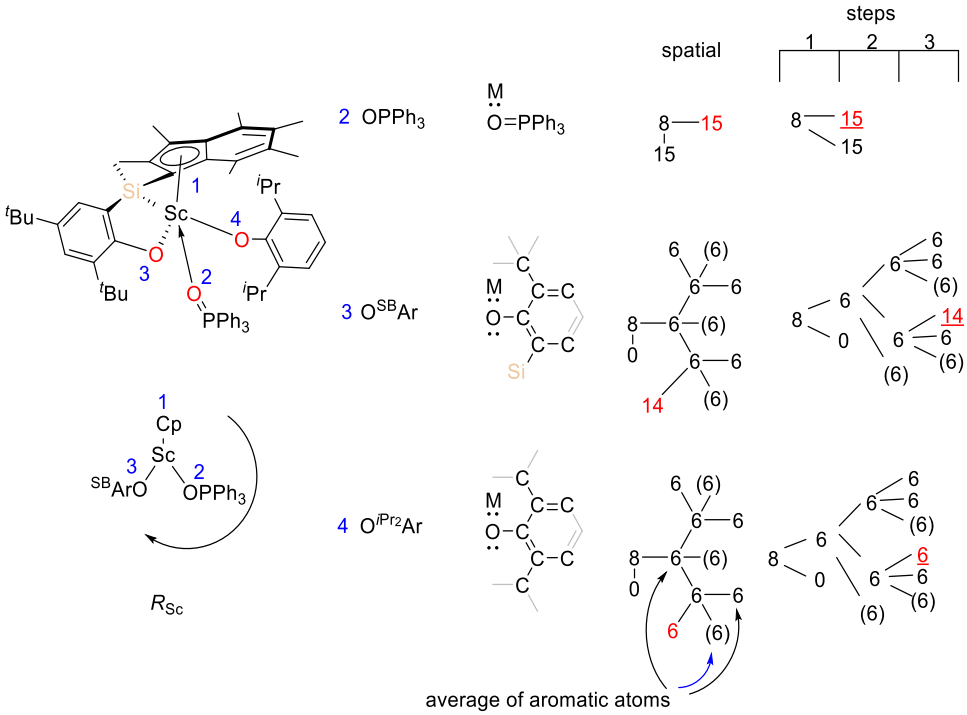


Figure 3.5 Priority for cases presented in this thesis Cp > $OPPH_3$ > $O^{SB}Ar$ > O^{iPr_2} Ar leading to R_{Sc} discriptor.

3.2.3. Asymmetric Ligand

A stereogenic unit arises at the indenyl-metal bond due to asymmetry of the indenyl *vs* Cp group. Where the *ansa*-bridge is bonded to the C1 carbon, it creates a chiral proligand with an asymmetric tetrahedral carbon. This results in asymmetry of the final complex (**Figure 3.6**).

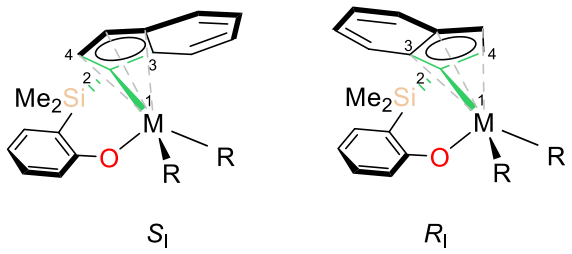


Figure 3.6 Asymmetry of the indeyl complex leading to sterogenic centre S_I and R_I.

Priority proceeds through IUPAC general rules, considering the atomic numbers of the atoms bonded to the C1 carbon involved both in the bonding to the metal centre, and the *ansa*- bridge. Where M = Sc, highest priority is the metal centre.

3.2.4. Operations and mechanisms for isomerism

Where these stereogenic units occur, the possible isomers are related through operations that alter one of the three stereogenic units to form one of the other diastereomers. Operations, as depicted in **Figure 3.7**, lead to distinct isomers that include (a) A-*proximal*/B-*distal* isomerisation through inversion of the metallocyclic ring, (M); (b) inversion of the metal chirality via ligand exchange (S); (c) inversion of the asymmetric stereogenic unit *via* indenyl face flip (I). By considering the operations, M, S, I, and E (no chirality change) on the set of enantiomers (W, X, Y, and Z, and W′, X′, Y′, and Z′**;** the respective enantiomers), results in the interconversion of isomers. Further, {MSI} leads to enantiomerisation, W → W′ (**Figure 3.7** (d)), when all operations are allowed.

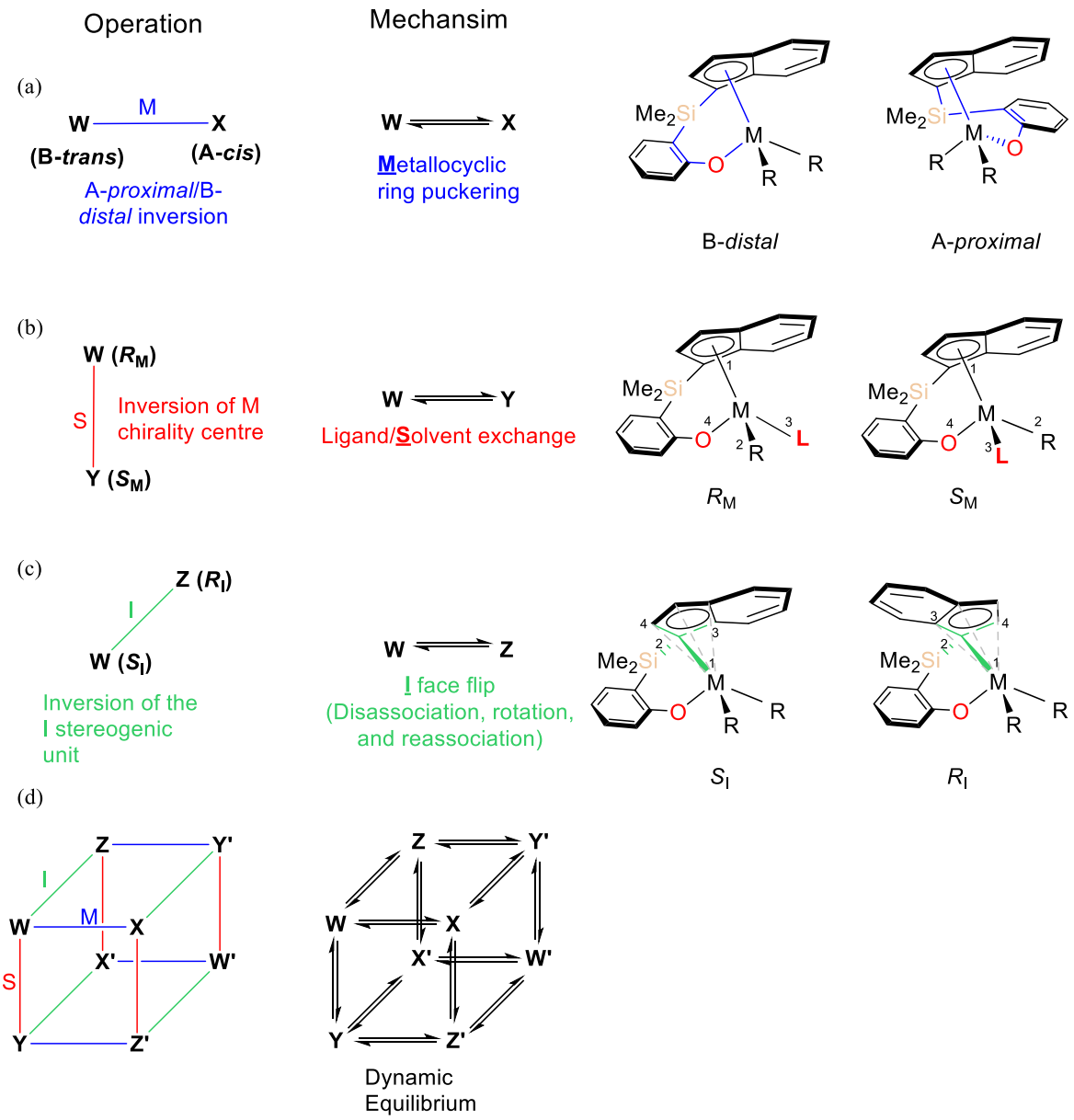


Figure 3.7 Operations and possible mechanisms for interconversion of PHENI* isomers. Possible operations leading to distinct isomers are (a) A-*proximal*/B-*distal* inversion of the metallocyclic ring, (b) inversion of the metal chirality *via* ligand exchange, and (c) inversion of the asymmetric stereogenic unit *via* indenyl face flip. (d) Operations linked through vertices of cube where W′, X′, Y′, and Z′ denote the enantiomers of W, X, Y, and Z.

In some cases, reactions can occur in solution that result in an inversion of one or more stereogenic unit(s). Any equilibria can be monitored *via* chemical exchange NMR spectroscopic experiments and used to determine the isomers of the complexes in solution.

3.2.5. Metallocyclic ring puckering

^{1}H NMR spectroscopy is used to evaluate the PHENI* scandium species in solution (**Chapter 2**). For **1**, there is a temperature and solvent dependency on the number of species observed in solution.

For example, dissolving **1** in THF-d_8 rather than benzene-d_6 or toluene-d_8 leads to an increase in the number of species stable in solution as seen in **Figure 3.8**. Labelled variable temperature for **1** can be found in **Appendix Figure A.18–22.**

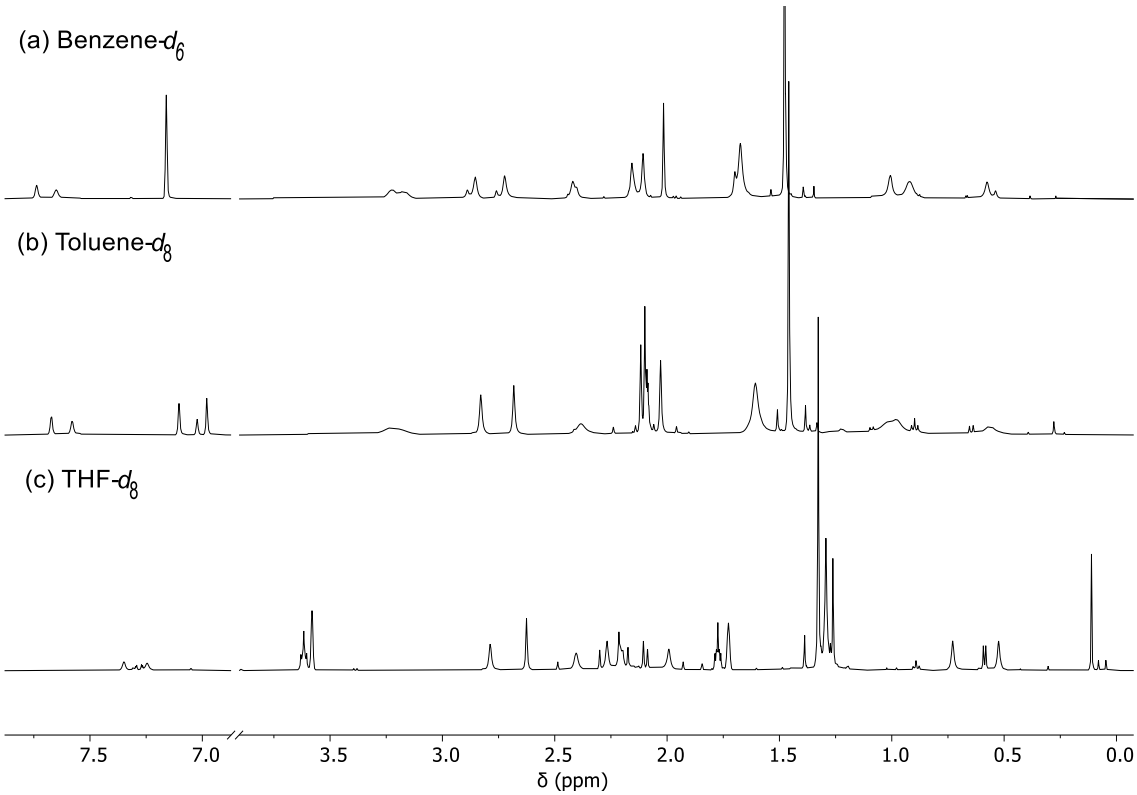


Figure 3.8 ^{1}H NMR spectrum (500 MHz, 298 K) in (a) benzene-d_6, (b) toluene-d_8, (c) THF-d_8, of ^{Me_2}SB($^{t Bu_2}$ArO,I*)Sc(Cl).THF (**1**).

Distinct species from metallocyclic ring puckering can be observed, often at lower temperature. When larger ligands were substituted, such as ODipp for Cl in **5**, and DMAP for THF in **9**, the signals corresponding to the protons of conformers (in a ratio of 40:1 and >400:1 respectively for major:minor conformers) are observed and resonances

relating to the protons in the major species are sharper than in **1**. Additionally, as there are >2 species in exchange, NMR spectroscopic experiments were unable to determine the activation energy for these interconversions. This suggests that increasing the ligand size slows isomerisation and causes conformations to be more stable.

The PHENICS-Ti complex $^{Me2}(^{tBu,Me}ArO,Cp^*)TiCl_2$ reported by Imai *et al*. (**Figure 3.9**) also exhibited rapid exchange between conformers on the NMR spectroscopic timescale. The reported solid-state structure showed unsymmetrical C_1 symmetry; however, the ^1H NMR spectrum matched a species with C_s symmetry. This led to the conclusion that the flexibility of the extended metallocyclic ring enables the exchange between conformers.[17] Typically, stable configurations occur where the energy barrier between conformational isomers is greater than 20 kcal mol^{-1}.

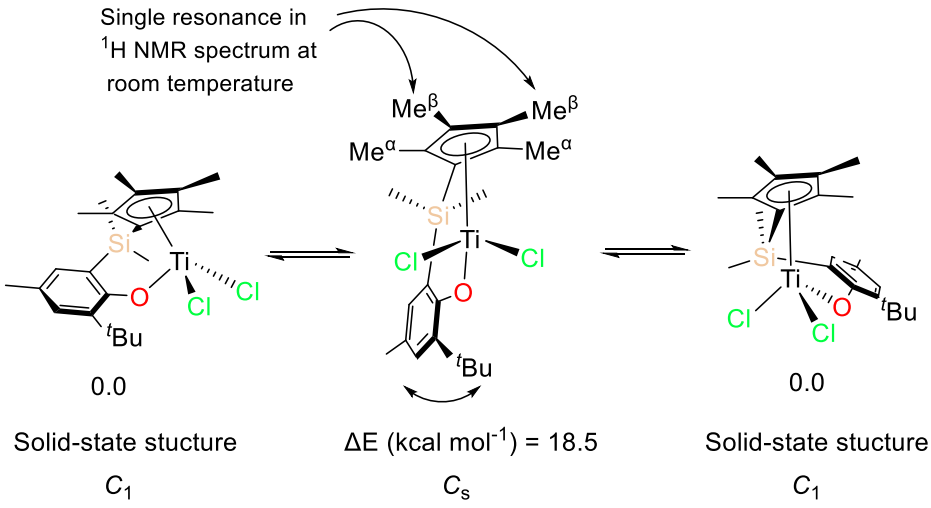


Figure 3.9 "Osciallation" of $^{Me2}SB(^{tBu,Me}ArO,Cp^*)Ti(Cl)_2$; stability differences at the RHG/LANL2DZ level calculated with Gaussian 98[18] relative to solid-state structure (0.0).[17]

The asymmetric sandwich zirconium complexes $^{Me2}SB(Cp,I^*)Zr(CH_2Ph)_2$ reported by O'Hare *et al.* contains two stereogenic units: an asymmetric ligand, and stable conformers in solution (**Figure 3.10**). The complex shows the coalescence of the silyl bridge methyl

proton resonances in the ^{1}H NMR spectrum at temperatures over 363 K. This was one reported example from the family that showed spectral changes during variable temperature solution ^{1}H NMR experiments.[19]

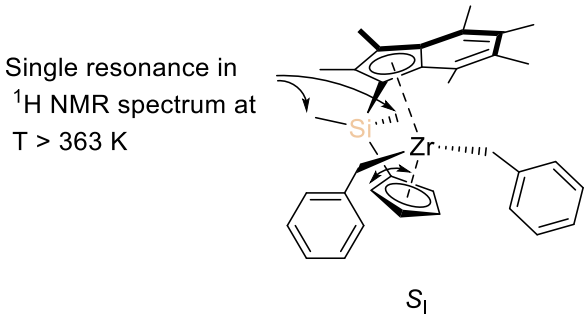


Figure 3.10 Structure of ^{Me2}SB(Cp,I*)Zr($CH_2Ph)_2$. One of the *ansa*-bridged Cp-I* Zr complexes reported by O'Hare *et al*. that showed temperature dependent flexibility [19, 20]

3.2.6. Ligand/solvent exchange

Inversion of a chirality centre requires a bond to be broken and reform. This can occur when a bond is labile and prone to substitution either *via* an associative or dissociative mechanism.[21] Chiral-at-metal centre half-metallocene sandwich complexes have been reported to invert on exchange with larger ligands.[13, 22, 23] The reaction of complex **5** with $OPPh_3$ to form ^{Me2}SB(^{t}Bu$_2$ArO,I*)Sc(ODipp)$OPPh_3$ (**12**) presents a system where dynamic equilibrium occurs between the diastereomers. Epimerisation of the four-coordinate scandium centre can be observed. When **12** forms initially, the isomers B-*distal*,R_{Sc},S_I)/(B-*distal*,S_{Sc},R_I)-**12 (12-K)** and (A-*proximal*,S_{Sc},S_I)/(A-*proximal*,R_{Sc},R_I)-**12** (**12-T**) are observed in a ratio of 1:3 after 5 minutes. After 18 hours at RT, the ratio reverses to 10:1 (**Figure 3.11**). The reaction is under thermodynamic control and **12-T** is favoured; DFT calculations were consistent with this isomer having the lowest free Gibbs energy; (**Figure 3.12**).[21, 24]

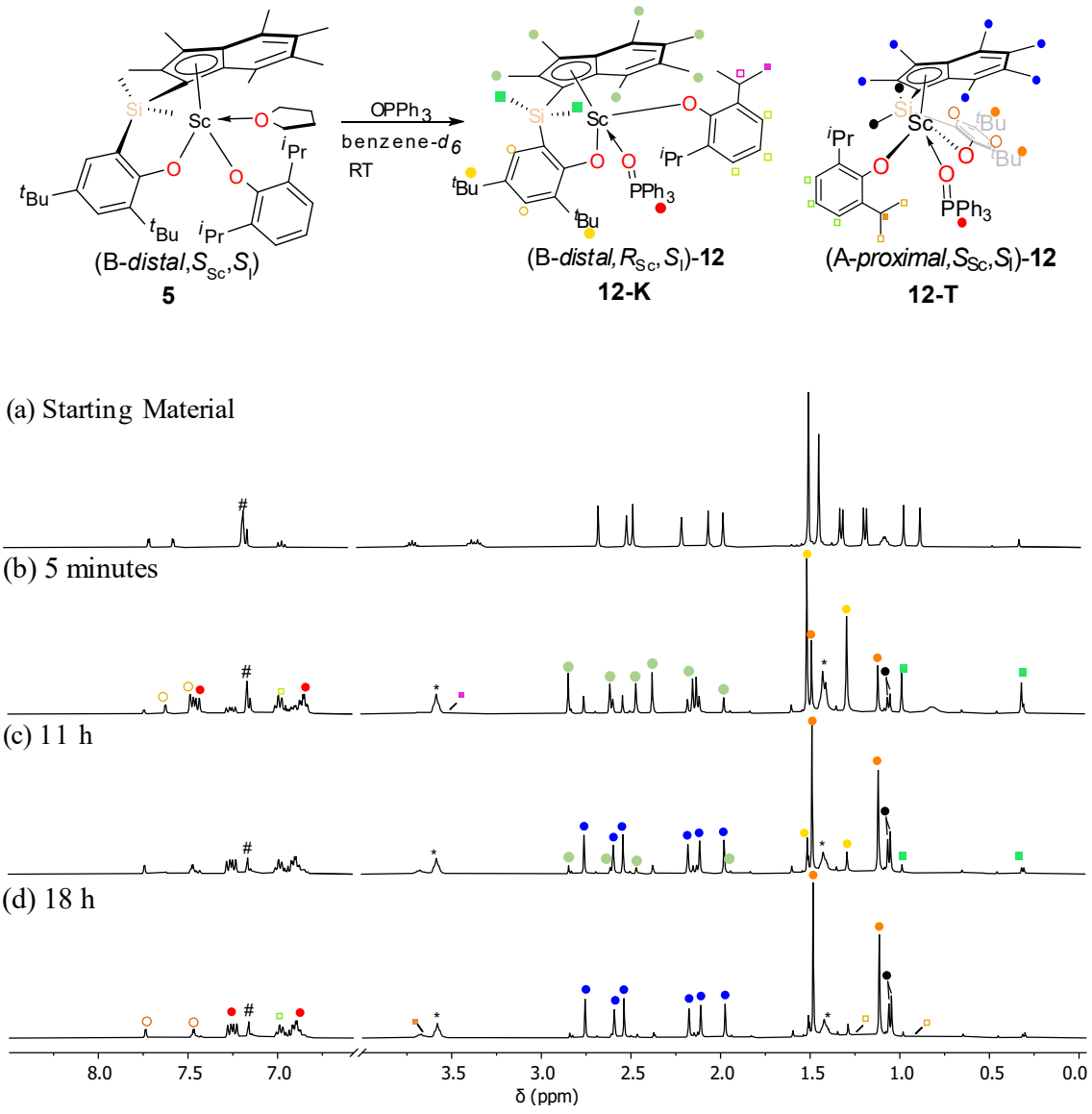


Figure 3.11 Synthesis of ^{Me_2}SB(^{tBu_2}ArO,I*)Sc(ODipp)OPPh$_3$ (**12**), showing the formation of (B-*distal*,R_{Sc},S_I)/(B-*distal*,S_{Sc},R_I)-**12** (**12-K**) and (A-*proximal*,S_{Sc},S_I)/(A-*proximal*,R_{Sc},R_I)-**12** (**12-T**) which reaches dynamic equilibrium (one enantiomer draw for clarity). ^{1}H NMR spectra (benzene-d_6, 400 MHz, 298 K) of (a) ^{Me_2}SB(^{tBu_2}ArO,I*)Sc(ODipp)THF (**5**) and **12** after (b) 5 minutes (c) 11 h and (d) 18 h

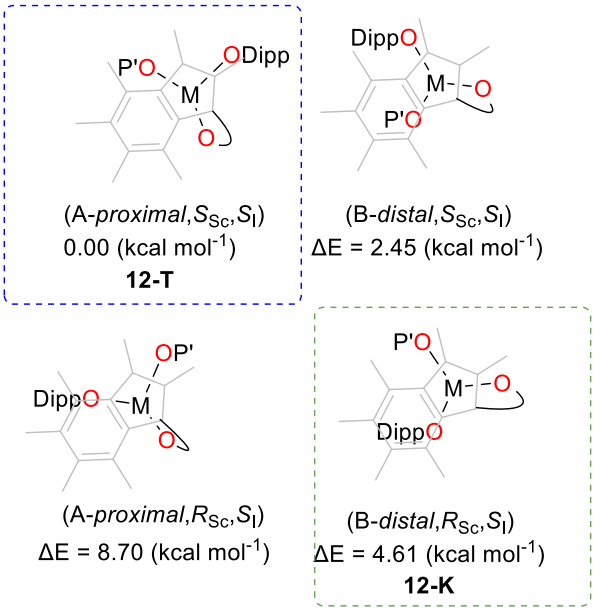


Figure 3.12 Computed Gibbs energy profile for isomers of **12**. The relative energies of enatiomer pairs are computed using r^{2}SCAN-3c and presented as ΔG (kcal mol^{-1}) relative to the lowest energy configuration of **12** (**12-T**).

The dependence of the time to reach dynamic equilibrium on the ratio of $OPPh_3$ was studied through changing the equivalents of $OPPh_3$ added relative to **5** (**Figure 3.13**). In all cases the final equilibrium ratio remains unaffected. The rate equilibrium was reached increased with ratio of $OPPh_3$ from 50 h for 4 eq. down from 150 h from 1.1 eq. Hence, $OPPh_3$ appears in the rate equation for the interconversion of the two species.

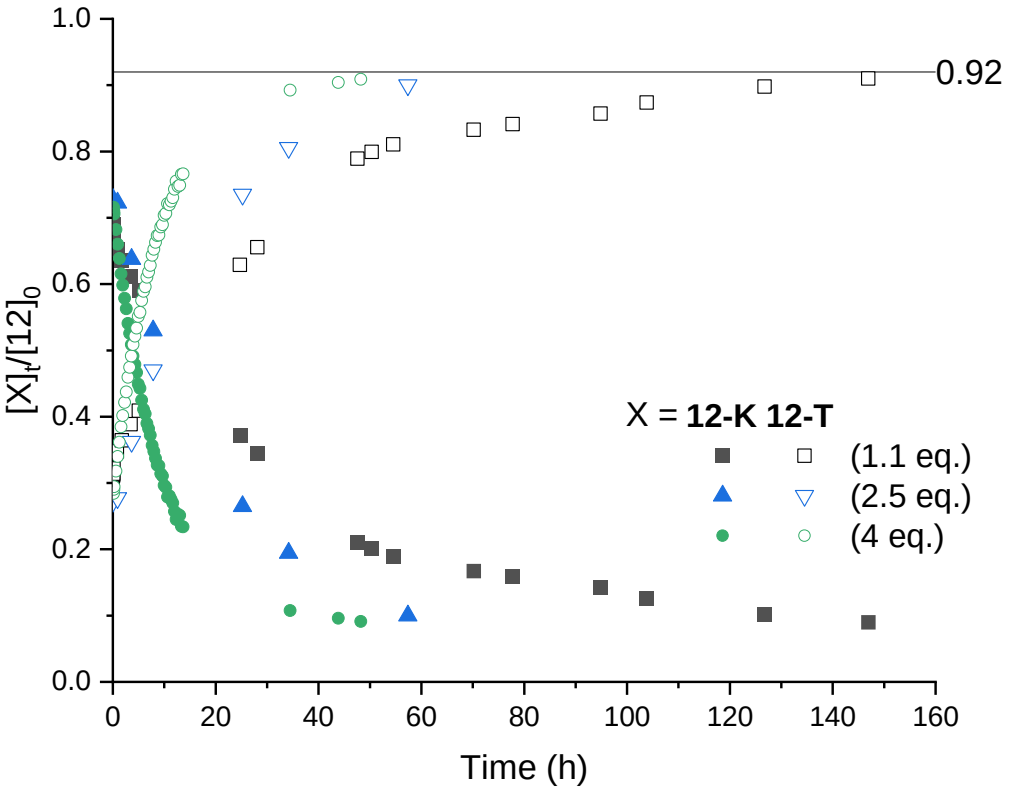


Figure 3.13 Addition of *x* eq.$OPPh_3$ to **5**; plot of [**12-T**]:[**12-K**] as a function of time observed by ^{1}H NMR spectroscopy (toluene-d_8, 298 K,) (black square 1.1, blue triangles 2.5, and green cirles 4.0 eq.) $[12]_0 = [12\text{-K}]_0 + [12\text{-T}]_0$; X = 12-K and 12-T. Equilibrium ratio is approximately 10:1 (**12-T**:**12-K**).

For **12**, the isomers of **12-T/K** are not distinguishable *via* ^{1}H NMR spectroscopy. These were previously observed *via* NOESY experiments for **1** and **5**, but not observed for **12** at RT.

Although the operations M, S, and I relate diastereomers, not all of these species are observed in solution. Where reaction mechanisms that lead to the operations are allowed, the rate of some of the reaction rates are much higher than others. Hence, reactions can be closely followed by another, leading to pre-equilibria. For example, when observing ligand exchange for **12**, the activation barrier for metallocyclic ring puckering (M) is lower than ligand exchange of $OPPh_3$. Ligand exchange therefore takes place in

combination with metallocyclic ring puckering and the intermediate diastereomer is not observed. For example, the conversion of **12-K** → **12-T** is described by {MS}.

By considering the solid-state data collected for the PHENI* scandium complexes **1** – **5** in different conformations, substitutions can be made through a structure drawing program and the resultant spatial data optimised and relative energies calculated. This can then be used as an approximate guide to the relative energy order for the various isomers of the compounds. Further, through comparison of a five and three coordination compound, the relative energy of an associative substitution or dissociative substitution transition states can be compared.

Structures were drawn with substituted $OPPh_3$ ligands and optimised in Avogadro using UFF (4 steps).[25] Additional geometry optimisation was done using Kohn-Sham density functional theory (DFT). In recent years, use of composite correction methods, such as the '3c' family, in combination with small optimised bases sets, allow for lower computational cost and excellent accuracy. One method is the regularised-restored (r^2) version of the strongly constrained and appropriately normed (SCAN) functional, a type of meta-generalised-gradient approximation (meta-GGA) functional(r^2-SCAN).[26]

The r^2SCAN-3c functional includes tailored corrections of a balanced triple-ζ Gaussian-type atomic orbital (GTO) basis set with the D4 London dispersion correction, and a geometrical counterpoise (gCP) correction for remaining inter- and intramolecular basis set superposition errors. GTO-based r^2SCAN-3c yields excellent results for the calculation of conformational energies for systems involving main-group and transition metals.[26, 27]

R^2SCAN is the second revision of the SCAN meta-GGA density-function approximation and can be used to construct high performance for conformational energies and structures. An estimate for the overall free energetic profile in the gas phase is shown in **Figure 3.14** for the dissociative and associated isomerisation routes, which proceed through 3- and 5-coordinate intermediates respectively can be made. The values are relative to the lowest energy isomer. The five-coordinate intermediate, with η^3-I* (13.25 kcal mol^{-1}) is calculated to be considerably lower in energy than the 3-coordinate intermediate (29.08 kcal mol^{-1}) and closer in energy to the (A-*proximal*,R_{Sc},S_I)/(A-*proximal*,S_{Sc},R_I) enantiomeric pair (8.70 kcal mol^{-1}). Therefore, the inversion of the metal chirality centre of **12** (**12-T** → **12-K** and **12-K** → **12-T**) *via* ligand exchange is proposed to go *via* a reaction pathway that includes (A-*proximal*,R_{Sc},S_I)/(A-*proximal*,S_{Sc},R_I) isomer.

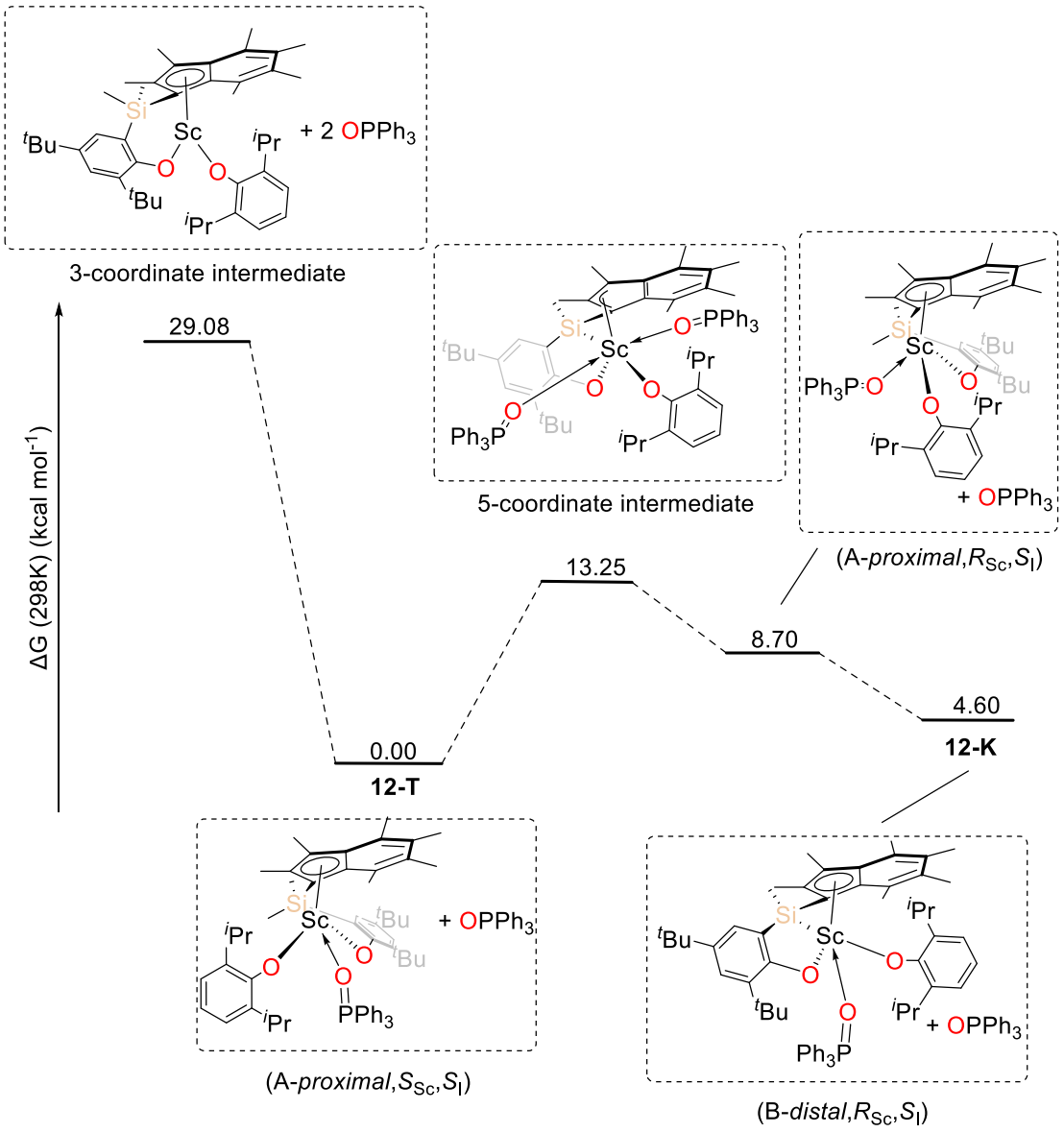


Figure 3.14 The overall computed Gibbs energy profile for $OPPh_3$ ligand exchange and metallocyclic ring puckering between **12-T** and **12-K**. The relative energies are computed using r^{2}SCAN-3c and presented as ΔG (kcal mol^{-1}). Five-coordinate intermeditate and three-cooridate intermediate are displayed.

The nature of the indenyl ligand allows facile ring slip to an η^3- donor (5-coordinate intermediate in **Figure 3.14**) to accommodate associative mechanisms.[28] Initially the four-coordinate tetrahedral scandium follows the 12e$^-$ rule.[29] Aromatisation of the C_6 ring during the haptotropic shift reduces the thermodynamic cost. This could allow additional coordination from neutral donor, here $OPPh_3$, and lead to a five-coordinate transition state

with 12 e^- filling only the metal ligand bonding orbitals. The five-coordinate geometry has been reported for the addition of PH_3 to η^5-(Ind)$Mn(CO)_3$ to form a 'pseudo-octahedral' complex, η^3-(Ind)$Mn(CO)_3(PH_3)$.[28] The DFT study, by Verios, described addition of PH_3 that occurs at the less crowded position (under the Me^{α} group), rather than at the site under to the C_6 ring.

Other four-coordinate scandium complexes have shown similar behaviour involving labile bonds that allow inversion of conformation or stereochemistry. The four-coordinated scandium imido complex reported by Parvez *et al.* occurred in endo/exo structures as shown in **Figure 3.15**.[30] A proposed dissociative mechanism, *via* a three-coordinate intermediate, forms first to allow scandium N-H insertion at 70 °C. In this case, both the *endo-* and *exo-* compounds were observed and shown to be in dynamic equilibrium. The reaction is slow and dissociation is rate limiting.

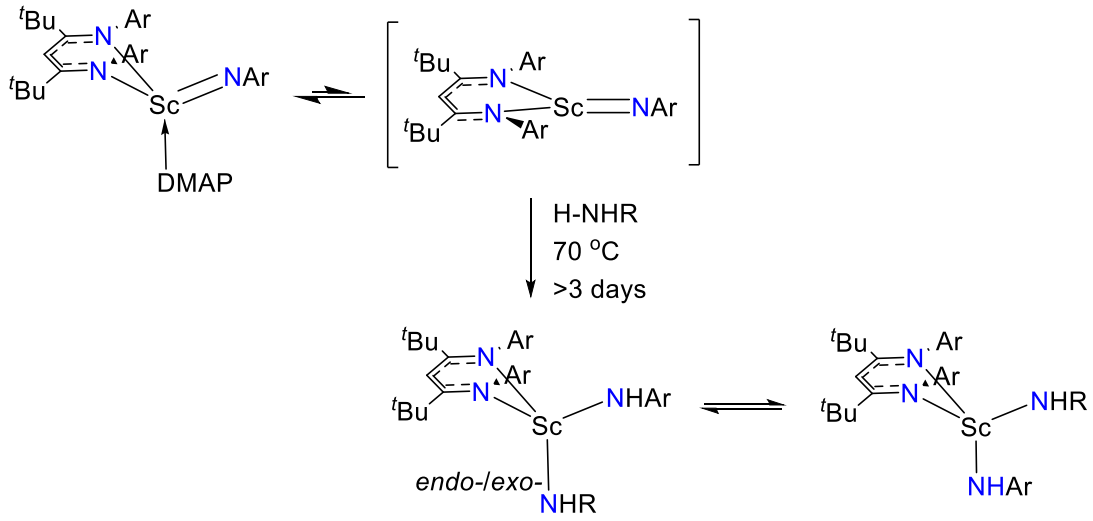


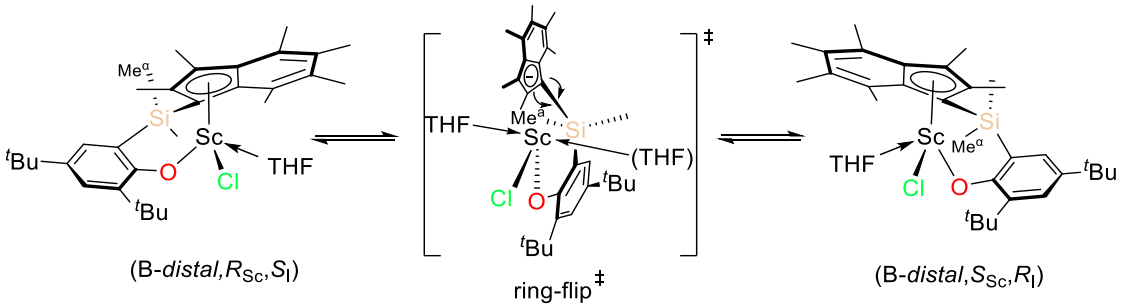
Figure 3.15 Slow interconversion *via* dissociation. Three-coordinate intermediate is reactive towards N-H bonds.[30]

Isomerisation half-sandwich Cp scandium complexes have been reported before, such as the compound $^{Me_2}Si(^{tBu}N,Cp^*)Sc(C_6H_5)(PMe_3)$ reported by Bercaw and co workers. At

elevated temperatures (80 °C), a mixture of isomers form from a single enantiomer.[31] For I* complexes **1**–**13** , coordination of neutral donors is facile, inversion of the metal centre occurs rapidly leading to broader resonances, and in some cases, several observed species observed in the ^{1}H NMR spectrum.

3.2.7. Disassociation, rotation, and reassociation of the indenyl moiety (I* face flip)

For the PHENI* complexes **1**, in solution the enantiomers are in equilibrium as depicted in **Scheme 3.1**.



Scheme 3.1 Proposed equilibria and realtionship between stereoisomers in solution of **1**.

The scheme shows both a chirality change (through substitution of THF) and dis/re-association of the indenyl moiety. Both the metal and indenyl chirality are altered.

The ^{1}H NMR spectrum of **1** in benzene-d_6 at 298 K shows a mixture of 2 isomers with the formula ^{Me_2}SB($^{t Bu_2}$ArO,I*)Sc(Cl)THF (**1**) in a ratio of 7:1. (**Figure 3.16**).

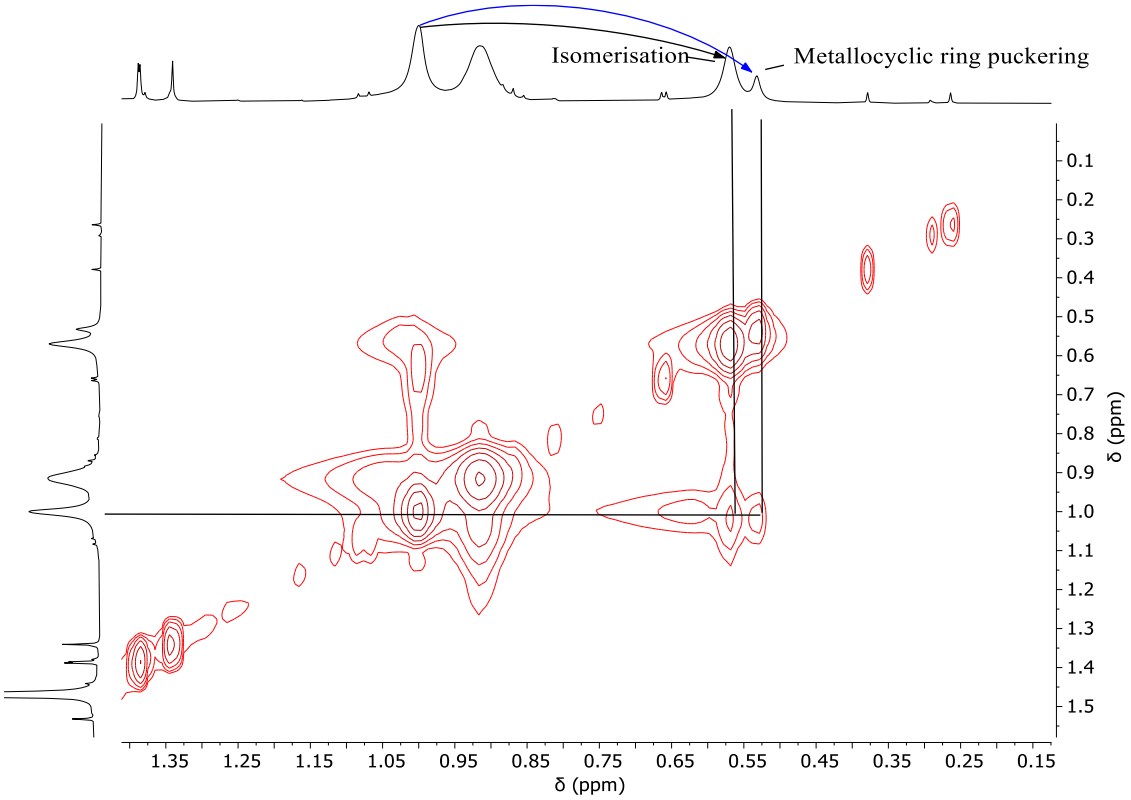


Figure 3.16 ^{1}H-^{1}H NOESY spectrum (500 MHz, benzene-d_6, 298 K) of ^{Me_2}SB($^{t Bu_2}$ArO,I*)Sc(Cl)THF (**1**). Chemical exhange between Si*Me* environments through isomerisation and metallocylic ring puckering.

The reaction mechanism in **Scheme 3.1** relates the enantiomer pair and includes all operations {MSI} shown in **Figure 3.17.** I* face flip, ligand exchange, and metallocyclic ring puckering all have allowed associated mechanisms and therefore lead to the isomerisation possible for **1**.

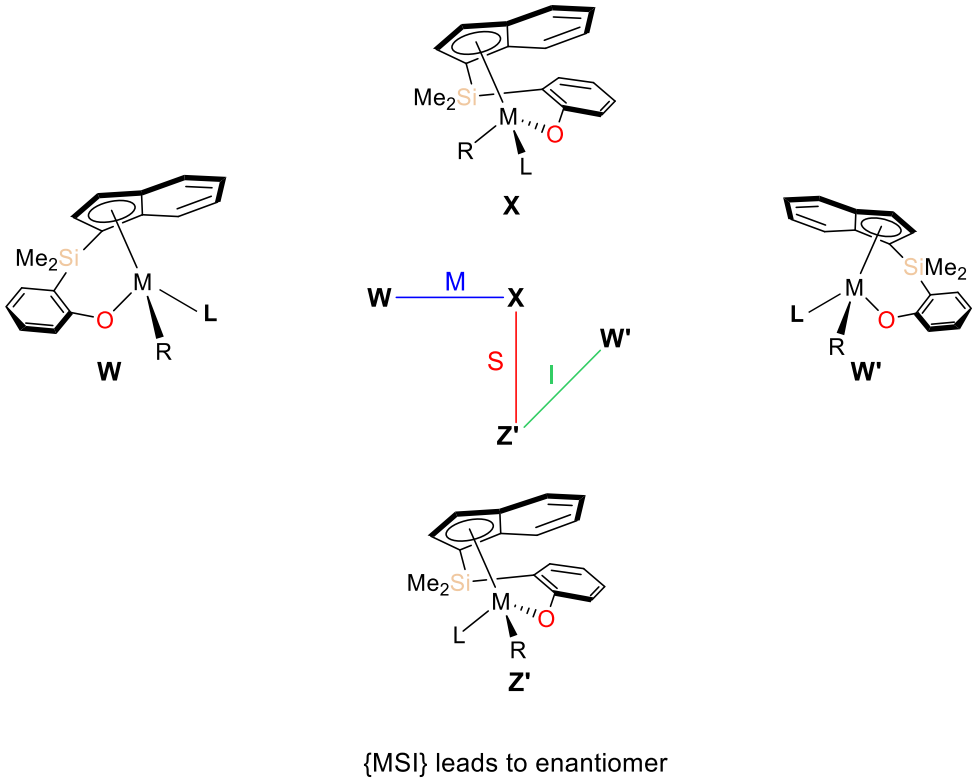


Figure 3.17 Allowed chemical distalformation/reactions required for isomerism of PHENI* complexes.

The ^{1}H-^{1}H NOESY spectra can be used to confirm chemical exchange and the presence of additional isomers in solution. For **2**, **5**, **6**, and **11** positive correlations between the Si*Me* proton environments for A-*proximal*/B-*distal* conformers is observed (**Figure 3.18**). For **11** (^{Me2}SB(^{tBu2}ArO,I*)Sc(Cl)OPPh$_3$), additional cross peaks are present between the Si*Me* proton resonances at δ 1.08 and 0.65 ppm, indicative of isomerisation in solution.

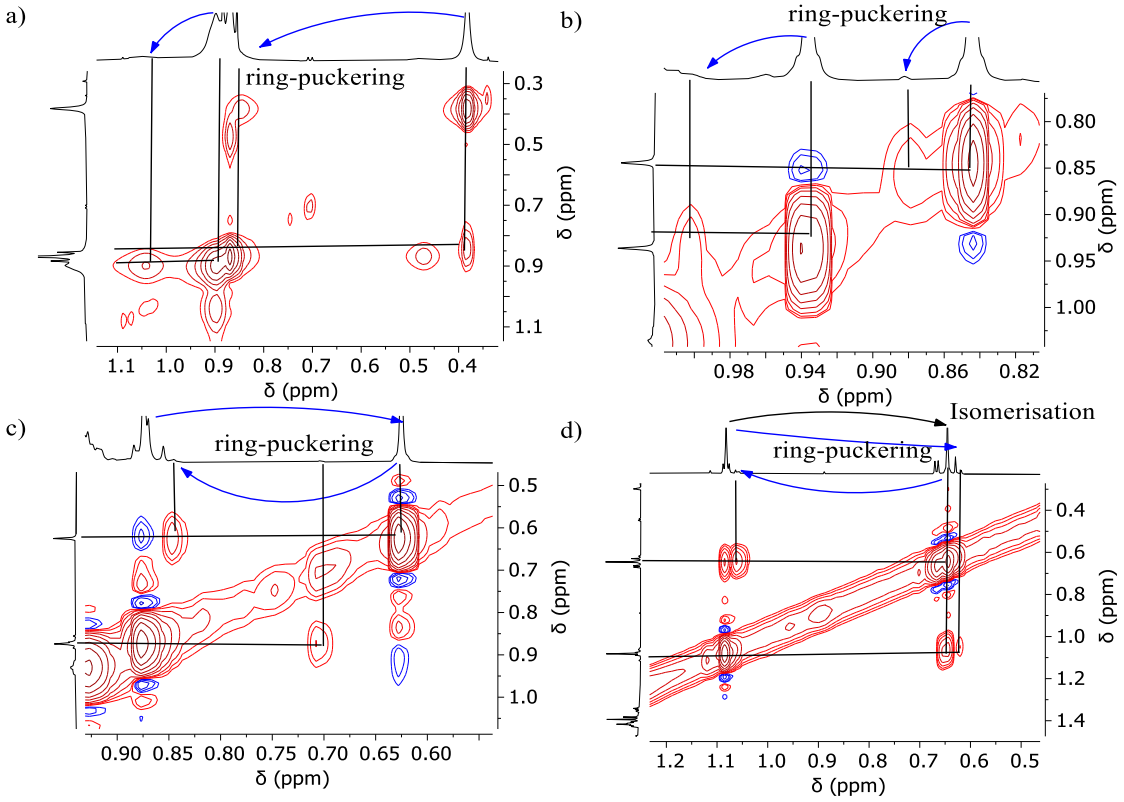
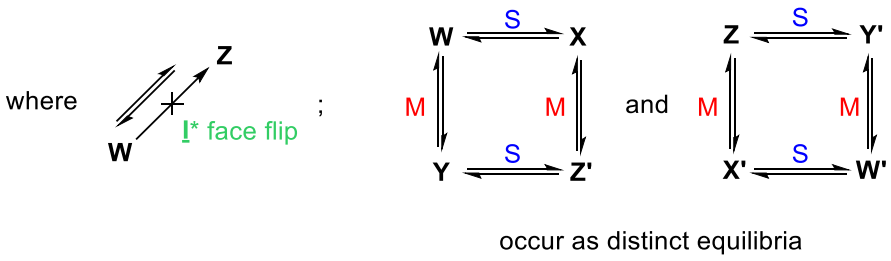


Figure 3.18 ^{1}H-^{1}H NOESY spectrum (600 or 400 MHz, benzene-d_6 298 K) of (a) **2**, (b) **5**, (c) **6**, and (d) **11** showing the exchange of Si*Me* groups. Blue cross peaks are through space coupling, red cross peaks are due to chemical exhange.

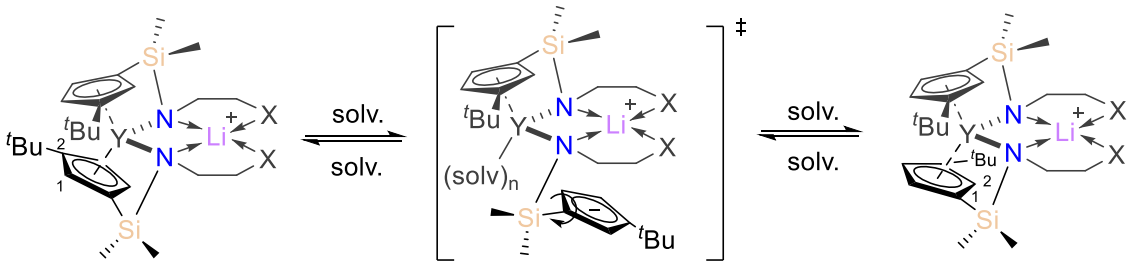
For **2**, **5**, and **6** where I*face flip is not observed, distinct equilibria are shown to exist as depicted in **Scheme 3.2**.



Scheme 3.2 Distinct equilibria between isomers where ligand exchange and metallocyclic ring puckering is possible but I* face flip is not

Cp derivatives have been proposed to go through a 'ring-flip' rearrangement mechanism through disassociation, rotation, and reassociation of the η^5-Cp–M bond; possible

mechanistic pathways have been studied for a number of asymmetric metallocene and chiral-Cp complexes.[32, 33] Reports of Cp and indenyl ring flipping have been noted previously by Okuda *et al*. (**Scheme 3.3**).[34]



Scheme 3.3 Isomerisation through dissociation, rotation, and re-coordination with the opposite face of the cyclopentadienyl ligand moiety reported by Okuda *et al*..[32]

For the synthesis of metallocene complexes *via* salt metathesis, residual LiCl can form an adduct with THF coordinated to the metal centre. Use of this synthetic route is suspected to lead increased rates of 'face flipping' in metallocene systems.[35] The ring flip involves the formation of an intermediate 'lithium Cp ion pair', as reported by Okuda *et al.*, in tandem with solvent stabilisation of the metal centre.[32, 36]

3.3. Conclusion

A unified approach to describe the stereochemistry and conformational dynamics of PHENI* complexes has been proposed. Possible pathways for isomerisation were explored with examples of metallocyclic ring puckering, metal centre chirality and indenyl face flipping.[13, 22, 23] PHENI* scandium complexes **1–13** are all present as a mixture of isomers. The labile ligands allow the product distribution to under thermodynamic control about the R_{Sc}/S_{Sc} chiral centre, elongated *ansa*-bridges allows for a low barrier for conversion between diastereomers.

Inversion of chirality at the metal stereogenic centre occurs through ligand disassociation and reassociation or *via* associative substitution, which can be observed through addition of $OPPh_3$ to form a dynamic equilibrium of isomers. The substitution of labile neutral donors is promoted due to the low energy barrier required for the I* ring slip (η^5- to η^3- to η^5-). Thus, scandium (III) can coordinate with an additional ligand without changing oxidation state.[21]

Large ligands (ODipp over Cl; DMAP and $OPPh_3$ over THF) reduce the relative ratio of minor isomers in solution. PHENI* complexes **1**, **2**, **5**, **8**, **9**, **11**, **12** present conformational isomerism in the form of distinct A-*proximal* or B-*distal* conformers in solution. LiCl catalyses isomerisation of PHENI* Sc complexes, as seen for **1,** through ring-flipping of the η^5-permethylindenyl moiety. Indenyl face flipping occurs through ligand disassociation and reassociation or *via* associative substitution.[8, 32]

3.4. References

1. , International Union of Pure and Applied Chemistry (IUPAC), 3.0.1 edn., 2019, DOI: doi:10.1351/goldbook.S05980.
2. P. International Union of and C. Applied, DOI: 10.1351/goldbook.C01262.
3. G. P. Goryunov, M. I. Sharikov, A. N. Iashin, J. A. M. Canich, S. J. Mattler, J. R. Hagadorn, . . . A. Z. Voskoboynikov, *Acs Catal*, 2021, **11**, 8079-8086.
4. E. Kirillov, T. Roisnel, A. Razavi and J.-F. Carpentier, *Organometallics*, 2009, **28**, 5036-5051.
5. T. Agapie, L. M. Henling, A. G. DiPasquale, A. L. Rheingold and J. E. Bercaw, *Organometallics*, 2008, **27**, 6245-6256.
6. W. P. Freeman, Y. J. Ahn, T. K. Hollis, J. A. Whitaker, V. C. Vargas, R. J. Rubio, . . . F. S. Tham, *J Organomet Chem*, 2008, **693**, 2415-2423.
7. K. B. Wagener, *Science*, 1995, **267**, 191.
8. G. W. Coates and R. M. Waymouth, *Science*, 1995, **267**, 217-219.
9. T. Arnold, D.Phil. Thesis, Oxford University, UK, 2015.
10. L. Chan, G. R. Hutchison and G. M. Morris, *J Chem Inf Model*, 2021, **61**, 743-755.
11. I. K. Boessenkool and J. C. A. Boeyens, *J Mol Struct*, 1980, **10**, 11-18.
12. J. H. Fu, Z. Y. Wang, F. L. Xue and J. P. Huo, *Acta Crystallogr Sect E Struct Rep Online*, 2010, **67**, o73.
13. P. S. Steinlandt, L. Zhang and E. Meggers, *Chem Rev*, 2023, **123**, 4764-4794.
14. T. D. Neil G. Connelly, Richard M. Hartshorn, Alan T. Hutton, *Nomenclature of Inorganic Chemistry IUPAC Recommendations 2005*, The Royal Society of Chemistry, 2005.
15. R. S. Cahn, C. Ingold and V. Prelog, *Angew Chem Int Ed Engl*, 1966, **5**, 385-415.
16. V. Prelog and G. Helmchen, *Angew Chem Int Ed Engl*, 1982, **21**, 567-583.
17. M. Nabika, H. Katayama, T. Watanabe, H. Kawamura-Kuribayashi, K. Yanagi and A. Imai, *Organometallics*, 2009, **28**, 3785-3792.

18. M. J. T. Frisch, G. W.; Schlegel, H. B.; Scuseria, G. E.; Robb, M. A.; Cheeseman, J. R.; Zakrzewski, V. G.; Montgomery, J. A., Jr.; Stratmann, R. E.; Burant, J. C.; Dapprich, S.; Millam, J. M.; Daniels, A. D.; Kudin, K. N.; Strain, M. C.; Farkas, O.; Tomasi, J.; Barone, V.; Cossi, M.; Cammi, R.; Mennucci, B.; Pomelli, C.; Adamo, C.; Clifford, S.; Ochterski, J.; Petersson, G. A.; Ayala, P. Y.; Cui, Q.; Morokuma, K.; Malick, D. K.; Rabuck, A. D.; Raghavachari, K.; Foresman, J. B.; Cioslowski, J.; Ortiz, J. V.; Baboul, A. G.; Stefanov, B. B.; Liu, G.; Liashenko, A.; Piskorz, P.; Komaromi, I.; Gomperts, R.; Martin, R. L.; Fox, D. J.; Keith, T.; Al-Laham, M. A.; Peng, C. Y.; Nanayakkara, A.; Challacombe, M.; Gill, P. M. W.; Johnson, B.; Chen, W.; Wong, M. W.; Andres, J. L.; Gonzalez, C.; Head-Gordon, M.; Replogle, E. S.; Pople, J. , *Gaussian, Inc*, 1998, A.GAUSSIAN 98, Revision A.9.
19. J. V. Lamb, D.Phil. D.Phil. Thesis, University of Oxford, 2019.
20. J. V. Lamb, J. C. Buffet, Z. R. Turner and D. O'Hare, *Polym Chem-Uk*, 2019, **10**, 1386-1398.
21. H. Brunner, *Angew Chem Int Ed Engl*, 1999, **38**, 1194-1208.
22. P. Kumar, R. K. Gupta and D. S. Pandey, *Chem. Soc. Rev.*, 2014, **43**, 707-733.
23. J. Z. Shezaf, C. G. Santana, C. Saludares, E. S. Briceno, K. Sakata and M. J. Krische, *J Am Chem Soc*, 2023, **145**, 18676-18683.
24. S. Akine and H. Miyake, *Coordin Chem Rev*, 2022, **468**.
25. M. D. Hanwell, D. E. Curtis, D. C. Lonie, T. Vandermeersch, E. Zurek and G. R. Hutchison, *J Cheminform*, 2012, **4**, 17.
26. T. Gasevic, J. B. Stückrath, S. Grimme and M. Bursch, *J Phys Chem A*, 2022, **126**, 3826-3838.
27. S. Grimme, A. Hansen, S. Ehlert and J.-M. Mewes, *J Chem Phys*, 2021, **154**.
28. L. F. Veiros, *Organometallics*, 2000, **19**, 3127-3136.
29. G. Frenking and N. Fröhlich, *Chem Rev*, 2000, **100**, 717-774.
30. T. Chu, W. E. Piers, J. L. Dutton and M. Parvez, *Organometallics*, 2013, **32**, 1159-1165.
31. P. J. Shapiro, PhD, California Institute of Technology, 1991.
32. K. C. Hultzsch, T. P. Spaniol and J. Okuda, *Organometallics*, 1997, **16**, 4845-4856.
33. C. M. Haar, C. L. Stern and T. J. Marks, *Organometallics*, 1996, **15**, 1765-1784.
34. O. J. Curnow, G. M. Fern, M. L. Hamilton and E. M. Jenkins, *J Organomet Chem*, 2004, **689**, 1897-1910.
35. S. Bellemin-Laponnaz, M. M. C. Lo, T. H. Peterson, J. M. Allen and G. C. Fu, *Organometallics*, 2001, **20**, 3453-3458.
36. A. Fridrichová, A. Růžička, M. Lamač and M. Horáček, *Inorg Chem Commun*, 2017, **76**, 62-66.

Chapter 4 – Using scandium complexes for the polymerisation of cyclic esters

4.1. Introduction

4.1.1. Chapter synopsis / Overview

Complexes **1**, **2**, **3**, **5**, and **7** are studied in this chapter for the ring-opening polymerisation of ϵ-caprolactone (ϵ-CL), *L*-lactide (*L*-LA), and ω-pentadecalactone (ω-PDL) (**Figure 4.1**).

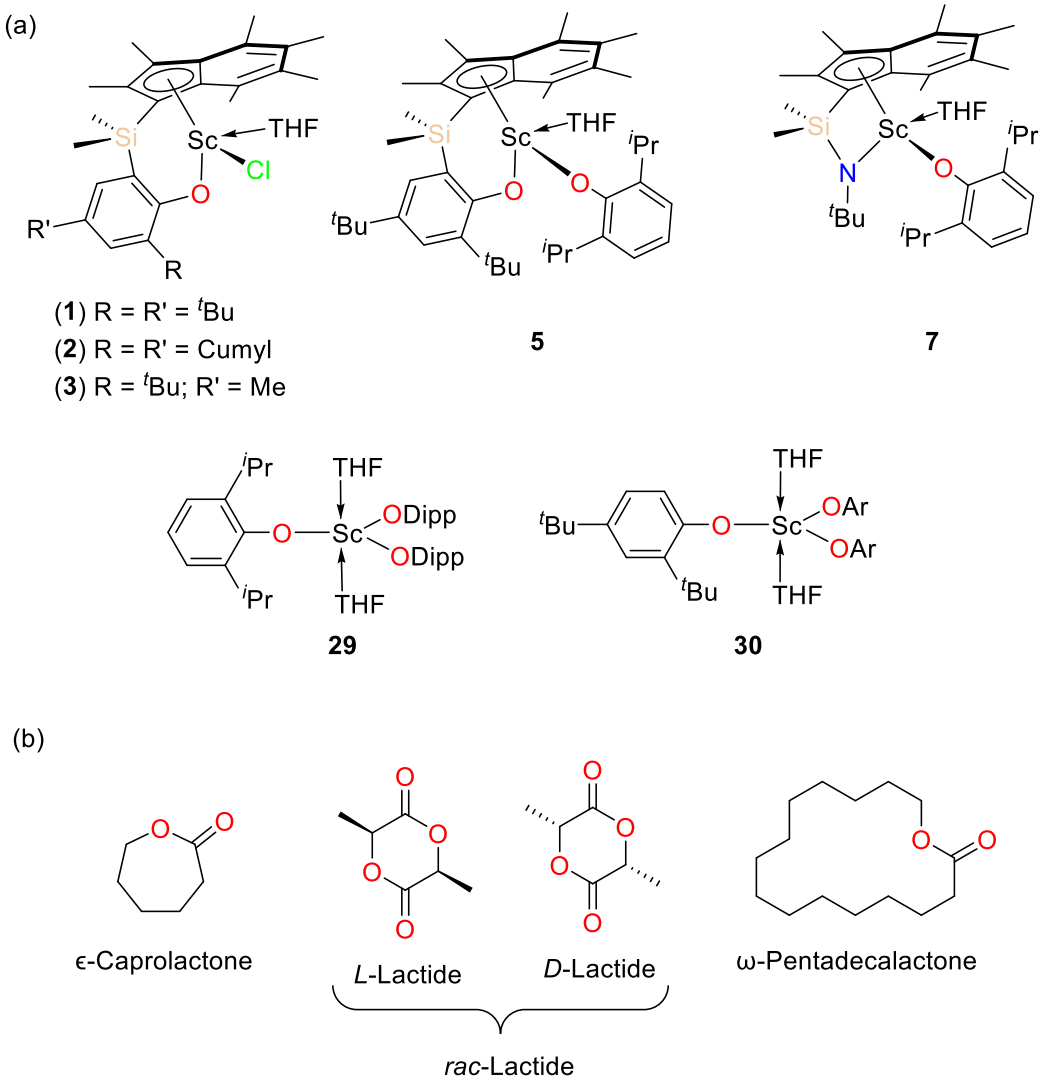
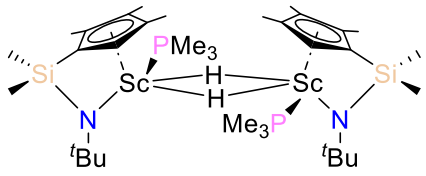


Figure 4.1 Summary of (a) initiators and (b) monomers used in this Chapter.

The effects of the addition of a co-initiator are studied. Solid-state structures of the adducts of **1** with *L*-LA and ω-PDL in addition to **5** and ϵ-CL, have been isolated and characterised (**24**–**26**). Temperature and monomer loading have been varied for a series of kinetic and thermodynamic studies. An attempt for the copolymerisation of ϵ-CL and *L*-LA was also carried out in addition to exploring the effects of neutral donors on activity and side reaction control. A series of polymer characterising techniques have been deployed.

4.1.2. Organometallic Scandium Catalysts for polymerisation

Rare earth metals have shown excellent catalysts for the coordination (co)polymerisation of α-olefins and cyclic esters. The first scandium half-metallocene complex, developed by Bercaw and co-workers, was commercialised as a α-olefin catalyst in the 1980s.



1989

Figure 4.2 (^{Me_2}SB($^{t Bu}$N,Cp*)Sc(H)PMe$_3$)$_2$ reported by Bercaw and co-workers.[1]

The field developed to using half-sandwich scandium bis(alkyl) complexes, activated with [Ph_3C][$B(C_6F_5)_4$] to form cationic scandium capable of co and tri polymerisation of a range of α-olefins and cyclic esters (**Figure 4.3**). They exhibit high stereoselectivity and activity. Further, neutral organometallic scandium complexes have been used for the polymerisation of cyclic esters such as LA and ϵ-Cl.

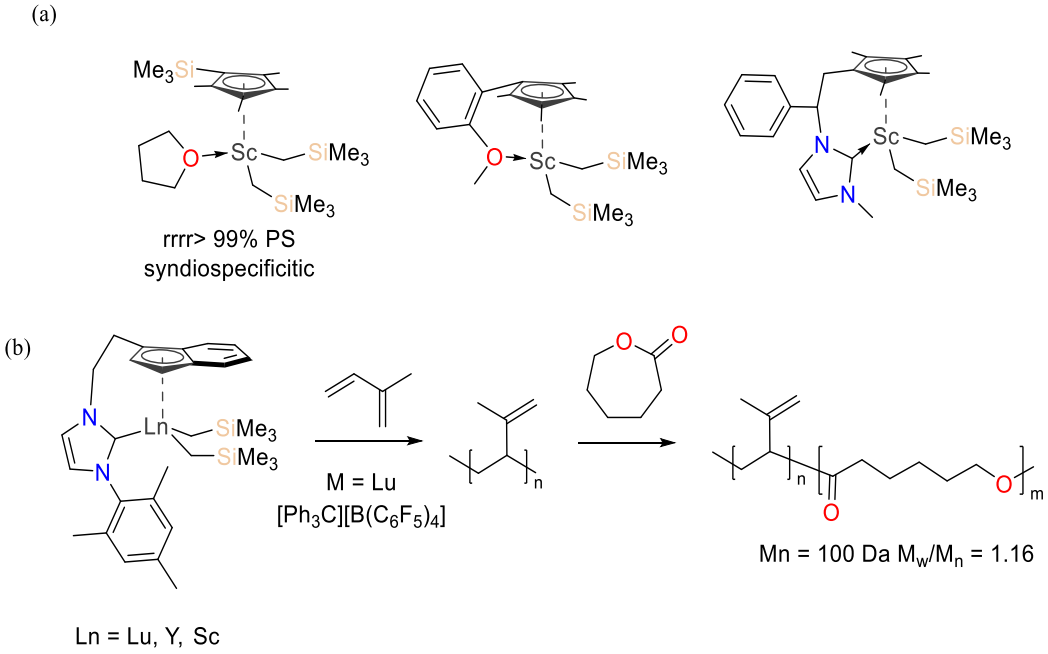


Figure 4.3 (a) Selection of bis(alkyl) rare earth (III) complexes[2-4] THF free scandium complexes, which (b) when activated with $[Ph_3C][B(C_6F_5)_4]$ and show highly active polymerisation of esters and olefins.

Fluxional complexes have been shown to rearrange *in-situ* during the polymerisation of cyclic esters. The fluxional bis(phenolato)scandium complex, reported by Okuda *et al*., switch between *Λ* and *Δ* configurations to yield highly heterotactic PLA with $P_r = 0.95$, reaching 81% conversion after 8 h at 25 °C ($[LA]_0:[Sc]_0 = 300:1$, THF) (**Figure 4.4**).[5]

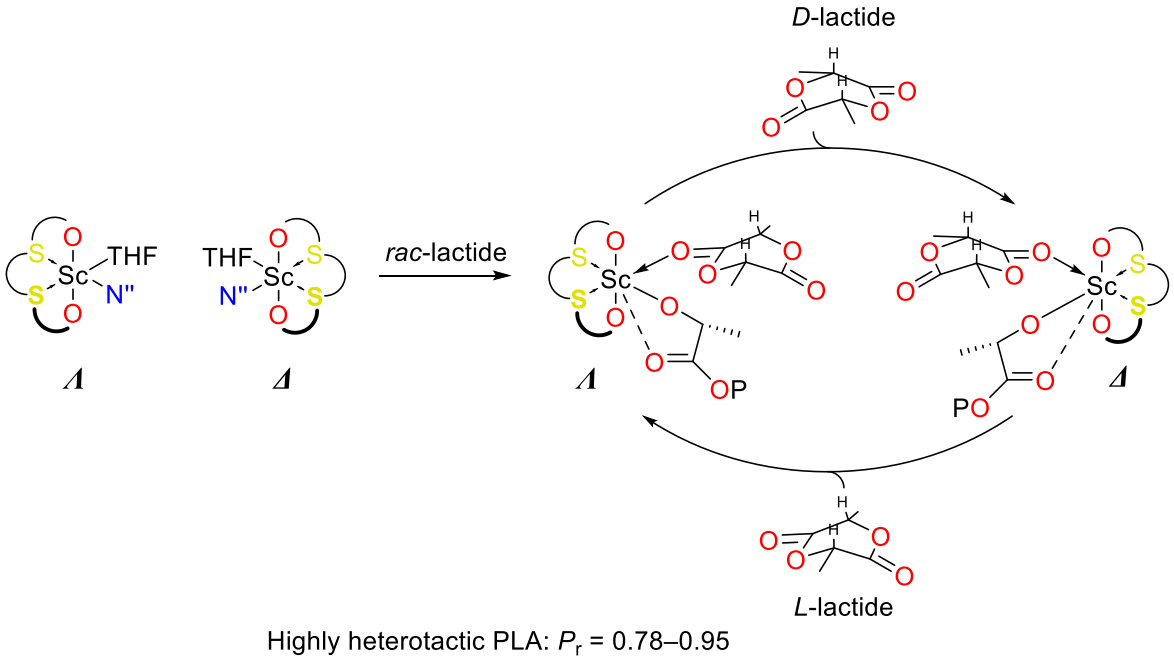


Figure 4.4 Fluxional bis(phenolato)scandium complexes capable of producing highly heterotactic PLA.[5]

In a similar manner, it could be possible that the fluxional bridge in CGCI* or PHENI* complexes also produce a similar effect, leading to enantiomeric site control depending on the stereoisomers present. O'Hare *et al.* reported the polymerisation of *rac*- and *L*-lactide using a variety of group 3 and 4 Pn* and I* type complexes. Atactic PLA was produced from the Pn* derivatives (**Figure 4.5** (a)).[6] Zirconium *ansa*-bridged I*-Cp systems produced heterotically enriched PLA with P_r = 0.81, in the presence of BnOH (**Figure 4.5** (b)).[7] Moderate stereo-control was reported for CGC-I* scandium complex ^{Me2}SB(^{R}N,I*)Sc(X)THF, where R = ^{i}Pr, ^{t}Bu, Ph; (**Sc-2** *P*r = 0.59; **Sc-3** *P*r = 0.68; **Sc-5** *P*r = 0.63) at elevated temperature (70 °C), where chain end control dictating the final tacticity of the polymer produced rather that site control.[8] From **Chapter 2** and **3**, the CGCI* more is ridged than the PHENI* ligand.

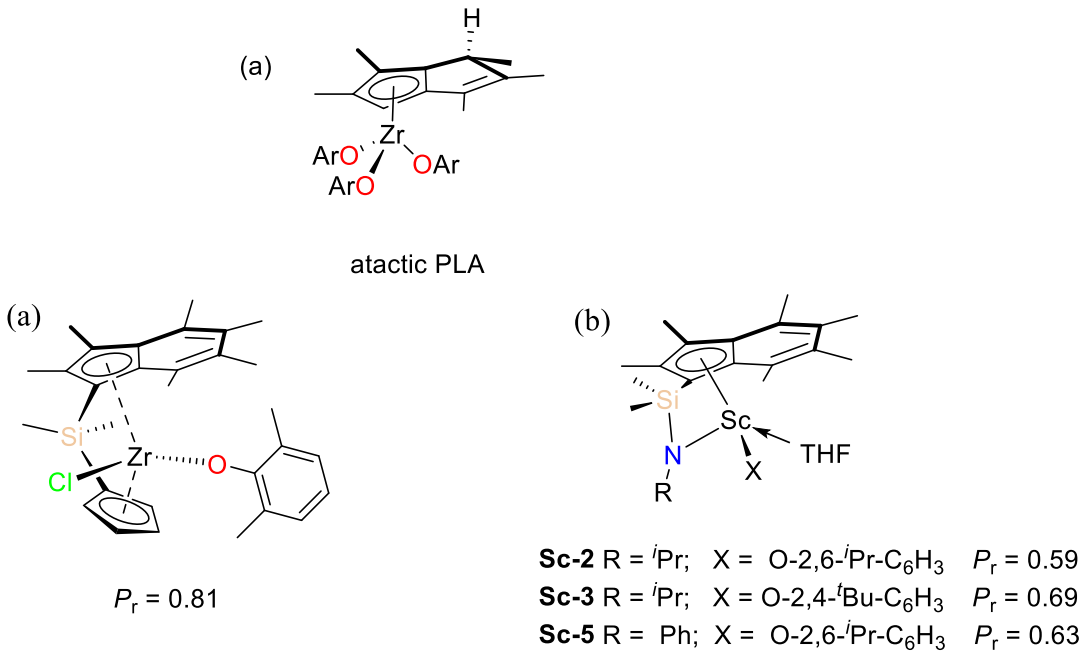


Figure 4.5 (a) Pn* zr complex[6] (b) ansa-bridged I*-CP zirconium complexes (c) CGC-I* ^{Me_2}SB(^{R}N,I*)Sc(R)THF reported by O'Hare *et al*.; for the polymerisation of lactide.[7, 9, 10]

Rare earths (RE) M(III) complexes have been used to study the polymerisation of ϵ-CL, proving to be some of the most active reported.[11] The reports of scandium over other RE metals is limited, despite high activity and control being reported for scandium catalysts.[12]

4.1.3. Reaction kinetics

Some simple methods are used as a guide to compare the polymerisation activities. The propagation rate constant , $k_{p,}$ is derived from the rate law of polymerisation.[13] Subtleties of the polymerisation mechanism are independent of this simplified kinetic equation which involves measuring the consumption of monomer as a basis for comparing activity.

$$-\frac{d[M]}{dt} = k_p[M]^x[cat]^y$$

k_p is calculated from the integrated plot from the experimentally observed rate constant k_{obs} at different catalyst concentrations. Using plots of $-\ln(k_{obs})$ *vs* $-\ln([cat]_0)$, and k_{obs} *vs* $[cat]_0$, an approximation of k_p can be made.

$$Ln\left(\frac{[M]_0}{[M]}\right) = k_p[cat.]t$$

De*via*tions from linearity can provide insights into the reactions, such as if the concentration of active initiator is changing, or if propagation is being outweighed by chain transfer or intra/intermolecular transesterification.

Other more complex methods to understand kinetics have also been developed as analysis of the kinetic profile of the reaction can lead to greater mechanistic insights. These include deterministic and stochastics optimisation models, which focus on the probability of chemical reactions occurring. These models provide detailed insights into polymer microstructure, but require extensive computing time and storage due to the required large sample sizes.[14-17] Direct analysis of a single, whole reaction profile through Variable Time Normalisation Analysis (VTNA) or Reaction Progress Kinetic Analysis (RPKA) methods can allow detailed kinetic analysis from smaller sample sizes.[18, 19] The most simple methods involve 'linearization methods', such as the plots of $-\ln(k_{obs})$ *vs.* $-\ln([cat]_0)$, and k_{obs} *vs.* $[cat]_0$, outlaid above, is only as good as the data fit (hence R^2 is included).[20] Where direct fitting is done in this thesis, the initiation period (first 10% of monomer consumption) has not been included in the fit.

4.1.4. Polymerisation conditions

Polymerisation reactions were performed in J. Young's tap NMR tubes unless otherwise stated. This does not allow for stirring which decreases reproducibility. The initial

concentration of monomer ([ϵ-CL]) is 0.5 M. Polymerisations were carried out in toluene or benzene dried over potassium and monitored directly through ^{1}H NMR spectroscopy for kinetic studies[21], or aliquots taken and the specified time intervals and quenched in (wet) pentane, before conversion is determined *via* ^{1}H NMR spectroscopy.

4.1.5. Considerations regarding Mark Houwink correction factor

When undertaking GPC (SEC) analysis, a calibration is done to take into consideration of the interaction of the polymer with the stationary phases.

For linear ϵ-CL, the Mark-Houwink correction factor of $K = 13.95 \times 10^{-5}$ dL/g; $a = 0.786$ is used.[22] For this thesis, due to the nature of oligomerisation and the effect that topology has on interaction with the stationary phase in the column, uncorrected values are quoted unless otherwise stated (in brackets). The uncorrected values are calculated using polystyrene standards ($K = 14.1 \times 10^{-5}$ dL/g; $a = 0.7$).

4.2. ϵ-CL polymerisation studies using PHENI* scandium chlorides (1–3)

4.2.1. The effect of BnOH

Complexes **1**, **2**, and **3** were selected for an initial study. Initial polymerisation studies employed the co-initiator benzyl alcohol ($C_6H_2CH_2OH$, BnOH) as a co-initiator. The Chloride complex **4** has previously shown to polymerise *L*-LA without a co-initiator, however, adding BnOH increased the polymerisation rate from 85% in 5 h to 94% in 50 mins.[23] Other RE chloride complexes have been reported to polymerise cyclic esters, such as the β-diketiminato (NacNac) Yb(III) chloride complex (NacNac)Yb(OAr)Cl(THF) reported by Zhang *et al*. was reported to act as initiators through M-O bonds for the ROP of ϵ-CL.[24] Commonly, alkoxide, alkyl, amide, and borohydrides groups are often used rather than halide groups as the target initiator group in ROP.[25]

1 equiv.of BnOH initiator was added prior to monomer addition. Where BnOH is used as a co-initiator, complexes **1**–**3** display a moderate rate of polymerisation at ambient temperature forming monomodal distributions with relatively low molar-mass dispersity ($Đ_M$ = 1.15–1.58) (**Figure 4.6** and **Table 4.1**).

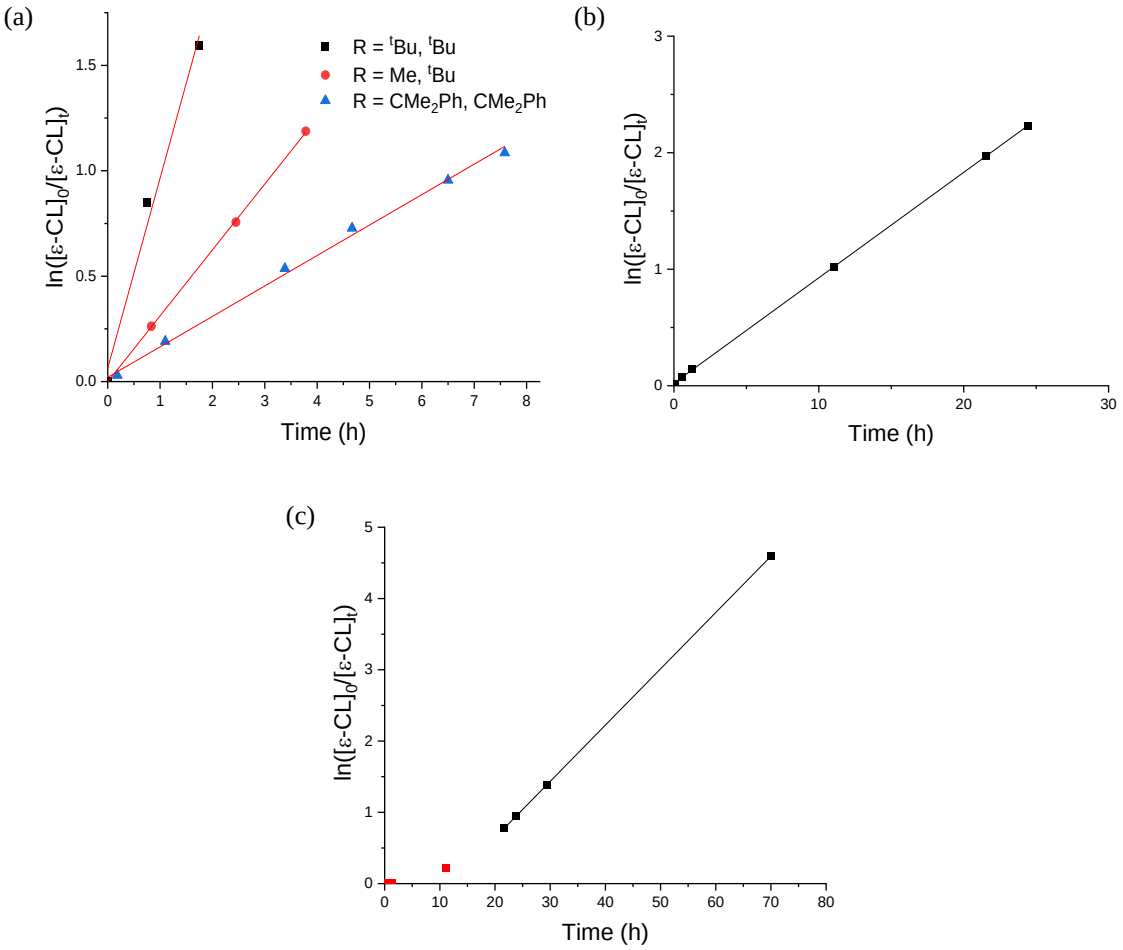


Figure 4.6 Plots of ln([ϵ-CL]$_0$/[ϵ-CL]$_t$) *vs.* Time (h) (a) 1, Black square (k_{obs} = 0.90±0.010^{-1}. R^2 = 0.993); **2** red circles (k_{obs} = 0.14±0.003^{-1}. R^2 = 0.999); **3**, blue upward triangles (k_{obs} = 0.31±0.003^{-1}). Conditions: : [ϵ-CL]$_0$:[**Sc**]$_0$:[BnOH] = 50:1:1, [ϵ-CL]$_0$ = 0.5 M in 0.6 mL benzene-d_6.(b) (k_{obs} = 0.09±0.003^{-1}. R^2 = 0.999). Conditions: [ϵ-CL]$_0$:[**1**]$_0$:[BnOH] = 400:1:1; [ϵ-CL]$_0$ = 0.5 M in 0.6 mL benzene-d_6. (c) Plot of ln([ϵ-CL]$_0$/[ϵ-CL]$_t$) *vs.* Time (h) (k_{obs} = 0.079±0.0002^{-1}. R^2 = 0.999). Conditions: [ϵ-CL]$_0$:[**1**]$_0$:[BnOH] = 50:1:0, [ϵ-CL]$_0$ = 0.5 M in 0.6 mL benzene-d_6.

Table 4.1 ROP of ϵ-CL initiated by **1**–**3** with BnOH co-initiator unless stated[e].

Cat.	$[M]_0/[Sc]_0$	Time (h)	Conv.[a] (%)	k_{obs} (h^{-1})	R^2	$M_{n,SEC}$[b] (kDa)	$M_{n,th}$[a,c] (kDa)	$Đ_M$[b]
1	50	2	80	0.90±0.010	0.993	9.7(6.3)	4.6	1.58(1.51)
1	400	24	90	0.09±0.003	0.999	15.8(10.0)	41	1.14(1.13)
1[e]	50	70	99	0.079±0.0002	0.999	44(27)	5	1.74(1.65)
2	50	7.6	66	0.14±0.003	0.999	7.7(5.1)	3.7	1.30(1.26)
3	50	3.8	70	0.31±0.003	0.999	12.4(7.6)	4.0	1.17(1.15)

Conditions: $[\epsilon\text{-CL}]_0$:$[Sc]_0$:[BnOH] as 50:1:1, $[\epsilon\text{-CL}]_0$ = 0.5 M in 0.6 mL benzene-d_6 at 25 °C. [a] Measured by ^{1}H NMR. First-order rate constant (k_{obs}) and R^2 were obtained from plots of $\ln([\epsilon\text{-CL}]_0/[\epsilon\text{-CL}]_t)$ *vs* time. [bc] Calculated from monomer conversion data: $[M]_0/[Sc]_0$ × conv. (%) × 114.14 × 0.01 + (MW of end groups (α+ω)) in kDa.[d] Houwink correction factor used for values in brackets; K = 13.95 × 10^{-5} dL/g; a = 0.786.[26] [e] No BnOH added.

However, the use of BnOH resulted in protonation of the permethylindenyl moiety as observed *via* the ^{1}H NMR spectroscopy. The I*H^{β} proton is present as a quartet resonance integrating to 1H at δ 3.02 ppm and I*Me^{β} protons are present as a doublet resonance at δ 1.07 ppm that integrates to 3H. The Me^{β} and H^{β} are mutually coupled with $^3J_{H\text{-}H}$ = 7.3 Hz, consistent with adjacent methyl and proton and the reported structure 1,2,3,4,5,6,7-heptamethyl-1H-indene (**Figure 4.7**).[27, 28]

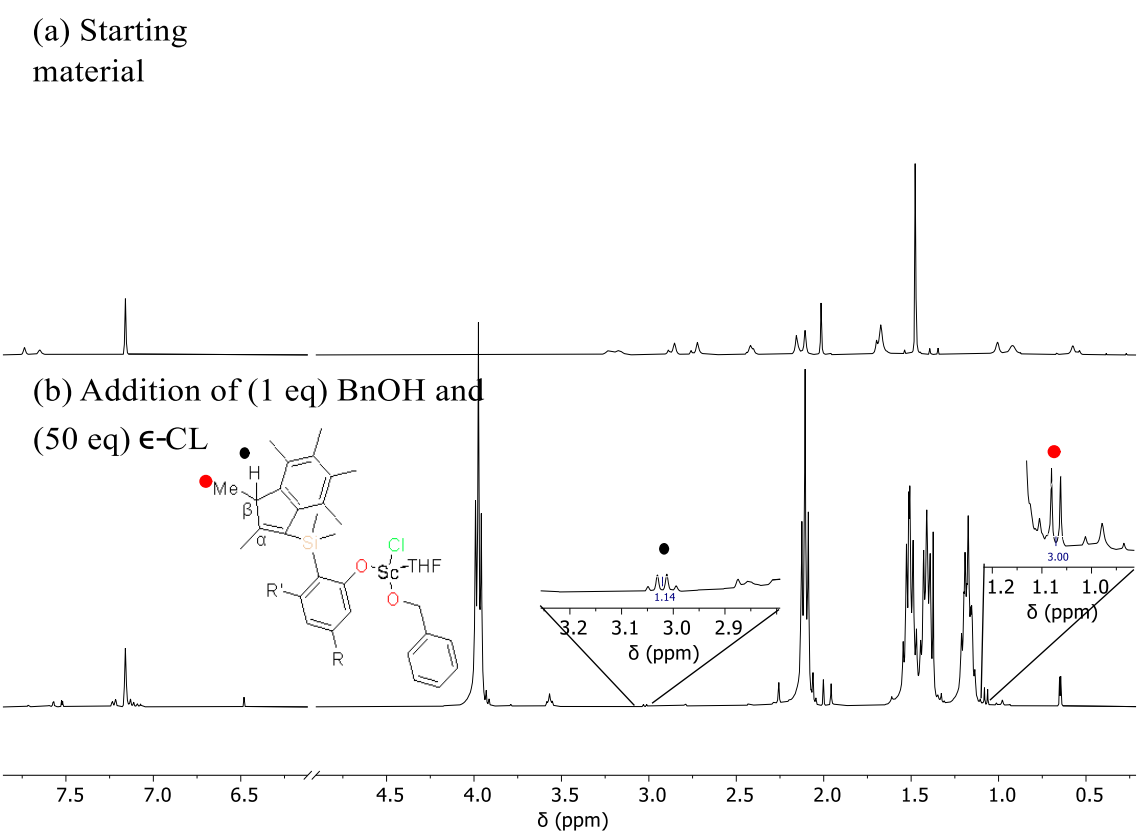


Figure 4.7 ^{1}H NMR spectra (benzene-d_6, 400 MHz, 298 K). of (a) **1**, and (b) addition of ϵ-CL and BnOH to **1** Conditions: [50]:[1]:[1], [ϵ-CL] = 0.5, 0.6 mL benzene-d_6 for 3h at 25 °C.

Adding other proton sources yielded a mixture of products through protonation of the indenyl in either the α- and β- positions of the Cp ring. This suggests that proton transfer occurs once the benzyl alcohol coordinates with the metal centre (**Figure 4.8** (a)). Another resonance of note, is free THF at δ 3.57 ppm, suggestive of the substitution of THF with ϵ-CL monomer during the polymerisation reaction. The resulting initiator is still active, with polymer chain growth from the scandium -benzyl group (**Figure 4.8** (b)), reacting, for **1**, 80% conversion in 2 h at ambient temperature for 50 equiv.of ϵ-CL.

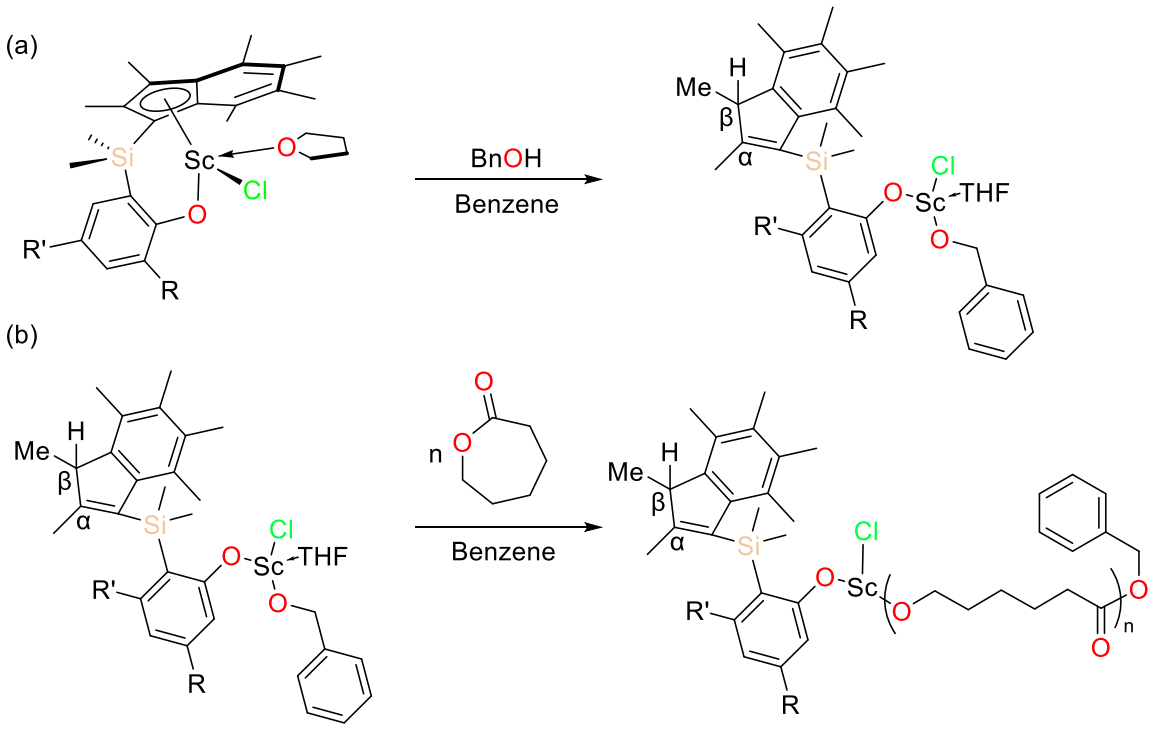


Figure 4.8 (a) Protonation of β-position through addition of BnOH. (b) Suggested active species during the polymerisation of ϵ-CL through insertion into the Sc-O($CH_2(C_6H_5)$) bond.

Bis-^{t}Butyl derivative **1** showed the highest activity under the conditions. The bis-cumyl derivative **2** presented with the slowest rate polymerising 50 equiv.of ϵ-CL in 7.6 h at ambient temperature. This shows the R,R′ groups leading to the reactivity order of **1** > **3** > **2;** ^{t}Bu, ^{t}Bu > ^{t}Bu, Me > Cumyl, Cumyl.

4.3. Polymerisation studies using PHENI*/CGCI* scandium aryloxide complexes

The aim was to target active catalytic species where the I* moiety is bonded to the scandium metal centre, to offer site control during polymerisation. To test the impact of altering the hetero atom, from N- to O-, a number of monomers were reacted with **5** and **7**. The macrolactone ω-pentadecalactone and *rac*-diolide have both been highlighted as potential alternatives to current commercial polyolefins. [29-33] Neither showed signs of polymerisation under the conditions tested.

4.3.1. Polymerisation of ϵ-CL varying the hetero atom (5 and 7)

Polymerisation studies were carried out using complexes **5** and **7** to compare the effects of altering the heteroatom on the kinetics and thermodynamics of polymerisation. The plots of conversion against time shows a slow initiation period and moderate rate for **5** and a fast initiation period and rate for **7** (**Figure 4.9).**

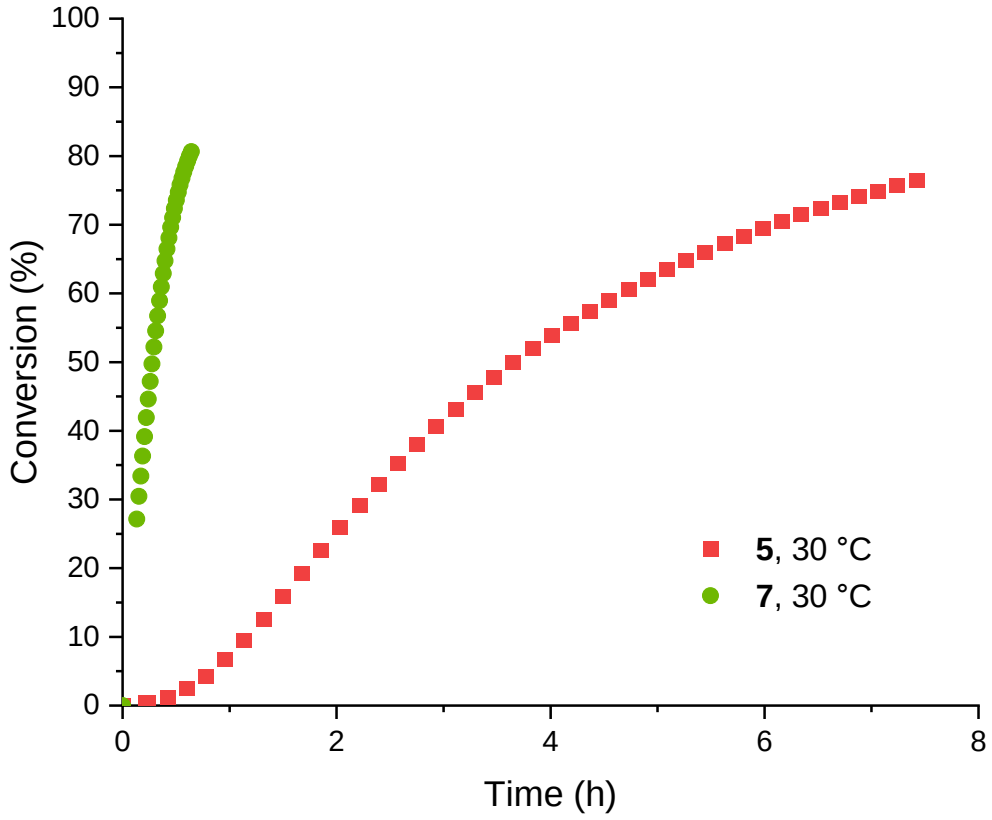


Figure 4.9 Plots of percentage conversion *vs.* time for **5** and **7**. **5**, red squares: (k_{obs} = 0.220 h^{-1}. R^2 = 0.999. **7**, green circles (k_{obs} = 2.79 h^{-1}. R^2 = 0.999) Conditions: [ϵ-CL]$_0$:[Sc]$_0$ [200]:[1] for **5** and [750]:[1] for **7**; [ϵ-CL]$_0$ = 0.5 M in 0.6 mL Tol-d_8 at 30 °C.

Plots used to obtain observed rate constants can be found in the appendix, section **A.3.3.3** and **A.3.3.5.** For the polymerisation of ϵ-CL, **5** had poor rate (k_{obs} = 0.224±0.004) achieving 70% conversion after 1.1 h at 60 °C in a ratio of 200:1 [ϵ-CL]:[Sc]$_0$. **7** exhibited a good polymerisation rate (k_{obs} = 2.79±0.026) achieving 81% conversion after 0.64 h at 30 °C in a ratio of 750:1 [ϵ-CL]:[Sc]$_0$. Although the conditions differ, the significant

change in initiation period and rate leads to the conclusion that insertion occurs through the tethered heteroatom on the ligand (**Figure 4.10**)

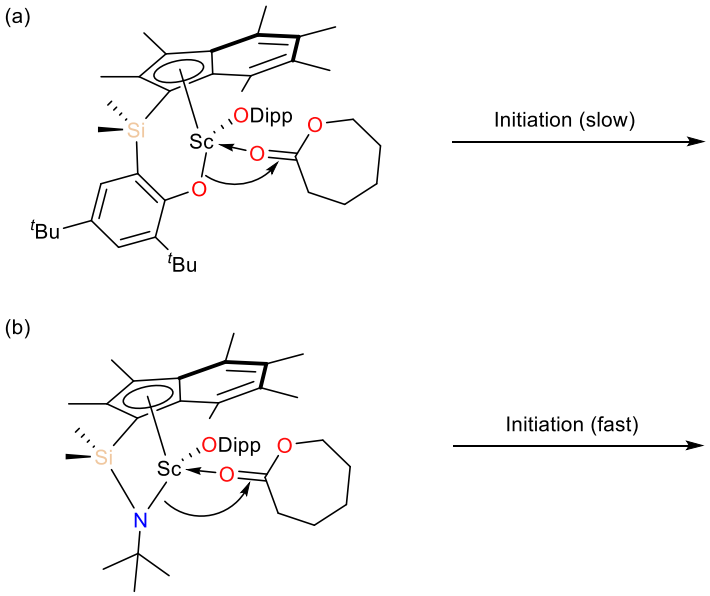


Figure 4.10 Proposed ring opening polymerisation through tethered initiating group. Initiation period for (a) PHENI* Sc is slow leading to larger M_n and $Đ_M$ than for (b) CGCI* Sc complex.

Similarly, a slow induction period was reported for the polymerisation of lactide using CGCI* complexes in **Figure 4.5** (c). The bis-isopropyl showed slower initiation compared to the bis-tert-butyl variants, this observation is considerd to be due to the coordination environment at the metal centre being more crowded due to the isopropyl groups on the aryl oxide. To further, more electron donating substituent on the amido ligand (^{i}Pr > ^{t}Bu > Ph) lead to higher activities (k_{obs} = 1.21 > 0.89 > 0.57).[9]

4.3.2. Initiator concentration dependency for 5 and 7

Kinetic order dependence of **5** and **7** were determined by changing the monomer to catalyst ratio The concentration of ϵ-CL was kept constant at 0.5 M as the concentration of initiator was varied. [ϵ-CL]$_0$:[**Sc**] ratios of 200, 400, and 800 were used for **5** and 250, 500, 750 for **7**. (**Table 4.2**).

Table 4.2 ROP of ϵ-CL initiated by **5** or **7** at various stoichiometries

Cat.	$[M]_0/[Sc]_0$	Temp. (°C)	Time (h)	Conv.[a] (%)	k_{obs} (h^{-1})	R^2	$M_{n,SEC}$[b]	$M_{n,th}$[a,c]	$Đ_M$[b]
5	200	25	7.7	80	0.24±0.01	0.998	93	23	1.82
5	400	25	29	80	0.067±0.01	0.999	111	44	2.30
5	800	25	29	45	0.02±0.003	0.998	-[d]	-	-[d]
7	250	30	0.17	72	6.61±0.136	0.998	73	21	2.20
7	500	30	0.25	60	3.55±0.048	0.999	110	34	1.85
7	750	30	0.33	61	2.79±0.018	0.999	118	52	1.51

Conditions: $[ϵ\text{-CL}]_0:[Sc]_0$ as stated; $[ϵ\text{-CL}]_0$ = 0.5 M in 0.6 mL (**5**) Benzene-d_6 or (**7**) Tol-d_8 First-order rate constant (k_{obs}) and R_2 were obtained from plots of $\ln([ϵ\text{-CL}]_0/[ϵ\text{-CL}]_t)$ *vs* time. [c] Calculated from monomer conversion data: $[M]_0/[Sc]_0$ × conv. (%) × 114.14 × 0.01 + (MW of end groups (α+ω)).[d] Sample blocked column, hence no measurement taken.

First-order dependence on monomer concentration was observed with the linear plots of $\ln([ϵ\text{-CL}]_0/[ϵ\text{-CL}]_t)$ *vs.* time for both **5** and **7**. The observed rate constants decreased with decreasing catalyst concentration. The rate law can be estimated from a plot of $-\ln(k_{obs})$ *vs* $-\ln[Sc]_0$, where a gradient of close to 1 was observed for both **5** and **7** at 0.972 ± 0.09 and 1.03 ± 0.16 respectively. Hence, a first-order rate law is applicable for both systems (**Figure 4.11** and **Figure 4.12**). In general, first order dependency is reported for ROP, however orders of less than 1 can suggest reversible catalyst-monomer equilibria and saturation kinetics being favoured.[34, 35]

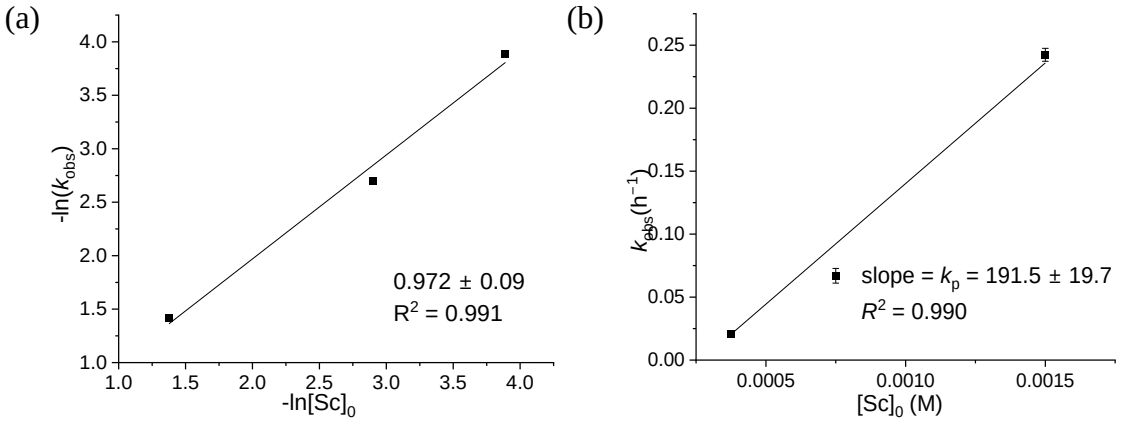


Figure 4.11 (a) Plot of −ln(k_{obs}) *vs.* −ln[Sc]$_0$ for ROP of ϵ-CL at 25°C with **5**. Order of reaction with respect to [Sc]$_0$ is 0.972 ± 0.09; R^2 = 0.991. (b) Plot of k_{obs} *vs.* [Sc]$_0$ for ROP of ϵ-CL using **5** where k_p = 191.5 ± 19.7 M^{-1} h^{-1}; R^2 = 0.990.

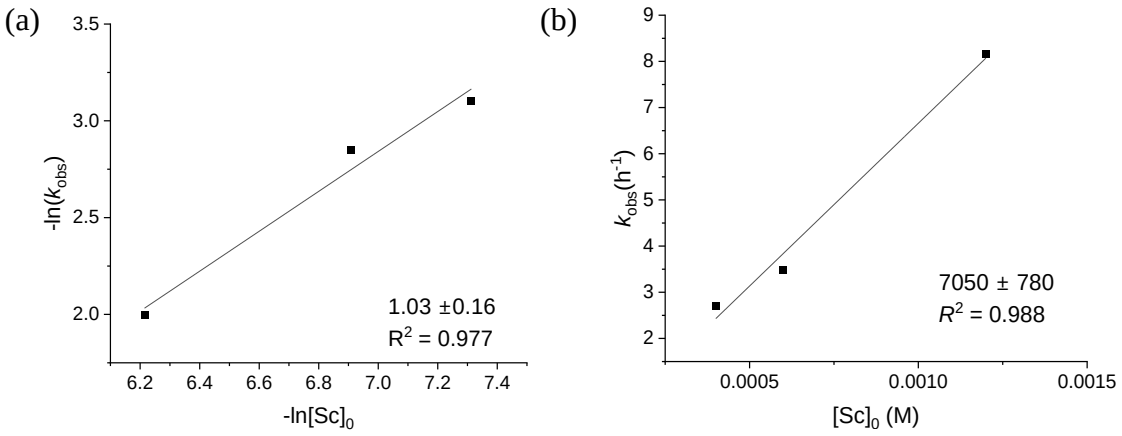


Figure 4.12 (a) Plot of −ln(k_{obs}) *vs.* −ln[Sc]$_0$ for ROP of ϵ-CL at 30°C with **7**. Order of reaction with respect to [Sc]$_0$ is 1.03 ± 0.15; R^2 = 0.977. (b) Plot of k_{obs} *vs.* [Sc]$_0$ for ROP of ϵ-CL using **7** where k_p = 7050 ± 780 M^{-1} h^{-1}; R^2 = 0.988

The propagation rate constant (k_p) is considerably higher for that of **7** (k_p = 7050 ± 780 M^{-1} h^{-1}; R^2 = 0.988) than for **5** (k_p = 191.5 ± 19.7 M^{-1} h^{-1}; R^2 = 0.990). This is likely due to the high amount of inactive initiator present in the reaction with **5**.

4.3.3. The effects of a competing neutral donor on polymerisation

The effects of adding a neutral donor on the kinetics of polymerisation of ϵ-CL was carried out with **5** and $OPPh_3$ as a neutral donor. Addition of other neutral donors or

Lewis bases, can be used to explore the effect of competing coordination on the reaction system.[36] For the ROP of *rac*-β-btyrolactone (*rac*-β-BL), the addition of tricyclohexylphosphine oxide ($OPCy_3$) to ($^{Dipp}/^{CH_2ArO}$BDI)Y($OCH(Ph)_2$)THF reported by Chen *et al*. showed an increase in polymerisation activity of from 1.7 to 64.7 h^{-1}. Further, the addition of $OPPh_3$ or other hard, monodentate phosphine oxides, the performance Y and La catalysts were shown to improve the rate and stereoselectivity.[37]

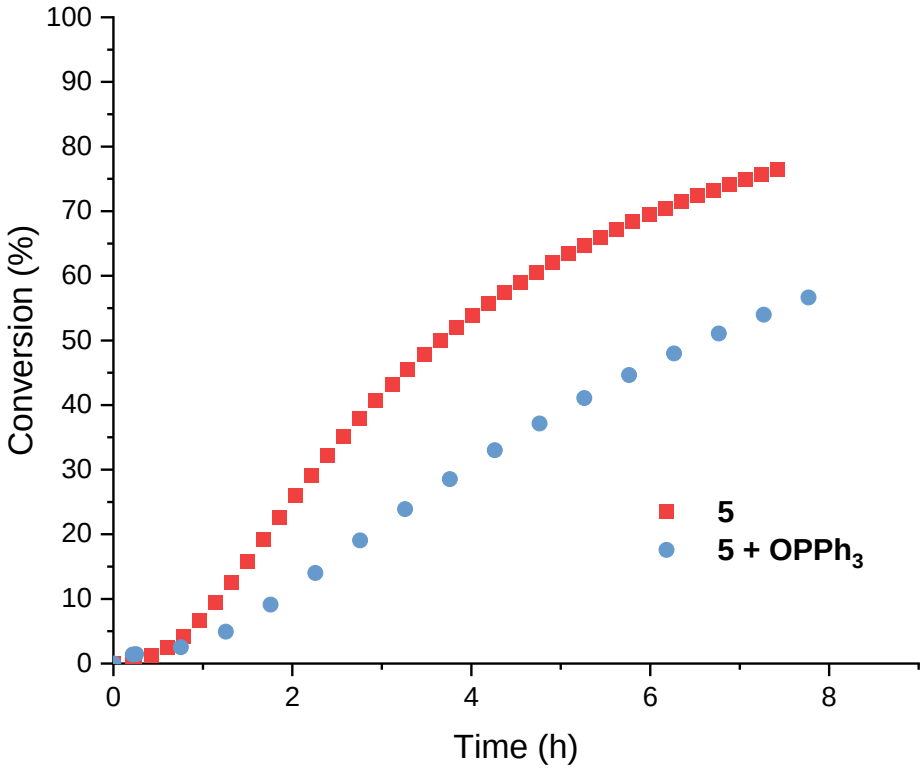


Figure 4.13 Plots of percentage conversion *vs.* time for **5**, **5** + $OPPh_3$ **5**, red squares: (k_{obs} = 0.224 h^{-1}. R^2 = 0.999. **5** + $OPPh_3$, blue circles (k_{obs} = 0.115 h^{-1}. R^2 = 0.999) Conditions: [ϵ-CL]$_0$:[Sc]$_0$ [200]:[1] for **5**; [ϵ-CL]$_0$ = 0.5 M in 0.6 mL Tol-d_8 at 30 °C.

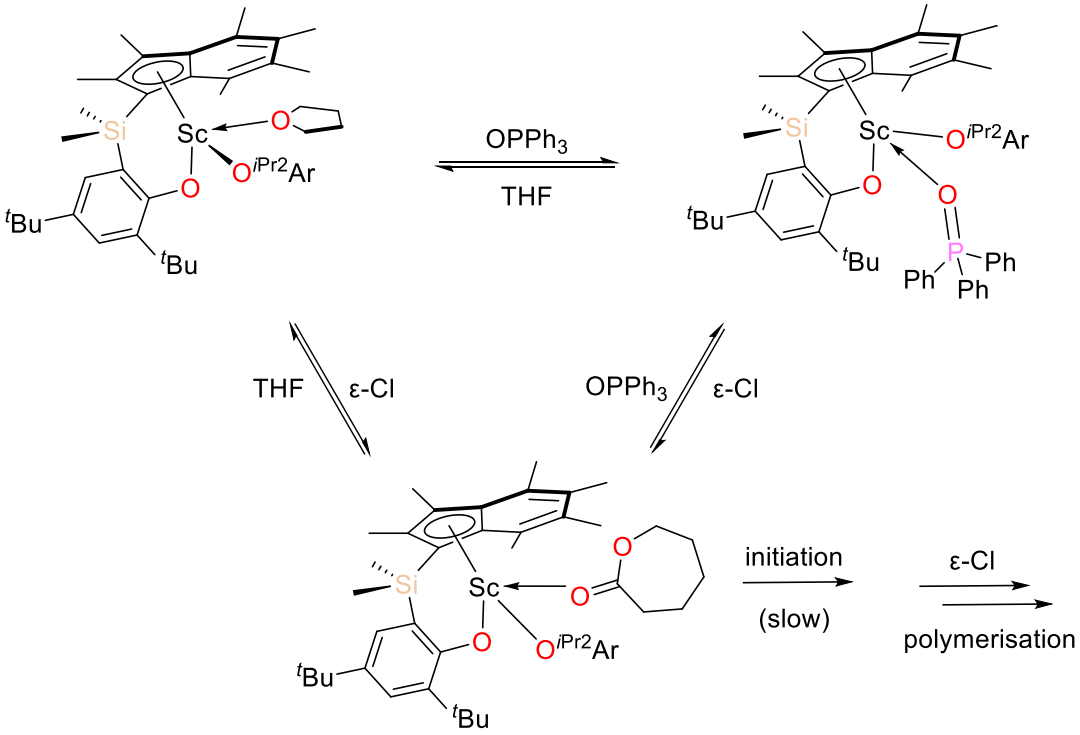
Plots used to obtain observed rate constants can be found in the appendix, section **A.3.3.4**. The rate of polymerisation was decreased on addition of $OPPh_3$ to **5** (**Figure 4.13** and **Table 4.3**).

Table 4.3 ROP of ϵ-CL initiated by **5** [200]:[1]:[x]

$OPPh_3$	Temp. (°C)	Time (h)	Conv.[a] (%)	k_{obs} (h^{-1})	R^2	$M_{n,SEC}$ (kDa)	$M_{n,\,th}$[a,c] (kDa)	$Đ_M$
0	30	7.4	76	0.224±0.004	0.999	154	23	1.89
1	30	11.2	65	0.115±0.05	0.996	180	15	1.45

Conditions: $[\epsilon\text{-CL}]_0:[Sc]_0:[OPPh_3]$ as stated; $[\epsilon\text{-CL}]_0$ = 0.5 M in 0.6 mL Tol-d_8 at 'T' °C. [a] Measured by ^{1}H NMR. First-order rate constant (k_{obs}) and R^2 were obtained from plots of $\ln([\epsilon\text{-CL}]_0/[\epsilon\text{-CL}]_t)$ *vs* time. [b,c] Calculated from monomer conversion data: $[M]_0/[Sc]_0$ × conv. (%) × 114.14 × 0.01 + (*M*W of end groups (α+ω)).

The molar-mass dispersity for all polymerisations was found to be dependent on the conversion %, suggestive of transesterification reactions occurring. It is well modelled that coordination is a possible rate limiting step during propagation for the Lewis acid mediated coordination-insertion ROP.[10] Coordination of polar solvent THF inhibits ROP as seen for other Lewis acid catalysts[7, 38, 39] As previously explored in **Chapter 2**, addition of Lewis bases $OPPh_3$ and DMAP exchanged with THF in solution to form new complexes (**Scheme 4.1**). When $OPPh_3$ is present, a longer initiation period is observed in conjunction with a decrease in polymerisation activity as seen in **Figure 4.13**. Where $OPPh_3$ was added, an increase in both molecular weight and monomodal molecular weight distributions were recorded for the PCL produced across the temperature range 30–60 °C ($Đ_M$ = 1.59–1.64; **Table 4.3**).



Scheme 4.1 Substitution of the neutral donors prior to polymerisation of ϵ-CL.

This result is similar with that of the polymerisation of lactide with $Sc(Oct)_2$ which shows lower activity in strong donor solvents.[40] Additionally, previous studies involving changing to a polar solvent (THF) also showed inhibition of activity for the polymerisation of lactide using **5.**[41]

4.3.4. Temperature variation

Higher temperatures increase the rate of polymerisation of ϵ-CL using **5** and **7**. **5** (k_{obs} = 1.116±0.004) achieves a 70% conversion after 1.1 h at 60 ℃ in a ratio of 200:1 $[\epsilon\text{-CL}]_0$:$[Sc]_0$. By decreasing the temperature to 0–20 ℃, the rate could be monitored effectively for **7**, where the rate decreased (k_{obs} = 0.250±0.014) only achieving 75% conversion after 4.6 h (750:1, $[\epsilon\text{-CL}]_0$:$[Sc]_0$) at 0 ℃ (**Figure 4.14**) .

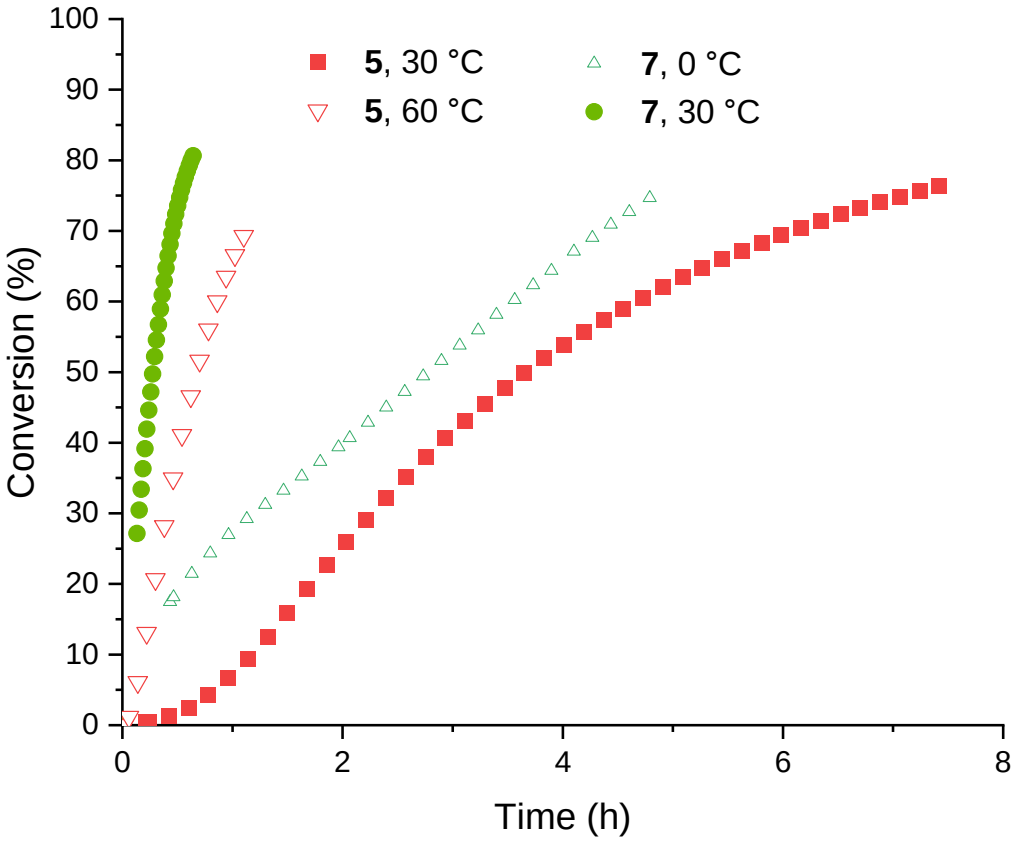


Figure 4.14 Plots of percentage conversion *vs.* time for **5** and **7**. **5**, red squares: (k_{obs} = 0.220 h^{-1}. R^2 = 0.999) and red triangles (k_{obs} = 1.116 h^{-1}. R^2 = 0.999 ±0.009). **7**, green circles (k_{obs} = 2.79 h^{-1}. R^2 = 0.999) and green upward triangles (k_{obs} = 0.250 h^{-1}. R^2 = 0.996). Conditions: $[\epsilon\text{-CL}]_0$:$[Sc]_0$ [200]:[1] for **5** and [750]:[1] for **7**; $[\epsilon\text{-CL}]_0$ = 0.5 M in 0.6 mL Tol-d_8 at 0/30/60°C).

Plots used to obtain observed rate constants can be found in the appendix, section **A.3.3.3** and **A.3.3.5.** For the polymerisation of ϵ-CL at elevated temperature with the addition of $OPPh_3$, **5** had moderate rate (k_{obs} = 0.917±0.006) achieving 63% conversion after 1.3 h at 60 °C in a ratio of 200:1 $[\epsilon\text{-CL}]$:$[Sc]_0$. (**Table 4.4**).

Table 4.4 ROP of ϵ-CL initiated by **5**[(d)] and **7**

Cat.	[M]	Temp. (°C)	Time (h)	Conv.[a] (%)	k_{obs} (h^{-1})	R^2	$M_{n,SEC}$ (kDa)	$M_{n,th}$[a,c] (kDa)	$Đ_M$
5	200	60	1.1	70	1.116±0.009	0.998	105	16	1.64
5[d]	200	60	1.3	63	0.917±0.006	0.998	151	14	1.62
7	750	0	4.8	75	0.250±0.014	0.996	183	64	1.99

Conditions: $[\epsilon\text{-CL}]_0$:$[Sc]_0$:$[OPPh_3]$ as stated; $[\epsilon\text{-CL}]_0$ = 0.5 M in 0.6 mL Tol-d_8 at 'T' °C. [a] Measured by ^{1}H NMR. First-order rate constant (k_{obs}) and R^2 were obtained from plots of $\ln([\epsilon\text{-CL}]_0/[\epsilon\text{-CL}]_t)$ *vs* time. [b,c] Calculated from monomer conversion data: $[M]_0/[Sc]_0$ × conv. (%) × 114.14 × 0.01 + (MW of end groups (α+ω)). [d] 1 equiv.of $OPPh_3$ added prior to addition of monomer.

The Eyring equation can be formed to calculate the thermodynamic parameters: entropy ($\Delta S^{‡}$) and enthalpy ($\Delta H^{‡}$), of activation.

$$\ln\left(\frac{k_{\text{obs}}}{T}\right) = -\frac{\Delta H^{‡}}{RT} + \ln\left(\frac{k_{\text{B}}}{h}\right) + \frac{\Delta S^{‡}}{R}$$

A plot of $\ln(\frac{k_{\text{obs}}}{T})$ against $\frac{1}{T}$ has a gradient of $-\frac{\Delta H^{‡}}{R}$ and an intercept of $\ln(\frac{k_{\text{B}}}{h}) + \frac{\Delta S^{‡}}{R}$. For **5**, $\Delta G^{‡}$ is calculated to be −21.3±1.9 k mol^{-1} at 298 K. Where $OPPh_3$ is added, an increase of $\Delta H^{‡}$ is observed from 41.6 ± 1.8 to 56.0 ± 2.8 kJ mol^{-1}. This is likely due to the stronger competition of $OPPh_3$ over THF, slowing the rate of polymerisation. In addition, $\Delta S^{‡}$ is seen to decrease in magnitude from −71.4 ± 5.6 to –29.5 ± 8.6 J mol^{-1} K^{-1} on addition of $OPPh_3$. The transition state is only slightly more ordered than the **5** for **12 (5+OPPH$_3$)**. For **7**, the $\Delta G^{‡}$ is −21.3±1.9 k mol^{-1} at 298 K from the observed $\Delta S^{‡}$ = −48.8 ± 6.2 J mol^{-1} and $\Delta H^{‡}$ = 56.9±1.8 kJ mol (**Figure 4.15** and **Table 4.5**).

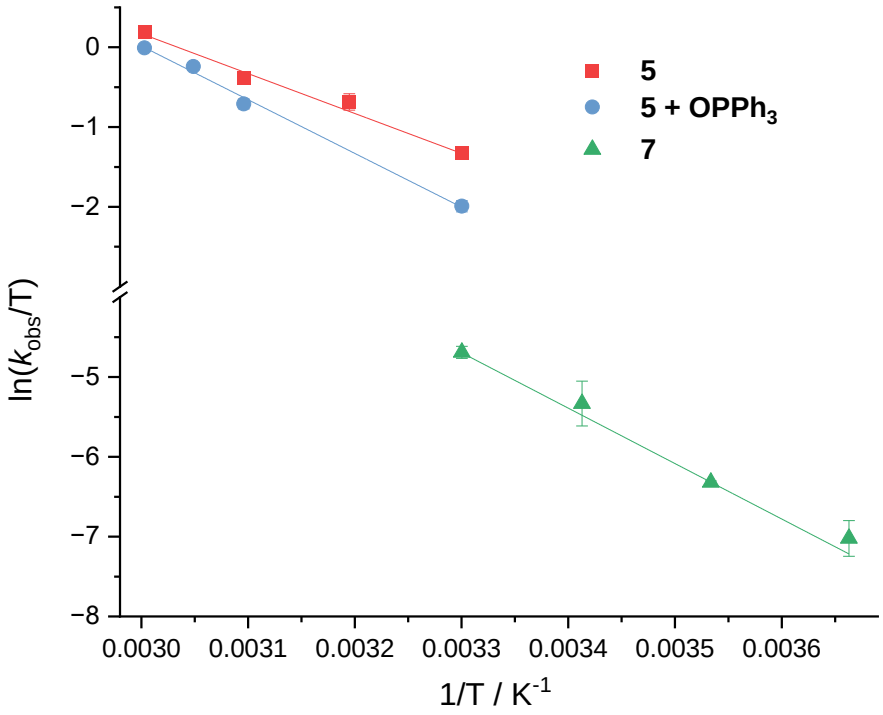


Figure 4.15 Eyring plot of ln(k_{obs}/T) *vs.* 1/T: **5**, red squares (Slope = –5001.1 ± 214.7, intercept = 15.17 ± 0.67, R^2 = 0.9688); **5** and $OPPh_3$, blue circles (slope = –6731.5 ± 332, intercept = 20.21 ± 1.04, R^2 = 0.9951). **7** Green upward triangles (Slope = –6843.3 ± 214.6, intercept = 17.9 ± 0.7, R^2 = 0.9398) Conditions: [ϵ-CL]$_0$:[Sc]$_0$:[$OPPh_3$] as (red squares) 200:1:0 and (blue circles) 200:1:1, (green upward triangles) 750:1:0 [ϵ-CL]$_0$ = 0.5 M in 0.6 mL toluene-d_8.

Table 4.5 Summary of Eyring calculation for the enthalpy and entropy of activation for the polymerisation of ϵ-CL using **5**, **5** + $OPPh_3$, and **7**.

Cat.	[M]$_0$/[Sc]$_0$	Monomer	Solvent	$\Delta H^{\ddagger}$ kJ mol^{-1}	$\Delta S^{\ddagger}$ J K^{-1} mol^{-1}
5	200	ϵ-CL	Toluene	41.6±1.8	−71.4 ± 5.6
5 + OPPh$_3$	200	ϵ-CL	Toluene	56.0 ± 2.8	–29.5 ± 8.6
7	750	ϵ-CL	Toluene	56.9±1.8	−48.8 ± 6.2

Within these, higher temperatures can lead to increased termination and a decline in activity, either through catalyst decomposition, or with interaction with solvent and monomer impurities as was observed with **7** when T > 30 °C.[42 14]

4.3.5. Polymerisation of ϵ-CL using scandium tris-aryloxide complexes (29 and 30)

Simple systems, such as lanthanide tri-aryl and -alkyl complexes, have been shown to have moderate to good polymerisation activity. The use of $Sc(OTf)_3$ was reported by Hendrick *et al.* and Okuda *et al*. for the controlled and highly active polymerisation of ϵ-CL.[43, 44] The polymerisation requires facile coordination to the scandium centre and the addition of a co-initiator leading to cationic living polymerisation. Okada and co-workers reported the polymerisation of 50 equiv. of ϵ-CL in 2 h at 25 ℃ ($Đ_M$ = 1.1) using $Sc(OTf)_3$ with 1 equiv. of BnOH.[45]

To test if any insertion was possible through insertion into scandium aryl oxide bonds, a study was conducted to test the five coordinate scandium tris-aryloxide complexes **29** and **30**. Although the rate of polymerisation was significantly higher for **30** than for **29**, both are shown to polymerise ϵ-CL over a number of days rather than hours for **5** and **7 (Table 4.3**). **29** achieved 67% conversion after 83 h at 30 ℃ in a ratio of 50:1 $[\epsilon\text{-CL}]:[Sc]_0$. Further, **30** proved to have a poor ROP initiator achieving 95% conversion after 30 h at 30 ℃ in a ratio of 50:1 $[\epsilon\text{-CL}]:[Sc]_0$. The molar-mass dispersity was found to be dependent on the conversation % suggestive of living polymerisation reactions occurring with molecular weights being much higher (over 10x) than theoretical molecular weights (**Table 4.6**).

Table 4.6 ROP of ϵ-CL initiated by Sc complexes **29** and **30**.

Cat.	$[M]_0/[Sc]_0$	Temp. (℃)	Time (h)	Conv.[a] (%)	$M_{n,SEC}$[b] (kDa)	$M_{n,\,th}$[a,c] (kDa)	$Đ_M$[b]
29	50	30	83	67	98	3.8	2.17
30	50	30	30	95	32	5.4	1.59

Conditions: $[\epsilon\text{-CL}]_0:[Sc]_0$ as 50:1, $[\epsilon\text{-CL}]_0$ = 0.5 M in 0.6 mL benzene-d_6 at 30 ℃. [a] Measured by ^{1}H NMR spectroscopic analyses. First-order rate constant (k_{obs}) and R^2 were obtained from plots of ln([ϵ-

$CL]_0/[\epsilon\text{-}CL]_t$) *vs* time. [b,c] Calculated from monomer conversion data: $[M]_0/[Sc]_0 \times$ conv. (%) × 114.14 × 0.01 + (MW of end groups (α+ω)) in kDa.

Other five coordinate RE tris-aryloxides Ln = Sm, Dy, Y, Yb for $n = 2$ and have been studied for the polymerisation of lactide showing efficient but poorly controlled polymerisation. The presence of a co-initiator such as BnOH is required to form $Ln(OBn)_3.x$THF in order for polymerisation to proceed.[46-49] For the THF free Ln aryloxide $Sm(ArO)_3$, high activity (including large amounts of transesterification) for the polymerisation of ϵ-CL was reported by Shen *et al*.[50] The samarium aryloxides with bulky ortho groups showed the highest reactivity, with >99% conversion for $[\epsilon\text{-}CL]_0$:$[Sm]_0$ (Sm = $Sm(^{t}Bu_2^{Me}ArO)_3$ [800]:[1]) after 1 h at 60°C.

4.3.6. Polymer characterisation

4.3.6.1. Gel permeation chromatograms

There is a clear trend for higher molar-mass dispersity at lower concentration, for 250:1 ($Đ_M$ = 2.20), whereas the 750:1 polymerisation ratio has much lower dispersity (($Đ_M$ = 1.48) at the same conversion %.

Table 4.7 ROP of ϵ-CL using PHENI*-AMIDO scandium complex **7** at various stoichiometries

$[M]_0/[Sc]_0$	Temp. (°C)	Time (min)	Conv.[a] (%)	$M_{n,SEC}$[b]	$M_{n,\,th}$[a,c]	$Đ_M$[b]
750	30	20	61	118	52	1.51
750	30	30	66	136	57	1.49
750	30	40	71	183	61	1.48

Conditions: $[\epsilon\text{-}CL]_0$:$[Sc]_0$ as stated; $[\epsilon\text{-}CL]_0$ = 0.5 M in 0.6 mL Tol-d_8 at 30 °C. Reported for outlined shapes in **Figure 4.13**; measured by ^{1}H NMR spectroscopic analyses. [c] Calculated from monomer conversion data: $[M]_0/[Sc]_0 \times$ conv. (%) × 114.14 × 0.01 + (MW of end groups (α+ω)).

GPC and MALDI-TOF analysis were carried out on the polymer produced from the reactions. All polymer produced showed a monomodal distribution (**Figure 4.16**), there

is a dependence on the concentration of monomer on the molecular weights of the polymer produced suggesting a living polymerisation.

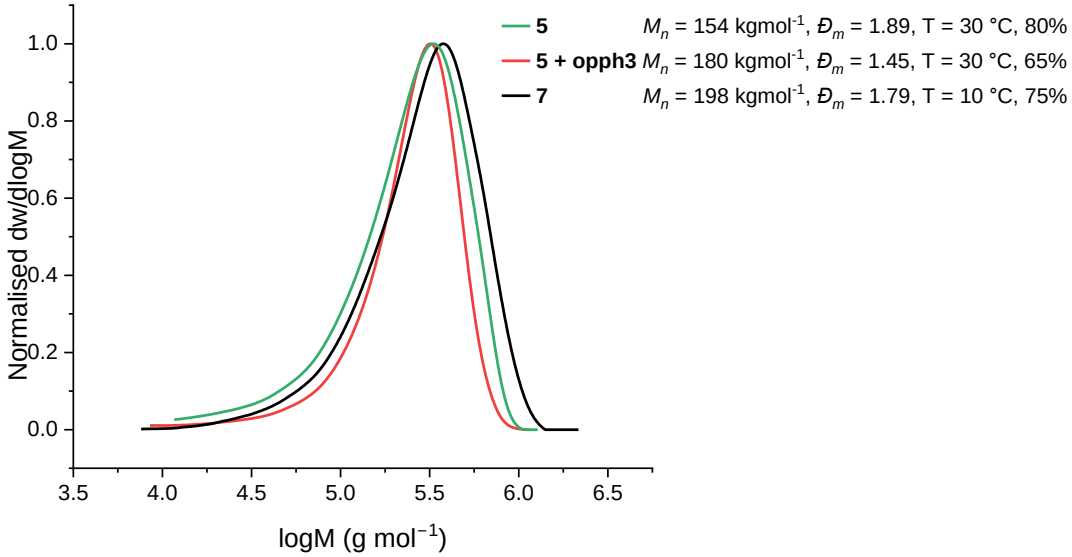


Figure 4.16 Gel permeation chromatograms (GPC) traces of PCL synthesised from the ROP of ϵ-CL with **5**, **5** and $OPPh_3$, and **7.** Conditions: $[\epsilon\text{-CL}]_0$:$[Sc]_0$ as stated $[\epsilon\text{-CL}]_0$ = 0.5 M in 0.6 mL.

For **5**, there is an increase in molar-mass dispersity at higher conversions and a decrease in molecular weight, suggestive of transesterification as the concentration of free monomer is depleted (**Figure 4.17**).[51] Where the conversion reaches 80% or above, the molar-mass dispersity rises sharply (**Figure 4.17** (b)).

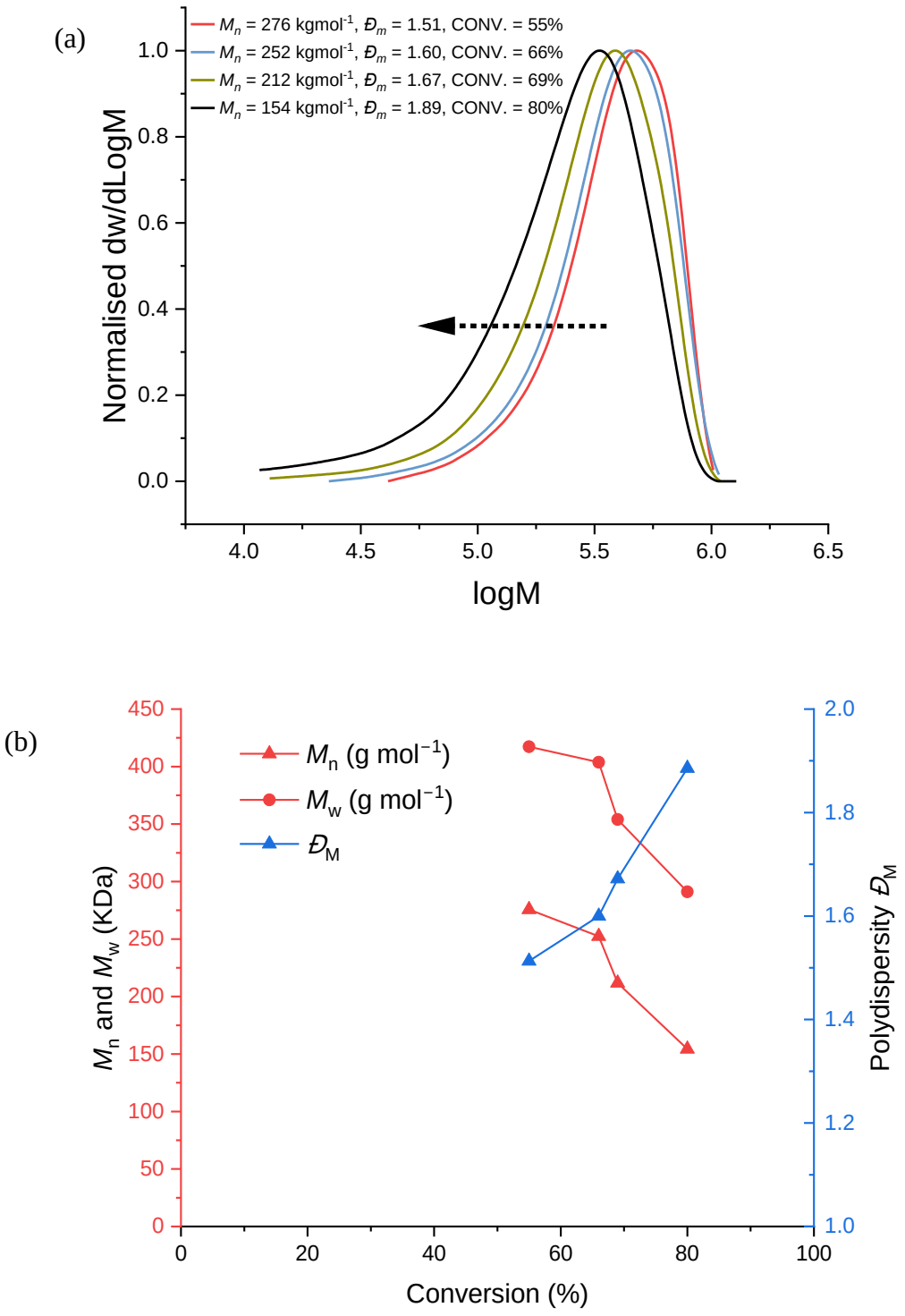


Figure 4.17 (a) GPC traces of PCL synthesised from the ROP of ϵ-CL with **5**. (b) Conversion *vs* M_n (red circles) and M_w (red triangles, left). Conversion *vs* molar-mass dispersity ($Đ_M$) (blue triangles, right). $[ϵ\text{-CL}]_0$:$[Sc]_0$ [200]:[1] $[ϵ\text{-CL}]_0$ = 0.5 M in 0.6 mL tol.

4.3.6.2. Matrix-assisted laser desorption/ionisation time of flight (MALDI-TOF)

Matrix-assisted laser desorption/ionisation time of flight (MALDI-TOF) mass spectrometry can be used to determine the end groups of the polymers produced. The end groups, or lack of end groups, can be established by comparing the measured mass peaks in the spectra to calculated molecules of X-repeating units with β and ω end groups in addition to a cation (such as H^+ or K^+).[40]

PCL produced using **5, 29** and **30** was loaded onto a grounded steel plate with DCTB matrix and KTFA cationising agent and the following MALDI-TOF spectra were recorded (**Figure 4.18**). A series of distributions are overlayed which can be seen as a pattern of repeating signals with an interval of 114.1(4) m/z, corresponding to the ϵ-CL sub unit.

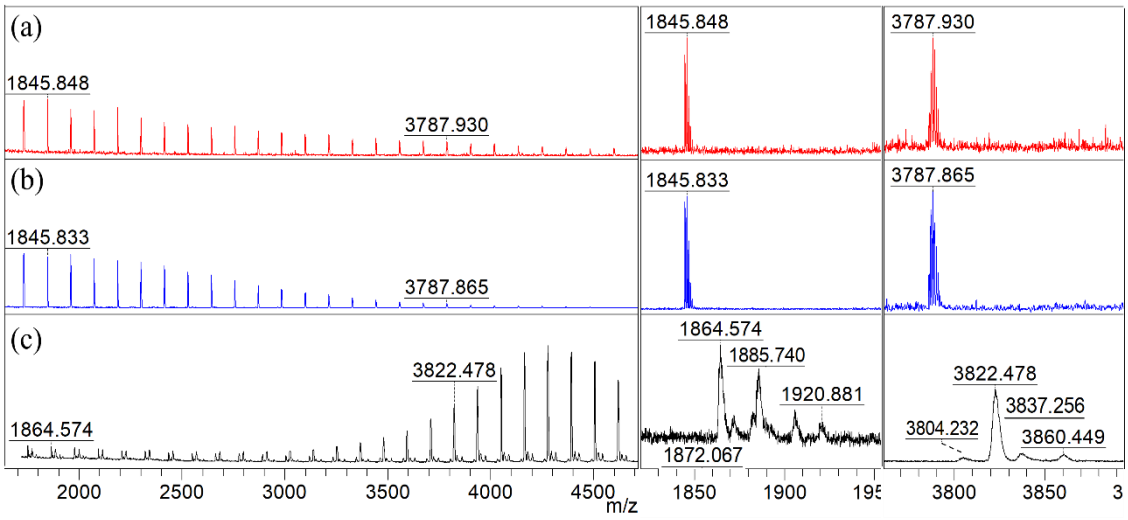


Figure 4.18 MALDI-ToF mass spectrum of ϵ-PCL synthesised using (a) **30**, (b) **29**, and (c) **5**. Conditions: (a) [ϵ-CL]:[**30**]$_0$ = 50:1(b) [ϵ-CL]:[**29**]$_0$ = 10:1 (c) low (10%) conversion, [ϵ-CL]:[**5**]$_0$ = 200:1, [ϵ-CL]$_0$ = 0.5 M, 6.0 mL Toluene at 25 °C. The cationisation agent was KTFA, and the matrix was DCTB. Δm/z = 114.1(4) Da between peak envelopes.

29 and **30** present with identical MALDI-TOF patterns with polymer matching that of linear PCL/H^+ (H/OH) (114.14*13 + 18 + 1 = 1845.33Da). (**Figure 4.18** (a and b)). A *L*-

LA polymerisation study carried out with Y(O-2,6-^{t}Bu$_2$OAr)$_3$.2THF (without the presence of a co-initiator) reported similar results.[49] It was suggested that initiation occurred through proton transfer either from the solvent or another protic impurity, rather than through insertion of the M-OAr bonds.

The polymer produced from a low conversion sample of **5** displays as two overlapping distributions. An orange distribution that decreases as mass increases, which grows to be the dominate distribution at higher conversion (**A.125**). The other (green **Figure 4.19**) appears as a normal distribution, formed from the living chains, quenched during the workup of the reaction to form polymer with H/OH end groups.[51, 52] The molecular masses the living chains are observed through MALDI-ToF, are centred around ~ 4300 Da. This is higher than $M_{n,th}$ for 10% conversion at 200:1 [M]:[Cat.] of ~2300 Da. The slow initiation period leads to higher molecular weights, also observed *via* SEC.

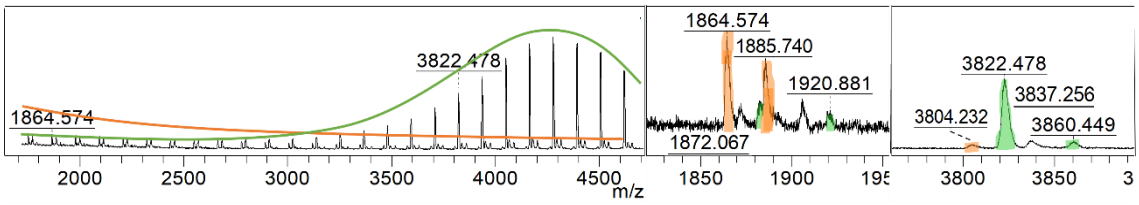


Figure 4.19 MALDI-ToF mass spectrum of ϵ-PCL synthesised using **5**. Low (10%) conversion, [ϵ-CL]:[**5**]$_0$ = 200:1, [ϵ-CL]$_0$ = 0.5 M, 6.0 mL Toluene at 25 °C. Orange and green lines showing two polymer distributions overlayed.

Table 4.8 Mass fragments from MALDI-TOF spectrum **Figure 4.18** and **Figure 4.19**

Cat.	*m/z* [a]	End group (α\ω)	Cation	Calculated *m/z*	Chain length
29/30	1845.8	O/OH	H^+	1845.33	17
5	1864.6	Cyclic	K^+	1865.34	16
5	1883.1	H/OH	K^+	1883.24	16
5	1885.7	DCTB, KTFA	K^+	1886.27	13
5	3804.2	Cyclic	K^+	3805.72	33
5	3822.5	H/OH	K^+	3823.72	33

The peak at 1885.740 Da (**Figure 4.18 (c)**/**Figure 4.19**) can be assigned to PCL, the matrix DCTB and the cationising agent KTFA (114.14*13 + 250.34 + 152.11 = 1885.7 Da). The mass peaks at 1864.574 Da, can be assigned to cyclic PCL/K^+ (114.14*16 + 39.1 = 1865.34 Da). The peak at 3822.5 Da can be assigned to linear PCL/K^+ OH/H end groups (114.14*33 +18 + 39.1 = 3823.72 Da).

O'Hare *et al*. using ^{Me2}SB(^{iPr}N,I*)Sc(ODipp)THF for the polymerisation of lactide, reported polymer capped with -^{iPr}N ligand in addition to -OH terminated and cyclic polymer.[9] In the reported case, no sign of insertion in to the Sc-ODipp bond was observed as no ODipp capped polymer was detected *via* MALDI-ToF. Other examples of ϵ-CL insertion into amido-M bonds include Okuda *et al.,* whom reported ROP of ϵ-CL through ring expansion with the yttrium amido complex Li[Y(η5:η1-$C_5Me_4SiMe_2NCH_2CH_2OMe)_2$]. Insertion into the Y-amido bond followed by intramolecular transesterification produces mainly cyclic-PCL in the process.[53] Another sample of **5** also showed signs of ligand attached to the polymer and is included in the Appendix (**Figure A.126**).

4.3.7. Discussion on proposed reaction mechanism for 5, 7, 29 and 30

The polymerisation of ϵ-CL using **5** and **7** produces polymer either -OH terminated or apparent cyclic or unterminated polymer. The formation of polymer with no end-groups can either be through chain scission through ionisation or oligomerisation during the polymerisation reaction.[54] The formation of oligomers through transesterification is known to occur towards the latter stages of the reaction, as reported for the polymeriation

of *L*-LA using $Sn(Oct)_2$ salt catalysts, resulting in increasing $Đ_M$ and decreasing M_n (**Figure 4.20**).[51]

(a)

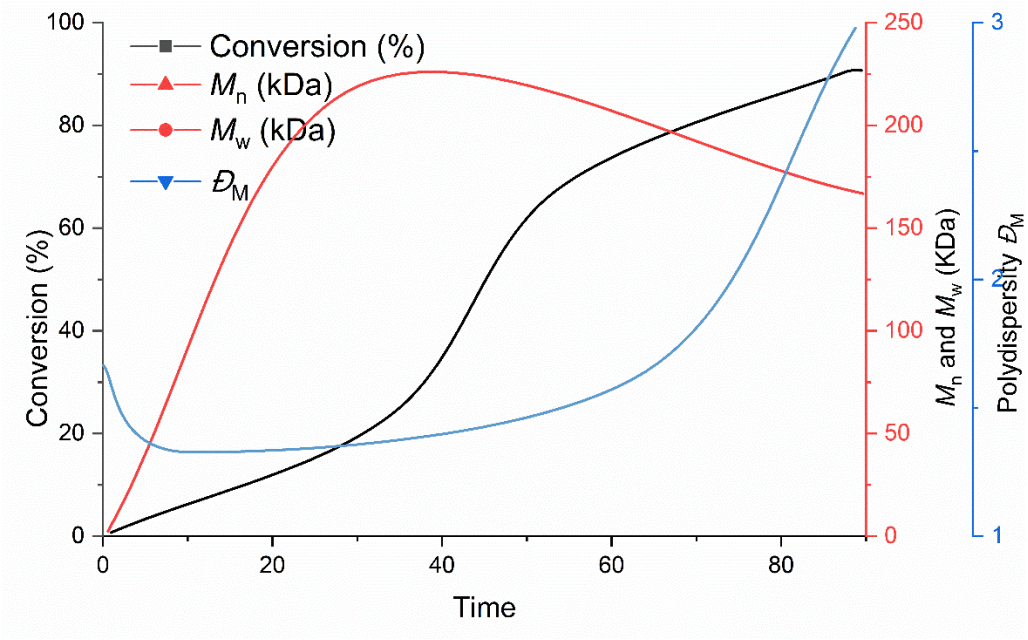


Figure 4.20 Conversion % *vs* Time *vs* M_n and M_w *vs* $Đ_M$ drawings representative of polymerisation using PHENI* sc **5** and **S**n(Oct)$_2$[51] where transesterification is prevalent at latter stages of the reaction.

Concentration of monomer has been reported to have a significant impact on whether linear or cyclic molecules are produced. Slow addition of ϵ-CL to a samarium catalyst reported by Visseaux *et al.* produced cyclic oligo-ϵ-CL, whereas rapid addition lead to linear polymer being obtained.[55] For **5** and **7**, as [M] → 0, transesterification is favoured as evidenced by increasing molecular wight dispersity at high conversion. One possible mechanism is through intramolecular cyclisation, promoted by the chain being tethered to the scandium through the I* moiety as shown in **Figure 4.21** (b).

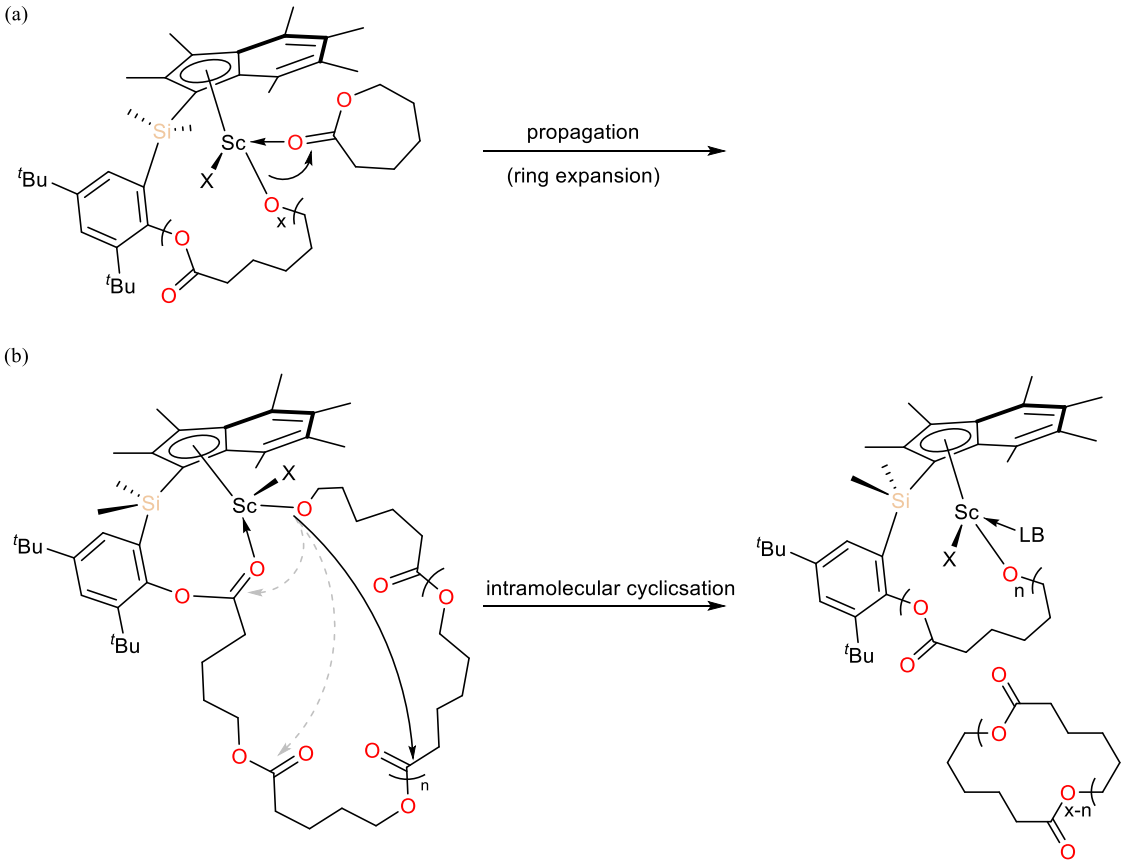


Figure 4.21 (a) Ring expansion polymerisation through tethered active chain. (b) Intramolecular cyclisation to form cyclic PCL.

4.4. *L*-LA polymerisation using 5 and 7

Polymerisation studies carried out using ^{Me2}SB(^{tBu2}ArO,I*)Sc(Cl)THF (**1**) and ^{Me2}SB(^{tBu2}ArO,I*)Sc(ODipp)THF (**5**) for the ROP of *L*- and *rac*- LA have previously been reported by I. Stephens.[41] It was reported that **1** had no reactivity towards *L*-La under the conditions tested. Atactic PLA was produced using **5** with a k_{obs} = 0.41 h^{-1} at 70 °C in benzene-d_6 [40:1] [*L*-LA]$_0$:[Sc]$_0$ achieving >95% conversion after 10 h. The rate of polymerisation for **5** was shown not to be dependent on toluene *vs* benzene as a solvent. Polymerisation of *L*-LA and *rac*-LA was reported by O'Hare *et al.*, using **7**, where k_{obs} = 0.66 h^{-1} at 70 °C in toluene for [*rac*-LA]$_0$:[Sc]$_0$ = 1000:1 with Pr = 0.71.[23] Initiation of ROP of *L*-LA using the chloride complex ^{Me2}SB(^{tBu}N,I*)Sc(Cl)THF (**4**) was also

reported, reaching 85% conversion after 5 h at 70 °C in a 100:1 ratio without the use of a co-initiator.

Table 4.9 Summary of Eyring calculation for the enthalpy and entropy of activation for the polymerisation of ϵ-CL and *L*-LA for selected complexes.

Cat.	Monomer	Solvent	$\Delta H^{\ddagger}$ kJ mol^{-1}	$\Delta S^{\ddagger}$ J K^{-1} mol^{-1}
5	ϵ-CL	Toluene	41.6±1.8	−71.4 ± 5.6
5 + OPPh$_3$	ϵ-CL	Toluene	56.0 ± 2.8	–29.5 ± 8.6
7	ϵ-CL	Toluene	56.9±1.8	−48.8 ± 6.2
5	L-LA	Toluene	64	−69
5	L-LA	Benzene	44	−105
7	L-LA	Toluene	56±5	−86 ± 13
Pn*	L-LA	Chloroform	75.9	−52

Pn* = Pn*(H)Zr(O-2,6-^{i}Pr-C$_6$H$_3$)$_3$[6]

$\Delta S^{\ddagger}$, the entropy of activation gives an indication of the relative disorder of the SM *vs* TS; the larger the negative value, the more ordered the TS *vs* SM. A negative value of a smaller magnitude means the order is closer to that of the starting material.[56] The relative disorder of each entry can be compared within the same standard conditions.[9] Through this, the following conclusions can be made: (a) regarding the ROP of LA, TS of **5** is more ordered than for **7** These values are in agreement literature values indicating a high ordered transitions state, which is to be expected for coordination-insertion mechanism.[57, 58] (b). The enthalpy of activation of **5** and **7** is similar for both at 41.6±1.8 and 56.9±1.8 kJ mol^{-1} respectively. On addition of OPPh$_3$ to **5**, the enthalpy of activation is recorded as 56.0±2.8 kJ mol^{-1}.

4.5. Synthesis and solid-state characterisation of scandium-cyclic ester adducts

A number of lactone monomer-metal adducts have been characterised in the solid state previously. The yttrium chloride ϵ-CL adduct $Y(Cl)_3(\epsilon\text{-CL})_3$[59] and yttrium metallocene ($Cp^*_2Y(Cl)\epsilon\text{-CL}$)[60] in addition to a cationic niobium (IV) complex which presents isomerisation at elevated temperature leading to ROP of ϵ-CL (**Figure 4.22**).[61, 62]

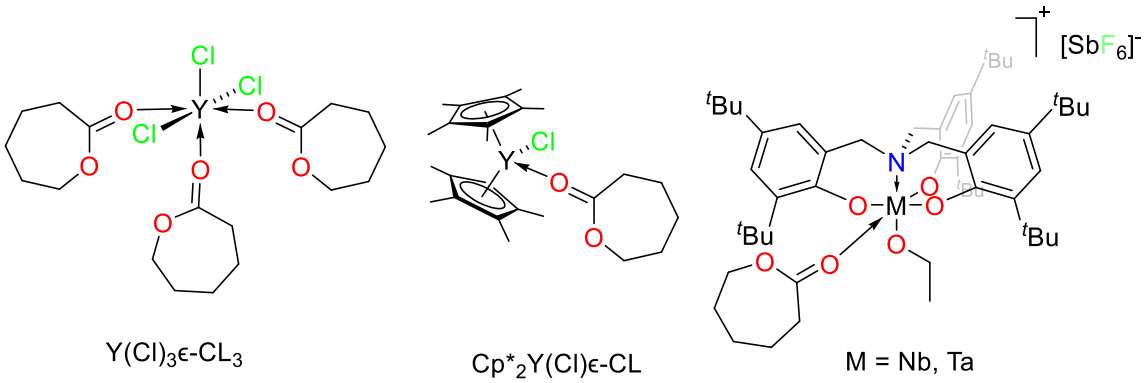


Figure 4.22 Metal ϵ-CL adducts reported in the solid state of **(**a) $Y(Cl)_3\epsilon\text{-CL}_3$.[59] (b) $Cp^*_2Y(Cl)\epsilon\text{-CL}$[60], and (c) cationic M(V) alkoxides[61, 62]

Additionally, Darensbourg *et al.* reported the stereoselective site dependent coordination of *L*- and *D*- lactide to the aluminium half-salen complex and a scandium lactide insertion product, which does not lead to polymerisation, reported by Williams *et al.* although no solid state structure was reported (**Figure 4.23**).[63]

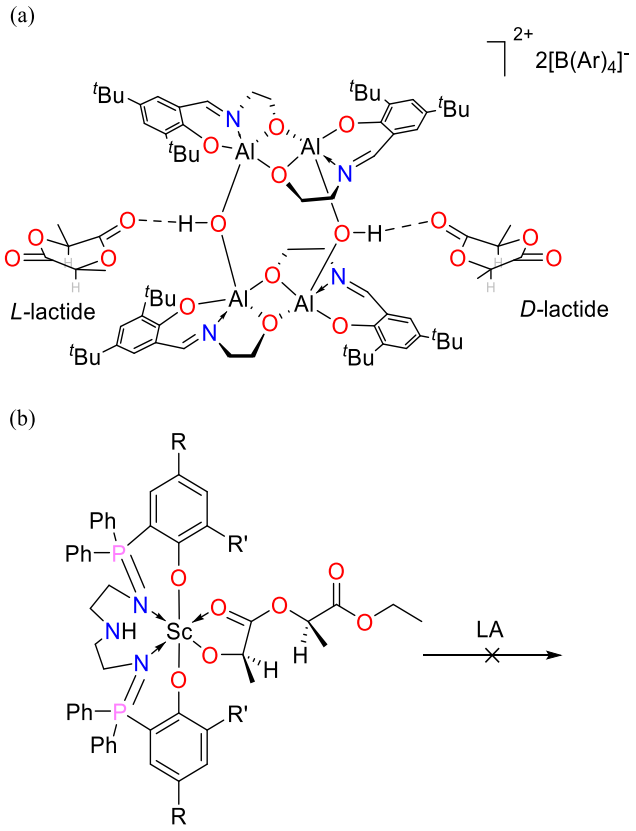
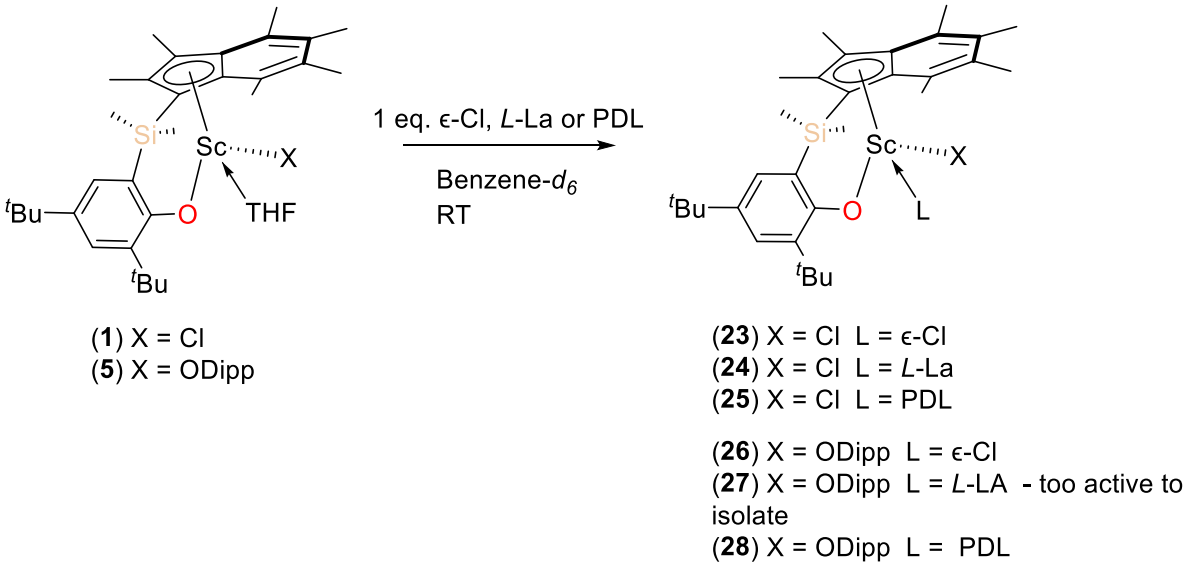


Figure 4.23 (a) Half-salen aluminium complex with *L* and D- lactide hydrogen bonded to the hydroxy ligands.[63] Suggestive of enantiomorphic site control during polymerisation reported by Darensbourg *et al.*[63] (b) Proposed structure of scandium phosphasalen lactide complex

Exploring the reactivity of new catalysts for a range of monomers is key to understanding reactivity. Complexes **1** and **5** were reacted with 1 equiv. of ϵ-CL, *L*-LA and ω-PDL in Youngs tap NMR tube to form the respective scandium adducts **23**–**25** and **26**–**28** in benzene-d_6 (**Equation 4.1**). The samples were freeze dried *in vacuo* to form **23**–**26** and **28** as off-white powders in 80–91% yield. The complexes were characterised *via* NMR, EA and IR.



Equation 4.1 Synthesis of cyclic ester-scandium adducts **23**–**26** and **28**

Attempts to form **27** resulted in the formation of PLA. A species, proposed to be the lactide adduct (**27**) was observed in the reaction mixture as seen in **Figure 4.24** (b). The species was not isolated or characterised further. The IR of the *v*(CO) carbonyl are 1655 and 1668 cm^{-1} for the ϵ-CL adducts **24** and **26**, and 1647 and 1656 cm^{-1} for the ω-PDL adducts **25** and **28**. The *v*(CO) for **24** occurred as a broad peak.

Table 4.10 The CO stretching vibrations, *v*(CO) for **23–26**, **28** and monomers.[64-66] Carboxylic acid *v*(CO) for *L*-LA, ϵ-CL, and ω-PDL are in the range 1720–1740 cm^{-1}.

adduct.	Monomer	*v*(CO) cm^{-1}
23	ϵ-CL	1655
24	La	1773-1670
25	ω-PDL	1647
26	ϵ-CL	1668
28	ω-PDL	1656
	ϵ-CL	1729[64]
	La	1770[65]
	ω-PDL	1736[66]

All are of a lower wavelength than free monomers where v(CO) in the range 1720–1740 cm^{-1}. Similarly, the v(CO) absorption band for the methylaluminium bis(phenoxide) ϵ-CL adduct was reported around 1640 cm^{-1} by Kolodziejczyk *et al.*[67] ^{1}H NMR spectroscopy shows the formation of new species **23**–**28** on addition of the cyclic esters, in addition to free THF with a characteristic broad singlet at δ 3.58 ppm. Examples shown for adducts **26**–**28** from **5** in **Figure 4.24**.

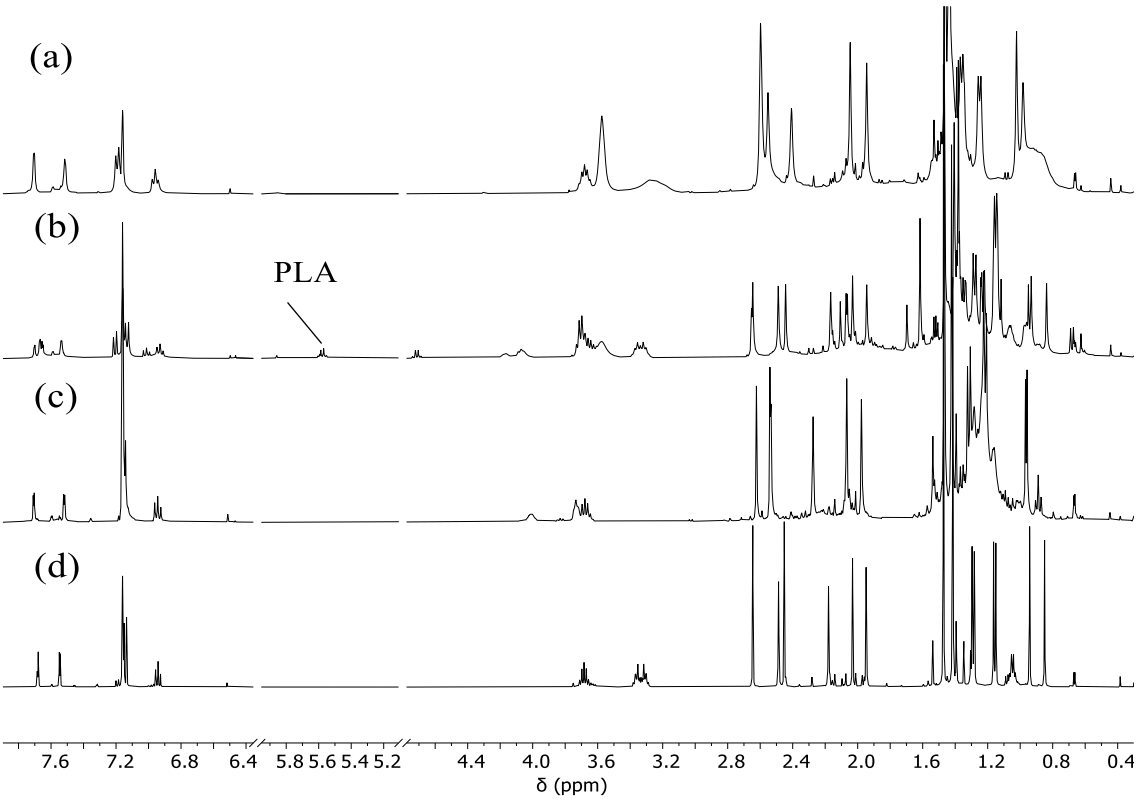


Figure 4.24 ^{1}H NMR spectrum (benzene-d_6, 400/600 MHz, 298 K) of ^{Me_2}SB(^{tBu}OAr,I*)Sc(ODipp)*'cyclic ester'* (a) **26**, (b) **27**, and (c) **28** and synthesised from *'cyclic ester'* + (d) **5**

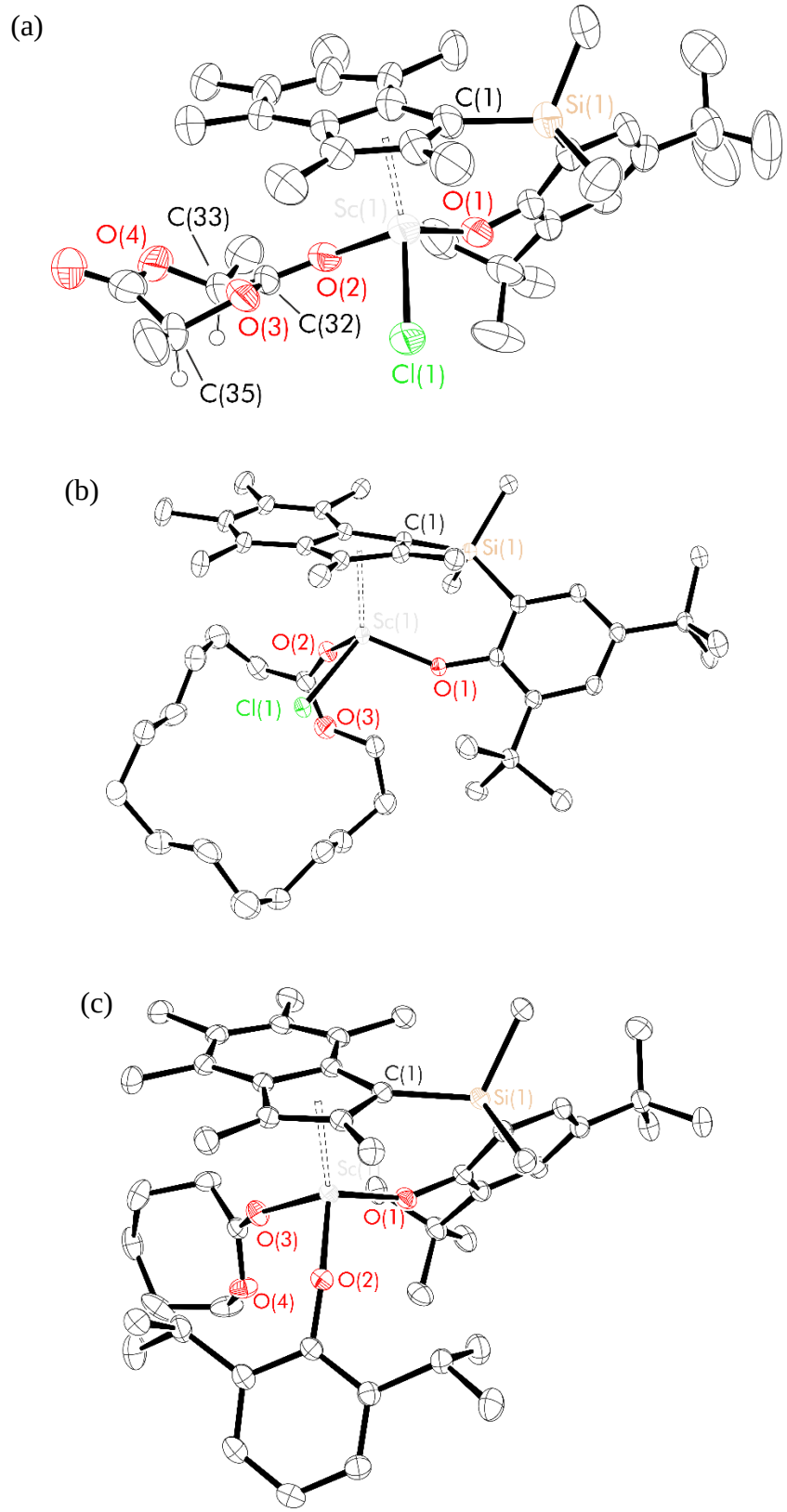


Figure 4.25 Solid state structures of (a) (A-*cis*,R_{Sc},R_{I})-**24**, (b) **25**, and (c) **26**. For **25** and **26** only one enantiomer shown but a pair is present in the unit cell. Ellipsoids are drawn at 30% probability and all non-chiral hydrogen atoms are omitted for clarity (only relevant for **24**).

Crystals suitable for an X-ray diffraction study of **24**, **25**, and **26** were grown from slow evaporation of n-hexane. The solid-state structure of **24** was present as the single enantiomer (A-*cis*,R_{Sc},R_I), whereas **25** and **26** were present as the enantiomeric pair (R_{Sc},S_I)/(S_{Sc},R_I) (**Figure 4.25**). **24** was found to have a chiral monoclinic space group, $P2_1$; **25** a monoclinic space group, $P2_{1/c}$ and in the B-*trans* conformation; and **26** a triclinic space group, $P\bar{1}$ and in the A-*cis* conformation. A list of selected parameters is presented in **Table 4.11** for **24–26**.

Table 4.11 Experimental metrical parameters (bond lengths (Å) and angles (°)) for **24**, **25**, and **26.** Estimated standard de*via*tions shown in brackets

Parameter	**24**	**25**	**26**
X[a]	Cl	Cl	ODipp
Cyclic ester	*L*-LA	ω-PDL	ϵ-CL
Conformation	A-*cis*	A-*cis*	B-*trans*
Sc–I*$_{cent}$	2.143(5)	2.1371(12)	2.1716(8)
Sc–X	2.427(3)	2.4022(7)	1.9376(13)
Sc–O^{ester} [b]	2.159(6)	2.1346(18)	2.1227(13)
Sc–O^{Ar} [c]	1.920(8)	1.9169(15)	1.9357(12)
^{ester}O=C	1.228(11)	1.289(6)	1.234(2)
I*$_{cent}$–Sc–X	117.96(17)	118.71(4)	117.18(5)
I*$_{cent}$–Sc–O^{ester}	112.7(2)	116.53(6)	116.62(4)
I*$_{cent}$–Sc–O^{Ar}	117.9(2)	113.37(5)	114.96(4)
X–Sc–O^{ester}	99.28(18)	94.01(5)	99.58(5)
X–Sc–O^{Ar}	108.9(2)	104.40(5)	108.91(5)
O^{ester}–Sc–O^{Ar}	96.4(3)	107.57(5)	96.83(5)
TA(M) ϕ	87.5(9)	29.2(2)	87.76(14)
τ_4'	0.880(2)	0.8845(1)	0.8947(1)
Δ_{M-C}	0.225	0.096	0.158

For ^{Me_2}SB(^{t}Bu$_2$ArO,I*)Sc(X).(Cyclic ester), [a] X is anionic ligand, [b] O^{ester} is carbonyl oxygen on cyclic ester bonded to Sc and [c] O^{Ar} represents ^{t}Bu$_2$ArO

With respect to Sc–O^{ester} bonds, the order follows that *L*-lactide adduct has a longer bond than the ω-PDL adduct where (*2.1227(13)* <) 2.1346(18) < 2.159(6) Å for (***26*** <) **25** < **24** and a shorter ^{ester}O=C carbonyl bond where 1.228(11) (< *1.234(2)*) < 1.289(6) Å for **24** (< ***26***) < **25**. It has previously been suggested that the carbonyl C=O bond distance is suggestive of the level of activation of the coordinated monomer.[61] As all the adducts

contain different monomers, a comparison on the carbonyl activity is difficult. The steric bulk of each monomer has a significant impact on the proximity of the bonded carbonyl oxygen to the scandium centre (**Figure 4.26**). The average bond length in the solid state would suggest the ω-PDL is the most activated, having the longest C=O bond. However, polymerisation activity shows the lactide is the most readily polymerised.

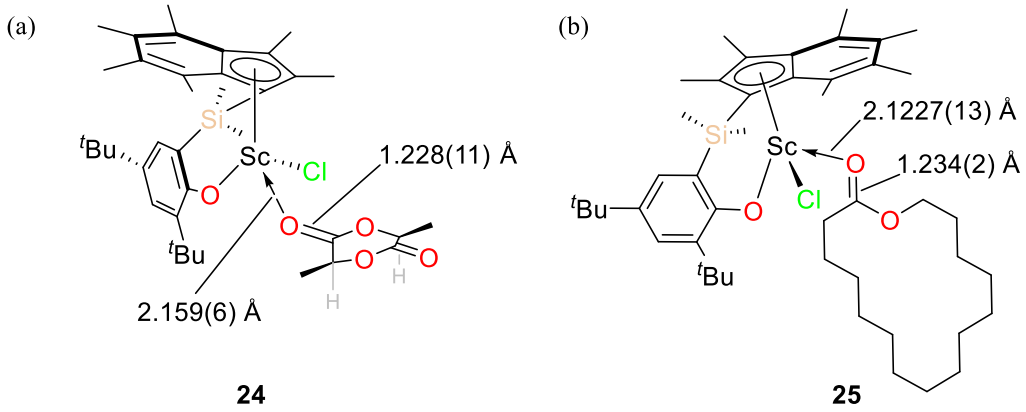
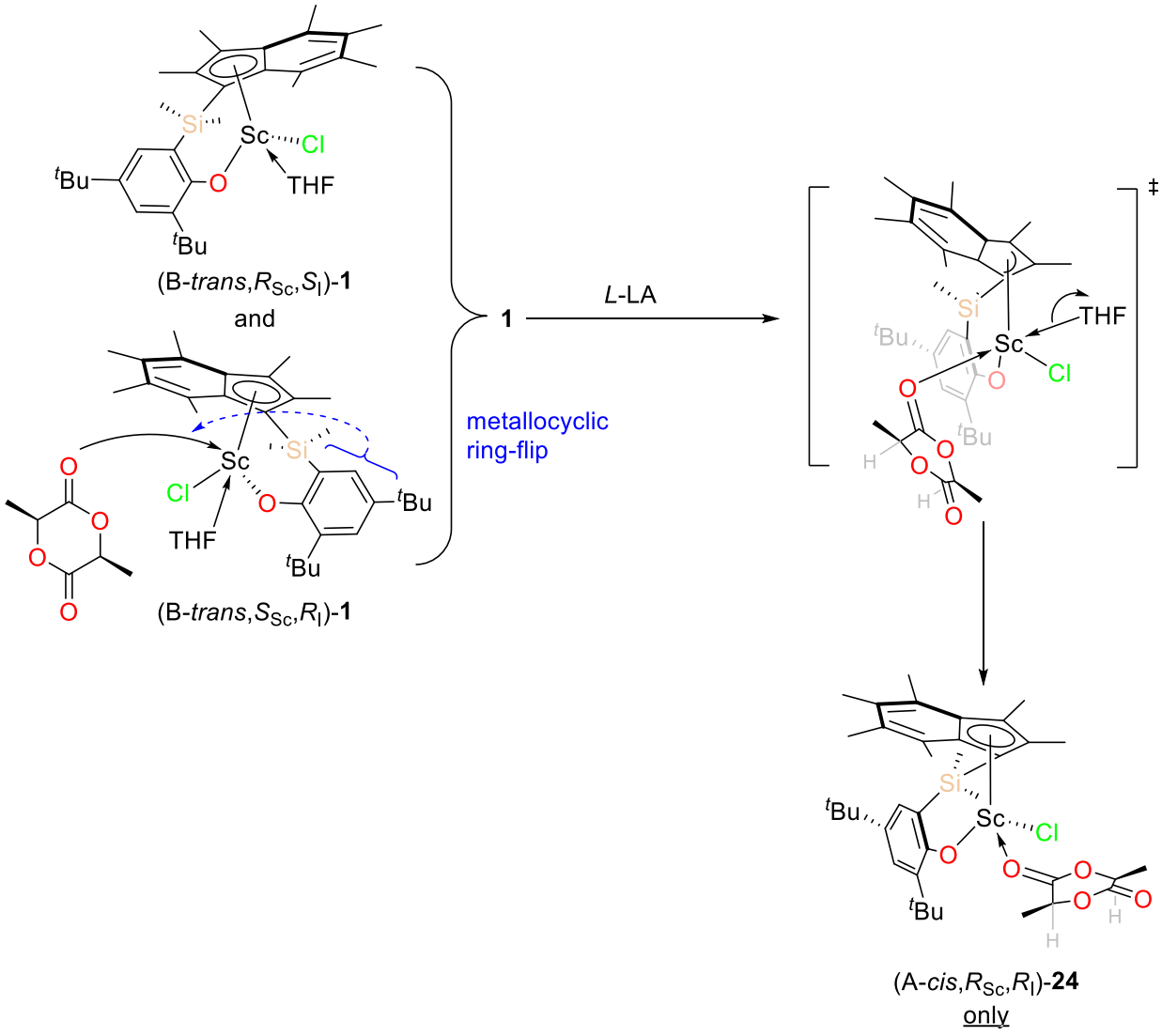


Figure 4.26 Bond lengths (Å) of the Sc-O and C=O bonds of (a) **24** and (b) **25**

When considering ϵ-CL adducts of neutral metal complexes, reports are within the range 1.226(4)–1.246(6) Å[59, 60, 67] with the yttrium metallocene adduct Cp*$_2$Y(Cl)ϵ-CL reported by W. Evans and co-workers presenting a C=O bond distance of 1.238(5)Å[60] close to the bond distance for **26** at 1.234(2) Å.[67] Cationic metal ϵ-CL coordination complexes have been reported with carbonyl bonds in the range of 1.217(6)–1.244(4)[61, 62, 68] and non-coordinated co-crystals of ϵ-CL in the region of 1.203–1.230(8) Å[69, 70]. There is definite O=C bond elongation from non-coordinated to coordinated lactone. However, change between cationic and neutral ϵ-CL adducts is insignificant from the set of data currently available.

24 forms through the associative substitution from (B-*trans*,S_{Sc},R_I)-**1** similar to that of the formation of the kinetic product **12-K** from **5** as discussed in **3.2.6.**. The solid-state

structure presents as enantiomerically pure. The formation of a single enantiomer could have occurred either through selection of a chance crystal or through a thermodynamical preference for the formation of this particular enantiomer in solution as shown in (**Scheme 4.2**).



Scheme 4.2 Synthesis of enantiomerically pure (A-*cis*,R_{Sc},R_I)-**24** from **1**. Rapid rearrangement of ligand conformation similar to that reported by Okuda *et al.*[71]

4.6. *L*-Lactide and ϵ-CL copolymerisation using 5 and 7

4.6.1. Literature reports and mechanism

The ring opening copolymerisation (ROCOP) of cyclic esters has been a rapidly expanding field.[72-75] ROCOP provides routes to controlling the macroscopic properties that can have a greater commercial market than homopolymers.[76, 77] Aluminium catalysts have been the main success for the copolymerisation of La and ϵ-CL.[74, 78, 79] Incorporation of lactide into PCL is of interest as this leads to a faster degradation period than homo-PCL.[80] This is useful for biomedical therapeutic applications where controlling the degradation period is important. Determining whether homo-polymerisation rather than copolymerisation occurs can be done by analysis of NMR spectroscopy, GPC and MALDI-ToF spectrometry data.[74, 81] It has been demonstrated that when both monomers are in the initial reaction, all of lactide monomer is polymerised followed by ϵ-CL. Incorporation can occur either through propagation or transesterification with PLA molecules in solution to form copolymer.[82] Where incorporation through transesterification occurs, two different modes occur, T_I and T_{II}. The mechanism of T_I and T_{II} are the same other than location of the break in the chain. T_I leaves even numbers of lactyl (half the lactide unit) units in the chain; T_{II} leaves odd. In addition, transesterification leads to higher than theoretical molecular. For reports in literature, high temperatures (>80 °C) or time (>h) are required.[83-85] Limited examples are reported at ambient conditions, such as the lanthanum shiff base complex.[86] Another route to obtaining PCL-b-PLA is through first polymerisation of ϵ-CL, then addition of LA to the living PCL chain.[72, 87]

^{1}H NMR spectroscopic analysis is used to identify the presence of ϵ-CL and *L*-LA linkages in the copolymers. The signals for the methylene protons of–C**H**$_2$CO–and–

C(O)OC**H**$_2$**–**attributed to ϵ-CL–ϵ-CL homo-sequences are observed around δ 2.3 and 4.0 ppm whereas the signals assigned to methylene protons of CL**–**LA hetero sequences are observed at δ 4.4 and 2.4 ppm.

4.6.2. Preliminary Results

The copolymerisation of ϵ-CL and *L*-LA was explored using several methods. First, a 50:50 mixture of ϵ-CL and *L*-LA was dissolved in 0.51 mL of toluene-d_8 and **7** dissolved in 0.09 mL of toluene added with 0 or 1 equiv.of $OPPh_3$ 250:250:1:*x*, [ϵ-CL]:[*L*-LA]:[**7**]:[$OPPh_3$] to a Youngs tap NMR tube and monitored over through NMR spectroscopy. After 3 days at 80℃, 90% conversion of *L*-LA was observed however no ϵ-CL was consumed during the reaction and the polymer did not contain any lactone proton signals in the ^{1}H NMR spectra (Entry 1 **Table 4.12**). Additionally, a series of reactions were undertaken where ϵ-CL was first polymerised; then L-LA was added to form a co-polymer 25:25:1:1, [ϵ-CL]:[*L*-LA]:[**Sc**]:[$OPPh_3$] (Entry 2 **Table 4.12**).

Table 4.12 ROP of *L*-LA;ϵ-CL initiated by **7**.

Entry	ϵ-CL	L-LA	$OPPh_3$	Temp. (℃)	Time (h)	Conv. (ϵ-CL/L-LA)[a] (%)	$M_{n,SEC}$[b] (kDa)	$Đ_M$[b]
1	250	250	1	60	4.23	0/87	56	1.36
2	25	25[d]	1	30	3/	60/80	5	2.15

Conditions: $[ϵ\text{-CL}]_0$:$[Sc]_0$ as 50:1, $[ϵ\text{-CL}]_0$ = 0.5 M in 0.6 mL toluene-d_6 at stated temperature. [a] Measured by ^{1}H NMR with ϵ-CL conversion in brackets. First-order rate constant (k_{obs}) and R^2 were obtained from plots of $\ln([ϵ\text{-CL}]_0/[ϵ\text{-CL}]_t)$ *vs* time. [b,c] Calculated from monomer conversion data: $[M]_0/[Sc]_0$ × conv. (%) × 114.14 × 0.01 + (MW of end groups (α+ω)) in kDa. [d] *L*-Lactide added after 3 mins at RT

The formation of a ϵ-CL–*L*-LA co-polymer was produced as evidenced by MALDI-TOF spectroscopy. MALDI-TOF spectra shows a pattern of peaks separated by either 72.1 or 114.2 m/z as depicted in **Figure 4.27**.

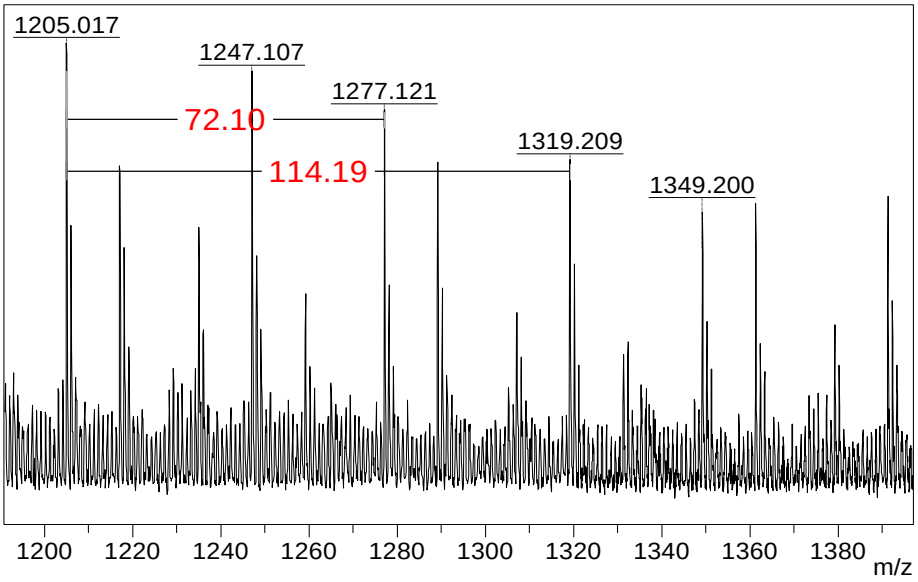


Figure 4.27 MALDI-TOF spectra of MALDI-ToF mass spectra of ϵ-PCL synthesised using (**7**). Conditions: [ϵ-CL]:[L-LA]:[**7**]$_0$:[opph$_3$] = 25:25:1:1, [ϵ-CL]$_0$ = 0.05 M, 0.6 mL toluene-d_8 at 25 °C. The cationisation agent was KTFA, and the matrix was DCTB. Peak separation of 72.1 and 114.19 m/z shown.

Through forming a matrix of all possible combinations of lactyl ($C_3H_4O_2$), and ϵ-CL units, all mass peaks present in the MALDI-TOF spectrum can be matched to chains of *n* lactyl and *m* ϵ-CL units (**Table 4.13**).

Table 4.13 Measured *m/z* from MALDI-TOF spectrum of PLLA-PLC copolymer. The cationisation agent was KTFA, and the matrix was DCTB Conditions: [ϵ-CL]:[*L*-LA]:[**7**]$_0$:[OPPh$_3$] = 25:25:1:2, [ϵ-CL]$_0$ = 0.05 M, 0.6 mL toluene-d_8 at 80 °C for 2 days

m/z (Da)	Calculated *m/z*[a] (Da)	No. lactyl units (*m/z* = 72.1 Da)	No. caprolactone units (*m/z* = 114.1 Da)
1205.0	1204.6	13	2
1217.2	1216.6	10	4
1235.0	1234.7	15	1
1247.1	1246.7	13	3
1259.2	1258.7	10	5
1277.2	1276.7	14	2
1289.2	1288.7	11	4
1307.1	1306.9	16	1
1319.3	1318.8	13	3
1349.3	1348.8	15	2
1361.4	1360.8	12	4
1391.3	1390.9	14	3
1421.3	1420.9	16	2

[a] (114.1*(j) + 72.1*(k) + 39.1), where: *j* = no. of lactone units; *k* = no lactyl units.

It is possible that this is occurring *via* random transesterification reactions or through intramolecular cyclisation which the polymer is being produced (**Figure 4.28**).

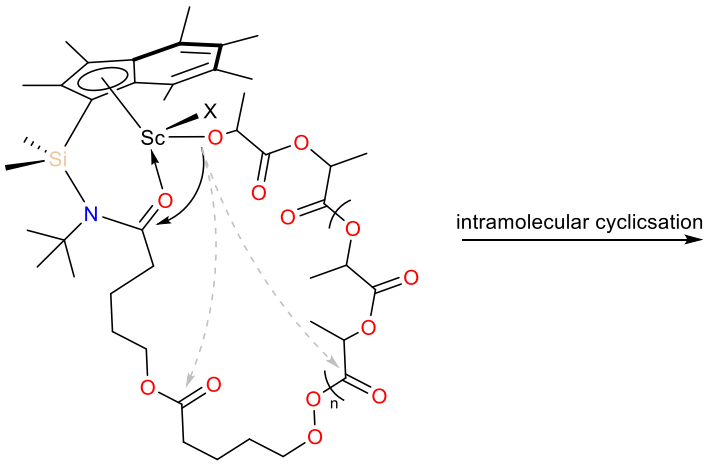


Figure 4.28 Possible intramolecular cyclisation to form cyclic PCL-b-L-LA copolymer.

The results are consistent with the literature, where ϵ-CL is first added, followed by the addition of LA, leading the formation of a random ϵ-CL-LA copolymer.[88]

4.7. Conclusion

The complexes **1–3** were shown to be active for the ROP of ϵ-CL, showing well controlled polymerisation in the presence of BnOH ($Đ_M$ = 1.1–1.5). Without BnOH, **1** showed activity, albeit reduced. Addition of BnOH the PHENI* indenyl complexes lead to protonation of the I* moiety and the structural constraints around the metal centre are disrupted. This increased the activity significantly.[39]

The 4-coordinate PHENI* and CGCI* scandium aryloxide complexes **5** and **7** were found to be active for the polymerisation of ϵ-CL and *L*-LA without the use of a co-initiator but showed no activity towards ω-pentadecalactone. For the polymerisation of ϵ-CL, **5** had poor rate (k_{obs} = 0.224±0.004) achieving 70% conversion after 1.1 h at 60 ℃ in a ratio of 200:1. **7** had good polymerisation rate (k_{obs} = 2.79±0.026) achieving 81% conversion after 0.64 h at 30 ℃ in a ratio of 750:1. Both showed a first-order dependence on monomer concentration. The poly(ϵ-CL) obtained were of medium-high molecular weights (M_n >80 000) and moderate to low molar-mass dispersity ($Đ_M$ = 1.4–2.3) with M_n and $Đ_M$ being dependent on monomer ratio and conversion %. The difference in rate was concluded to be the difference in nucleophilicity of the ligand *phenoxy*- and *amido*-hetero atom.

When a neutral donor was added, the rate for **5** decreases and showed a longer initiation period in addition to a low molar-mass dispersity. The results of variable temperature studies showed that the thermodynamic parameters of the scandium catalysed

polymerisations lay in the ranges: $41.6 < \Delta H^{\ddagger} < 56.9$ kJ mol^{-1}, $-29.5 < \Delta S^{\ddagger} < -71.4$ J K^{-1} mol^{-1}.

5-coordinate tris-aryl oxide scandium complexes (Sc(O-2,4-R-C_6H_3), where R = ^{i}Pr (**29**) and ^{t}Bu (**30**)) show an increase in rate from substitute R group from R = ^{i}Pr (**29**) to ^{t}Bu (**30**)). Both **29** and **30** showed living polymerisation with molecular weights increase during the course of the reaction through initiation by protic impurity rather than insertion of the Sc-aryloxide bond. The 4 coordinate I* systems are fluxional in solution and the neutral ligand can exchange easily through a 5-coordinate transition state mediated by the η^5- to η^3- indenyl ring-slip. This facilitates the coordination of monomer and increases activity.

Complexes **1** and **5** were reacted with ε-CL, *L*-LA, and ω-PDL to form scandium-monomer adducts **23**–**26**, and **28**. Monomer-metal adducts **24**–**26** have been characterised in the solid state, and are some of the few examples of coordinated initiator-monomer adducts. The formation of **24** might occur through crystal selection or thermodynamic preference. Sc–O dative bond for *L*-lactide adduct is longer than in ω-PDL adduct, with C=O bond distances suggesting the lactide scandium adducts is strained due to steric bulk of the lactide molecule. Comparisons with other metal ε-CL complexes showed minimal difference in C=O bond lengths between cationic and neutral ε-CL adducts, but elongation relative to non-coordinated complexes.

A preliminary co-polymerisation study was conducted which showed the formation of random ϵ-CL-*L*-LA copolymer is possible using 4 coordinate PHENI* and CGC Sc aryloxide catalysts.

4.8. References

1. P. J. Shapiro, PhD, California Institute of Technology, 1991.
2. B. Wang, D. Wang, D. Cui, W. Gao, T. Tang, X. Chen and X. Jing, *Organometallics*, 2007, **26**, 3167-3172.
3. X. Xu, Y. Chen, J. Feng, G. Zou and J. Sun, *Organometallics*, 2010, **29**, 549-553.
4. Y. Luo, J. Baldamus and Z. Hou, *J Am Chem Soc*, 2004, **126**, 13910-13911.
5. H. Ma, T. P. Spaniol and J. Okuda, *Angew. Chem. Int. Ed.*, 2006, **45**, 7818-7821.
6. Z. R. Turner, J. C. Buffet and D. O'Hare, *Organometallics*, 2014, **33**, 3891-3903.
7. J. V. Lamb, J. C. Buffet, J. E. Matley, C. M. R. Wright, Z. R. Turner and D. O'Hare, *Dalton Trans*, 2019, **48**, 2510-2520.
8. M. J. Stanford and A. P. Dove, *Chem Soc Rev*, 2010, **39**, 486-494.
9. N. Diteepeng, I. A. P. Wilson, J.-C. Buffet, Z. R. Turner and D. O'Hare, *Polym Chem-Uk*, 2020, **11**, 6308-6318.
10. Z. R. Turner, J. V. Lamb, T. P. Robinson, D. Mandal, J. C. Buffet and O. H. D, *Dalton Trans*, 2021, **50**, 4805-4818.
11. A. Arbaoui and C. Redshaw, *Polym Chem-Uk*, 2010, **1**, 801-826.
12. D. M. Lyubov, A. O. Tolpygin and A. A. Trifonov, *Coordin Chem Rev*, 2019, **392**, 83-145.
13. S. Penczek, J. Pretula and S. Slomkowski, *Chem. Teach. Int.*, 2021, **3**, 33-57.
14. D. Meimaroglou, P. Pladis and C. Kiparissides, *Macromol React Eng*, 2016, **11**, 1600039.
15. G. P. Paul and N. Virivinti, *Iran Polym J*, 2022, **31**, 59-81.
16. F. Weng, X. Li, Y. Wang, W. J. Wang and S. J. Severtson, *Macromol. React. Eng.*, 2015, **9**, 535-544.
17. R. P. Rosa, F. V. Ferreira and L. M.F. Lona, *Chem. Eng. Sci.*, 2021, **246**, 116934.
18. C. D. T. Nielsen and J. Burés, *Chem. Sci.*, 2019, **10**, 348-353.
19. J. S. Mathew, M. Klussmann, H. Iwamura, F. Valera, A. Futran, E. A. C. Emanuelsson and D. G. Blackmond, *J. Org. Chem.*, 2006, **71**, 4711-4722.
20. J. Burés, *Angew. Chem. Int. Ed.*, 2016, **55**, 2028-2031.
21. C. Alamillo-Ferrer, G. Hutchinson and J. Burés, *Nat. Rev, Chem.*, 2022, **7**, 26-34.
22. S. Sinnwell, A. J. Inglis, T. P. Davis, M. H. Stenzel and C. Barner-Kowollik, *Chem. Commun.*, 2008, DOI: 10.1039/b718180a, 2052.
23. N. Diteepeng, J. C. Buffet, Z. R. Turner and D. O'Hare, *Dalton Trans*, 2019, **48**, 16099-16107.
24. M. Xue, H. Sun, H. Zhou, Y. Yao, Q. Shen and Y. Zhang, *J. Polym. Sci., Part A: Polym. Chem.*, 2006, **44**, 1147-1152.
25. A. Kowalski, A. Duda and S. Penczek, *Macromol. Rapid Commun.*, 1998, **19**, 567-572.
26. A. Fernández-Tena, R. A. Pérez-Camargo, O. Coulembier, L. Sangroniz, N. Aranburu, G. Guerrica-Echevarria, . . . A. J. Müller, *Macromolecules*, 2023, **56**, 4602-4620.
27. T. Arnold, D.Phil. Thesis, Oxford University, UK, 2015.
28. J. C. Buffet, T. A. Q. Arnold, Z. R. Turner, P. Angpanitcharoen and D. O'Hare, *RSC Adv.*, 2015, **5**, 87456-87464.
29. J. A. Wilson, Z. Ates, R. L. Pflughaupt, A. P. Dove and A. Heise, *Prog. Polym. Sci.*, 2019, **91**, 29-50.
30. D. Myers, T. Witt, A. Cyriac, M. Bown, S. Mecking and C. K. Williams, *Polym Chem-Uk*, 2017, **8**, 5780-5785.
31. X. Tang, A. H. Westlie, L. Caporaso, L. Cavallo, L. Falivene and E. Y. X. Chen, *Angew. Chem. Int. Ed.*, 2020, **59**, 7881-7890.
32. X. Y. Tang, C. X. Shi, Z. Zhang and E. Y. X. Chen, *Macromolecules*, 2021, **54**, 9401-9409.
33. X. Tang and E. Y. Chen, *Nat Commun*, 2018, **9**, 2345.
34. S. Gesslbauer, G. Hutchinson, A. J. P. White, J. Burés and C. Romain, *Acs Catal*, 2021, **11**, 4084-4093.
35. K. Y. Ding, M. O. Miranda, B. Moscato-Goodpaster, N. Ajellal, L. E. Breyfogle, E. D. Hermes, . . . W. B. Tolman, *Macromolecules*, 2012, **45**, 5387-5396.
36. X. Dong and J. R. Robinson, *New J Chem*, 2022, **46**, 444-453.
37. X. Dong and J. R. Robinson, *Chem Sci*, 2020, **11**, 8184-8195.
38. J. Ling, J. Shen and T. E. Hogen-Esch, *Polymer*, 2009, **50**, 3575-3581.
39. W. A. Munzeiwa, B. O. Omondi and V. O. Nyamori, *Polym. Bull.*, 2024, DOI: 10.1007/s00289-024-05149-5.
40. H. R. Kricheldorf and S. M. Weidner, *Eur Polym J*, 2023, **185**, 111822.
41. I. Stephens, M. Chem Part II Thesis, University of Oxford, 2021.
42. L. D. Henderson, G. D. MacInnis, W. E. Piers and M. Parvez, *Can J Chem*, 2004, **82**, 162-165.
43. N. Nomura, A. Taira, T. Tomioka and M. Okada, *Macromolecules*, 2000, **33**, 1497-1499.

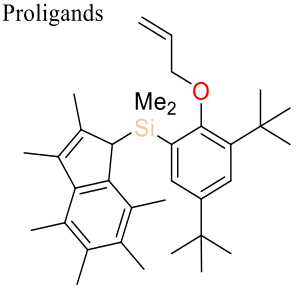
44. M. Möller, R. Kånge and J. L. Hedrick, *J. Polym. Sci., Part A: Polym. Chem.*, 2000, **38**, 2067-2074.
45. N. Nomura, A. Taira, A. Nakase, T. Tomioka and M. Okada, *Tetrahedron*, 2007, **63**, 8478-8484.
46. S. Hamidi, G. B. Deacon, P. C. Junk and P. Neumann, *Dalton Trans.*, 2012, **41**, 3541.
47. L. Clark, G. B. Deacon, C. M. Forsyth, P. C. Junk, P. Mountford and J. P. Townley, *Dalton Trans.*, 2010, **39**, 6693.
48. W. M. Stevels, M. J. K. Ankoné, P. J. Dijkstra and J. Feijen, *Macromolecules*, 1996, **29**, 3332-3333.
49. W. M. Stevels, M. J. K. Ankoné, P. J. Dijkstra and J. Feijen, *Macromolecules*, 1996, **29**, 6132-6138.
50. F. Peng, J. Ling, Z. Shen and W. Zhu, *J. Mol. Catal. A: Chem.*, 2005, **230**, 135-141.
51. Y. C. Yu, G. Storti and M. Morbidelli, *Ind Eng Chem Res*, 2011, **50**, 7927-7940.
52. Y. Liu, X. Yuan, J. Wu, X. Hu, N. Zhu and K. Guo, *Polym. Chem.*, 2022, DOI: 10.1039/d1py01340h.
53. K. C. Hultzsch, T. P. Spaniol and J. Okuda, *Organometallics*, 1998, **17**, 485-488.
54. S. Penczek, R. Szymanski, A. Duda and J. Baran, *Macromol Symp*, 2003, **201**, 261-269.
55. M. Visseaux, C. H. Brachais, C. Boisson and K. Tortosa, *Cr Acad Sci Ii C*, 2000, **3**, 631-638.
56. J. Klosin, W. J. Kruper, P. N. Nickias, G. R. Roof, P. De Waele and K. A. Abboud, *Organometallics*, 2001, **20**, 2663-2665.
57. V. C. Gibson and S. K. Spitzmesser, *Chem. Rev.*, 2003, **103**, 283-316.
58. A. F. Douglas, B. O. Patrick and P. Mehrkhodavandi, *Angew. Chem. Int. Ed. Engl.*, 2008, **47**, 2290-2293.
59. W. J. Evans, J. L. Shreeve and R. J. Doedens, *Inorg. Chem.*, 1993, **32**, 245-246.
60. W. J. Evans, C. H. Fujimoto, M. A. Johnston and J. W. Ziller, *Organometallics*, 2002, **21**, 1825-1831.
61. A. Buchard, M. G. Davidson, G. Gobius du Sart, M. D. Jones, G. Kociok-Köhn, S. N. McCormick and P. McKeown, *Inorg. Chem.*, 2023, **62**, 15688-15699.
62. A. Buchard, M. G. Davidson, G. Gobius du Sart, M. D. Jones, G. Kociok-Köhn, S. N. McCormick and P. McKeown, *Inorg. Chem.*, 2024, **63**, 27-38.
63. D. J. Darensbourg, W. Choi, O. Karroonnirun and N. Bhuvanesh, *Macromolecules*, 2008, **41**, 3493-3502.
64. W. Saiyasombat, R. Molloy, T. M. Nicholson, A. F. Johnson, I. M. Ward and S. Poshyachinda, *Polymer*, 1998, **39**, 5581-5585.
65. L. Nikolic, I. Ristic, B. Adnadjevic, V. Nikolic, J. Jovanovic and M. Stankovic, *Sensors*, 2010, **10**, 5063-5073.
66. PubChem, PubChem Compound Summary for CID 235414, Oxacyclohexadecan-2-one https://pubchem.ncbi.nlm.nih.gov/compound/Oxacyclohexadecan-2-one, (accessed November 14, 2024).
67. J. Lewiński, P. Horeglad, E. Tratkiewicz, W. Grzenda, J. Lipkowski and E. Kolodziejczyk, *Macromol. Rapid Commun.*, 2004, **25**, 1939-1942.
68. S. Dagorne, F. Le Bideau, R. Welter, S. Bellemin-Laponnaz and A. Maisse-François, *Chem. – Eur. J.*, 2007, **13**, 3202-3217.
69. A. A. Yartseva, L. S. Koldrov, S. S. Galibeev, V. P. Arkhireev, N. I. Naumkina, I. A. Litvinov and A. T. Gubaidullin, *J. Struct. Chem.*, 2007, **48**, 1138-1144.
70. M. Yan, Y. Liu, J. Xu, L. Yang, L. Zhang, F. Nie and S. Huang, *Cryst. Growth Des.*, 2020, **20**, 5387-5394.
71. A. Kapelski, J. C. Buffet, T. P. Spaniol and J. Okuda, *Chem. – Asian J.*, 2012, **7**, 1320-1330.
72. M. Abdul Rahman, T. J. Neal and J. A. Garden, *Chem. Commun.*, 2024, **60**, 5530-5533.
73. F. Kayser, G. Fleury, S. Thongkham, C. Navarro, B. Martin-Vaca and D. Bourissou, *Polym. Chem.*, 2022, DOI: 10.1039/d2py00101b.
74. B. Beament, D. Britton, T. Malcomson, G. R. Akien, N. R. Halcovitch, M. P. Coogan and R. H. Platel, *Inorg. Chem.*, 2024, **63**, 280-293.
75. F. Y. Weng, X. H. Li, Y. J. Wang, W. J. Wang and S. J. Severtson, *Macromol React Eng*, 2015, **9**, 535-544.
76. S. Paul, Y. Zhu, C. Romain, R. Brooks, P. K. Saini and C. K. Williams, *Chem. Commun.*, 2015, **51**, 6459-6479.
77. Y. Zhu, C. Romain and C. K. Williams, *Nature*, 2016, **540**, 354-362.
78. M. Florczak and A. Duda, *Angew. Chem. Int. Ed.*, 2008, **47**, 9088-9091.
79. N. Nomura, A. Akita, R. Ishii and M. Mizuno, *J. Am. Chem. Soc.*, 2010, **132**, 1750-1751.
80. M.-H. Huang, S. Li and M. Vert, *Polymer*, 2004, **45**, 8675-8681.
81. J. Kasperczyk and M. Bero, *Die Makromolekulare Chemie*, 1991, **192**, 1777-1787.
82. E. Piedra-Arroni, C. Ladaviere, A. Amgoune and D. Bourissou, *J Am Chem Soc*, 2013, **135**, 13306-13309.

83. R. L. Webster, N. Noroozi, S. G. Hatzikiriakos, J. A. Thomson and L. L. Schafer, *Chem Commun (Camb)*, 2013, **49**, 57-59.
84. D. J. Gilmour, R. L. Webster, M. R. Perry and L. L. Schafer, *Dalton Trans*, 2015, **44**, 12411-12419.
85. H. Ouyang, D. Yuan, K. Nie, Y. Zhang, Y. Yao and D. Cui, *Inorg. Chem.*, 2018, **57**, 9028-9038.
86. J. Shao, H. Zhou, Y. Wang, Y. Luo and Y. Yao, *Dalton Trans.*, 2020, **49**, 5842-5850.
87. H. R. Kricheldorf, S. M. Weidner and A. Meyer, *Macromol. Chem. Phys.*, 2022, DOI: 10.1002/macp.202200385.
88. J. Kasperczyk and M. Bero, *Die Makromolekulare Chemie*, 1993, **194**, 913-925.

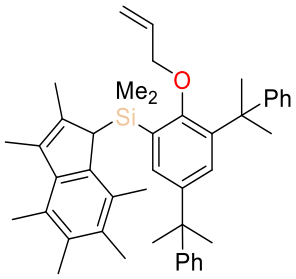
Chapter 5 – **Experimental Detail**

5.1. Compound Key

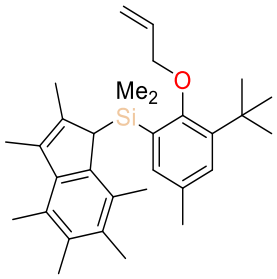
Proligands



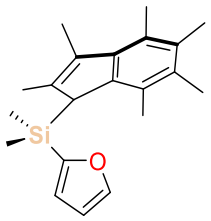
$Me_2SB(^{tBu_2}ArOAllyl,I^*)H$



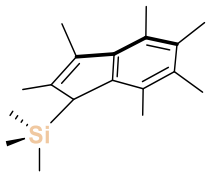
$Me_2SB(^{Cumyl_2}ArOAllyl,I^*)H$



$Me_2SB(^{Me,tBu}ArOAllyl,I^*)H$

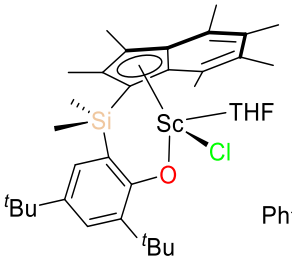


$Me_2SB(Furan,I^*)H$

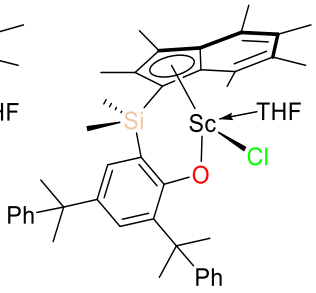


$I^{\#}SiMe_3$

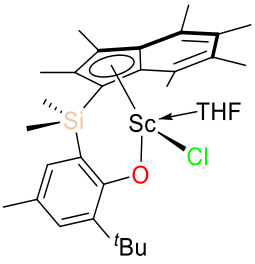
Complexes



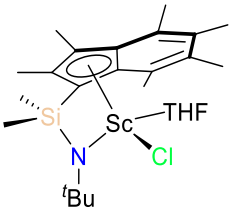
1



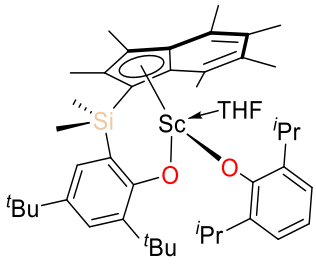
2



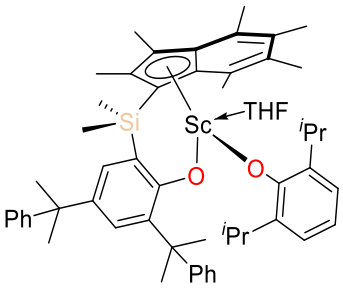
3



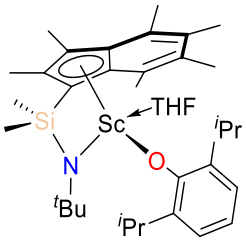
4



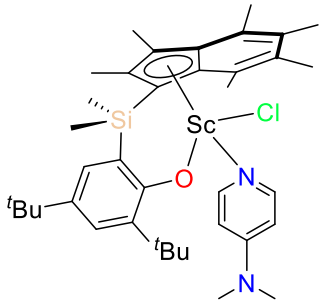
5



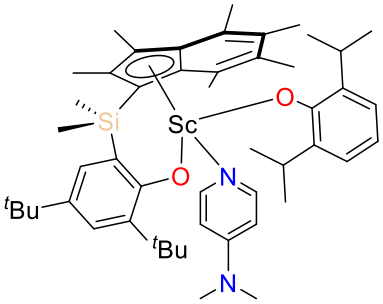
6



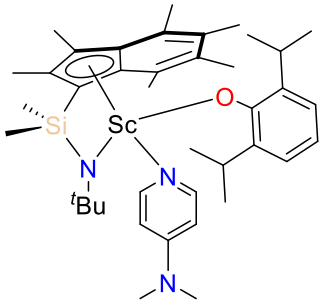
7



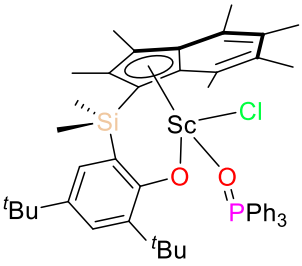
8



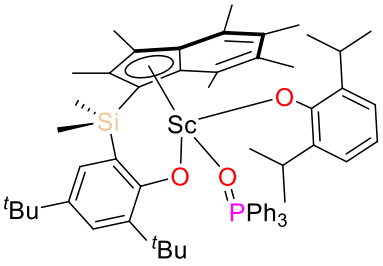
9



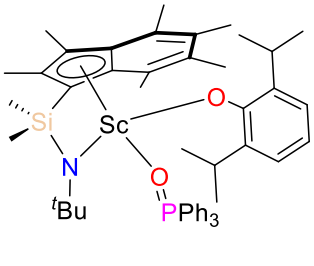
10



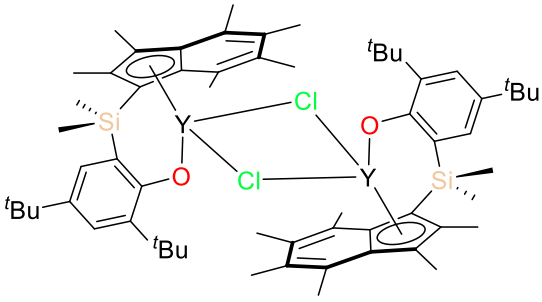
11



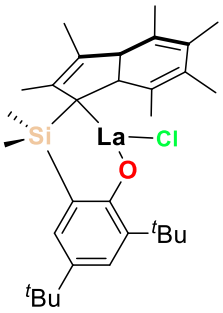
12



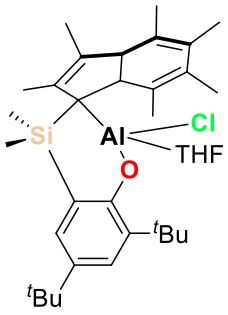
13



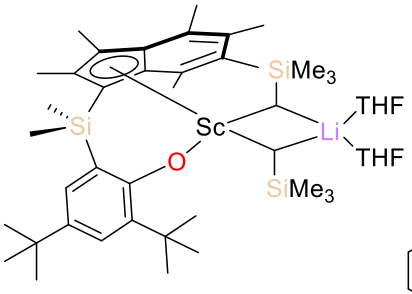
14



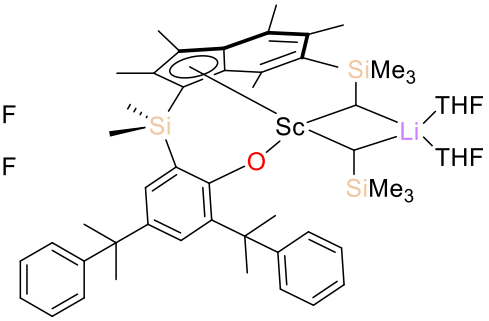
15



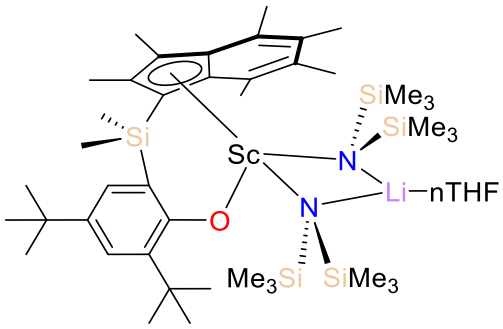
16



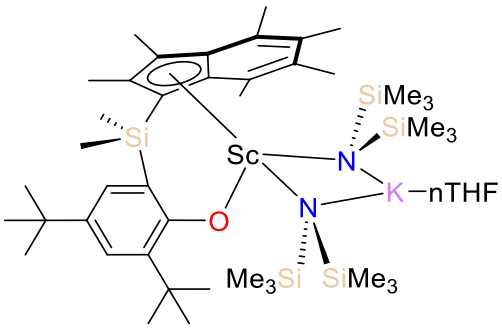
17



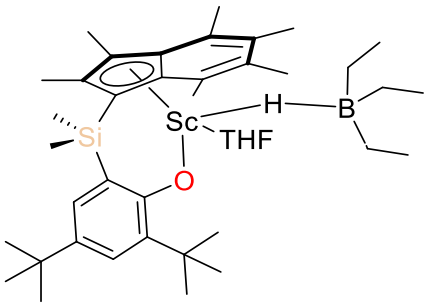
18



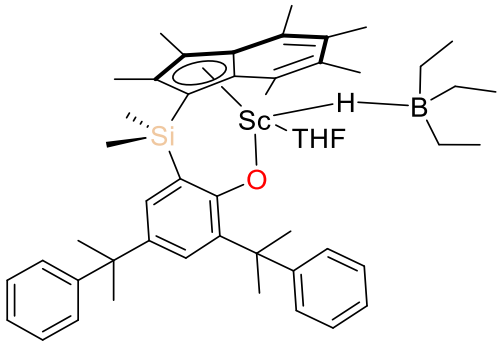
19



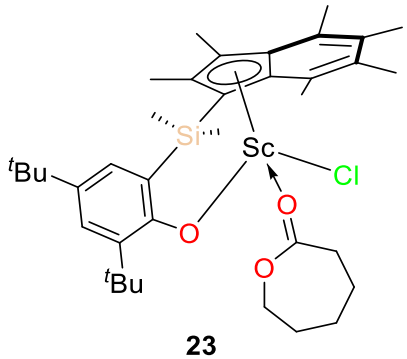
20



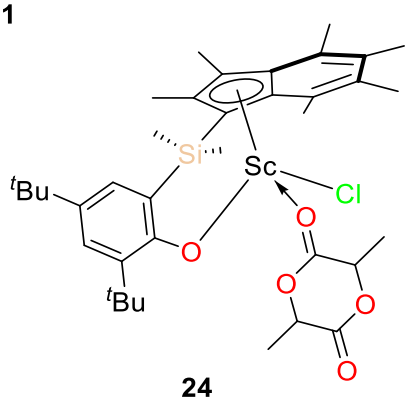
21



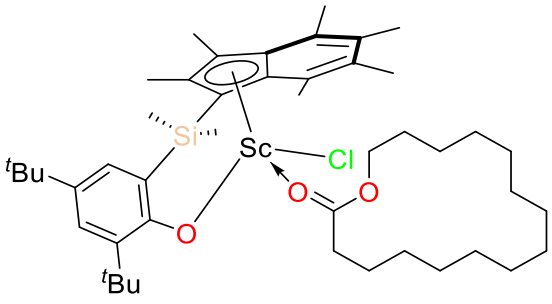
22



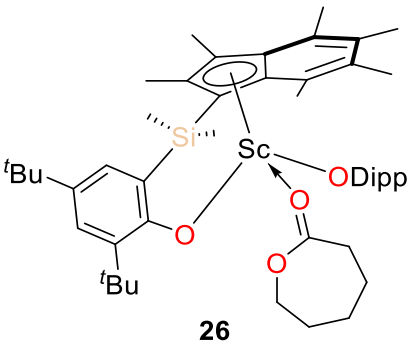
23



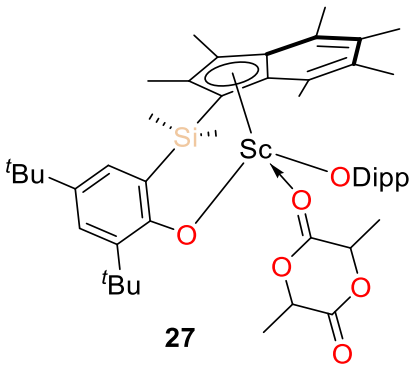
24



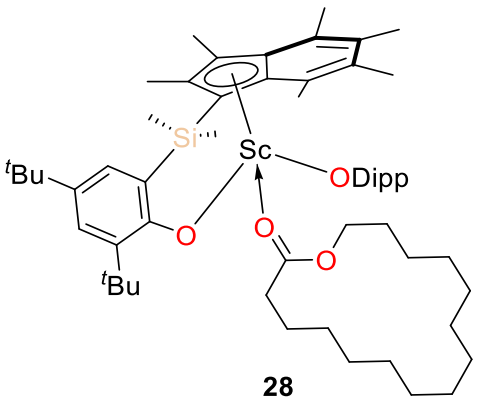
25



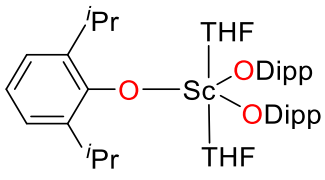
26



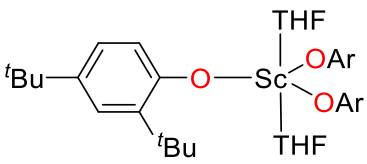
27



28



29



30

5.2. General procedures

Air- and moisture-sensitive compounds were manipulated under an inert atmosphere of nitrogen, using standard Schlenk line techniques[1] on a dual manifold vacuum/nitrogen line or in an MBraun Labmaster 100 glovebox.

5.2.1. Literature preparations and commercially supplied reagents

Furan (Fluorochem), hydrochloric acid (Fischer Scientific), ^{n}BuLi (1.6 M solution in hexanes; Sigma Aldrich), 6-bromo-2,4-di-tert-butylphenol (Alfa Aesar), 2,6-diisporopyl phenol (Sigma Aldrich), 2,4-*tert*-butyl-phenol (Fluorochem), pyridine (Sigma Aldrich), potassium hydroxide (Sigma Aldrich), sodium amide (Sigma Aldrich), scandium (III) oxide (Sigma Aldrich) and were all used as received. Benzyl alcohol (Sigma Aldrich) were stored over 3 Å molecular sieves and freeze-pump-thaw degassed three times prior to use. 2,6- diisopropylaniline (Apollo Scientific), and tetramethylethylenediamine (TMEDA; Sigma Aldrich) were dried over calcium hydride.

Lanthanum trichloride, yttrium trichloride, and aluminium trichloride (Sigma Aldrich) were dried under reduced pressure and stored under an inert atmosphere prior to use. Potassium hydride (Sigma Aldrich) was purchased as a 30 wt% dispersion in mineral oil. Any excess oil was decanted away before the solid was washed with portions of diethyl ether until a free-flowing powder was obtained; this was dried under reduced pressure before use. Sodium bis(trimethylsilyl)amide (Sigma Aldrich) was washed with portions of pentane and dried under reduced pressure before use. (Trimethylsilyl)methyllithium (1.0M) pentane (Sigma Aldrich) was tried under vacuum, then sublimed at 75°C. Potassium and lithium bis(trimethylsilyl)amide (Sigma Aldrich)

$KBEt_3H.THF_{0.25}$ was prepared by drying a solution of potassium triethylborohydride (1.0 M in THF, Sigma Aldrich), under vacuum for 1 day and THF ratio determined *via* ^1H NMR spectroscopy. 2,3,4,5,6,7-hexamethylindene ($C_9Me_6H_2$, $Ind^{\#}H$) was supplied by SCG Chemicals Co., Ltd. (Thailand) and used as received. and. Me_2SiCl_2 and Me_3SiCl (Sigma Aldrich) was stored over 4 Å molecular sieves. $ScCl_3.3THF$ was synthesised using a modified literature procedure.[2] The reaction between Sc_2O_3 and HCl produced $ScCl_3.(H_2O)_6$, which subsequently reacted with trimethylsilyl chloride (Me_3SiCl) in THF to afford ScCl3·3THF. Me_3SiCl was used as an alternative to thionyl chloride ($SOCl_2$). L-lactide (L-LA) was provided courtesy of Corbion, was recrystallised twice from toluene and sublimed (70 °C, 10–3 mbar) as standard procedure.[3] Et_3N was dried over KOH, filtered, and then degassed under partial vacuum before use. K(O-2,6-^{i}Pr-C_6H_3) was synthesised from an adapted salt metathesis route by Dr Nichabhat Diteepeng. Furan-2-yl lithium (Organolithium formation) was prepared by addition of 1.1 eq. of ^{n}BuLi (1.6 M in hexanes, 9.4 mL, 15.1 mmol, 1.1 eq.) to furan (0.936 g cm^{-1}, 13.7 mmol, 1 mL) in THF (20 mL) at 0 °C. The mixture was dried and washed with cold hexanes (0 °C, 3 x 5 mL) to give an off-white powder.[4]

5.2.1.1. Monomer preparation

Rac-DL[5] was synthesised from 3-Chloroperbenzoic acid (Sigma Aldrich) and dimethyl succinate (Sigma Aldrich) following literature. ω-pentadecalactone (Sigma Aldrich) was distilled from calcium hydride and stored under an inert atmosphere. ϵ-caprolactone (Fisher scientific) was dried over calcium hydride and triple distilled after the addition of 3 drops of ^{n}BuLi (1.6M, n-hexanes) and stored under an inert atmosphere.

The ϵ-caprolactone ϵ-CL was dried first over anhydrous calcium hydride (CaH_2). Then fractional distilled under dynamic vacuum at 80 °C, with the first and last 10% of each

fraction being removed. A few drops of ^{n}BuLi (1.6 mol in Hexanes) were added during the final distillation step to yield dry ϵ-Cl.

5.2.2. Solvent Preparation

Pentane, hexane, toluene, and benzene were dried using an MBraun SPS 800 solvent purification system, stored over a potassium mirror, and degassed under partial vacuum before use. Anhydrous dichloromethane, dimethylformamide, and acetonitrile were dried using an MBraun SPS 800 system, stored over pre-activated 3 Å molecular sieves and degassed under partial vacuum before use. Tetrahydrofuran was distilled from sodium/benzophenone, stored over pre-activated 3 Å molecular sieves and degassed under partial vacuum before use. Diethyl ether was distilled from NaK, stored over a potassium mirror, and degassed under partial vacuum before use. Dioxane was distilled from sodium, stored over pre-activated 3 Å molecular sieves and degassed under partial vacuum before use.

Deuterated solvents were dried over potassium metal (benzene-d_6, and toluene-d_8) or CaH_2 (chloroform-d_1, pyridine-d_5, and tetrahydrofuran-d_8) and refluxed under reduced pressure, distilled under static vacuum, freeze-pump-thaw degassed three times and stored over pre-activated 3 or 4 Å molecular sieves. Chloroform-d_1 used as supplied for samples which were not air- and moisture-sensitive.

5.2.3. Solution NMR spectroscopy

NMR spectra were recorded on either a Bruker Avance III HD NanoBay NMR (9.4 T, 400.2 MHz), a Bruker Avance III NMR (11.75 T, 499.9 MHz), a Bruker Avance NMR (11.75 T, 500.3 MHz) with a ^{13}C-detect cryoprobe, or a Bruker NEO 600 (14.1 T, 600.4 MHz) with a broadband helium cryoprobe. Spectra were recorded at 298 K unless

otherwise stated and referenced internally to the residual *protio* solvent resonance. Chemical shifts, δ, are reported in parts per million (ppm) relative to tetramethylsilane (δ = 0 ppm). Air-sensitive samples were prepared in a glovebox under an inert atmosphere of nitrogen, using dried deuterated solvents and sealed in 5 mm Young's tap NMR tubes.

5.2.4. X-ray crystallography

Single-crystal X-ray diffraction data collection and structure determination were performed by Dr Zoë R. Turner or Dr Clement G. Collins Rice (University of Oxford). Crystals were mounted on MiTeGen MicroMounts using perfluoropolyether oil and rapidly transferred to a goniometer head on a diffractometer fitted with an Oxford Cryosystems Cryostream open-flow nitrogen cooling device.[6] Data collections were carried out at 150 K on an Oxford Diffraction Supernova diffractometer using mirror-monochromated Cu Kα radiation (λ = 1.54178 Å) and data were processed using CryAlisPro.[7] The structures were solved using direct methods (SIR-92)[8] or a charge flipping algorithm (SUPERFLIP)[9] and refined by full-matrix least-squares using either the Win-GX or CRYSTALS software suites.[10, 11] Molecular bond lengths and angles were calculated, where required, using PLATON.[12] Illustrations of the solid state molecular structures were created using ORTEP.[13] Thermal ellipsoids were shown at 30% probability unless otherwise specified.

5.2.5. Elemental analysis

Samples were prepared in a glovebox under a nitrogen atmosphere and sealed in glass vials. CHN analyses were carried out in duplicate by Ms Orla McCullough (London Metropolitan University).

5.2.6. Infrared spectroscopy

Fourier-transform infrared (FTIR) spectra were measured using a ThermoScientific Nicolet iS 5 FTIR spectrometer, and either the iD1 Transmission, or germanium iD3 Attenuated Total Reflection accessories. A background spectrum was run prior to the samples and subtracted from the sample spectra. Air-sensitive samples were prepared in a glove box, ground with anhydrous potassium bromide (KBr), and pressed into discs.

5.2.7. Gel permeation chromatography

Polymer molecular weights and dispersity (M_n, M_w and M_w/M_n) were determined by GPC using a Polymer Laboratories PLGPC50 Plus instrument equipped with a Polymer Laboratories PLgel Mixed-D column (300mm length, 7/5 mm diameter) and a refractive index (RI) detector. THF (sigma Aldrich, HPLC grade) with BHT (0.244 gL^{-1}) inhibitor was used as an eluent at 35 °C with a flow rate of 1.0 mL min^{-1}. Samples were dissolved in THF at a concentration of 1.0 mg mL^{-1} and filtered with PTFE filters before injection. Linear polystyrenes were used as primary calibration standards and a correction factor of 0.58 was applied for lactide samples and 0.786 for PCL where appropriate.

5.2.8. Proligand synthesis

Substituted phenol, $^{R,R'}$ArOH (1 equivalent), was dissolved in dichloromethane in a round-bottomed flask. To this, Br_2 (1 eq.) was added dropwise. The reaction was stirred for 90 minutes, after which the crude mixture was washed with distilled water. The organic portion was dried over $MgSO_4$, filtered, and the solvent removed under vacuum to yield the monobrominated product quantitatively as a thick oil.

The bromophenol $^{Br,R,R'}$ArOH and allyl bromide (CH_2CHCH_2Br, 1.5 eq.) were then dissolved in acetone in a round-bottomed flask. This solution was then added dropwise

to a 10% aqueous solution of NaOH (1.5 eq.) and stirred for 4 h. The reaction mixture was neutralised with 5% aqueous H_2SO_4 and the volatiles removed under vacuum. The product, ^{Br,Me_2}ArOAllyl, was extracted in toluene, dried over $MgSO_4$ and the solvent removed under vacuum to give the desired product in quantitative yields as off-white solids.

The allylphenol $^{Br,R,R'}$ArOAllyl was dissolved in toluene in a Schlenk flask. To this was added dropwise at –70 °C 1.3 eq. of ^{n}BuLi solution (1.6 M in hexanes) and the reaction was allowed to warm to –20 °C. If the reaction is allowed to warm to 0 °C a rearrangement product is formed at this stage. This mixture was then dropwise added to a toluene solution of 3 eq. Me_2SiCl_2 at –20 °C. The reaction was allowed to warm to room temperature and stirred for 18 h. The solid by products were removed by filtration, and the volatiles removed under vacuum, leaving the chlorosilyl product, $^{Me_2ClSi,R,R'}$ArOAllyl, as a pale yellow to colourless oil. This was then combined with 1.1 equivalents of (2,3,4,5,6,7-hexamethyl-1*H*-inden-1-yl)lithium ($Ind^{\#}$Li) and dissolved in THF at 0 °C. The reaction was allowed to warm to room temperature and stirred for 18 h, after which it was dried under vacuum; the product was extracted in pentane and the solvent removed under vacuum to yield the proligand ^{Me_2}SB($^{R,R'}$ArOAllyl,I*)H or the rearrangement product, benzofuran. The proligand was then redissolved in toluene. 3.5 equivalents of triethylamine were added and the mixture cooled to –78 °C. 2.25 eq. of ^{n}BuLi solution (1.6 M in hexanes) was added dropwise. The reaction was allowed to warm to room temperature and stirred for 3–18 h, during which the solution gradually darkens. In the stepwise process, removal of the volatiles under vacuum yielded the ligands as dilithium salts, ^{Me_2}SB($^{R,R'}$ArO,I*)Li_2, as bright orange powders in approximately quantitative

yields. The crude products can then be used to synthesise metal complexes without further purification.[14]

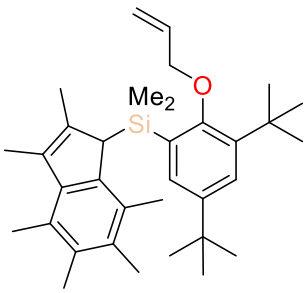
5.3. Experimental Detail for Chapter 2

Compounds have been previously synthesised and obtained as orange oils. The compounds reported here are obtained as crystalline solids

Crystals of the R=R′=^{t}Bu and R = R′ = Cumyl were also grown following an adapted procedure: the crude yellow oil/wax was redissolved in minimum volume of hexanes and cooled to −20 °C. A white crystalline solid formed and the supernatant solution was filtered away. The white solid was then washed with cold (−20 °C) hexanes.

^{Me2}SB($^{R,R'}$ArOAllyl,I*)H can be further purified from crude product. After combining 1.1 eq. of (2,3,4,5,6,7-hexamethyl-1*H*-inden-1-yl)lithium (Ind$^{\#}$Li) with ^{Me2}SiCl$^{R,R'}$ArOAllyl in THF at 0 °C; the reaction was allowed to warm to room temperature and stirred for 18 h. After the reaction mixture was dried under vacuum; the product was extracted in hexane, concentrated and cooled to -20 °C. White crystals form suitable for X-ray crystallography are collected and washed with cold hexanes. Multiple crops yielded 26% ^{Me2}SB($^{t Bu2}$ArOAllyl,I*)H and 51% ^{Me2}SB(^{Cumyl2}ArOAllyl,I*)H.

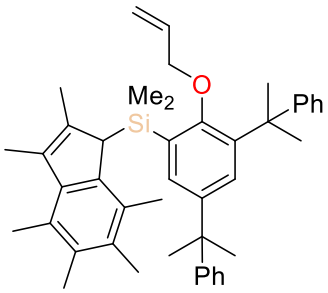
5.3.1. Synthesis of ^{Me2}SB(^{tBu2}ArOAllyl,I*)H



^{1}H NMR (benzene-d_6, 600 MHz, 298 K): δ 7.59 (d, $^{4}J_{H–H}$ = 2.5 Hz, 1H, Ar**H**), 7.37 (d, $^{4}J_{H–H}$ = 2.5 Hz, 1H, Ar**H**), 5.87 (ddt, $^{3}J_{H–H}$ = 17.3, 10.8, $^{4}J_{H–H}$ = 4.1 Hz 1H, $OCH_2C\mathbf{H}CH_2$), 5.56 (dq, $^{3}J_{H–H}$ = 17.3, $^{4}J_{H–H}$ = 2.0 Hz 1H, $OCH_2CHC\mathbf{H}_2$), 5.16 (app. dq, $^{3}J_{H–H}$ = 10.8, $^{4}J_{H–H}$ = 1.9 Hz 1H, $OCH_2CHC\mathbf{H}_2$), 4.47 (ddt, $^{3}J_{H–H}$ = 14.1, $^{4}J_{H–H}$ = 4.0, 2.0 Hz 1H, $OC\mathbf{H}_2CHCH_2$), 4.26 (ddt,

$^{3}J_{H–H}$ = 14.1, $^{4}J_{H–H}$ = 4.1, 2.0Hz 1H, OC**H**$_2$CHCH$_2$), 3.98 (s, 1H, I***H**), 2.53 (s, 3H, I***Me**), 2.24 (s, 3H, I***Me**), 2.21 (s, 3H, I***Me**), 2.18 (s, 3H, I***Me**), 2.14 (s, 3H, I***Me**), 1.86 (s, 3H, I***Me**), 1.53 (s, 9H, C**Me**$_3$), 1.30 (s, 9H, C**Me**$_3$), 0.28 (s, 3H, Si**Me**), 0.17 (s, 3H, Si**Me**) ppm. **^{13}C{^{1}H} NMR** (benzene-d_6, 126 MHz, 298 K): δ 161.70 (1-**C**$_6$H$_2$), 145.45 (2,4-**C**$_6$H$_2$), 142.51 (**I***), 142.29 (**I***), 141.58 (2,4-**C**$_6$H$_2$), 139.74 (**I***), 134.21 (OCH$_2$**C**HCH$_2$), 132.96 (**I***), 132.31 (6-**C**$_6$H$_2$), 132.17 (**I***), 132.03 (3,5-**C**$_6$H$_2$), 129.67 (**I***), 127.45 (**I***), 126.51 (3,5-**C**$_6$H$_2$), 126.12 (**I***), 115.91 (OCH$_2$CH**C**H$_2$), 76.00 (O**C**H$_2$CHCH$_2$), 48.45 (**I***Si), 35.76 (**C**Me$_3$), 34.65 (**C**Me$_3$), 31.69 (C**Me**$_3$), 31.46 (C**Me**$_3$), 19.10 (I***Me**), 16.51 (I***Me**), 16.43 (I***Me**), 16.39 (I***Me**), 15.27 (I***Me**), 15.05 (I***Me**), 0.20 (Si**Me**), −2.32 (Si**Me**) ppm. **^{29}Si NMR** (benzene-d_6): δ –0.72 ppm. Anal. calcd for C$_{34}$H$_{50}$OSi: C, 81.21, H, 10.02. Found: C, 81.20, H, 9.64.

5.3.2. Synthesis of ^{Me2}SB(^{Cumyl2}ArOAllyl,I*)H

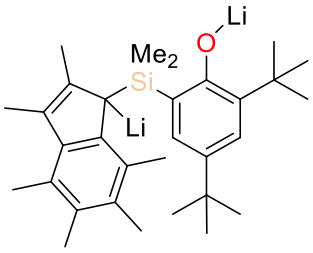


^{1}H NMR (benzene-d_6, 400 MHz, 298 K): δ 7.63 (d, $^{4}J_{H–H}$ = 2.5 Hz, 1H, 3,5-C$_6$**H**$_2$), 7.35−7.28 (m, 5H, CMe$_2$**Ph** and 3,5-C$_6$**H**$_2$), 7.23−6.97 (m, 6H, CMe$_2$Ph**H**), 5.49 (ddt, $^{3}J_{H–H}$ = 17.4 Hz, $^{3}J_{H–H}$ = 10.7 Hz, $^{3}J_{H–2H}$ = 4.4 Hz, 1H, OCH$_2$C**H**CH$_2$), 5.15 (dd, $^{3}J_{H–H}$ = 17.3 Hz, $^{2}J_{H–H}$ = 2.0 Hz, 1H, OCH$_2$CHC**H**$_2$), 4.96 (dd, $^{3}J_{H–H}$ = 10.8 Hz, $^{2}J_{H–H}$ = 1.9 Hz, 1H, OCH$_2$CHC**H**$_2$), 3.83 (I***H**), 3.49 (ddt, $^{2}J_{H–H}$ = 13.2 Hz, $^{3}J_{H–H}$ = 4.2 Hz, $^{4}J_{H–2H}$ = 1.9 Hz, 1H, OC**H**$_2$CHCH$_2$), 3.26 (ddt, $^{2}J_{H–H}$ = 13.2 Hz, $^{3}J_{H–H}$ = 4.1 Hz, $^{4}J_{H–2H}$ = 1.9 Hz, 1H, OC**H**$_2$CHCH$_2$), {2.50 (3H) 2.21 (3H) 2.17 (6H) 2.04 (3H) 1.78 (3H) 1.75 (3H) 1.71 (3H) 1.70 (3H) 1.67 (3H) (s, I***Me** and C**Me**$_2$Ph)}, 0.14 (s, 3H, Si**Me**), and 0.02 (s, 3H, Si**Me**) ppm.

^{13}C{^{1}H} NMR (benzene-d_6, 126 MHz, 298 K): δ 161.12 (O**Ar**), 151.80 (CMe$_2$**Ph**), 151.05 (CMe$_2$**Ph**), 145.28 (Ar), 142.45 (**I***), 142.17 (**I***), 142.04 (**Ar**), 139.57 (**I***),

134.97 ($OCH_2\mathbf{C}HCH_2$), 134.34 (O**Ar**), 132.93 (**I***), 132.78 (**I***), 132.10 (**I***), 129.61 (**I***), 128.38 (CMe_2**Ph**), 128.35 (CMe_2**Ph**), 128.16 (**Ar**), 128.12 (**Ar**), 127.97 (O**Ar**), 127.35 (Ar), 127.17 (Ar), 126.62 (Ar), 126.07 (I*), 126.04 (CMe_2**Ph**), 125.62 (CMe_2**Ph**), 114.95 ($OCH_2CH\mathbf{C}H_2$), 74.34 ($O\mathbf{C}H_2CHCH_2$), 48.41 (**I***Si), 43.11 (**C**Me_2Ph), 42.85 (**C**Me_2Ph), 31.15 (C**Me**$_2$Ph), 31.08 (C**Me**$_2$Ph), 30.88 (C**Me**$_2$Ph), 30.59 (C**Me**$_2$Ph), 19.11 (I***Me**), 16.54 (I***Me**), 16.39 (I***Me**), 16.36 (I***Me**), 15.25 (I***Me**), 15.08 (I***Me**), –0.39 (Si**Me**), –2.29 (Si**Me**) ppm.

5.3.3. Synthesis of ^{Me_2}SB(^{t}Bu$_2$ArOAllyl,I*)Li$_2$.(NEt$_3$)$_x$



The proligand was dissolved in toluene. 3.5 eq. of Et_3N were added and the mixture cooled to –78 °C. 2.25 eq. of ^{n}BuLi solution (1.6 M in hexanes) was added dropwise. The reaction was allowed to warm to room temperature and stirred for 3–18 h, during which the solution gradually darkens. Removal of the volatiles under vacuum yielded the ligands as dilithium salts, ^{RaRb}SB(^{t}Bu$_2$ArOAllyl,I*)Li$_2$, as a bright orange powder in approximately quantitative yield.

^{1}H NMR (pyridine-d_5, 600 MHz, 298 K): δ 7.88 (d, $^{4}J_{H–H}$ = 2.78 Hz, 1H, Ar**H**), 7.60 (d, $^{4}J_{H–H}$ = 2.8 Hz, 1H, Ar**H**), 2.95 (s, 3H, I***Me**), 2.86 (s, 3H, I***Me**), 2.84 (s, 3H, I***Me**), 2.67 (s, 3H, I***Me**), 2.48 (s, 3H, I***Me**), 2.31 (s, 3H, I***Me**), 1.86 (s, 9H, C**Me**$_3$), 1.56 (s, 9H, C**Me**$_3$), 1.03 (s, 6H, Si**Me**) ppm. Resoance recorded at δ 2.43 (q, $^{3}J_{H–H}$ = 6.5 Hz, 6H, $NC\mathbf{H}_2CH_3$), 0.98 (t, $^{3}J_{H–H}$ = 6.5 Hz, 9H, $NCH_2C\mathbf{H}_3$) ppm correspond to NEt_3 adduct.

^{13}C{^{1}H} NMR (pyridine-d_5, 151 MHz, 298 K): δ 162.90 (1-$\mathbf{C}_6H_2$), 136.20 (2,4-$\mathbf{C}_6H_2$), 136.07 (**I***), 135.75 (**I***), 134.44 (2,4-$\mathbf{C}_6H_2$), 129.45 (**I***), 128.92 (**I***), 126.02 (6-$\mathbf{C}_6H_2$), 124.67 (**I***), 124.11 (3,5-$\mathbf{C}_6H_2$), 123.47 (**I***), 122.38 (**I***), 119.97 (3,5-$\mathbf{C}_6H_2$), 119.45 (**I***),

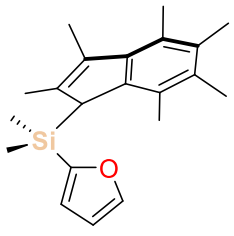
105.62 (**I***Si), 36.03 (**C**Me$_3$), 34.62 (**C**Me$_3$), 33.26 (C**Me**$_3$), 30.85 (C**Me**$_3$), 22.85 (I***Me**), 18.25 (I***Me**), 17.87 (I***Me**), 17.60 (I***Me**), 16.96 (I***Me**), 16.29 (I***Me**), 6.50 (Si**Me**) ppm. δ 46.90 (, N**C**H$_2$CH$_3$) and 12.60 (, NCH$_2$**C**H$_3$) ppm correspond to NEt$_3$.

5.3.3.1. Synthesis of rearrangement product benzofuran D

Obtained as final product from one-pot synthesis attempt of ^{Me2}SB(^{t}Bu$_2$ArOAllyl,I*)H. Temperature for the previous step was too close to 0 °C and rearrangement was possible. Obtained as off-white solid in 0.67 g (60 %) Yield.

^{1}H NMR (chloroform-*d*$_1$, 400 MHz, 298 K) δ 6.95 (d, $^4J_{H–H}$ = 2.0 Hz, 1H , Ar**H**), 6.78 (d, $^4J_{H–H}$ = 2.0 Hz, 1H, Ar**H**), 4.38 (dt, $^3J_{H–H}$ = 12.2, $^4J_{H–H}$ = 8.7 Hz 1H, OC**H$_a$**H$_b$C(Ar)HCH$_2$Si), 3.71(dt, $^2J_{H–H}$ = 19.2 $^3J_{H–H}$ = 8.5, 1H, OCH$_a$**H$_b$**C(Ar)HCH$_2$Si), 3.31 (m, 1H, I***H**), 3.21-3.15 (m, 1H, OCH$_a$H$_b$C(Ar)**H**CH$_2$Si), 2.41 (s, 3H, I*), 2.15 (s, 3H, I***Me**), 2.12 (s, 3H I***Me**), 2.12 (s, 3H, I***Me**), 2.10 (s, 3H, I***Me**), 1.95 (s, 3H, I***Me**), 1.21 (s, 9H, C**Me**$_3$), 1.18 (s, 9H, C**Me$_3$**), 0.95 (dd, *J* = 15.0, 3.4 Hz, 1H OCH$_a$H$_b$C(Ar)HC**H$_2$**Si), 0.76 (t, $^3J_{H–H}$ = 6.7 Hz, 2H), 0.53 (dd, $^3J_{H–H}$ = 15.0, 11.0 Hz, 1H, OCH$_a$H$_b$C(Ar)HC**H$_2$**Si), -0.00 (s, 3H, Si**Me**) and (s, 3H, Si**Me**) ppm.

5.3.4. Synthesis of ^{Me2}SB(Furan,I*)H



To a THF solution (40 mL) of I$^{\#}$SiMe$_2$Cl (2.180 g, 7.18 mmol), furan-2-yl lithium (1 eq., 0.531 g, 7.18 mmol) was added dropwise at 0 °C. The reaction mixture was allowed to warm to 25 °C and stirred for 18 h and darkened to an orange-brown solution. Volatiles were removed *in vacuo*, followed by extraction with *n*-pentane (4 x 10 mL) to yield a yellow solution. The resulting yellow solution was dried *in vacuo* and washed with *n*-pentane (3 x 20 mL) to afford ^{Me2}SB(Furan,I*)H as a pale yellow waxy solid in 87% yield

(6.00 mmol, 1.950 g). **^{1}H NMR** (benzene-d_6, 400 MHz, 298 K): δ 7.43 (d, $^3J_{H\text{-}H}$ = 1.6 Hz, 1H, $C_4\mathbf{H}_3O$), 6.39 (d, $^3J_{H\text{-}H}$ = 3.2 Hz, 1H, $C_4\mathbf{H}_3O$), 6.17 (dd, $^3J_{H\text{-}H}$ = 1.6, 3.2 Hz, 1H, 3-$C_4\mathbf{H}_3O$), 3.62 (s, 1H, I*__H__), 2.50 (s, 3H, I*__Me__), 2.22 (s, 3H, I*__Me__), 2.18 (s, 3H, I*__Me)__ , 2.18 (s, 3H, I*__Me)__, 2.17 (s, 3H, I*__Me__), 2.01 (s, 3H, I*__Me)__, 1.86 (s, 3H, I*__Me)__, 0.08 (s, 3H, Si__Me__), and 0.06 (s, 3H, Si__Me__) ppm.

^{13}C{^{1}H} NMR (benzene-d_6, 126 MHz, 298 K): δ 159.21 (1-$\mathbf{C}_4H_3O$), 146.71 (x-$\mathbf{C}_4H_3O$), 141.93 (**I***), 141.53 (**I***), 138.87 (**I***), 133.16 (**I***), 132.27 (**I***), 129.86 (**I***), 127.44 (**I***), 126.17 (**I***), 120.87 (y-$\mathbf{C}_4H_3O$), 110.02 (3-$\mathbf{C}_4H_3O$), 47.55 (I*Si), 22.05 (I*__Me__), 16.42 (I*__Me__), 16.37 (I*__Me__), 16.36 (I*__Me__), 15.26 (I*__Me__), and 14.88 (I*__Me__), -2.96 (Si__Me__), and -4.39 (Si__Me__) ppm. Anal. Calcd for $C_{21}H_{30}SiO$: C, 77.72; H, 8.70. Found: C, 75.98; H, 7.90.

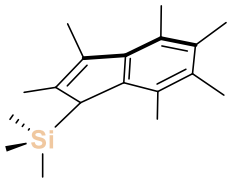
5.3.5. Synthesis of ^{Me2}SB(Furan,I*)Li

To an Et_2O solution (30 mL) of ^{Me2}SB(Furan,I*)H (5.650 g, 17.4 mmol), ^{n}BuLi (1.6 M, 1.10 eq., 12.00 mL, 19.1 mmol) was added dropwise at −78 °C. The reaction mixture was allowed to warm to 0 °C and stirred for 18 h. A light-yellow precipitate formed, mixture filtered and solid was washed with cold (−78 °C) n-hexanes (3 x 10 mL). Volatiles were removed *in vacuo* to afford ^{Me2}SB(Furan,I*)Li an off-white powder in 12% yield (0.674 g, 2.04 mmol,). **^{1}H NMR** (pyridine-d_5, 400 MHz, 298 K): δ 7.43 (d, $^3J_{H\text{-}H}$ = 1.6 Hz, 1H, $C_4\mathbf{H}_3O$), 6.39 (d, $^3J_{H\text{-}H}$ = 3.2 Hz, 1H, $C_4\mathbf{H}_3O$), 6.17 (dd, $^3J_{H\text{-}H}$ = 1.6, 3.2 Hz, 1H, 3-$C_4\mathbf{H}_3O$), 3.62 (s, 1H, I*__H__), 2.50 2.22 2.18 2.17 2.01 1.86 (s, 3H each, I*__Me__), 0.08 0.06 (s, 3H each, Si__Me__) ppm.

^{13}C{^{1}H} NMR (benzene-d_6, 126 MHz, 298 K): δ 159.21 (1-$\mathbf{C}_4H_3O$), 146.71 (x-$\mathbf{C}_4H_3O$), 141.93 (**I***), 141.53 (**I***), 138.87 (**I***), 133.16 (**I***), 132.27 (**I***), 129.86 (**I***), 127.44 (**I***),

126.17 (**I***), 120.87 (y-**C**$_4$H$_3$O), 110.02 (3-**C**$_4$H$_3$O), 47.55 (I*Si), 22.05 (I***Me**), 16.42 (I***Me**), 16.37 (I***Me**), 16.36 (I***Me**), 15.26 (I***Me**), and 14.88 (I***Me**), -2.96 (Si**Me**), and -4.39 (Si**Me**) ppm.

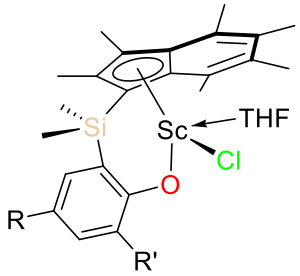
5.3.6. Synthesis of I$^{\#}$SiMe$_3$



To a THF solution (40 mL) of I$^{\#}$Li (4.400 g, 21.3 mmol), TMSCl (1 eq., 2.90 ml, 21.3 mmol) was added dropwise at 0 °C. The reaction mixture was allowed to warm to 25 °C and the resulting light-brown solution stirred for 18 h. Volatiles were removed *in vacuo* and product extracted with *n*-pentane (3 x 10 mL). The resulting light brown solution was dried *in vacuo* and washed with cold (0 °C) pentane (3 x 5 mL) to afford I$^{\#}$SiMe$_3$ as a pale-yellow solid in 12% yield (0.70 g, 2.57 mmol). **^{1}H NMR** (benzene-d_6, 400 MHz, 298 K): δ 3.25 (s, 1H, I***H**), 2.51 (s, 3H, I***Me**), 2.25 (s, 3H, I***Me**), 2.20 (s, 3H, I***Me)**, 2.19 (s, 3H, I***Me)**, 2.18 (s, 3H, I***Me**), 1.95 (s, 3H, I***Me)**, -0.10 (s, 9H, Si**Me**) ppm.

5.3.7. Synthesis of ^{Me2}SB($^{R,R'}$ArO,I*)Sc(Cl)THF R = R′ = ^{t}Bu (1) and Cumyl (2); R = ^{t}Bu, R′ = Me (3)

General procedure



(1) R=R'=^{t}Bu,
(2) R=R'=Cumyl,
(3) R=^{t}Bu R'=Me

To a toluene solution (30 mL) of the respective proligand ^{Me2}SB($^{R,R'}$ArOAllyl,I*)H and triethylamine (4 eq) cooled to −78 °C, a solution of ^{n}BuLi (1.6 M in hexanes, 2.2 eq.) was added dropwise. The reaction mixture was allowed to warm to 23 °C and stirred for 5 h. $ScCl_3$.3THF (1 eq.) as a slurry in toluene (20 mL) was added to the reaction mixture at 0 °C. The resulting mixture was stirred for 18 h and formed a yellow suspension. Volatiles were removed *in vacuo* and product extracted with benzene (4 x 10 mL). The resulting yellow solution was dried *in vacuo* and washed with cold pentane (3 x 10 mL) to afford ^{Me2}SB($^{R,R'}$ArO,I*)Sc(Cl)THF (**1–3**) as an off-white powder. Crystals suitable for X-ray crystallography were grown from cold hexanes (−30 °C) of **1** and **2**.

R = R′ = ^{t}Bu (**1**) (0.600 g, 30%)

^{Me2}SB($^{R,R'}$ArOAllyl,I*)H: (1.500 g, 3.26 mmol), triethylamine (4 eq., 1.3 mL, 13.0 mmol), ^{n}BuLi (1.6 M in hexanes, 2.2 eq., 4.6 mL, 7.23 mmol).

^{1}H NMR (benzene-d_6, 400 MHz, 298 K): δ 7.74 7.65 (s, 1H each, 3,5-C_6**H**$_2$), 3.27–3.11 (m, 4H, 2,5-C_4**H**$_8$O), 2.85 2.71 2.42 2.15 2.11 2.02 (s, 3H each, I***Me**), 1.67 (s, 9H, 2-C**Me**$_3$), 1.47 (s, 9H, 4-C**Me**$_3$), 1.11–1.01 (s, 3H, Si**Me**), 0.92 (m, 4H, 3,4-C_4**H**$_8$O), and 0.58 (s, 3H, Si**Me**) ppm. **^{13}C{^{1}H} NMR** (benzene-d_6, 126 MHz, 298 K): δ 164.12 (1-**C**$_6$H$_2$), 142.92 (2,4-**C**$_6$H$_2$), 141.95 (**I***), 136.00 (2,4-**C**$_6$H$_2$), 135.15 (**I***), 131.39 (6-**C**$_6$H$_2$), 130.95 (**I***), 130.51 (**I***), 130.09 (**I***), 128.85 (**I***), 128.56 (**I***), 128.16 (**I***), 127.52 (3,5-

C$_6$H$_2$), 125.16 (3,5-**C**$_6$H$_2$), 99.88 (**I***Si), 72.41 (2,5-**C**$_4$H$_8$O), 35.35, and 34.72 (**C**Me$_3$), 32.21, and 30.45 (C**Me**$_3$), 24.73 (3,4-**C**$_4$H$_8$O) 22.05, 17.37, 16.90, 16.25, 15.41, and 14.92 (I***Me**), 4.57, and 1.39 (Si**Me**) ppm. **^{45}Sc NMR** (121.5 MHz, benzene-d_6, 298 K): δ 140.81 ppm. Anal. Calcd for $C_{35}H_{52}ClO_2SiSc$: C, 68.55; H, 8.55. Found C, 66.34; H 8.55

5.3.8. Synthesis of ^{Me2}SB(^{Cumyl2}ArO,I*)Sc(Cl)THF (2)

<u>R = R′ = Cumyl</u> (**2**) (0.482 g, 41%)

^{Me2}SB(^{Cumyl2}ArOAllyl,I*)H (.00 g, 1.60 mmol), triethylamine (4 eq., 0.9 mL, 6.39 mmol), ^{n}BuLi (1.6 M in hexanes, 2.25 eq., 2.25 mL, 3.60 mmol). $ScCl_3$.3THF (1 eq., 0.5880 g, 1.60 mmol).

^{1}H NMR (benzene-d_6, 500 MHz, 298 K): δ 7.64 (broad s, 2H, 3,5-C$_6$**H**$_2$), 7.48–7.41 (m, 4H, CMe$_2$**Ph**), 7.29–7.20 (m, 2H, CMe$_2$**Ph**), 7.12–7.08 (m, 1H, CMe$_2$**Ph**), 7.00–6.95 (m, 2H, CMe$_2$**Ph**), 6.78–6.73 (m, 1H, CMe$_2$**Ph**), 2.85 (s, 3H, I***Me**), 2.72-2.71 (overlapping s, 5H, I***Me** and 2,5-C$_4$**H**$_8$O), 2.51 (broad s, 2H, 2,5-C$_4$**H**$_8$O) 2.34 (s, 3H, I***Me**), 2.09 (overlapping s, 6H, I***Me**, I***Me**), 2.03 (s, 3H, C**Me**$_2$Ph), 1.99 (s, 3H, I***Me**), 1.85 (overlapping s, 6H, C**Me**$_2$Ph), 1.51 (s, 3H, C**Me**$_2$Ph), 0.90 (broad s, 4H, 3,4-C$_4$**H**$_8$O), 0.87 (s, 3H, Si**Me**), and 0.39 (s, 3H, Si**Me**) ppm. **^{13}C{^{1}H} NMR** (benzene-d_6, 126 MHz, 298 K): δ 163.40 (1-**C**$_6$H$_2$), 153.45, and 152.24 (1-**C**$_6$H$_5$), 142.54, and 141.43 (2,4-**C**$_6$H$_5$), 131.37 (**I***), 130.32 (**I***), 135.04 (3,5-**C**$_6$H$_2$), 130.02 (**I***), 128.95 (**I***), 128.73 (**I***), 128.56 (**I***), 128.37 (CMe$_2$**Ph**), 128.30 (CMe$_2$**Ph**), 127.76 (CMe$_2$**Ph**), 127.53 (**I***), 127.32 (CMe$_2$**Ph**),127.22 (3,5-**C**$_6$H$_2$), 127.07 (**I***), 126.47 (CMe$_2$**Ph**), 125.82 (CMe$_2$**Ph**), 124.22 (CMe$_2$**Ph**), 99.37 (**I***Si), 71.62 (2,5-**C**$_4$H$_8$O) 43.34, and 42.92 (**C**Me$_2$Ph), 33.78, 31.68, 31.60, and 26.40 (C**Me**$_2$Ph), 25.00 (3,4-**C**$_4$H$_8$O). 21.47, 16.90, 16.55, 15.85, 15.14, and 14.44 (I***Me**), 4.24, and 0.02 (Si**Me**) ppm. Additional unassigned carbon peaks at δ

71.62, 34.40, 22.70, 17.35 ppm. Anal. Calcd. for $C_{45}H_{55}ClO_2SiSc$: C, 73.90; H, 7.53. Found C, 72.45; H, 7.46.

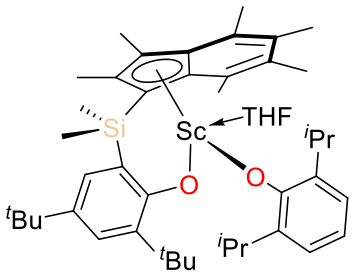
5.3.9. Synthesis of ^{Me2}SB($^{t\text{Bu, Me}}$ArO,I*)Sc(Cl)THF (3)

R = ^{t}Bu, R′ = Me (**3**) (0.083 g, 6%)

^{Me2}SB($^{t\text{Bu,Me}}$ArOAllyl,I*)H (1.000 g, 2.170 mmol)), triethylamine (4 eq., 0.878 mL, 8.68 mmol), ^{n}BuLi (1.6 M in hexanes, 2.25 eq., 3.05 mL, 4.81 mmol). $ScCl_3$.3THF (1 eq., 0.5880 g, 1.60 mmol).

^{1}H NMR (400 MHz, benzene-d_6, 298 K): δ 7.43 (d, $^4J_{H–H}$ = 2.3 Hz, 1H, 3,5-C_6**H**$_2$), 7.31 (d, $^4J_{H–H}$ = 2.3 Hz, 1H, 3,5-C_6**H**$_2$),), 3.27–3.23 (broad s, 4H, 2,5-C_4**H**$_8$O), 2.85 (s, 3H, I***Me**), 2.71 (s, 3H, I***Me**), 2.40 (s, 3H, I***Me**), 2.14 (s, 3H, I***Me**), 2.11 (s, 3H, I***Me)** , 2.02 (s, 3H, I***Me)**, 1.59 (s, 9H, C**Me**$_3$), (s, 3H, 4-C_6H_2-**Me**), 0.92 (s, 3H, Si**Me**), 0.56 (m, 4H, 3,4-C_4**H**$_8$O), and 0.58 (s, 3H, Si**Me**) ppm. **^{13}C{^{1}H} NMR** (126 MHz, benzene-d_6, 298 K): δ 164.12 (1-**C**$_6H_2$), 142.92 (2,4-**C**$_6H_2$), 141.95 (**I***), 136.00 (2,4-**C**$_6H_2$), 135.15 (**I***), 131.39 (6-**C**$_6H_2$), 130.95 (**I***), 130.51 (**I***), 130.09 (**I***), 128.85 (**I***), 128.56 (**I***), 128.16 (**I***), 127.52 (3,5-**C**$_6H_2$), 125.16 (3,5-**C**$_6H_2$), 99.88 (**I***Si), 72.41 (2,5-**C**$_4H_8$O), 35.35, and 34.72 (**C**Me$_3$), 32.21, and 30.45 (C**Me**$_3$), 24.73 (3,4-**C**$_4H_8$O) 22.05, 17.37, 16.90, 16.25, 15.41, and 14.92 (I***Me**), 4.57, and 1.39 (Si**Me**) ppm. Anal. Calcd for $C_{35}H_{52}ClO_2SiSc$: C, 68.55; H, 8.55. Found C, 66.34; H 8.55

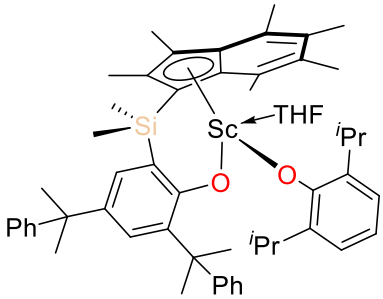
5.3.10. Synthesis of ^{Me2}SB(^{tBu2}ArO,I*)Sc(ODipp)THF (5)



5

To a benzene solution (20 mL) of the complex ^{Me2}SB(^{tBu2}ArO,I*)Sc(Cl)THF (**1**) (0.600 g, 0.978 mmol), KODipp 1.05 eq., 0.222 g, 0.103 mmol) was added. The cloudy yellow reaction mixture was allowed to stir for 1.5 h at 23 ℃. The insoluble materials were removed by filtration and the volatiles were removed *in vacuo*. The resulting off-white solid was washed with pentane (3 x 10 mL) to afford ^{Me2}SB(^{tBu2}ArO,I*)Sc(ODipp)THF (**5**) as a white powder in 56% yield (0.543 mmol, 0.41 g). **^{1}H NMR** (400 MHz, benzene-d_6, 298 K): δ 7.68 (d, $^{4}J_{H–H}$ = 2.4 Hz, 1H, 3,5-C$_6$**H**$_2$), 7.55 (d, $^{4}J_{H–H}$ = 2.4 Hz, 1H, 3,5-C$_6$**H**$_2$), 7.15 (d, $^{3}J_{H–H}$ = 7.6 Hz, 2H, 3,5-C$_6$**H**$_3$), 6.94 (t, $^{3}J_{H–H}$ = 7.6 Hz, 1H, 4-C$_6$**H**$_3$), 3.68 (m, $^{3}J_{H–H}$ = 6.9 Hz, 2H, C**H**Me$_2$), 3.41–3.26 (m, 4H, 2,5-C$_4$**H**$_8$O), 2.65 (s, 3H, I***Me**), 2.49 (s, 3H, I***Me**), 2.45 (s, 3H, I***Me**), 2.18 (s, 3H, I***Me**), 2.03 (s, 3H, I***Me**), 1.95 (s, 3H, I***Me**), 1.47 (s, 9H, C**Me**$_3$), 1.40 (s, 9H, C**Me**$_3$), 1.29 (d, $^{3}J_{H–H}$ = 6.8 Hz, 6H, CH**Me**$_2$), 1.16 (d, $^{3}J_{H–H}$ = 6.8 Hz, 6H, CH**Me**$_2$), 1.11–0.98 (m, 4H, 3,4-C$_4$**H**$_8$O), 0.94 (s, 3H, Si**Me**), and 0.85 (s, 3H, Si**Me**) ppm. **^{13}C{^{1}H} NMR** (126 MHz, benzene-d_6, 298 K): δ 166.13 (1-**C**$_6$H$_2$), 157.24 (1-**C$_6$**H$_3$), 140.29 (2,4-**C**$_6$H$_2$), 140.19 (**I***), 137.45 (2,4-**C**$_6$H$_2$), 136.39 (**I***), 134.01 (2,4-**C**$_6$H$_2$), 131.94 (6-**C**$_6$H$_2$), 130.42 (**I***), 129.43 (**I***), 129.00 (**I***), 128.85 (**I***), 128.69 (**I***), 128.35 (3,5-**C**$_6$H$_2$), 125.53 (**I***), 124.36 (3,5-**C**$_6$H$_2$), 123.50 (3,5-C$_6$**H**$_3$), 119.28 (4-C$_6$**H**$_3$), 100.25 (**I***Si), 72.20 (2,5-**C**$_4$H$_8$O), 35.29, and 34.53 (**C**Me$_3$), 32.21, and 30.54 (C**Me**$_3$), 25.99, and 24.99 (**C**HMe$_2$), 24.26 (3,4-**C**$_4$H$_8$O) 24.95, and 24.86 (CH**Me**$_2$) 21.94, 17.62, 17.02, 16.32, 16.16, and 15.26, (I***Me**), 5.18, and 3.50 (Si**Me**) ppm. **^{45}Sc{^{1}H} NMR** (121.5 MHz, benzene-d_6, 298 K): δ 52 ppm. Anal. Calcd for $C_{47}H_{69}O_3ScSi$: C, 74.76; H 9.12.Found, C, 73.08; H 8.50.

5.3.11. Synthesis of ^{Me_2}SB(^{Cumyl_2}ArO,I*)Sc(ODipp)THF (6)



6

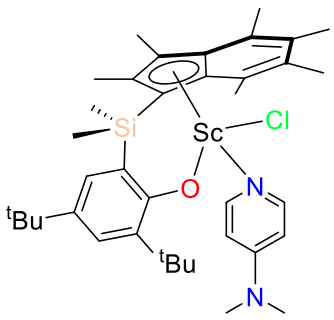
To an benzene solution (20 mL) of the complex ^{Me_2}SB(^{Cumyl_2}ArO,I*)Sc(Cl)THF (0.250 g, 0.036 mmol), potassium(2,6-diisopropyl)phenoxide (1.05 eq., 0.082 g, 0.038 mmol) was added. The off-white reaction mixture was allowed to stir for 1.5 h at 23 °C. The insoluble materials were removed by filtration and the volatiles were removed *in vacuo*. The resulting white solid was washed with pentane (3 x 10 mL) to afford ^{Me_2}SB(^{Cumyl_2}Ar,I*)Sc(ODipp)THF as an off-white solid in 26% yield (0.0094 mmol, 0.066 g). **^{1}H NMR** (benzene-d_6, 500 MHz, 298 K): δ 7.65 (d, $^4J_{H–H}$ = 2.6 Hz 1H, 3,5-C_6**H**$_2$), 7.46 (d, $^4J_{H–H}$ = 2.6 Hz 1H, 3,5-C_6**H**$_2$), 7.44–7.41 (overlapping m, 2H, CMe_2**Ph**), 7.25–7.17 (overlapping m, 6H, CMe_2**Ph** and 3,5-C_6**H**$_3$), 7.11–7.06 (m, 1H, CMe_2**Ph**), 6.99 (t, $^3J_{H–H}$ = 7.5 Hz, 1H, 4-C_6**H**$_3$), 7.95–6.88 (m, 2H, CMe_2**Ph**), 6.80–6.73 (m, 1H, CMe_2**Ph**), 3.29 (hept, $^3J_{H–H}$ = 6.8 Hz, 2H, C**H**Me_2), 2.73–2.66 (m, 4H, 2,5-C_4**H**$_8$O), 2.48 (s, 3H, I***Me**), 2.39 (s, 3H, I***Me**), 2.36 (s, 3H, I***Me**), 2.34 (s, 3H, I***Me**), 2.06 (s, 3H, I***Me**), 2.03 (s, 3H, I***Me**), 1.93 (s, 3H, C**Me**$_2$Ph), 1.81 (overlapping s, 6H, C**Me**$_2$Ph), 1.54 (s, 3H, C**Me**$_2$Ph), 1.26 (d, $^3J_{H–H}$ = 6.8 Hz, 6H, CH**Me**$_2$), 1.19 (d, $^3J_{H–H}$ = 6.8 Hz, 6H, CH**Me**$_2$), 0.98–0.89 (m, 4H, 3,4-C_4**H**$_8$O), 0.87 (s, 3H, Si**Me**), and 0.63 (s, 3H, Si**Me**) ppm. **^{13}C{^{1}H} NMR** (benzene-d_6, 126 MHz, 298 K): δ 164.91 (1-**C**$_6$H$_2$), 157.97 (1-**C**$_6$H$_3$), 153.37 and 152.29 (2,4-**C**$_6$H$_2$), 140.03 (CMe_2**Ph**), 139.81(**I***), 136.87 (2,6-**C**$_6$H$_3$), 135.76 (**I***), 133.89 (CMe_2**Ph**), 132.01 (6-**C**$_6$H$_5$), 130.78 (3,5-**C**$_6$H$_2$), 129.68 (**I***), 129.23 (**I***), 128.50 (**I***), 128.35 (CMe_2**Ph**), 128.27 (3,5-**C**$_6$H$_2$), 127.97 (**I***), 127.89 (CMe_2**Ph**), 127.31 (CMe_2**Ph**), 126.81 (**I***), 126.66 (CMe_2**Ph**), 125.71 (CMe_2**Ph**), 124.69 (CMe_2**Ph**), 123.28 (3,5-**C**$_6$H$_3$), 118.86 (4-**C**$_6$H$_3$), 98.21 (**I***Si), 71.28 (2,5-**C**$_4$H$_8$O) 42.72, and 42.63 (**C**Me_2Ph), 34.28, 31.13 and 27.57 (C**Me**$_2$Ph), 26.13 (**C**HMe_2), 24.81 (3,4-**C**$_4$H$_8$O), 24.67

and 24.50 (CH**Me**$_2$), 21.77, 17.06, 16.65, 15.96, 14.81, and 14.70 (I***Me**), 4.48, and 2.89 (Si**Me**) ppm. Unassigned peaks at δ 34.08, 22.37, 13.92 ppm.

5.3.12. General synthesis of DMAP (8–10) and $OPPh_3$ (11–13) adducts

To an Youngs tap NMR tube containing the respective scandium complexes **1**, **5**, and **7,** (0.006 mmol) dissolved in 0.6 mL of benzene-d_6 or toluene-d_8, 1 eq. of DMAP or $OPPh_3$ was added. ^{1}H NMR spectroscopy was used to monitor the reactions. In all cases, the off-white (**5** and **7**) or yellow (**1**) solutions became slightly lighter in colour. Conversion >99% was observed for all **8–13** *via* ^{1}H NMR spectroscopy and isolated as off-white microcrystalline solids in 61–83 % yields as stated.

5.3.13. Synthesis of ^{Me2}SB(^{tBu2}ArO,I*)Sc(Cl)DMAP (8)

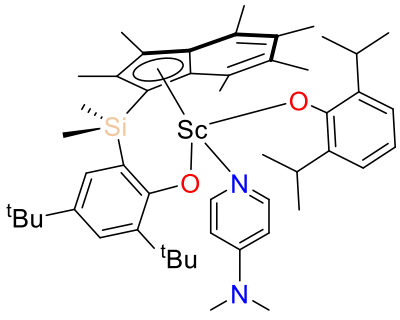


8

85% spectroscopic yield.

^{1}H NMR (benzene-d_6, 600 MHz, 298 K):δ 7.79 (d, $^{4}J_{H\text{-}H}$ = 2.6 Hz, 1H, 5-C$_6$**H**$_2$), 7.66 (d, $^{4}J_{H\text{-}H}$ = 2.5 Hz, 1H, 3-C$_6$**H**$_2$), 7.38 – 7.34 (m, 2H, 2,6-NC$_6$**H**$_4$), 5.47 – 5.42 (m, 2H, 3,5-NC$_6$**H**$_4$), 2.91 (s, 3H, I***Me**), 2.71 (s, 3H, I***Me**), 2.49 (s, 3H, I***Me**), 2.42 (s, 3H, I***Me**), 2.01 (d, *J* = 1.6 Hz, 3H), 1.94 (s, 3H), 1.86 (s, 6H, N**Me**$_2$), 1.66 (s, 9H, C**Me**$_3$), 1.50 (s, 9H,C**Me**$_3$), 0.98 (s, 3H, Si**Me**), and 0.83 (s, 3H, Si**Me**) ppm. Multiplets at δ 3.59 (8H) and correspond to free THF. **^{13}C{^{1}H} NMR** (benzene-d_6, 151 MHz, 298K):δ 164.53 (1-**C**$_6$H$_2$), 154.86 (4-N**C**$_6$H$_4$), 148.02 (2,6-N**C**$_6$H$_4$), 141.58 (**I***), 141.37 (2,4-**C**$_6$H$_2$), 135.33 (2,4-**C**$_6$H$_2$), 135.29 (**I***), 132.26 (6-**C**$_6$H$_2$), 130.38 (**I***), 129.04 (**I***), 128.68 (**I***), 128.59 (**I***), 128.35 (**I***), 128.14 (**I***), 127.98 (3,5-**C**$_6$H$_2$), 124.96 (3,5-**C**$_6$H$_2$), 119.08(4-**C**$_6$H$_3$), 105.00 (3,5-N**C**$_6$H$_4$), 99.99 (**I***Si), 38.02 (N**Me**$_2$**)**, 35.48 and 34.72 (**C**Me$_3$) 32.27 and 30.62 (C**Me**$_3$), 21.90, 17.47, 16.94, 16.31, 15.68, (I***Me**), 5.18, and 3.75 (Si**Me**) ppm. Peaks at δ 67.93 and 25.77 correspond to free THF. **^{45}Sc NMR** (121.5 MHz, benzene-d_6, 298 K):δ 148.23 ppm.

5.3.14. Synthesis of ^{Me2}SB(^{tBu2}ArO,I*)Sc(ODipp)DMAP (9)



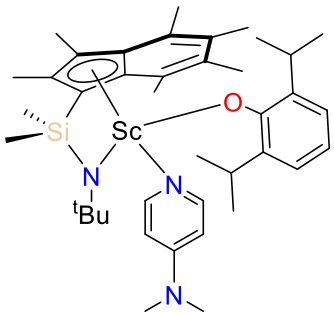
9

(25.0 mg, 61%); fine white microcrystalline powder.

^{1}H NMR (benzene-d_6, 400 MHz, 298 K): δ 7.76 (d, $^{4}J_{H–H}$ = 2.6 Hz, 1H, 3,5-C$_6$**H**$_2$), 7.58 (d, $^{4}J_{H–H}$ = 2.6 Hz, 1H, 3,5-C$_6$**H**$_2$), 7.39 (dd, $^{3}J_{H–H}$ = 5.7, $^{4}J_{H–H}$ = 1.6 Hz, 2H, 2,6-NC$_6$**H**$_4$), 7.23 (d, $^{3}J_{H–H}$ = 7.6Hz, 2H, 3,5-C$_6$**H**$_3$), 6.99 (t, $^{3}J_{H–H}$ = 7.6 Hz, 1H, 4-C$_6$**H**$_3$), 5.63 (dd, $^{3}J_{H–H}$ = 5.6, $^{4}J_{H–H}$ = 1.5 Hz, 2H, 3,5-

$NC_6\mathbf{H}_4$), 3.87 (hept, $^3J_{H–H}$ = 6.8 Hz, 2H, C**H**Me$_2$), 3.32 (broad s, 1H, C**H**Me$_2$), 2.68 (s, 3H, I***Me**), 2.59 (s, 3H, I***Me**), 2.37 (s, 3H, I***Me**), 2.33 (s, 3H, I***Me**), 2.09 (s, 3H, I***Me**), 2.01 (s, 3H, I***Me**), 1.88 (s, 6H, N**Me**$_2$), 1.49 (s, 9H, C**Me**$_3$),), 1.40 (s, 9H, C**Me**$_3$) 1.37 (d, $^3J_{H–H}$ = 6.8 Hz, 6H, CH**Me**$_2$) 1.08 (s, 9H, NC**Me**$_3$), 1.27 (d, $^3J_{H–H}$ = 6.8 Hz, 6H, CH**Me**$_2$), 1.00 (s, 3H Si**Me**), 0.97 (s, 3H, Si**Me**) ppm. δ 3.58 and 1.44–1.42 ppm corresponds to free THF. **^{13}C{^{1}H} NMR** (benzene-d_6, 101 MHz, 298 K): δ 166.03 (1-**C**$_6$H$_2$), 157.94 (1-**C**$_6$H$_3$) ,154.88 (4-N**C**$_6$H$_4$), 148.36 (2,6-N**C**$_6$H$_4$), 139.99 (2,4-**C**$_6$H$_2$), 139.52 (**I***), 137.51 (2,6-**C**$_6$H$_3$), 135.96 (**I***), 134.64 (2,4-**C**$_6$H$_2$), 132.21 (6-**C**$_6$H$_2$), 130.07 (**I***), 129.49 (**I***), 128.59 (**I***), 128.18 (**I***), 127.94, (3,5-**C**$_6$H$_2$), 126.68 (**I***), 124.53 (3,5-**C**$_6$H$_2$), 123.47 (3,5-C$_6$**H**$_3$), 118.86 (4-**C**$_6$H$_3$), 115.62 (**I***), 105.11 (3,5-N**C**$_6$H$_4$), 99.47 (**I***Si), 38.06 (NMe$_2$**)**, 35.22, and 34.58 (**C**Me$_3$), 32.30, and 30.84 (C**Me**$_3$), 26.33 (**C**HMe$_2$), 24.95 (CH**Me**$_2$), 24.91 (CH**Me**$_2$), 21.83, 17.29, 17.10, 16.46, 16.17, and 15.18 (I***Me**), 5.28 and 3.53 (Si**Me**) ppm. δ 67.87and 25.82 ppm correspond to free THF. **^{45}Sc{^{1}H} NMR** (121 MHz, benzene-d_6, 298 K) δ 60.79 ppm. Anal. Calcd for $C_{50}H_{71}N_2O_2ScSi$: C, 74.59; H, 8.89; N, 3.48. Found: C, 74.54; H, 9.17; N, 3.13.IR strong absorption bands at 1613, 1537, and 1430 cm^{-1} of ν(C=N). [15]

5.3.15. Synthesis of ^{Me2}SB(^{tBu}N,I*)Sc(ODipp)DMAP (10)



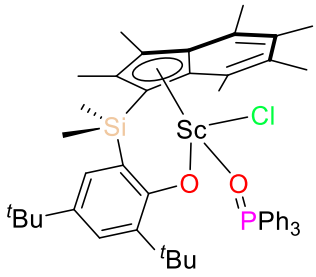
10

(21.5 mg, 83%); off-white microcrystalline powder.

^{1}H NMR (toluene-d_8, 400 MHz, 298 K): δ 7.62 (dd, $^3J_{H–H}$ = 7.2, $^4J_{H–H}$ = 1.6 Hz, 2H, 2,6-NC$_6$**H**$_4$), 7.14 (d, $^3J_{H–H}$ = 7.6Hz, 2H, 3,5-C$_6$**H**$_3$), 6.91 (t, $^3J_{H–H}$ = 7.6Hz, 1H, 4-C$_6$**H**$_3$), 5.74 (dd, $^3J_{H–H}$ = 7.2, $^4J_{H–H}$ = 1.6 Hz, 2H, 3,5-$NC_6\mathbf{H}_4$), 3.66 – 3.52 (overlapping m, 5H, THF and C**H**Me$_2$), 2.75 (s, 3H, I***Me**), 2.60 (s, 3H, I***Me**), 2.57 (s, 3H, I***Me**), 2.50 (s, 3H, I***Me**), 2.08 (s, 6H, N**Me**$_2$), 1.90 (s, 3H,

I*Me), 1.63 (s, 3H, I*Me), 1.51 – 1.41 (m, 3H, THF), 1.38 (d, $^{3}J_{H-H}$ = 7.0 Hz, 6H, CHMe$_2$) 1.36 (s, 9H, NCMe$_3$), 1.25 (d, $^{3}J_{H-H}$ = 6.8 Hz, 6H, CHMe$_2$), 1.03 (s, 3H SiMe), 0.99 (s, 3H, SiMe) ppm. **^{13}C{^{1}H} NMR** (toluene-d_8, 101 MHz, 298 K): δ 158.43 (1-C$_6$H$_3$), 157.49, 154.93, 154.57(4-NC$_6$H$_4$), 149.27 (2,6-NC$_6$H$_4$), 139.68 (I*), 137.86 (2,6-C$_6$H$_3$), 136.97 (I*), 129.34 (I*), 128.02 (I*), 127.97 (I*), 127.68 (I*), 126.80 (I*), 123.66 (3,5-C$_6$H$_3$), 118.51 (4-C$_6$H$_3$), 117.56 (I*), 104.36 (3,5-NC$_6$H$_4$), 94.15 (I*Si), 55.02 (NCMe$_3$), 38.51 (NMe$_2$), 35.66 (NCMe$_3$), 26.21 (CHMe$_2$), 25.60 (CHMe$_2$), 25.08 (CHMe$_2$), 22.36, 17.71, 17.02, 16.63, 16.51, and 15.41 (I*Me) , 12.34 and 10.84 (SiMe) ppm. δ 68.14 and 26.54 correspond to free THF. Anal. Calcd for $C_{40}H_{60}N_3OScSi$: C, 71.50; H, 9.00; N, 6.25. Found: C, 67.73; H, 8.69; N, 4.67.

5.3.16. Synthesis of ^{Me2}SB(^{tBu2}ArO,I*)Sc(Cl)OPPh$_3$ (11)



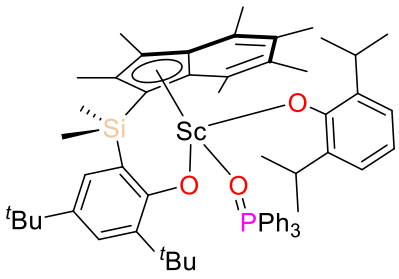
11

85% spectroscopic yield

^{1}H NMR (benzene-d_6, 600 MHz, 298 K): δ 7.77 (s, $^{4}J_{H-H}$ = 2.5 Hz 1H, 5-C$_6$H$_2$), 7.65 (s, $^{4}J_{H-H}$ = 2.5 Hz 1H, 3-C$_6$H$_2$), 7.44 – 7.36 (m, 6H, 2,6-C$_6$H$_5$), 7.06 – 6.94 (m, 9H, 3,4,5-C$_6$H$_5$), 2.83 (s, 3H, I*Me), 2.69 (s, 3H, I*Me), 2.50 (s, 3H, I*Me), 2.37 (s, 3H, I*Me) , 1.93 (s, 3H, I*Me), 1.82 (s, 3H, I*Me), 1.60 (s, 9H, *2*-CMe$_3$), 1.50 (s, 9H, *4*-CMe$_3$), 1.08 (s, 3H, SiMe), and 0.65 (s, 3H, SiMe) ppm. Multiplets at δ 3.60 and 1.42 ppm correspond to free THF. **^{13}C{^{1}H} NMR** (benzene-d_6, 151 MHz, 298 K) δ 165.38 (1-C$_6$H$_2$), 141.93 (I*), 140.74 (4-C$_6$H$_2$), 136.39 (I*), 135.00 (2-C$_6$H$_2$), 133.31 (d, $^{4}J_{P-C}$ = 3.1 H, 4-C$_6$H$_5$), 132.87 (d, $^{2}J_{P-C}$ = 11.2 Hz, 2,6-C$_6$H$_5$), 131.47 (6-C$_6$H$_2$),.129.89 (I*), 128.99 (d, $^{3}J_{P-C}$ = 12.7 Hz, 3,5-C$_6$H$_5$), 128.59 (I*), 128.35 (I*), 128.14 (I*), 127.98 (3,5-C$_6$H$_2$), 127.38 (I*), 124.83 (3,5-C$_6$H$_2$), 118.28 (I*) 98.81 (I*Si), 35.44 (*o*-CMe$_3$), 34.68 (*p*-CMe$_3$), 32.32 (*p*-CMe$_3$), 30.63 (*p*-CMe$_3$), 22.15, 17.24, 17.23,

16.31, 15.69, 15.61 (I***Me**), 4.00 (Si**Me**), 2.17 (Si**Me**). Peaks at δ 67.84 and 25.82 ppm correspond to free THF. **^{31}P{^{1}H} NMR** (243 MHz, benzene-d_8, 298 K):δ 40.96 ppm. **^{45}Sc{^{1}H} NMR** (121.5 MHz, benzene-d_6, 298 K):δ 129 ppm.

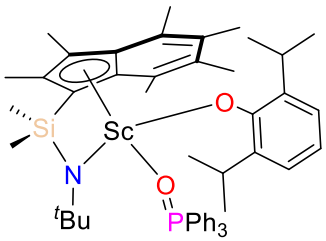
5.3.17. Synthesis of ^{Me2}SB(^{tBu2}ArO,I*)Sc(ODipp)OPPh$_3$ (12)



12

(25.0 mg, 65%); fine white microcrystalline powder **^{1}H NMR** (benzene-d_6, 400 MHz, 298 K): δ 7.74 (d, $^{4}J_{H–H}$ = 2.6 Hz, 1H, 3,5-C$_6$**H**$_2$), 7.47 (d, $^{4}J_{H–H}$ = 2.6 Hz, 1H, 3,5-C$_6$**H**$_2$), 7.30 – 7.20 (overlapping m, 6H, 2,6-C$_6$**H**$_5$), 7.14 (d, 2H, 3,5-C$_6$**H**$_3$), 7.03 – 6.82 (overlapping m, 10 H, 3,4,5-C$_6$**H**$_5$ and 4-C$_6$**H**$_3$), 3.67 (hept , $^{3}J_{H–H}$ = 6.7, 2H, C**H**Me$_2$), 3.61 – 3.55 (m, 4H, THF), 2.75 (s, 3H, I***Me**), 2.59 (s, 3H, I***Me**), 2.54 (s, 3H, I***Me**), 2.18 (s, 3H, I***Me**), 2.11 (s, 3H, I***Me**), 1.97 (s, 3H, I***Me**), 1.48 (s, 9H, C**Me**$_3$), 1.42 (m, 4H, THF), 1.11 (s, 9H, C**Me**$_3$) 1.37 (broad s, 12H, CH**Me**$_2$) 1.06 (s, 3H Si**Me**), 1.05 (s, 3H, Si**Me**). **^{13}C{^{1}H} NMR** (benzene-d_6, 101 MHz, 298 K): δ 167.05 (1-**C**$_6$H$_2$), 158.22 (1-**C**$_6$H$_3$), 138.47 (2,4-**C**$_6$H$_2$), 138.39 (**I***), 136.57 (2,6-**C**$_6$H$_3$), 134.29 (2,4-**C**$_6$H$_2$), 133.57 (**I***), 133.37, 133.35, 132.97, 132.87, 132.79 and 132.68, (**Ar**), 133.60 (6-**C**$_6$H$_2$), 131.48 (**I***), 131.84 (**Ar**), 128.98 (**I***), 128.18 (**I***), 128.80, (3,5-**C**$_6$H$_2$), 127.95 (**I***), 125.92 (**I***), 124.13 (3,5-**C**$_6$H$_2$), 122.68 (3,5-C$_6$**H**$_3$), 118.19 (4-**C**$_6$H$_3$), 114.18 (**I***), 99.26 (**I***Si), 35.20, and 34.48 (**C**Me$_3$), 32.28, and 30.67 (C**Me**$_3$), 26.13 (**C**HMe$_2$), 24.98 (CH**Me**$_2$), 25.81 (CH**Me**$_2$), 22.36, 17.40, 17.24, 16.60, 16.00, and 15.58 (I***Me**), 7.22 and 5.99. (Si**Me**) ppm. δ 67.87 and 25.81 correspond to free THF. **^{31}P{^{1}H} NMR** (benzene-d_6, 202.4 MHz, 298 K) δ 40.53 ppm. **^{31}P{^{1}H} NMR** (toluene-d_8, 202.4 MHz, 233 K) A:40.71 B: 39.87 ppm **^{45}Sc{^{1}H} NMR** (benzene-d_6, 121 MHz, 298 K) δ 34.46 ppm. Anal. Calcd for C$_{61}$H$_{76}$O$_3$PScSi: C, 76.22; H, 7.97. Found: C, 76.38; H, 7.84.

5.3.18. Synthesis of ^{Me2}SB($^{t Bu}$N,I*)Sc(ODipp)OPPh$_3$ (13)



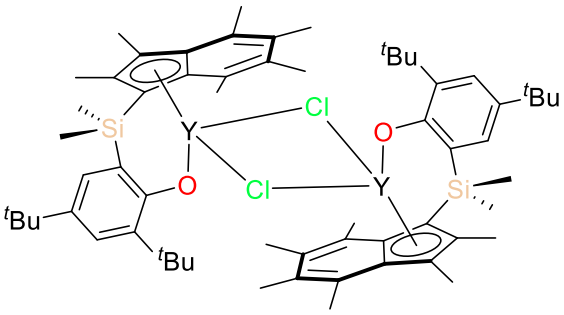
13

(15.0 mg, 64%); fine white microcrystalline powder.

^{1}H NMR (toluene-d_8, 400 MHz, 298 K): δ 7.62 (dd, $^3J_{H–H}$ = 7.2, $^4J_{H–H}$ = 1.6 Hz, 2H, 2,6-NC$_6$**H**$_4$), 7.14 – 6.95 (overlapping m, 11H, 3,5-C$_6$**H**$_3$ and Ar-**H**), 6.89 (t, $^3J_{H–H}$ = 7.5 Hz, 1H, 4-C$_6$**H**$_3$), 4.04 (broad s, 1H, C**H**Me$_2$), 3.32 (broad s, 1H, C**H**Me$_2$), 2.72 (s, 3H, I***Me**), 2.57 (s, 3H, I***Me**), 2.54 (s, 3H, I***Me**), 2.00 (s, 6H, N**Me**$_2$), 1.90 (s, 3H, I***Me**), 1.47 (s, 3H, I***Me**), 1.35 (broad s, 12H, CH**Me**$_2$) 1.08 (s, 9H, NC**Me**$_3$), (CH**Me**$_2$), 1.04 (s, 3H Si**Me**), 0.99 (s, 3H, Si**Me**). Peaks at δ 3.55 and 1.45 ppm correspond to free THF. **^{13}C{^{1}H} NMR** (toluene-d_8, 101 MHz, 298 K): δ 158.12 (1-**C**$_6$H$_3$), 139.19 (**I***), (2,6-**C**$_6$H$_3$), 136.12 (**I***), 133.57 (**Ph**), 132.83 (**C**$_6$H$_3$), 132.74 (**C**$_6$H$_3$), 131.84 (**Ph**), 129.08 (**I***), 128.88 (**I***), 128.76 (**I***), 127.75 (**I***), 126.46 (**I***), 123.66 (3,5-C$_6$**H**$_3$), 117.92 (4-**C**$_6$H$_3$), 117.86 (**I***), 94.94 (**I***Si), 54.39 (**C**Me$_3$), 36.00 (C**Me**$_3$), 26.21 (**C**HMe$_2$), 25.60 (CH**Me**$_2$), 25.08 (CH**Me**$_2$), 22.58, 18.33, 17.19, 17.09, 16.69, and 15.47 (I***Me**) , 13.04 and 11.86 (Si**Me**) ppm. δ 68.11 and 26.20 correspond to free THF. **^{31}P{^{1}H} NMR** (toluene-d_8, 202 MHz, 233 K) δ 40.71 (kinetic product) 39.87 (thermodynamic product) ppm. **^{45}Sc{^{1}H} NMR** (benzene-d_6, 121 MHz, 298 K) δ 124.30ppm. Anal. Calcd for $C_{51}H_{65}NO_2PScSi$: C, 73.97; H, 7.91; N, 1.69. Found: C, 72.83; H, 7.42; N, 1.69.

5.3.19. Synthesis of [^{Me2}SB($^{t Bu2}$ArO,I*)Y(Cl)THF]$_2$ (14)

To an orange solution of the lithiated proligand ^{Me2}SB($^{t Bu2}$ArOAllyl,I*)Li$_2$ (1.976g, 4.656 mmol) in 20 mL of benzene, a slurry of YCl_3 (1.1 eq., 1.000 g, 5.122 mmol) in



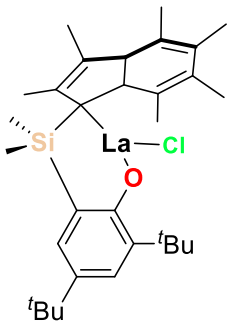
14

10 mL of benzene, was added. The reaction mixture was stirred for 5 days at 70°C resulting in the formation of an off-white solution with white precipitate. The product was extracted *via* filtration and the volatiles were removed *in vacuo;* the resulting yellow/orange solid was washed with pentane (3 x 20 mL) and remaining solid dried *in vacuo* to yield [^{Me2}SB(^{tBu2}ArO,I*)Y(Cl)THF]$_2$ as a light orange solid in 38% yield (1.03 g, 1.763 mmol).

^{1}H NMR (benzene-d_6, 400 MHz, 298 K): δ 7.65 and 7.57 (d, ^3J = 2.5 Hz, 1H each, 3,5-C$_6$**H**$_2$), 7.50 and 7.20 (d, ^3J = 2.6 Hz, 1H each, 3,5-C$_6$**H**$_2$), 2.74, 2.72, 2.57, 2.49, 2.41, 2.37, 2.36, 2.21, 2.18, 2.02, 1.85, 1.73, and 1.72 (s, 3H each, I***Me**), 1.49, 1.36, 1.34, and 0.76 (s, 9H each, C**Me**$_3$), 0.87, 0.86, 078, and 0.71 (s, 3H each, Si**Me**) ppm.

^{13}C{^{1}H} NMR (benzene-d_6, 126 MHz, 298 K): δ 166.60 and 162.20 (1-**C**$_6$H$_2$), 140.32, 138.67, 134.62, and 133.36 (2,4-**C**$_6$H$_2$), 141.67, 140.99, 140.99, 138.07, 133.13, 131.79, 131.34, 131.11, 129.54, 128.42, 128.42, 127.97, 126.62, 126.17, 125.95, 123.92, 117.41, 115.39, and 141.95 (**I***),133.58 and 130.89 (6-**C**$_6$H$_2$), 129.83, 127.84, 124.72, and 124.03 (3,5-**C**$_6$H$_2$), 99.27 and 96.75 (**I***Si), 35.35, 34.09, 34.00, and 32.96 (**C**Me$_3$), 31.66, 31.63, 31.20, and 30.00 (C**Me**$_3$), 22.18, 21.38, 18.47, 18.15, 17.19, 16.86, 16.54, 16.38, 26.22, 16.06, 15.74, 14.77, and 14.12 (I***Me**), 6.55, 5.43, 2.06, and 1.61 (Si**Me**) ppm. Anal. Calcd for C$_{45}$H$_{55}$ClSiY: C, 63.63; H, 8.08; N, 0. Found C, 63.27; H 8.08; N, 0.3. Nitrogen as a result of proligand-NEt$_3$ adduct (starting material) impurity.

5.3.20. ^{Me2}SB(^{tBu2}ArO,I*)LaCl (15)



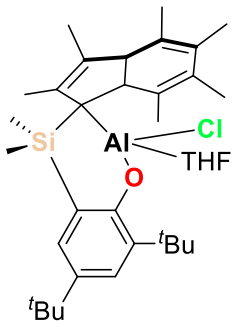
15

To a Young's NMR tube containing the proligand ^{Me2}SB(^{tBu2}ArO,I*)Li$_2$ (10 mg, 0.0211 mmol) dissolved in THF-d_8 as a pale yellow solution, LaCl$_3$.3THF (10.2 mg, 0.0211 mmol) was added and heated to 60 ℃ for 3 days. A pale yellow solution was observed and >95% conversion was recorded *via* ^{1}H NMR spectroscopy.

^{1}H NMR (THF-d_8, 600 MHz, 298 K): δ 7.32 (d, $^4J_{H\,H}$ = 2.6 Hz, 1H, 3-C$_6$**H**$_2$),, 7.16 – 7.14 (s, 1H, 5-C$_6$**H**$_2$), 2.62 (broad s, 3H, I***Me**), 2.39 (broad s, 3H, I***Me**), 2.37 (broad s, 3H, I***Me**), 2.28 (s, 3H, I***Me)** , 2.25 (s, 3H, I***Me)**, 2.21 (s, 3H, I***Me**), 1.48 (s, 9H, *o*-C**Me**$_3$), 1.30 (s, 9H, *p*-C**Me**$_3$), 0.23 (s, 3H, Si**Me**), −0.20 (s, 3H, Si**Me**) ppm. Resoance at δ 3.66–3.60 and 1.80–1.76 ppm corresponds to free THF

^{13}C{^{1}H} NMR (THF-d_8, 151 MHz, 298 K): δ 160.46 (1-**C**$_6$H$_2$), 144.97 (**I***), 141.89 (**I***), 141.62 (2,4-**C**$_6$H$_2$), 140.78 (2,4-**C**$_6$H$_2$), 130.01 (**I***), 129.87 (6-**C**$_6$H$_2$), 129.14 (**I***), 128.86 (3-**C**$_6$H$_2$), 128.52 (**I***), 128.51 (5-**C**$_6$H$_2$), 126.98 (**I***), 125.75 (**I***), 125.72 (**I***Si), 35.69, and 34.80 (**C**Me$_3$), 32.12 and 30.63 (C**Me**$_3$), 23.15, 20.93, 19.58, 16.89, 16.77, 15.83, , and 14.34 (I***Me**), 3.39 and 0.64 (Si**Me**) ppm. Peaks at δ 68.03 and 26.10 ppm correspond to free THF. Additional peaks relating to minor compound are present at δ 162.58, 160.66, 147.00, 145.76, 143.75, 141.93, 141.27, 140.88, 139.44, 138.38, 137.65, 137.10, 135.06, 131.82, 129.25, 128.61, 128.16, 127.84, 127.21, 126.84, 126.46, 125.99, 124.45, 123.62, 115.87, 36.02, 35.02, 34.68, 32.36, 31.90, 31.63, 30.74, 18.96, 17.10, 16.93, 16.56, 16.07, 14.11, 1.35, 1.28, 1.10, -0.86 ppm but unassigned.

5.3.21. Synthesis of ^{Me2}SB(^{tBu2}ArO,I*)Al(Cl)THF (16)



16

To an orange solution of the lithiated proligand ^{Me2}SB(^{tBu2}ArOAllyl,I*)Li$_2$ (2.26 g, 0.04713 mmol) in toluene, a slurry of AlCl$_3$.THF (1.05 eq., 1 g, 0.04967 mmol) in benzene, was added. The reaction mixture was stirred for 1 day at 25℃ resulting in the formation of an off-white solution with white precipitate. The reaction mixture was filtered and the volatiles were removed *in vacuo*. The resultant solid was then washed with cold pentane to yield ^{Me2}SB(^{tBu2}ArO,I*)Al(Cl)THF as a white solid in 19 % yield (0.543 g 0.0090 mmol)

^{1}H NMR (benzene-d_6, 600 MHz, 298 K): δ 7.69 (d, $^{4}J_{H\text{-}H}$ = 2.7 Hz, 1H, 3,5-C$_6$**H**$_2$), 7.48 (d, $^{4}J_{H\text{-}H}$ = 2.7 Hz, 1H, 3,5-C$_6$**H**$_2$), 3.30 (m, 4H, 2,5-C$_4$**H**$_8$O), 2.69 (s, 3H, I***Me**), 2.59 (s, 3H, I***Me**), 2.50 (s, 3H, I***Me**), 2.41 (s, 3H, I***Me)** , 2.26 (s, 3H, I***Me)**, 2.17 (s, 3H, I***Me**), 1.76 (s, 9H, C**Me**$_3$), 1.43 (s, 9H, C**Me**$_3$), 0.92 (m, 4H, 3,4-C$_4$**H**$_8$O), 0.45 (s, 3H, Si**Me**), and 0.07 (s, 3H, Si**Me**) ppm.

^{13}C{^{1}H} NMR (benzene-d_6, 126 MHz, 298 K): δ 160.18 (1-**C**$_6$H$_2$), 144.90 (**I***), 140.86 (2,4-**C**$_6$H$_2$), 141.98 (**I***), 141.54 (**I***), 137.49 (2,4-**C**$_6$H$_2$), 132.07 (6-**C**$_6$H$_2$), 129.63 (**I***), 129.18 (3,5-**C**$_6$H$_2$), 128.51 (**I***Si), 128.73 (**I***), 128.06 (**I***), 127.39 (**I***), 125.59 (**I***),), 125.48 (3,5-**C**$_6$H$_2$), 73.04 (2,5-**C**$_4$H$_8$O), 35.59, and 34.53 (**C**Me$_3$), 31.90, and 30.59 (C**Me**$_3$), 24.44 (3,4-**C**$_4$H$_8$O) 20.41, 19.60, 16.70, 16.54, 16.38, and 15.74 (I***Me**), 3.93, and 0.51 (Si**Me**) ppm.

Minor Product – secondary resonances

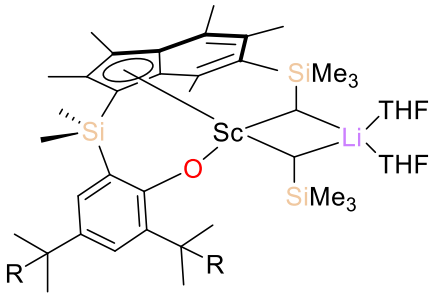
^{1}H NMR (benzene-d_6, 600 MHz, 298 K): δ 7.59 (d, $^{4}J_{H\text{-}H}$ = 2.5 Hz, 1H, 3,5-C$_6$**H**$_2$), 7.46 (d, $^{4}J_{H\text{-}H}$ = 2.5 Hz, 1H, 3,5-C$_6$**H**$_2$), 3.06 (m, 4H, 2,5-C$_4$**H**$_8$O), 2.77 (s, 3H, I***Me**), 2.74 (s,

3H, I*Me), 2.45 (s, 3H, I*Me), 2.27 (s, 3H, I*Me) , 2.24 (s, 3H, I*Me), 2.16 (s, 3H, I*Me), 1.51 (s, 9H, CMe$_3$), 1.34 (s, 9H, CMe$_3$), 0.63 (m, 4H, 3,4-C$_4$H$_8$O), 0.37 (s, 3H, SiMe), and 0.09 (s, 3H, SiMe) ppm.

^{13}C{^{1}H} NMR (benzene-d_6, 126 MHz, 298 K): δ 161.97 (1-C$_6$H$_2$), 145.58 (2,4-C$_6$H$_2$), 143.56 (I*), 141.55 (I*), 141.55 (I*), 141.54 (2,4-C$_6$H$_2$), 130.31 (I*), 130.08 (I*), 129.69 (I*), 129.11 (3,5-C$_6$H$_2$), 128.28 (6-C$_6$H$_2$), 128.96 (I*Si), 128.06 (I*), 126.55 (I*Si), 126.13 (3,5-C$_6$H$_2$), 125.14 (I*), 72.05 (2,5-C$_4$H$_8$O), 35.53, and 34.63 (CMe$_3$), 31.69, and 30.60 (CMe$_3$), 27.52 (3,4-C$_4$H$_8$O), 23.79, 17.11, 16.86, 16.61, 16.29, and 15.57 (I*Me), 3.17, and 0.10 (SiMe) ppm.

5.4. Experimental for unsuccessful chemistries in Chapter 2

5.4.1. Synthesis of ^{Me2}SB($^{R,R'}$ArO,I*)Sc(CH$_2$(SiMe$_3$))$_2$-μ^{2}Li.THF R = R′ = ^{t}Bu (17) and Cumyl (18)



17 R= Me
18 R = Ph

To an Youngs tap NMR tube containing **1** or **2**, (0.006 mmol) dissolved in 0.6 mL of benzene-d_6 2 eq. Li(CH$_2$SiMe$_3$) was added forming a pale-yellow solution with a white solid (LiCl) forming. The mixture was filtered through PTFE filters under an N$_2$ atmosphere (in glovebox). ^{1}H NMR spectroscopy was used to monitor the reactions and full conversion to scandiate **17** and **18** was recorded. Attempts to isolate the products led to decomposition and products were also unstable at room temperature in solution.

R = R′ = ^{t}Bu (17) spectroscopic NMR yield = >95%

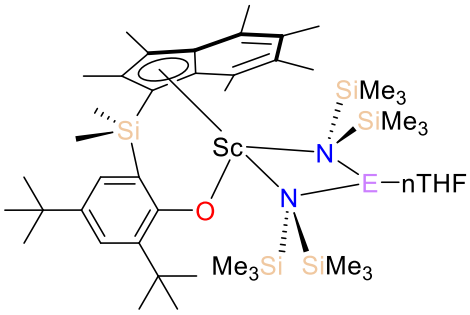
^{1}H NMR (benzene-d_6, 600 MHz, 298 K):δ 7.58 (d, $^{4}J_{H–H}$ = 2.6 Hz, 1H, 3-C_6**H**$_2$), 7.46 (d, $^{4}J_{H–H}$ = 2.6 Hz, 1H, 5-C_6**H**$_2$), 3.12 (s, 8H, 2,5-C_4**H**$_8$O), 2.89, 2.75, 2.33, 2.32, 2.17, 2.16 (s, 3H each, I*-**Me**), 1.51 (s, 9H, C**Me**$_3$), 1.36 (s, 9H, C**Me**$_3$), 1.11 (s, 8H, 3,4-C_4**H**$_8$O), 0.78, 0.74 (s, 3H each, Si**Me**), 0.31, 0.17 (s, 9H each, Si**Me**$_3$), -0.48, -1.42 (s, 2H each, C**H**$_2$SiMe$_3$). TMS at δ 0.00 ppm

^{13}C {H} NMR (benzene-d_6, 151 MHz, 298 K):δ 162.98 (1-**C**$_6$H$_2$), 142.24 (4-**C**$_6$H$_2$), 137.16 (**I***), 135.94 (6-**C**$_6$H$_2$), 132.98 (**I***), 129.59 (**I***), 129.12 (**I***), 128.35 (**I***), 128.22 (**I***), 128.06 (**I***), 127.90 (**I***), 127.42 (5-**C**$_6$H$_2$), 125.24 (3-**C**$_6$H$_2$), 111.54 (**I***), 96.18 (Si**I***), 68.49 (2,5-**C**$_4$H$_8$O), 35.60 (o-**C**Me$_3$), 34.52 (p-**C**Me$_3$), 32.36 (p-C**Me**$_3$), 32.00 (o-C**Me**$_3$), 25.17 (3,4-**C**$_4$H$_8$O), 21.92, 17.93, 17.18, 16.76, 16.55, and 15.69 (I*-**Me**), 5.16 (Si**Me**), 4.30 (Si**Me**$_3$), 4.07 (Si**Me**), 4.03 (Si**Me**$_3$), 1.42 and −0.76 (Sc**C**H$_2$) ppm. δ 0.02 ppm residual TMS.

R = R′ = Cumyl (18) spectroscopic NMR yield = >95%

^{1}H NMR (benzene-d_6, 400 MHz, 298 K):δ 7.59 (d, $^{4}J_{H–H}$ = 2.4 Hz, 1H, 3-C_6**H**$_2$), 7.47 (d, $^{4}J_{H–H}$ = 2.4 Hz, 1H, 5-C_6**H**$_2$), 7.39 (overlapping m, 2H, CMe$_2$**Ph**), 7.28–7.17 (overlapping m, 4H, CMe$_2$**Ph**), 7.12 (t, $^{3}J_{H–H}$ = 7.0 Hz, 1H, CMe$_2$**Ph**), 6.93 (t, $^{3}J_{H–H}$ = 7.8 Hz, 2H, CMe$_2$**Ph**), 6.70 (t, $^{3}J_{H–H}$ = 6.6 Hz, 1H, CMe$_2$**Ph**), 3.15 (broad s, 4H, 2,5-C_4**H**$_8$O), 2.80, 2.71, 2.25, 2.24, 2.21 , 2.07 (s, 3H each, I*-**Me**), 1.80 (s, 6H, C**Me**$_2$Ph), 1.61, 1.42 (s, 3H each, C**Me**$_2$Ph), 1.19 (m, 4H, 2,5-C_4**H**$_8$O), 0.69, 0.61 (s, 3H each, Si**Me**), 0.20 (s, 9H, Si**Me**$_3$), 0.10 (s, 9H, Si**Me**$_3$), −0.75 (broad s, 2H, ScC**H**$_2$), −1.81 (m, 2H each, ScC**H**$_2$).

5.4.2. Synthesis of ^{Me2}SB(^{tBu2}ArO,I*)Sc(N(SiMe$_3$)$_2$)$_2$.E.THF (E = Li (19) and K (20))



19 E = Li
20 E = K

In a Youngs NMR tube, ^{Me2}SB(^{tBu2}ArO,I*)Sc(Cl).THF (17 mg, 0.0259 mmol) dissolved in benzene-d_6 (0.6 mL), lithium bis(trimethylsilyl)amide (1.0 eq., 4.34 mg, 0.0259 mmol) was added at 25 °C followed by a further equivalent after 1 h. A bright yellow solution was formed with a white precipitate. Filtration to remove the LiCl and removal of volatiles under vacuum provided ^{Me2}SB(^{tBu2}ArO,I*)Sc(N(SiMe$_3$)$_2$)$_2$.Li·THF **19** and **20** which decomposed at room temperature when isolated.

E = Li **19** spectroscopic NMR yield = >95%

^{1}H NMR (benzene-d_6, 600 MHz, 298 K):δ 7.70 (d, $^4J_{H–H}$ = 2.4 Hz, 1H, 3,5-C$_6$**H**$_2$), 7.57 (d, $^4J_{H–H}$ = 2.4 Hz, 1H, 3,5-C$_6$**H**$_2$), 3.60 (m, 4H, 2,5-C$_4$**H**$_8$O), 2.64 (s, 3H, I***Me**), 2.55 (s, 3H, I***Me**), 2.41 (s, 3H, I***Me**), 2.27 (s, 3H, I***Me**), 2.11 (s, 3H, I***Me**), 1.99 (s, 3H, I***Me**), 1.50 (s, 9H, C**Me**$_3$), 1.45 (s, 9H, C**Me**$_3$), 1.23 (m, 4H, 3,4-C$_4$**H**$_8$O), 0.85 (s, 3H, Si**Me**), 0.82 (s, 3H, Si**Me**), 0.30 (s, 27H, NSi**Me**$_3$), 0.18 and −0.21 (s, 9H, Si**Me**$_3$) ppm. Unassigned peaks at,δ 0.10 ppm (H-HMDS),

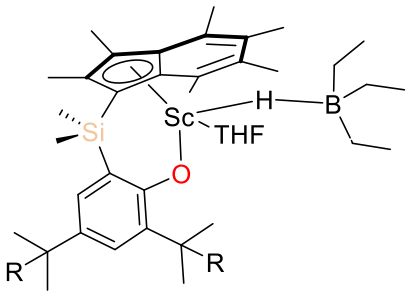
^{13}C{^{1}H} NMR (benzene-d_6, 151 MHz, 298 K):δ 164.32 (1-**C**$_6$H$_2$), 141.56 (4-**C**$_6$H$_2$), 140.47 (**I***), 135.54 (**I***), 135.07 (2-**C**$_6$H$_2$), 131.33 (**I***), 131.27 (**I***), 130.99 (6-**C**$_6$H$_2$), 130.45 (**I***), 128.78 (**I***), 128.14 (**I***), 127.98 (5-**C**$_6$H$_2$), 125.04 (3-**C**$_6$H$_2$), 116.84 (**I***), 102.42 (**I***Si), 68.72 (2,5-**C**$_4$H$_8$O), 35.43 (o-**C**Me$_3$), 34.64 (p-C**Me**$_3$), 32.17 (p-**C**Me$_3$),

30.82 (o-C**Me**$_3$), 24.99 (**C**HMe$_2$), 24.26 (3,4-**C**$_4$H$_8$O) 24.95, and 24.86 (CH**Me**$_2$) 21.94, 17.62, 17.02, 16.32, 16.16, and 15.26, (I***Me**), 5.18, and 3.50 (Si**Me**) ppm.

E = K (**20**) spectroscopic NMR yield = >95%

^{1}H NMR (benzene-d_6, 400 MHz, 298 K):δ 7.62 (d, $^4J_{H\,H}$ = 2.6 Hz, 1H, 3-C$_6$**H**$_2$), 7.46 (d, $^4J_{H\,H}$ = 2.6 Hz, 1H, 5-C$_6$**H**$_2$), 3.51–3.43 (m, 4H, 2,5-C$_4$**H**$_8$O), 2.84, 2.80, 2.51, 2.36, 2.18, 1.83 (s, 3H each, I***Me**), 1.42 (s, 9H, *o*-C**Me**$_3$), 1.40 (s, 9H, *p*-C**Me**$_3$), 1.39–1.37 (m, 4H, 3,4-C$_4$**H**$_8$O), 0.88, 0.79 (s, 3H each, Si**Me**$_3$), 0.54, 0.44, 0.41, 0.13 (s, 36H total, NSi**Me**$_3$) ppm. δ 0.10 ppm is H-HMDS (s, 21H).

5.4.3. Synthesis of ^{Me2}SB($^{R,R'}$ArO,I*)Sc(BH$_4$)THF R = R′ = ^{t}Bu (21) and Cumyl (22)



21 R = Me
22 R = Ph

To an Youngs tap NMR tube containing the respective scandium complexes **1**, **5**, and **7,** (0.006 mmol) dissolved in 0.6 mL of benzene-d_6 or toluene-d_8, 1 eq. of DMAP or OPPh$_3$ was added. ^{1}H NMR spectroscopy was used to monitor the reactions. In all cases, the off-white (**5** and **7**) or yellow (**1**) solutions became slightly lighter in colour.

R = R′ = ^{t}Bu (21) spectroscopic NMR yield >95%

^{1}H NMR (THF-d_8, 600 MHz, 298 K): δ 7.70 (d, $^4J_{H-H}$ = 2.6 Hz, 1H, 3-C$_6$**H**$_2$), 7.62 (d, $^4J_{H-H}$ = 2.6 Hz, 1H, 5-C$_6$**H**$_2$), 3.64 (broad s, 1H Sc-H), 3.46 (broad s, 4H, 2,5-C$_4$**H**$_8$O), 2.80, 2.68, 2.38, 2.13, (s, 3H each, I***Me**), 2.00–1.97 (overlapping m, 6H, I***Me)**, 1.56 (s, 9H, *o*-C**Me**$_3$), 1.42 (s, 9H, *p*-C**Me**$_3$), 1.21–1.09 (overlapping , 9H, BCH$_2$C**H**$_3$), 0.98 (overlapping m, 4H, 3,4-C$_4$**H**$_8$O), 0.94, 0.79 (s, 3H each, Si**Me**), 0.56 (m, 2H, BC**H**$_2$CH$_3$)

−0.42 (m, 2H, BC**H**$_2$CH$_3$) ppm. Peaks at δ 3.66–3.60 and 1.80–1.76 ppm correspond to free THF. **^{11}B{^{1}H}** (benzene-d_6, 128.4 MHz, 298 K):δ −2.79 ppm.

R = R′ = Cumyl (22) spectroscopic NMR yield >95%

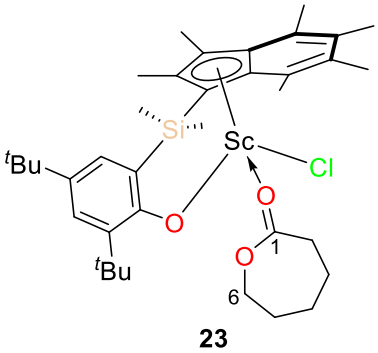
^{1}H NMR (benzene-d_6, 400 MHz, 298 K):δ 7.39 (d, $^4J_{H–H}$ = 2.6 Hz, 1H), 7.35 (d, $^4J_{H–H}$ = 2.6 Hz, 1H), 7.25–7.19 (m, 2H, CMe$_2$**Ph**), 7.05–6.97 (m, 4H, CMe$_2$**Ph**), 6.92–6.86 (m, 2H, CMe$_2$**Ph**), 6.70 (t, $^3J_{H–H}$ = 7.3 Hz, 1H, CMe$_2$**Ph**), 3.30 (broad s, 4H, 2,5-C$_4$**H**$_8$O), 2.98 (s, 1H, Sc**H**B(Et$_3$)), 2.54, 2.39, 2.19, 1.90, 1.82, 1.72(s, 3H each, I*__Me__), 1.59 (s, 6H, C__Me__$_2$Ph), 1.53, 1.44 (s, 3H, C__Me__$_2$Ph), 1.14 (broad s, 4H, 3,4-C$_4$**H**$_8$O), 0.94 – 0.73 (m, 25H), 0.60, 0.47 (s, 3H, Si__Me__), 0.01, −0.98 (m, 2H each, BC**H**$_2$CH$_3$).

5.5. Experimental detail for Chapter 4

5.5.1. Synthesis of ^{Me_2}SB(^{tBu_2}ArO,I*)Sc(X)L, X = Cl; L = ϵ-CL (23), L-La, (24) and PDL (25); X = ODipp, L = ϵ-CL (26), L-La (27) and PDL (28)

To an Youngs tap NMR tube containing **1** or **5**, (43 mg) dissolved in 0.6 mL of benzene-d_6 1 eq. lactone (ϵ-CL, L-La or PDL) was added forming a pale-yellow solution. The sample was freeze dried *in vacuo* at 0 °C and a heat gun used to dry gently. The solids foamed slightly and an off-white solid remained. N-hexanes were added to the NMR tube where for **23**, **24**, and **25**, the partial was only slightly soluble as an off-white solution which was filtered. Crystals suitable for X-ray study were collected for **24**, **25** and **26** from slow evaporation from n-hexanes at RT.

23



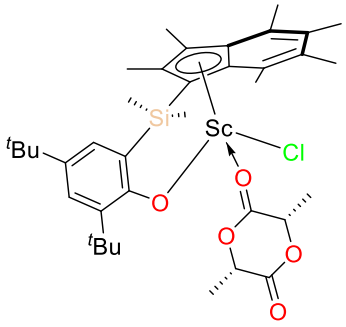
23

(31.1 mg, 64%); fine white microcrystalline powder.

^{1}H NMR (benzene-d_6, 400 MHz, 298 K): δ 7.75 (d, $^4J_{H-H}$ = 2.5 Hz, 1H, 3,5-C$_6$**H**$_2$), 7.62 (d, $^4J_{H-H}$ = 2.5 Hz, 1H, 3,5-C$_6$**H**$_2$), 3.24 (broad s 2H, 6-C$_6$**H**$_{12}$O$_2$) 2.84, 2.81, 2.42, 2.38, 2.13, and 2.04 (s, 3H each, I***Me**), 1.88 (broad s, 2H, 2-C$_6$**H**$_{12}$O$_2$), 1.63 (s, 9H, 2-C**Me**$_3$), 1.49 (s, 9H, 4-C**Me**$_3$), 0.98 (s, 3H, Si**Me**), 0.94, 0.83, 0.75 (broad s, 2H each, C$_6$**H**$_{10}$O$_2$) and 0.58 (s, 3H, Si**Me**) ppm. **^{13}C{^{1}H} NMR** (151 MHz, benzene-d_6, 298 K): δ 164.95 (1-**C**$_6$H$_2$), 142.92 (2,4-**C**$_6$H$_2$), 145.43 (**I***), 141.65 (**I***), 141.34 (2,4-**C**$_6$H$_2$), 135.15 (**I***), 135.77 (6-**C**$_6$H$_2$), 131.79 (**I***), 131.57 (**I***), 130.07 (**I***), 128.35 (**I***), 128.13 (**I***), 128.98 (**I***), 127.52 (3,5-**C**$_6$H$_2$), 125.16 (3,5-**C**$_6$H$_2$), 100.06 (**I***Si), 71.74 (6-**C**$_6$H$_{12}$O$_2$), 35.38, and 34.70 (**C**Me$_3$), 34.14 (2-**C**$_6$H$_{10}$O$_2$) 32.29, and 30.35 (C**Me**$_3$), 27.67, 27.30 (**C**$_6$H$_{10}$O$_2$), 22.06 (I***Me**), 21.46 (**C**$_6$H$_{12}$O$_2$), 17.59, 17.14, 16.59, 15.73, and 14.35 (I***Me**), 2.98, and 2.78 (Si**Me**) ppm. Signal for (1-**C**$_6$H$_{10}$O$_2$) not

observed. Anal. Calcd for $C_{37}H_{54}O_3ScSi$: C, 68.71; H 8.31.Found, C, 69.20; H 6.79 IR strong absorption bands at 2949, 2908, 2874 *v*(C-H) 1655, 1458, and 1251 cm^{-1}

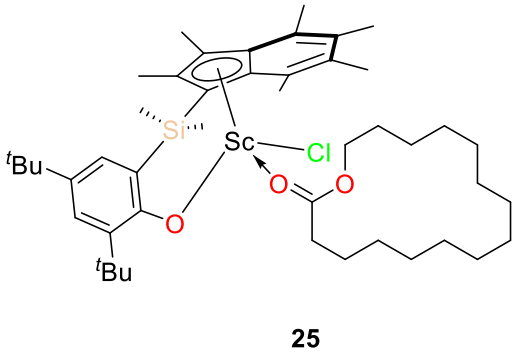
24



24

^{1}H NMR (benzene-d_6, 400 MHz, 298 K): δ 7.72 (d, $^4J_{H–H}$ = 2.5 Hz, 1H, 3,5-C_6**H**$_2$), 7.62 (d, $^4J_{H–H}$ = 2.5 Hz, 1H, 3,5-C_6**H**$_2$), 3.77 (q, $^3J_{H–H}$ = 6.7 Hz, 2H, C_6**H**$_8O_2$), 2.84, 2.70, 2.37, 2.15, 2.10, 2.01 (s, 3H each, I***Me**), 1.63 (s, 9H, 2-C**Me**$_3$), 1.47 (s, 9H, 4-C**Me**$_3$), 1.17 (d, $^3J_{H–H}$ = 6.6 Hz, 6H, C_6**H**$_8O_4$), 0.95 and 0.63 (s, 3H each, Si**Me**) ppm. **^{13}C{^{1}H} NMR** (benzene-d_6, 101 MHz, 298 K): δ 167.20 (C_6**H**$_8O_4$), 126.55 (1-**C**$_6$H$_2$), 141.92 (2,4-**C**$_6$H$_2$), 140.95 (**I***), 136.00 (2,4-**C**$_6$H$_2$), 135.12 (**I***), 130.65 (6-**C**$_6$H$_2$), 130.98 (**I***), 130.47 (**I***), 130.09 (**I***), 128.87 (**I***), 128.30 (**I***), 128.06 (**I***), 127.66 (3,5-**C**$_6$H$_2$), 124.27 (3,5-**C**$_6$H$_2$), 102.48 (**I***Si), 72.04 (C_6**H**$_8O_4$), 35.54, and 34.71 (**C**Me$_3$), 32.21, and 30.42 (C**Me**$_3$), 22.01, 17.43, 16.94, 16.30, (I***Me**), 15.48 (C_6**H**$_8O_4$), 15.47, 15.37 (I***Me**),4.57, and 1.39 (Si**Me**) ppm. Anal. Calcd for $C_{37}H_{52}ClO_5ScSi$: C, 64.85; H 7.65. Found, C, 62.10 ; H 7.24 IR strong absorption bands at 2995, 2964, 2908, 2874 *v*(C-H) 1773, 1268 and 1243 cm^{-1}

25

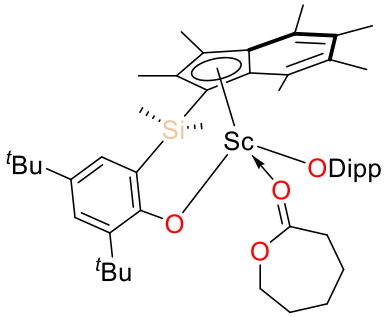


25

^{1}H NMR (benzene-d_6, 400 MHz, 298 K): δ 7.76 (d, $^4J_{H–H}$ = 2.6 Hz, 1H, 3,5-C_6**H**$_2$), 7.64 (d, $^4J_{H–H}$ = 2.6 Hz, 1H, 3,5-C_6**H**$_2$), 3.82 (broad s, 2H, C_{16}**H**$_{30}O_2$) 2.82, 2.78, 2.45 2.29 2.11 2.02 (s, 3H each, I***Me**), 1.65 (s, 9H, 2-C**Me**$_3$), 1.48 (s, 9H, 4-C**Me**$_3$), 1.30–1.06 (overlapping m, 24H, C_{16}**H**$_{30}O_2$) 1.03

(s, 3H, Si**Me**), and 0.71 (s, 3H, Si**Me**) ppm. Additional broad resonance in region **^{13}C{^{1}H} NMR** (benzene-d_6, 151 MHz, 298 K): δ 167.26 (1-**C**$_{16}$H$_{30}$O$_2$), 164.95 (1-**C**$_6$H$_2$), 142.55 (2,4-**C**$_6$H$_2$), 141.34 (**I***), 136.24 (2,4-**C**$_6$H$_2$), 135.76 (**I***), 131.79 (6-**C**$_6$H$_2$), 130.07 (**I***), 130.51 (**I***), 130.09 (**I***), 128.58 (**I***), 128.47 (**I***), 128.35 (**I***), 127.52 (3,5-**C**$_6$H$_2$), 125.16 (3,5-**C**$_6$H$_2$), 100.06 (**I***Si), 71.73 (**C**$_{16}$H$_{32}$O$_2$), 35.38, and 34.70 (**C**Me$_3$), 32.29, and 30.35 (C**Me**$_3$), 34.15 31.97 30.19 28.01, 27.67, 23.05, 21.25, 21.86, 21.25 (**C**$_{16}$H$_{30}$O$_2$) 22.06, 17.14, 16.59, 15.37, and 14.35 (I***Me**), 2.98, and 2.78 (Si**Me**) ppm. IR strong absorption bands at 3056, 2956, 2932, 2862 ν(C-H) 1735, 1647, 1458, 1418 cm^{-1} Anal. Calcd for C$_{46}$H$_{72}$ClO$_3$ScSi: C, 70.69; H 9.29. Found, C, 70.73; H 8.10

26

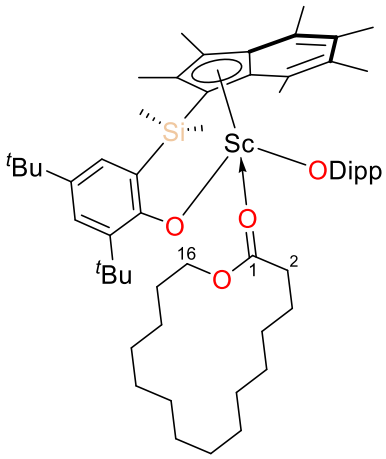


26

^{1}H NMR (benzene-d_6, 400 MHz, 298 K): δ 7.70 (d, $^{4}J_{H–H}$ = 2.5 Hz, 1H, 3,5-C$_6$**H**$_2$), 7.51 (d, $^{4}J_{H–H}$ = 2.5 Hz, 1H, 3,5-C$_6$**H**$_2$), 7.18 (d, $^{3}J_{H–H}$ = 7.2 Hz, 2H, 3,5-C$_6$**H**$_3$), 6.96 (t, $^{3}J_{H–H}$ = 7.6 Hz, 1H, 4-C$_6$**H**$_3$), 3.68 (m, $^{3}J_{H–H}$ = 6.9 Hz, 2H, C**H**Me$_2$), 3.57 (THF?), 3.26 (broad s, 2H, C$_6$**H**$_{10}$O$_2$), 2.60, 2.59, 2.55, 2.41, 2.05, 1.94 (s, 3H, I***Me**), 1.54 (overlapping m, 2H, C$_6$**H**$_{10}$O$_2$) 1.46 (s, 9H, C**Me**$_3$), 1.44 (s, 9H, C**Me**$_3$), 1.41–1.38 (overlapping m, 8H, C$_6$**H**$_{02}$O$_2$ and THF) 1.36 (d, $^{3}J_{H–H}$ = 6.4 Hz, 6H, CH**Me**$_2$), 1.25 (d, $^{3}J_{H–H}$ = 6.4 Hz, 6H, CH**Me**$_2$), 1.02 and 0.98 (s, 3H, Si**Me**) ppm. **^{13}C{^{1}H} NMR** (benzene-d_6, 126 MHz, 298 K): δ 166.13 (1-**C**$_6$H$_2$), 157.24 (1-**C**$_6$H$_3$), 140.29 (2,4-**C**$_6$H$_2$), 140.19 (**I***), 137.45 (2,4-**C**$_6$H$_2$), 136.39 (**I***), 134.01 (2,4-**C**$_6$H$_2$), 131.94 (6-**C**$_6$H$_2$), 130.42 (**I***), 129.43 (**I***), 129.00 (**I***), 128.85 (**I***), 128.69 (**I***), 128.35 (3,5-**C**$_6$H$_2$), 125.53 (**I***), 124.36 (3,5-**C**$_6$H$_2$), 123.50 (3,5-C$_6$**H**$_3$), 119.28 (4-C$_6$**H**$_3$), 100.25 (**I***Si), 35.29, and 34.53 (**C**Me$_3$), 32.21, and 30.54 (C**Me**$_3$), 25.99, and 24.99 (**C**HMe$_2$), 24.95, and 24.86 (CH**Me**$_2$) 21.94, 17.62,

17.02, 16.32, 16.16, and 15.26, (I*-**Me**), 5.18, and 3.50 (Si**Me**) ppm. Anal. Calcd for $C_{49}H_{71}O_4ScSi$: C, 73.83; H 8.98. Found, C, 75.02; H 8.13 IR strong absorption bands at 3051, 2957, 2862 *v*(C-H) 1668, 1435, and 1267 cm^{-1}

28



28

(31.1 mg, 64%); fine white microcrystalline powder.

^{1}H NMR (benzene-d_6, 400 MHz, 298 K): δ 7.71 (d, $^4J_{H–H}$ = 2.5 Hz, 1H, 3,5-C_6**H_2**), 7.52 (d, $^4J_{H–H}$ = 2.5 Hz, 1H, 3,5-C_6**H_2**), 7.15 (d, $^3J_{H–H}$ = 7.6 Hz, 2H, 3,5-C_6**H_3**), 6.94 (t, $^3J_{H–H}$ = 7.6 Hz, 1H, 4-C_6**H_3**), 3.74 (overlapping m, 2H, 16-C_{16}**$H_{30}O_2$**) 3.68 (m, $^3J_{H–H}$ = 6.9 Hz, 2H, C**H**Me_2), 2.63 2.56, 2.51, 2.28, 2.07, 1.98, (s, 3H each, I*-**Me**), 1.47 (s, 9H, C**Me**$_3$), 1.42 (s, 9H, C**Me**$_3$), 1.32 (d, $^3J_{H–H}$ = 6.8 Hz, 6H, CH**Me**$_2$), 1.22 (d, $^3J_{H–H}$ = 6.8 Hz, 6H, CH**Me**$_2$), 0.97, 0.95 (s, 3H each, Si**Me**) ppm. Regions including δ 2.19–2.13, 2.07–2.03, 1.60–1.10 (overlapping m, 30H C_{16}**$H_{30}O_2$**) ppm relate to PDL protons. δ 4.03 ppm is unreacted PDL.**^{13}C{^{1}H} NMR** (126 MHz, benzene-d_6, 298 K): δ 182.94 (1-**C**$_{16}H_{30}O_2$), 165.97 (1-**C**$_6H_2$), 158.06 (1-**C**$_6H_3$), 142.55 (2,4-**C**$_6H_2$), 140.14 (**I***), 139.90 (2,4-**C**$_6H_2$), 136.99 (**I***), 134.13 (2,4-**C**$_6H_2$), 131.86 (6-**C**$_6H_2$), 129.48 (**I***), 129.40 (**I***), 128.35 (**I***), 128.22 (**I***), 128.06 (**I***), 127.90 (3,5-**C**$_6H_2$), 126.34 (**I***), 125.92 (3,5-**C**$_6H_2$), 125.38 (3,5-**C**$_6H_3$), 118.78 (4-**C**$_6H_3$), 100.67 (**I***Si), 69.41 (16-**C**$_{16}H_{30}O_2$), 35.58 and 35.28 (**C**$_{16}H_{32}O_2$) 34.57 and 34.54 (**C**Me_3), 35.28 (2-**C**$_{16}H_{30}O_2$) 32.25, and 31.97 (C**Me**$_3$), 31.89, 30.56, 30.07, 27.88, 27.57, 27.36, 27.19, 26.85 (**C**$_{16}H_{30}O_2$), 26.33, and 26.31 (**C**HMe_2), , 26.22, 26.20, 26.18, 26.15, (**C**$_{16}H_{30}O_2$) 24.76, and 24.69 (CH**Me**$_2$) 21.74, 17.62, 17.17, 16.61, 16.02, and 15.13, (I*-**Me**), 4.79, and 3.10

(Si**Me**) ppm. Anal. Calcd for $C_{58}H_{89}O_4ScSi$: C, 75.44; H 9.72. Found, C, 72.82, H, 6.45. IR strong absorption bands at 3056, 2956, 2932, 2862 *ν*(C-H) 1738, 1656, 1435, and 1270 cm^{-1}

5.5.2. Synthesis of $Sc(OAr)_3.2THF$

The preparation of $Sc(OAr)_3.2THF$ was carried out using a modified literature procedure. $ScCl.3THF$[3] and 3.1 eq, of the selected potassium aryloxide (KOAr, where OAr = O-2,6-diisopropylphenyl and O-2,4-di*tert*butylphenyl) are dissolved in toluene and heated to 60 ℃ for 3 days. The reaction was then dried, and the product extracted with hexanes/pentanes and dried *in vacuo*. The products were collected as white powders in yields of 78 % and 56 % respectively. **29** and **30** were characterised via ^1H NMR spectroscopy. The resonances corresponding to O-2,6-diisopropylphenyl for **29** and the O-2,4-di*tert*butylphenyl moiety for **30** were found to be in a ratio of 3:2 compared to the THF resonances. Crystals of **29** and **30** suitable for solid-state analysis were formed by slow evaporation of a saturated solution at – 40 ℃ in hexanes.

5.6. References

1. D. F. Shriver and M. A. Drezdon, *The Manipulation of Air-Sensitive Compounds*, Wiley, 2 edn., 1986.
2. *Inorganic Syntheses*, 2010.
3. Z. R. Turner, J. C. Buffet and D. O'Hare, *Organometallics*, 2014, **33**, 3891-3903.
4. R. Mykura, R. Sánchez-Bento, E. Matador, V. K. Duong, A. Varela, L. Angelini, R. J. Carbajo, J. Llaveria, A. Ruffoni and D. Leonori, *Nature Chemistry*, 2024, **16**, 771-779.
5. X. Tang, A. H. Westlie, L. Caporaso, L. Cavallo, L. Falivene and E. Y. X. Chen, *Angew. Chem. Int. Ed.*, 2020, **59**, 7881-7890.
6. J. Cosier and A. M. Glazer, *J. Appl. Crystallogr.*, 1986, **19**, 105-107.
7. U. K. L. Oxford Diffraction Agilent Technologies, *Journal*.
8. A. Altomare, G. Cascarano, C. Giacovazzo and A. Guagliardi, *J. Appl. Crystallogr.*, 1993, **26**, 343-350.
9. L. Palatinus and G. Chapuis, *J. Appl. Crystallogr.*, 2007, **40**, 786-790.
10. L. Farrugia, *J. Appl. Crystallogr.*, 1999, **32**, 837-838.
11. P. W. Betteridge, J. R. Carruthers, R. I. Cooper, K. Prout and D. J. Watkin, *J. Appl. Crystallogr.*, 2003, **36**, 1487-1487.
12. A. L. Spek, *J. Appl. Crystallogr.*, 2003, **36**, 7-13.
13. L. J. Farrugia, *J. Appl. Crystallogr.*, 2012, **45**, 849-854.
14. C. G. Collins Rice, J. A. Hayden, A. D. Hawkins, L. J. Morris, Z. R. Turner, J. C. Buffet and D. O'Hare, *Organometallics*, 2024, **43**, 540-556.

15. K. Nakamoto, *Infrared and Raman Spectra of Inorganic and Coordination Compounds, Part B: Applications in Coordination, Organometallic, and Bioinorganic Chemistry*, John Wiley & Sons, 6 edn., 2009.

Chapter 6 – **Conclusions and outlook**

This thesis covers (i) the synthesis and reactivity of a number of group three, permethylindenyl-phenoxy (PHENI*) and constrained geometry permethylindenyl (CGCI*) complexes, mainly focusing on scandium; (ii) the dynamics of PHENI* complexes in solution; and (iii) the use of PHENI* and CGCI* scandium complexes as initiators for the ring opening polymerisation (ROP) of cyclic esters.

(i) Permethylindenyl-phenoxy (PHENI*) complexes

A novel set of PHENI* and CGCI* complexes, with a variety of phenoxide substituents, ancillary ligands, and trivalent metals have been synthesised and characterised. Chiral at metal complexes present as a mixture of distinct fluxional isomers in solution where I* and phenoxy- substituents can be *cis* or *trans*. Solid state structural analysis reveals crowded metal centres favours the A-*cis* conformation and less crowded metal centres favours the B-*trans* conformation.

bond distance derived from ^{45}Sc NMR spectroscopy correlates significantly to the shielding of the scandium centre and the reported signal, with scandium nuclei in PHENI* complexes being more shielded than in CGCI* complexes. This leads to the relationship of the activity of the CGCI* complex as the scandium can readily able to accept electron density than the PHENI* complexes. Scandiate complexes are prone to formation from low coordinate scandium THF complexes. Use of a stronger or more sterically hindered neutral donor may prevent the formation or stabilisation of these-*ate* compounds above −30 °C. For example, using crown ethers to bond to the lithium/potassium or phosphines to displace THF before adding any alkyl or amide salts.

(ii) Dynamics in solution

A unified approach to describe the stereochemistry and conformational dynamics of PHENI* complexes has been proposed. Possible pathways for isomerisation are explored with examples of metallocyclic ring puckering, metal centre chirality and indenyl face flipping. Chiral at metal PHENI* scandium complexes all present as a mixture of isomers in solution. The labile ligands allow the product distribution to be under thermodynamic control about the R_{Sc}/S_{Sc} chiral centre. The elongated *ansa*-bridges of PHENICS/ and PHENI* complexes allows for a lower barrier for conversion between diastereomers.

Inversion of chirality at the metal stereogenic centre occurs through ligand disassociation and reassociation or *via* associative substitution. The substitution of labile neutral donors is promoted due to the low energy barrier required for the I* ring slip (η^5- to η^3- to η^5-). Thus, scandium (III) can coordinate with an additional ligand and accept an additional $2e^-$ (net 0 change) without changing oxidation state. Large ligands reduce relative ratio of minor isomers in solution by increasing the relative energy difference of isomers. PHENI* complexes present conformational isomerism in the form of distinct A-*cis* and B-*trans* conformers in solution. LiCl catalyses isomerisation of PHENI* Sc complexes, as seen for **1,** through ring-flipping of the η^5-permethylindenyl moiety.

(iii) Polymerisation of cyclic esters using PHENI* and comparisons to CGCI*

The complexes **1**-**3** were shown to be active for the ROP of ϵ-CL. In this case, where BnOH is used as a co-initiator the PHENI* indenyl moiety is protonated and the structural constraints around the metal centre are lost. The 4-coordinate PHENI* and CGCI* scandium chloride and aryloxide complexes were found to be active for the polymerisation of ϵ-CL and *L*-La without the use of a co-initiator but showed no activity

towards ω-pentadecalactone. **5** showed low activity (200 eq to 70% conversion at 60℃ in 1.1 h) and **7** showed medium/good activity (750 eq to 61% conversion at 30℃ in 20 mins) with a first-order dependence on monomer concentration for both. Polymerisation is proposed to be through *phenoxy*- or *amido*- heteroatom which is the cause of the activity difference. Cyclic polymer, forms as the chain end is tethered to the scandium through the I* moiety, promoting intramolecular transesterification. When a neutral donor was added, the rate decreases and showed a longer initiation period in addition to a low polymer dispersity index. 5-coordinate tris-aryl oxide scandium complexes showed living polymerisation. Initiation is most likely caused by protic impurities rather than coordination insertion of the Sc-aryloxide bond.

Monomer-scandium adducts have been reported in the solid state. It is found that Sc–O ester bonds in *L*-lactide adduct are longer than in PDL adduct. Comparisons with other metal ε-CL complexes showed minimal difference in C=O bond lengths between cationic and neutral ε-CL adducts, but elongation relative to non-coordinated complexes. *L*-lactide adduct takes the A-*cis* conformation whereas ω-pentadecalactone the B-*trans*. A preliminary co-polymerisation study was conducted which showed the formation of random ϵ-CL-L-La copolymer is possible using 4 coordinate PHENI* and CGCI* Sc aryloxide catalysts. Due to the nature of other co-polymers produced using half metallocene scandium complexes, future work on this topic could involve the use of PHENI* catalysts as cationic initiators of α-olefins and cyclic esters, or by using the scandium chloride (**1–3)** as pre-catalysts. Using the PHENI* over the CGCI* for this would prevent initiation through the amido moiety and allow for polymer to be produced without disrupting the structure of the catalyst. Additionally, testing different initiating groups may provide routes to high activity, well controlled catalysts.